A Metabolomic Investigation of Rho-ROCK Signalling in Metastatic Melanoma

Kanno, Tokuwa

Awarding institution:
King's College London

King's College London

PhD Thesis

A METABOLOMIC INVESTIGATION OF RHO-ROCK SIGNALLING IN METASTATIC MELANOMA

Author: Tokuwa Kanno

Supervisors: Dr. A. James Mason

Dr. Victoria Sanz-Moreno

A thesis submitted for the degree of
Doctor of Philosophy
in the Institute of Pharmaceutical Science
of the Faculty of Life Science and Medicine
King's College London

ID: 0902158

Abstract

Metastatic spread is the cause of 90% of cancer-related deaths. Melanoma cells with high actomyosin contractility, driven by high Rho-Rho Kinase (ROCK) signalling, exhibit a rounded amoeboid type movement and are found at the invasive fronts of primary tumours and in metastases. ROCK is a novel therapeutic target of melanoma as it has recently been shown that small molecule inhibitors of ROCK can reduce melanoma growth and the number of metastases *in vivo*.

-Omics level studies of biological systems are quickly becoming an integral and routine part of biological research. Nuclear Magnetic Resonance (NMR) Metabolomics is a relatively cheap and highly reproducible means of identifying 30-100 different metabolites in a biological system. To date there has not been an -omic level study of ROCK regulation of cancer cell metabolism and this thesis addresses this gap in knowledge.

In this thesis, we investigate how ROCK controls proliferation and promotes the rounded morphology. Applying NMR metabolomics to murine melanomas and human A375M2 melanoma cells we identify a substantial shift from glutamine metabolism to anaerobic respiration as the main effect of ROCK inhibition/silencing/knockout with substantial reductions in intracellular glutamate and *myo*-inositol and increases in saturated lipids and the methyl groups of lipids also detected.

Further, analysis of glucose or glutamine-glutamate metabolism gene expression in melanoma patients reveals a greater dependence on the Warburg effect in primary tumours. Glutamine utilisation, correlated with ROCK, increases during metastasis.

In the final section of this work, we show that ROCK1/2 silenced morphological, proliferative and metabolomic phenotypes in A375M2 cells are reproduced by silencing selected glutamate and/or glutamine transporters and, respectively, inhibition and silencing of AMPA and kainate receptors. It is possible that autocrine ionotropic glutamate receptor mediated signalling underpins ROCK dependent control of proliferation and actomyosin contractility in metastatic melanoma.

Table of Contents

Table of Figures

Table of Tables

Acknowledgements

The past three years and a bit have been among the most difficult and yet most enjoyable years of my life. I cannot express enough how grateful I am to all the support I have received during this time and I do not think I can ever repay what has been given to me.

I want to thank the National Institute for Health Research Biomedical Research Council (NIHR-BRC) for funding my PhD project and my supervisors Dr. A. James Mason and Dr. Victoria Sanz-Moreno for guiding me through this project. I also want to thank other funding bodies who have made financial contributions to various projects and travels during my PhD; The International Metabolomics Society, The Biochemical Society and King's College London Graduate School.

I owe so much to Dr. Mason who first encouraged me to consider pursuing research during my undergraduate degree and has been supporting and encouraging me throughout the past four years. He has always supported my research ideas, even when they didn't lead to much. I am especially grateful for how he has actively encouraged me to develop lateral skills and take part in collaborations which has greatly enriched my overall experience. Dr. Sanz-Moreno has been instrumental in guiding me through the beginning stages of this project and consistently offered advice and encouragement while demonstrating a passion for research that has always impressed me.

I want to thank to everyone in the Mason, Sanz-Moreno and Ridley groups for always being there for advice, support and general chat. A special thanks to Dr. Andrew Atkinson, who always had good advice with the intricacies of setting up Magic Angles, shims and locks. I also want to thank those that took time to teach me and worked very closely with me on various aspects of this project: Dr. Justyna Kozlowska, Dr. Eva Crosas Molist, Dr. Sandra Kuemper, Francesca Di Giuseppe, Beatriz Padilla, Pahini Pandya. This would have never been possible without your support and patience. I have been lucky to supervise several talented students during this time. Simon Tin Hine Chu, Sogol Salamipour, and Thomas Gardner, it's been a pleasure. I learnt far more from you than you from me.

I want to thank all the students at the Randall, especially Richard Hodge and Raquel Brandão Haga. I really appreciated your friendship in my time at the Randall and beyond. I know you guys will go onto great things. Gaia Cantelli deserves particular praise for putting up with me as a bench mate and more recently as a house mate. Thanks for all the good times and helping me through bad times. You're a good friend.

Thanks to everyone at the IPS for making my time here so enjoyable Thanks especially Simona Di Blasio, Min Kim, and Dr. Giorgia Manzo. A big thank you to all the students in the KBI/BRC cohort. The first year together was memorable and showed me how great it can be to be a part of a community of scientists.

Thanks to the friends outside research who kept me grounded and made sure I didn't spend too much time in the lab. You guys are the best: Takao, Miriam, Masa, Yoshi and Calum. Maggie, you awoke me from a seven-year slumber, and I'm grateful for that. Thank you Amanda for being around as I picked up the pieces. Thank you Magda for giving me hope, and to Flora as we start on a new journey. To Steve Martinez: you're the brother I never had and an inspiration for me. Thank you.

Finally, the biggest thanks to my family: Mom, Dad, Nando, Elisa, Keimi, Mika, Yoshie, Gram, Aunt Anita, Aunt Judy, Drew, Austin and little Jason. You guys gave me life and love. There's no greater gift and for that I am forever grateful.

Abbreviations

ABBRIVATION	MEANING
2-HG	2-Hydroxyglutarate
ACO1	Aconitase 1
AKT	Protein Kinase B
AKT2	Protein Kinase B 2
AMPA	Aminomethylphosphonic acid
ASCT2	Amino Acid Transporter 2
ATP	Adenosine Triphosphate
BPTES	Bis-2-(5-phenylacetamido-1,3,4-thiadiazol-2-yl)ethyl sulfide
BRAF	B-Rapidly Accelerated Fibrosarcoma
CAMK2	Calmodulin Kinase 2
CAN	Copy Number Alterations
CNS	Central Nervous System
CNV	Copy Number Variant
CO-IP	co-immunoprecipitation
COSMIC	The Catalogue of Somatic Mutations in Cancer
COSY	Correlation Spectroscopy
COW	Correlation Optimised Warping
CPMG	Carr-Purcell-Meiboom-Gill
CRE	Causes recombination' protein
CREB	cAMP Response Element Binding Protein
CS	Citrate Synthase
CSA	Chemical Shift Anisotropy
CTL-4	Cytotoxic T-lymphocyte-associated Protein 4
CV	Cross Validation
DLD	Dihydrolipoamide Dehydrogenase
DMEM	Dulbecco's Modified Eagle Media
DMSO	Dimethyl Sulfoxide
DNA	Dioxyribonucleic Acid
DNP	Dynamic Nuclear Polarisation
ECM	Extra Cellular Matrix
ERK	Extracellular Signal Regulated Kinase
ES	Enrichment Score
EU	European Union
FBS	Foetal Bovine Serum
FDA	Food and Drug Administration
FDR	False Discovery Rate
FID	Free Induction Decay
FTIR	Fourier Transform Infrared Spectroscopy
GAP	GTPase Activating Protein
GAPDH	Glyceraldehyde 3-phosphate dehydrogenase
GBM	Glioblastoma Multiform
GCLC	Glutamate-Cysteine Ligase Catalytic Subunit
GCLM	Glutamate-Cysteine Ligase Modifier Subunit
GC-MS	Gas Chromatography Mass Spectrometry
GDP	Guanosine Diphosphate

GEF	Guanine Nucleotide Exchange Factor
GEO	Gene Expression Omnibus
GLC	Glucose
GLN	Glutamine
GLS	Glutaminase
GLU	Glutamate
GLUL	Glutamate-Ammonia Ligase
GLUT	Glucose Transporter 1
GM-CSF	Granulocyte Macrophage Colony-stimulating Factor
GOF	Gain of Function
GPCR	G-Protein Coupled Receptor
GRIA	Glutamate Receptor Ionotropic Type AMPA
GRIN	Glutamate Receptor Ionotropic Type NMDA
GRM	Glutamate Metabotropic Receptor
GSEA	Genes Set Enrichment Analysis
GSH	Glutathione
GSK269	GSK269962A
GSM	GEO Sample Number
GTP	Guanosine Triphosphate
GTP	Guanosine Triphosphate
HIV	Human Immunodeficiency Virus
HMDB	Human Metabolome Database
HR-MAS	High Resolution Magic Angle Spinning
HSQC	Heteronuclear Single Quantum Coherence Spectroscopy
HSV-1	Herpes Simplex Virus 1
IC50	Quantity of Drug required for 50% inhibition of a biological process
IDE	Interactive Development Environment
IDH	Isocitrate Dehydrogenase
IF	Invasive Front
JAK	Janus Kinase
J-RES	J-Resolved Spectroscopy
KD	Knock Down
KEGG	Kyoto Encyclopaedia of Genes and Genomes
KO	Knock Out
LAT1	Sodium-Independent Neutral Amino Acid Transporter 1
LOX	locus of X-over P1
MAPK	Mitogen-activated Protein Kinase
ME2	Malic Enzyme 2
MEK	Mitogen-activated Protein Kinase
MGWAS	Metabolic Genome Wide Association Study
MHZ	Mega Hertz
MIAME	Minimum Information about a Microarray Experiment
MLC	Myosin Light Chain
MLCK	Myosin Light Chain Kinase
MR	Magnetic Resonance
MSIGDB	Molecular Signatures Database
MTOR	Mammalian Target of Rapamycin

NADPH	Nicotinamide Adenine Dinucleotide Phosphate
NCBI	National Center for Biotechnology Information
NCI	National Cancer Institute
NIH	National Institute of Health
NMDA	N-Methyl-D-aspartic acid
NMR	Nuclear Magnetic Resonance
OAT	Ornithine Aminotransferase
OBA	Optimised Bucketing Algorithm
OGDH	Oxoglutarate Dehydrogenase
OPLS-DA	Orthogonal Partial Least Squares Discriminant Analysis
PCA	Principle Component Analysis
PDB	Protein Database
PDL-1	Programmed Death-ligand 1
PFKL	Phosphofructokinase, Liver Type
PI3K	Phosphoinositide 3 Kinase
PKA	Protein Kinase A
PKC	Protein Kinase C
PKG	Protein Kinase G
P-MLC	Phosphorylated Myosin Light Chain
PQN	Partial Quotient Normalisation
QPCR	Quantitative Polymerase Chain Reaction
RAC	Ras-related C3 botulinum toxin substrate 1
RAS	Rat Sarcoma Viral Oncogene Homolog
RDB	Rho Binding Domain
RNA	Ribonucleic Acid
RNAI	RNA interference
ROCK	Rho Kinase
ROS	Reactive Oxygen Species
SDHD	succinate dehydrogenase complex subunit D
SIRNA	Small Interfering Ribonucleic Acid
SKCM	Skin Cutaneous Melanoma
SLC	Solute Carrier
SNP	Single Nucleotide Polymorphism
STAT	Signal Transducer and Activator of Transcription Protein
SUCLG2	Succinate-CoA Ligase GDP-Forming Beta Subunit
SUMO	Small Ubiquitin-like Modifier
TB	Tumour Body
TCA	Tricarboxylic Acid
TCGA	The Cancer Genome Atlas
TET	Ten-Eleven Translocation
TGM	Transglutaminase
T-MLC2	Total Myosin Light Chain 2
TP53	Tumour Protein 53
TPI1	Triosephosphate Isomerase 1
UK	United Kingdom
US	United States
UV	Ultraviolet Radiation
XCT	Amino Acid Transport System Xc-

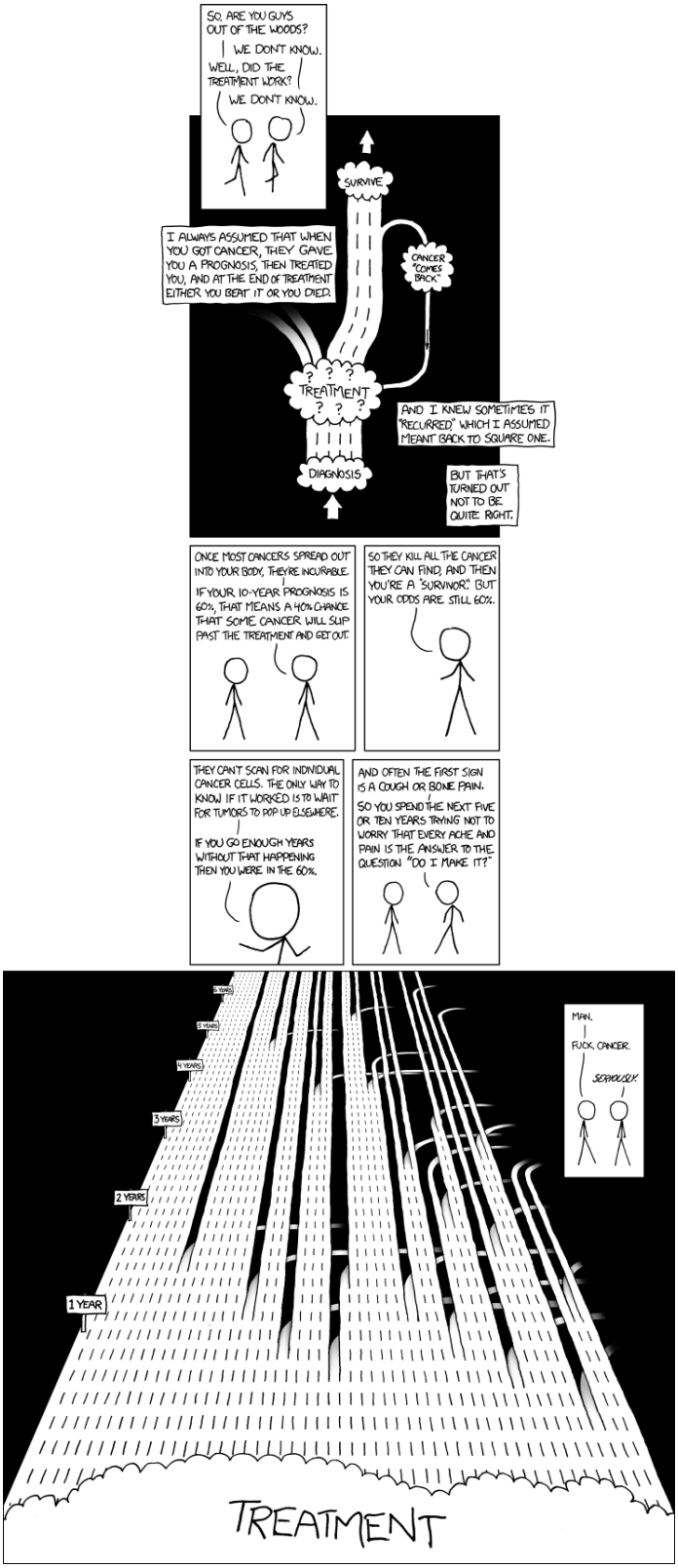

https://xkcd.com/931/ - Reproduced with Permission

Chapter 1 : Thesis Summary

Cancer is currently the leading cause of death in the UK (1) and while incredible advances have been made in the treatment of the disease, challenges still remain with regards to non-response to therapies and resistance that develops in patients. Thus there is still a need for new research into alternative targeted therapies. Melanoma Is the fifth most common form of cancer in the US and, while much less common in the UK, incidence has risen 400% since the 1970s (2). Rho Kinase (ROCK) has recently been suggested to be a therapeutic target of melanoma (3,4) and while its role in regulating the actin cytoskeleton and melanoma proliferation (5) are well established, much less is known about its regulation of cancer cell metabolism. Since metabolomics has now become an established part of biomedical research and NMR metabolomics is a highly reproducible, low cost method of conducting -omic levels studies of the metabolism of biological systems, the aim of this thesis is to address this gap in knowledge and conduct a metabolomic level study of melanoma cell metabolism after perturbing ROCK activity. Understanding the metabolic pathways that are altered by ROCK activity will give additional leads for further research into melanoma cell metabolism during disease progression and metastasis. The following paragraphs outline the chapter structure of the thesis.

Chapter 2 establishes the framework for this thesis. It will review the history and research background of first cancer metabolism and then NMR metabolomics, examining the history, sample preparation and data analysis required for successful metabolomic studies. It will then review malignant melanoma, the development of treatments of melanoma and current trends in targeting the metastatic cascade for therapy. Particular focus will be spent on cancer cell migration strategies and the Rho/ROCK signalling pathway, which promotes cancer cell invasion as well as melanoma proliferation. Finally, the available literature linking Rho/ROCK signalling to cancer metabolism will be examined.

Chapter 3 will detail the materials and methods used in this thesis with overviews of the data processing and pattern-recognition systems used in this thesis.

Chapter 4 is an NMR metabolomic study of ROCK activity in an *in vitro* model of metastatic melanoma. We will use the following strategies to interfere with ROCK activity or expression and study both whole cells with HR-MAS NMR and a liquid NMR study of the spent cell culture media:

- Small Molecule inhibition of ROCK activity in human A375M2 melanoma cells
- Silencing ROCK expression via siRNA in human A375M2 melanoma cells

- Genetic deletion of ROCK in a spontaneous murine model of malignant melanoma

The NMR metabolomics data combined with network analysis suggest that ROCK regulates intracellular levels of glutamine, glutamate and glutathione amongst other metabolites involved in lipid and inositol biology. *ROCK1* and *ROCK2* Knockout murine melanoma cells had distinct metabolic profiles, pointing to both redundant and unique regulation of metabolism by the two isoforms. These metabolic changes seem to be additive in the double knock-out model. ROCK inhibition leads to an increase in the Warburg effect, which can possibly be explained as a response to increases in oxidative stress resulting from ROCK inhibition and/or to make up for the loss of glutaminolysis. Melanoma cells were also observed to secrete glutamate, which points to the importance of glutamate in melanoma not just as a metabolite, but also as a signalling molecule.

Chapter 5 aims to address whether the data collected in chapter 4 can be applicable to the clinical setting. A conceptual integration of the metabolomic data and publically available transcriptomic data from melanoma patient microarrays is used to conduct a bioinformatics based search for potential therapeutic targets of metastatic melanoma. Echoing the experimental results of the previous chapter, the results point to the importance of glycolysis in primary tumour formation in melanoma while glutamine and glutamate metabolism plays a more important role in metastasis compared to primary tumours. Glutamine transport genes' expression also correlated with *ROCK* expression in melanoma patients and genes from both glycolysis and glutamine metabolism correlated with poor patient outcomes.

Chapter 6 returns to *in vitro* studies of metastatic melanoma, this time focussing on how interfering with glutamine/glutamate metabolism or glutamate signalling alters melanoma cell proliferation, morphology and metabolic profiles. siRNA and small molecule inhibitors targeting different stages of glutamine and glutamate metabolism as well as glutamate signalling are studied. siRNA knockdowns of genes involved in glutamine absorption and small molecule inhibition of glutaminase indicate that the ability of cells to maintain glutamine influx is essential for cell proliferation. Additionally, siRNA knockdowns of genes involved in glutamine and glutamate efflux suggest extracellular glutamine/glutamate to play a role in maintaining a rounded morphology in melanoma cells.

Antagonists of ionotropic glutamate signalling are shown to effectively inhibit cell proliferation at low does and siRNA knockdowns of an ionotropic glutamate receptor gene (*GRIK2*) is shown to regulate

cell morphology and actomyosin contractility in both human and mouse melanomas, while not affecting cell proliferation.

Chapter 7 concludes this thesis with a short discussion of all the collected data, suggests a model for how ROCK regulation of proliferation and actomyosin contractility may involve autocrine and/or paracrine signalling via ionotropic glutamate receptors and proposes future research directions.

The work presented in this thesis is currently being written for publication:

- **Kanno T**., Crosas Molist E., Padilla B., Chu T., Pandya P., Kozlowska J., Di Giuseppe F., Sanz-Moreno V., Mason AJ (2016) A role for glutamine-glutamate metabolism in the ROCK dependent control of proliferation and actomyosin contractility in A375M2 melanoma (in preparation)

Additional work not included in this thesis has been conducted that are significant contributions to current and future publications:

- Honeth, G., Schiavinotto, T., Vaggi, F., Marlow, R., **Kanno, T**., Shinomiya, I., … Dontu, G. (2015). Models of Breast Morphogenesis Based on Localization of Stem Cells in the Developing Mammary Lobule. *Stem Cell Reports*, *4*(4), 699–711.
- Choo J.M, **Kanno T.**, Zain N.M.M., Leong L.E.X, Abell G.C.J., Keeble J.E., Bruce K.D., Mason A.J., Rogers G.B. (2017) Divergent Relationships between Fecal Microbiota and Metabolome following Distinct Antibiotic-Induced Disruptions. *mSphere* **DOI:** 10.1128/mSphere.00005-17

Chapter 2 : Introduction, Background, and Review

2.1 Cancer and Therapy

Cancer has now surpassed cardiovascular disease as the leading cause of death in the UK. In 2014 there were 147,000 cancer related deaths, accounting for 29% of total deaths in the UK (1). However, breakthroughs in cancer awareness, prevention, diagnosis and treatment have resulted in an 8% decrease in cancer deaths for women and 11% decrease for men since 2004 in the UK(1). This is a testament to the resources dedicated to medical research and the resulting discoveries.

Cancer is a broad group of diseases characterised by uncontrolled cell proliferation with the potential to spread to secondary sites in the body. This process is known as metastasis (6). Great strides have been made in the last 40 years in understanding the molecular mechanisms driving the disease, which have permitted drastic improvements in diagnosis and treatment. For example, understanding the V600E BRAF (B-Rapidly Accelerated Fibrosarcoma) mutation in human melanoma demonstrates how understanding the biochemistry of cancer has translated into new hope for patients in the clinic. The last five years have seen the arrival of therapies such as vermurafenib which targets the V600E BRAF mutation present in 50% of human melanomas(7). There are also several other cancer therapies coming onto the market which would have been unthinkable just a decade ago; since 2011 seven immunotherapies that activate patient immune responses to melanoma have been approved for clinical use by the FDA(8). 2015 also saw a first in kind re-engineered viral therapy to target malignant melanoma cells approved by the FDA(9).

Despite these many exciting developments, several challenges remain. The incidence of certain cancers such as invasive breast, prostate and melanoma continue to increase (Figure 2.1). In the past ten years they have increased by 4%, 5% and 46% respectively (10).

There were 14,500 new cases of malignant melanoma in the UK diagnosed in 2013 (2). This rise in cancer incidence can largely be attributed to the increased life expectancy in the developed world as cancers are, for the most part, age-related diseases. In the specific case of melanoma, increased incidence can be attributed to increased exposure to ultraviolet radiation (UV) through exposure to sun, or artificially via sunbeds (11). Resistance to available therapies has always been an issue in the clinic. Amongst patients treated with vermurafenib, resistant tumours present within 6-7 months and 15% of patients treated do not respond (12). In addition, vermurafenib is only effective for patients whose melanomas harbour the V600E mutation of BRAF which is present in 50% of human melanomas (7). Patients treated with immunotherapies have shown a response rate between 45-52% (13) meaning that

a need remains for alternative therapies for the large number of patients who do not respond to currently available treatments. There is also a need to address how to treat not just the primary tumour but distant metastases. Current treatments have been suggested to increase the number of circulating tumour cells as the primary tumour is targeted, increasing the risk of metastasis (14).

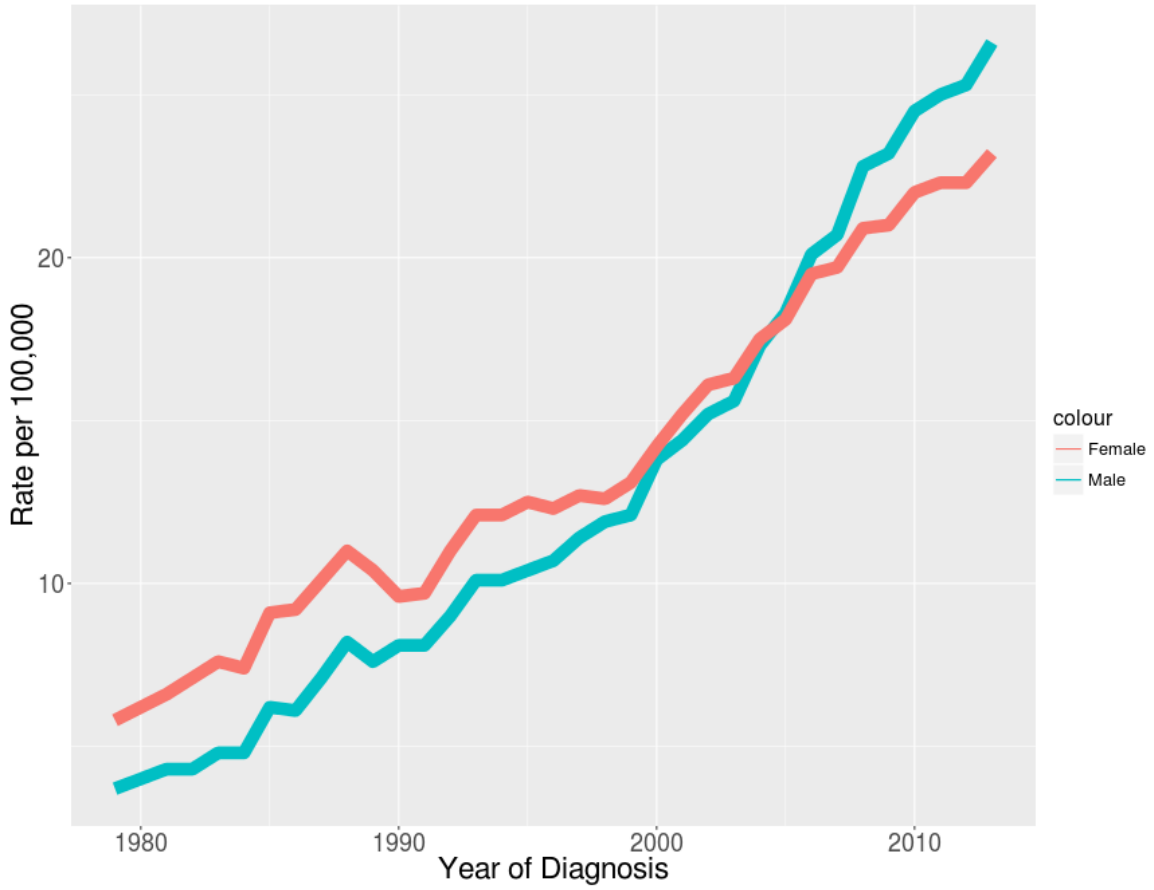

Figure 2.1. Melanoma Incidence per 100,000 people in the UK over time from 1980 to 2010. Data obtained from (2).

2.2 Oncology and Cancer Cell Metabolism

One potential avenue of research in oncology, which could reveal novel therapies for disease, is to target the altered energetics of tumour cells. Indeed, this thesis aims to study how cancer cell metabolism is altered in melanomas with higher metastatic potential. To help understand the purpose of this work, it is helpful to understand the history of our understanding of cancer metabolism and the direction this field of research has taken.

In 1923 Otto Warburg first reported that even in the presence of oxygen, tumour cells preferentially fermented glucose to lactic acid rather than converting it to pyruvic acid and channelling it into the more

efficient TCA cycle(15). He continued this line of research for decades and this observed phenomenon was denoted ‘The Warburg Effect’ in his honour (16).

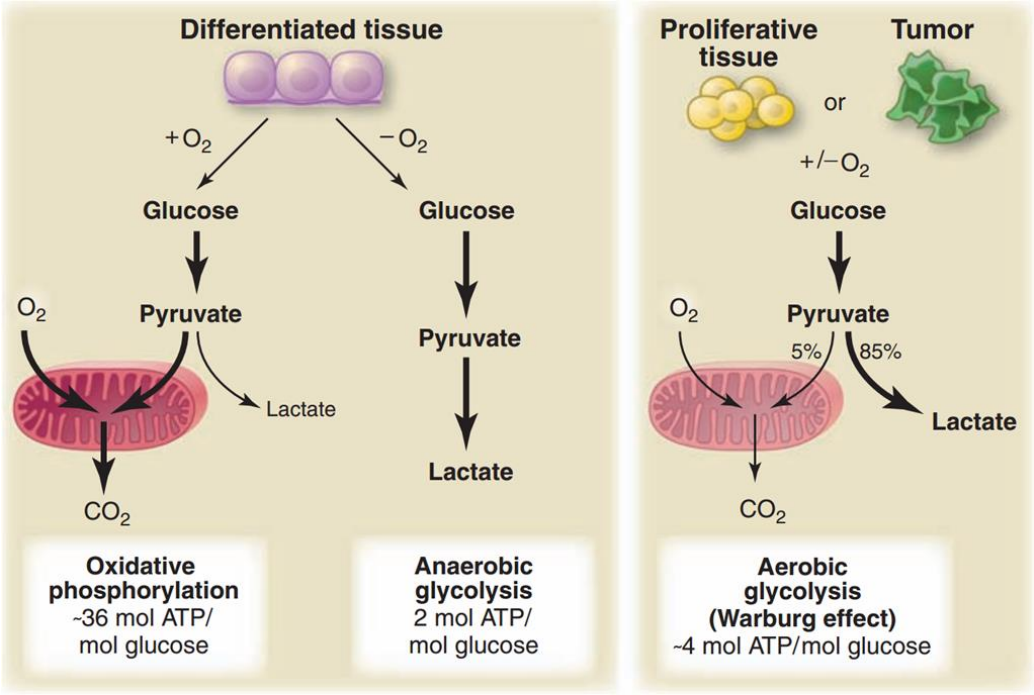

Vander Heiden et al 2008

Figure 2.2. The Warburg Effect. Even in the presence of oxygen, many tumour tissues and cells preferentially generate energy through glycolysis. This effect is observed by the secretion of large amount of lactic acid. Figure reproduced with permission from (15).

In his 1956 lecture he argued that cancer originates by two phases (17); the first being an ‘injury to respiration’ followed by the struggle of these injured cells to survive. Those that survive adopt anaerobic glycolysis as a metabolic strategy and have the side effect of rapid proliferation. Interestingly he concludes his lecture with this statement:

> ‘From this point of view, mutation and carcinogenic agent are not alternatives, but empty words, unless metabolically specified. Even more harmful in the struggle against cancer can be the continual discovery of miscellaneous cancer agents and cancer viruses, which, by obscuring the underlying phenomena, may hinder necessary preventive measures and thereby become responsible for cancer cases.’

It is interesting that, just three years after the publication of the structure of DNA, Warburg was so adamant that the only way to eventually reach a cure for cancer would be to target the damaged respiration of these cells. He maintained this stance of altered respiration as the prime cause of cancer well into 1966 (18), just a few years before his death.

His strong stance was erroneous as in the following years the genetics of cancer took the main focus of biochemical and biomedical research. The discovery of the *src* oncogene in 1970 initiated a string of discoveries of the genetics of oncogenesis that continues in our 'post-genomic' era. This is not to say that studies into cancer metabolism halted completely. In fact, there has been a steady increase in the number of papers published regarding cancer metabolism year on year. One example of the development of research into cancer metabolism was the discussion between Warburg and Weinhouse on whether oxidative phosphorylation still occurred in tumour tissue despite increased glycolysis. Isotope studies showed that the high glycolytic rate in tumours occurs despite normal levels of oxidative phosphorylation (19).

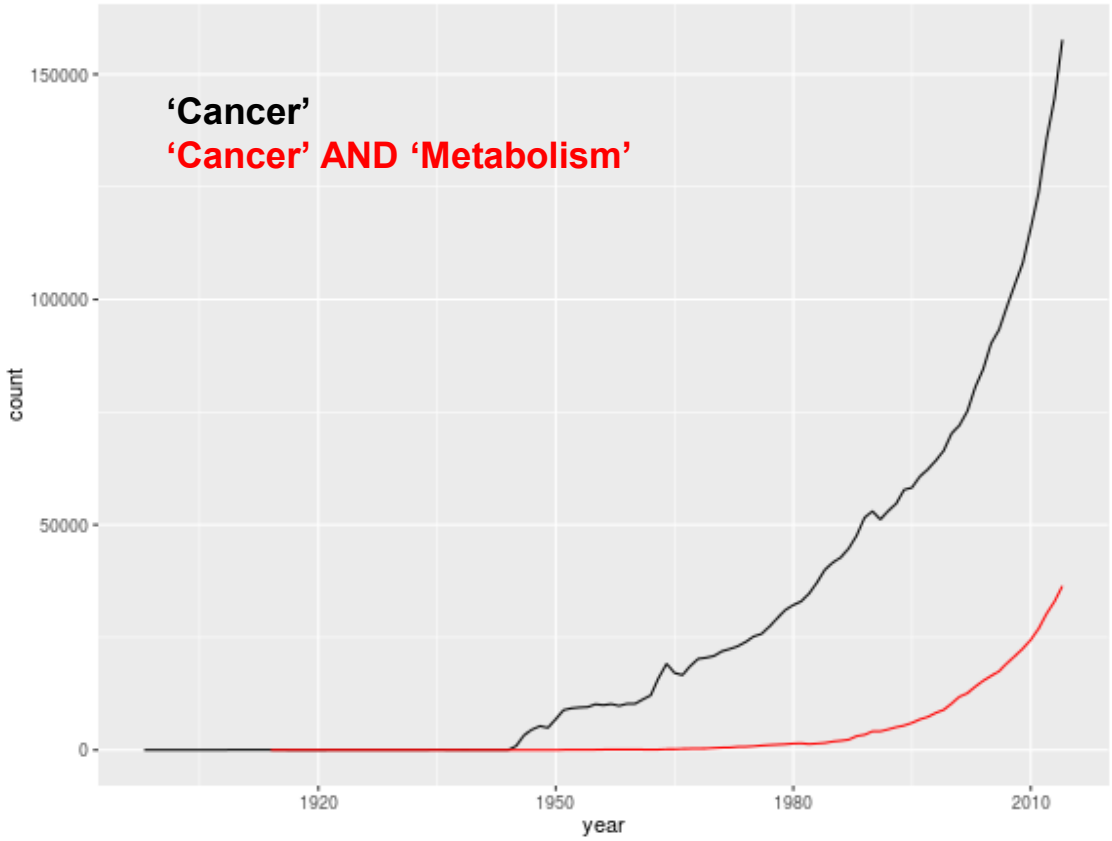

Figure 2.3. PubMed search results of the number of research papers published per year which contain the words "cancer" (in black) or "cancer metabolism" (in red). After 1980 there is a steady increase in publications regarding cancer metabolism.

It is only in the mid 1980's that we see a sharp transition in the number of published papers investigating cancer metabolism (Fig. 3). Since then each year has shown exponential growth in the field of cancer metabolism.

What has led to this growth of interest into cancer metabolism? There may not be any one definitive answer, however the development of technical platforms that allow for large scale studies of the metabolism of biological systems has contributed greatly to the renewed interest of studying cancer metabolism. In the early 20th Century Otto Warburg measured glucose and lactate using biochemical assays such as the Hagedorn-Jensen method for estimating glucose concentrations (20). Today's researchers have much more powerful tools such as mass spectrometry and nuclear magnetic resonance (NMR) spectroscopy available to obtain a biochemical 'snapshot' containing hundreds and even thousands of small molecules of their system of interest, discussed below.

2.3 Altered Energetics of Cancer Cells

The Warburg effect was the first metabolic pathway dysregulated in many cancer types to be understood. Since then there have been several other pathways and metabolites that are understood to be changed in different cancer types.

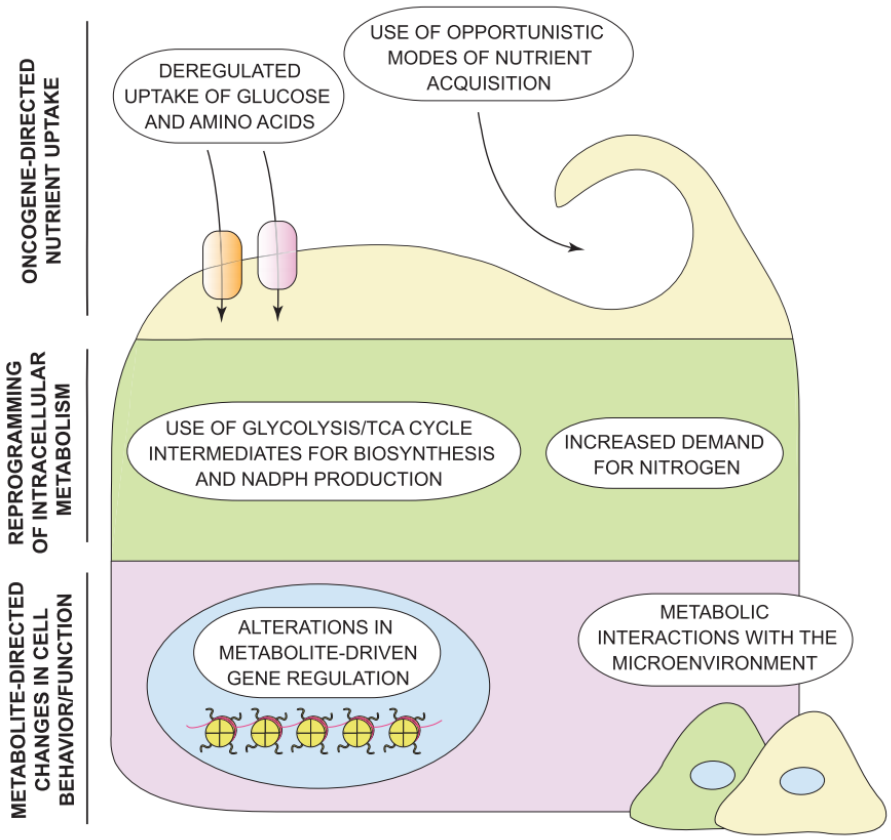

Figure 2.4. 'The Emerging Hallmarks of Cancer Metabolism'. Cancer cells rewire their metabolism to facilitate the behavioural changes in cancer cells. These can be largely categorised by increased nutrient uptake, reprogramming of intracellular metabolism, and metabolite directed changes in cell behaviour and/or function. Figure reproduced with permission from (21).

Pavlova *et al* propose six 'emerging hallmarks of cancer metabolism' (21). These are:

1. Deregulated uptake of glucose and amino acids
2. Use of opportunistic modes of nutrient acquisition
3. Use of glycolysis/TCA cycle intermediates for biosynthesis and NADPH production
4. Increased demand for nitrogen
5. Alterations in metabolite-driven gene regulation
6. Metabolic interactions with the microenvironment.

Cancers are a very heterogeneous set of diseases and do not necessarily present all six hallmarks simultaneously. Some specific examples are shortly discussed here. Many cancers seem to require exogenous glutamine to be able to sustain their increased levels of growth and proliferation. This phenomenon has been termed 'Glutamine addiction' (22). What makes it an interesting area for investigation is that glutamine is the most abundant amino acid present in the body and is a non-essential amino acid for most cell types. However not all cancers are addicted to exogenous glutamine. For example, breast cancers display distinct levels of glutamine dependence. Basal-type breast cancers tend to be glutamine dependent while luminal-type breast cancers tend to be independent of glutamine (23).

Another example of metabolic rewiring in cancer was demonstrated with the proposal of the first metabolic oncogene. Gain-of-function mutations in the Isocitrate Dehydrogenase genes *IDH1* and *IDH2* have been found in up to 80% of gliomas(24) and mutant IDH2 is sufficient to induce tumorigenesis in several classes of glioma (25). These mutated enzymes lead to the aberrant presence of 2-hydroxyglutarate (2-HG), which has been coined as an onco-metabolite. 2-HG is currently being clinically tested as a biomarker for gliomas (clinicaltrials.gov ID: NCT02388659). While the functional effects of this onco-metabolite are still being studied, it is already recognised that 2-HG interferes with the activity of TET (Ten-eleven translocation) hydroxylases which are responsible for the removal of DNA methylation (25).

The rewiring of cellular metabolism by cancer cells has many clear advantages in that it allows cells to sustain increased biosynthesis of building blocks for many aspects of cell growth and proliferation. It can also allow cells to avoid apoptosis by regulating reactive oxygen species and down-regulating pro-apoptotic signalling. The downside to this is that increased growth and proliferation lead to large

increases in energy demands and toxic metabolites such as lactate can accumulate either intracellularly or in the extracellular environment (16).

2.4 Metabolomics

The idea of using metabolic features to study biological systems can be traced all the way back to the idea that changes in biological fluids (humours) were indicative of diseases in the time of ancient Greece. In the middle ages of diagnostic 'urine wheels' linking various colours, smells and taste of urine to various pathological conditions (26). The term 'metabolome' appears first in the 1998 study by Oliver *et al.* (27) and the term was further defined by Oliver Fiehn in 2002(28) as 'the set of metabolites synthesised by an organism'. The field of metabolomics is thus the study of the metabolome.

Additionally, a slightly different field of study of metabolic responses of organisms to diverse stimulation was defined as the field of metabonomics by Jeremy Nicholson in 1999 (29):

> `the quantitative measurement of the dynamic multi-parametric metabolic response of living systems to pathophysiological stimuli or genetic modification'

As in most fields, the formal definition that facilitates deeper discussion is usually proposed once a body of research has been established that requires definition. Thus it is not a straightforward task to establish when the metabolomics field began. The first paper using the phrase 'metabolic profile' was published in 1971 by Horning and Horning (30) just a year after the death of Otto Warburg. There are also many examples of metabolomics type studies in the 70s, 80s and 90s, mainly developing the platforms and technologies that are still used today. Linus Pauling himself dabbled in some 'metabolomic' work; in 1971 he published work attempting metabolic profiling of urine and breath vapour by gas-liquid partition chromatography (31).

NMR had also been used to study complex mixtures of biological systems well before metabolomics was defined. In the 1970's there are examples of NMR being used to study the pH of animal blood by 31P NMR (32), red blood cell metabolism by ^{1}H spin echo NMR (33), and of whole organs (34). However, these types of studies weren't widely adopted until the development of higher field magnets and the appropriate computational methods that make these techniques more accessible to biologists rather than specialist chemists or physicists.

Currently the main methods used for metabolomic studies are Mass Spectrometry (MS) coupled with Chromatography (liquid or gas) and by NMR (35). Each method has its respective advantages and

disadvantages (Table 1). NMR is a highly reproducible technique that can process samples within a few minutes in a non-destructive manner(36). However, its main limitation is its low sensitivity. MS is a highly sensitive technique that can reveal information on thousands of different metabolites. The main challenges associated with MS are questions about reproducibility(37) and the identification of metabolites in the signal. There are other lesser used methods, such as Fourier Transform Infrared Spectroscopy (FTIR) (38) and Raman Spectroscopy (39,40), however they will not be discussed here as they are beyond the scope of this thesis.

	Mass Spectrometry	NMR	HR-MAS NMR
Pros	• high sensitivity (pM range) • 1000 -10,000 detected metabolites	• Highly reproducible • speed of spectra acquisition • sample integrity maintained	• Whole Cells - no extraction protocols needed
Cons	• questions about reproducibility • sample destroyed	• low sensitivity (low uM range) • tens to low hundred metabolites detected	• Less Resolution than liquid-state NMR

Table 1. Comparison of Mass Spectrometry, NMR and HR-MAS NMR for Metabolomic studies.

The growth of the field has led to many more systematic investigations to establish optimal methods and protocols for various metabolomic methods and various centres have been developed across the world spearheading these methods. The development of the field of metabolomics and a resurgence in interest in cancer cell metabolism has led to the acceptance of the recognition of the altered energetics of cancer cells as an emerging hallmark of cancer in Weinberg and Hannahan's 2011 update to their seminal review of the hallmarks of cancer (41). These topics were then expanded in more cancer metabolism specific reviews referenced above (Figure 2.4)(21).

Metabolomic studies can be designed to be non-targeting, aiming to gain a general picture of the biological system of interest (35); these types of studies are used to generate hypotheses for further investigation. Following these studies, metabolomic methods can often be altered for a targeted study to investigate a particular pathway of interest; in these types of studies labelled metabolites are

introduced into the system and how they are metabolised can be studied. These targeted ‘flux’ studies can be used with mass spectrometry (42) and, to a lesser extent, NMR (43).

Metabolomics methods are very flexible and have been applied to clinical studies (44) as well as basic biological research, to gain more mechanistic knowledge into biological systems of interest (45).

2.5 Nuclear Magnetic Resonance Spectroscopy

NMR is a technique that has found applications in a wide range of physical, chemical and biological research. In metabolomics it has proven to be a highly reproducible technique with the added benefit of not destroying the samples of interest. The following section, while not an exhaustive review, will give a short overview of the theoretical and practical aspects of applying NMR to metabolomics research, in particular the study of whole cells with High Resolution Magic Angle Spinning NMR (HR-MAS NMR).

2.5.1 Theory

The theory of NMR can be broadly explained by classical models. However, more in depth understanding of NMR requires an understanding of quantum mechanical models, which goes beyond the scope of this work. In this brief description of the physics driving NMR, we will be using the classical vector models.

NMR spectroscopy takes advantage of the behaviour of the magnetic properties of atoms. Atomic nuclei are comprised of protons and neutrons and are thus positively charged. Any object with an electrical charge creates a magnetic field. The magnetic moment arises from the inherent angular momentum or ‘spin’ of the nuclei. Due to the quantum nature of atomic particles, the spin states of nuclei are discrete values.

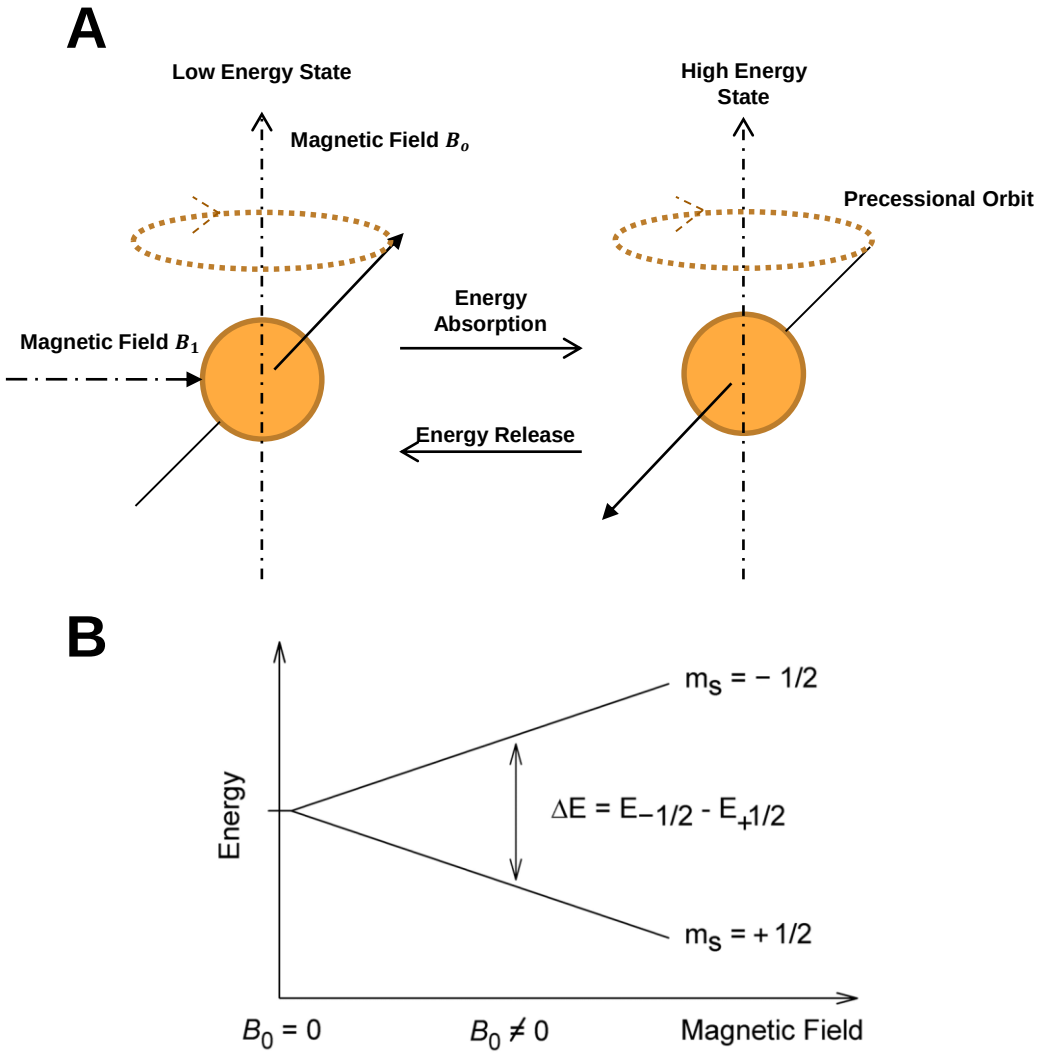

Figure 2.5. Atomic nuclei with non-zero spin can release detectable electromagnetic energy. A) A nucleus placed in a static external magnetic field will 'spin' or precess with a certain frequency. When a second perpendicular electromagnetic field is imposed, the nucleus can absorb this energy and 'flip' its spin state. When B_1 is removed, nuclei may return to their original natural state (relaxation) and will release the absorbed energy in the process. B) The energy required to induce a change in orientation is dependent on the strength of the external magnetic field B_0.

If the number of protons and neutrons are equal in the nucleus, then the total spin state is equal to zero. However, if the number of protons and neutrons are not equal then the spin state is non-zero. Therefore, certain nuclei ($^{1}\boldsymbol{H}$, $^{13}\boldsymbol{C}$, $^{31}\boldsymbol{P}$, $^{15}\boldsymbol{N}$) possess a non-zero spin. The most commonly studied nucleus is the hydrogen atom (^{1}H) comprised of a single proton. We can imagine the hydrogen atom (comprised of a single proton) as an object with its spin represented as a vector.

When placed in a static external electrical field, if the magnetic moment of the nucleus does not oppose the applied magnetic field it is said to be in the lower energy level. In this magnetic field, the nucleus precesses around the magnetic field (Figure 2.5A). The frequency of this precession is called the

Larmor precession frequency. When the electromagnetic radiation applied is equal to the Larmor precession frequency, resonant absorption can occur. When the nucleus absorbs energy, the magnetic moment of the nucleus 'flips' to oppose the applied field, and this is termed the higher energy state. The energy required to induce a change in orientation corresponds to the energy difference between the two orientations and depends on the strength of the magnetic field ($\boldsymbol{B_o}$, Figure 2.5B) in which the nucleus is placed. This can be described by the following equation:

$$\boldsymbol{\Delta E = \gamma h B_o / 2\pi}$$

where $\boldsymbol{h}$ is Planck's constant ($\boldsymbol{6.63 * 10^{-27} J\,s}$) $\boldsymbol{B_o}$ is the strength of the magnetic field and $\boldsymbol{\gamma}$ is the gyromagnetic ratio ($26.7522128 * 10^7\ rad\ T^{-1}s^{-1}$ for proton). The transition from the lower energy state to the higher energy state absorbs energy while the transition from the higher energy state to the lower energy state emits energy. At the Bohr condition ($\boldsymbol{\Delta E = h\nu}$), where the angular momentum is an integer multiple of $\boldsymbol{h}$ the frequency $\boldsymbol{\nu o}$ of the nuclear transition can be written as

$$\boldsymbol{\nu_o = \gamma B_o / 2\pi}$$

Thus far we have only been considering a single nucleus. In an experimental sample we deal with many more nuclei, each which their own magnetic moment. At this scale we then deal with bulk magnetization. When all the individual magnetic moments are averaged out, we can visualise the bulk magnetisation as a vector (Figure 2.6A).

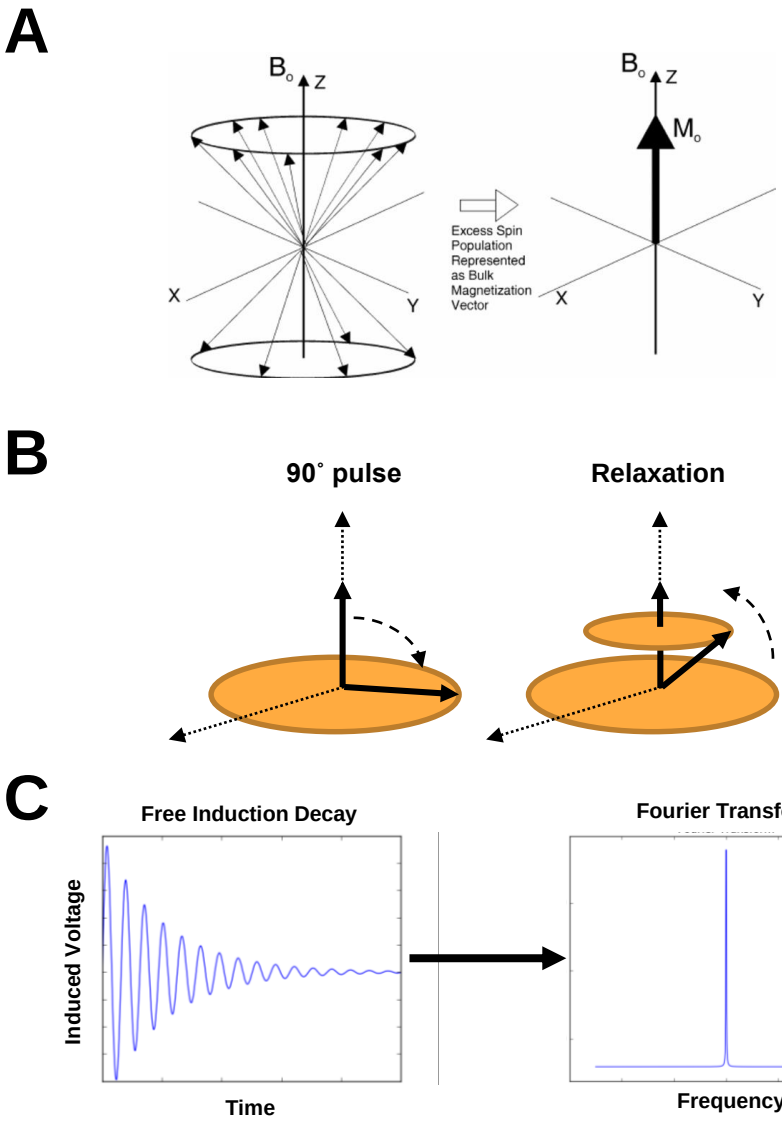

Figure 2.6. Bulk magnetisation and the classic NMR experiment. A) when all the magnetic moments in a sample are averaged out, the resulting bulk magnetisation can be visualised as a vector. B) In the classic NMR experiment, a perpendicular electromagnetic pulse is applied to the sample so as to induce a 90˚ change in orientation of the bulk magnetisation. This is known as the 90˚ pulse. When the pulse is switched off, the sample 'relaxes' back to its original orientation emitting the induced voltage. C) this relaxation can be detected by a receiving coil around the sample. The resulting data presents itself as a wave function of time and is known as the Free induction decay (FID). This data can be Fourier transformed into a function of frequency. This mathematical transformation is what gives the typical NMR spectra.

In the simplest NMR experiment, a radiofrequency pulse of the same frequency of the nuclei of interest is applied perpendicular to $\boldsymbol{B_o}$. The duration of the pulse is enough that the bulk magnetisation is tilted by 90˚, thus the name of the 90˚ pulse. Nuclei then absorb energy and when the radiofrequency pulse is removed, the nuclei 'relax' back into their natural state and release energy as a radio wave (Figure 2.6C). This energy can be detected by a receiver coil in the NMR magnet and the resulting data presents itself as a decaying wave function over time. This is known as the Free induction decay (FID) (Figure

2.6C). This data can be mathematically manipulated, namely via Fourier transform, which transforms the wave function into a function of frequency. This transformation gives a resulting NMR spectra which is then used for analysis.

NMR is a very powerful technique that has the main strength of being highly reproducible. However, one of its major limitations is its lack of sensitivity. This limitation is an inherent part of NMR and can be explained by the population distributions of spin states in a sample.

The energy difference between the spin states in hydrogen can be used in the Boltzmann Equation to calculate the population distributions. The occupancy of spin states can be described by a Boltzmann distribution:

$$N\beta/N\alpha = e^{-\gamma B_o/k_B T}$$

Where $N\beta$ and $N\alpha$ represent the population of nuclei in upper and lower energy states, k_B is the Boltzmann constant, and T is the absolute temperature (K). The signal intensity any spectroscopic method depends on the population difference between the two energy levels $N\beta$ and $N\alpha$. NMR is a low sensitivity technique due to the ratio between $N\beta$ and $N\alpha$ being close to 1. For example, with a 500MHz / 11.75 Telsa spectrometer at room temperature, the population ratio is calculated to be:

$$\frac{N\beta}{N\alpha} = \mathrm{e}^{\frac{-2.67519*10^{8}\ \mathrm{rad}s^{-1}\mathrm{T}^{-1}*11.75\mathrm{T}*6.626176*10^{-34}\ \mathrm{Js})}{1.380662*10^{-23}\ \mathrm{JK}^{-1}*293\mathrm{K}}} = 0.999485259\ \ldots$$

This means that the upper and lower energy states are almost equally populated and thus cancel each other out(46). It is only in the population difference of spins where a net absorption or release of energy is detected and makes up the signal intensity in NMR. This factor describes the relative low sensitivity of NMR and represents a limitation for the application of NMR to biological systems.

As seen from the equations of the Boltzmann distribution, the use of stronger magnetic fields will increase the population ratio and consequently the resolution of the NMR spectra (47). In addition, the signal to noise ratios (S/N) of spectra can also be improved by increasing the number of nuclei in the sample, e.g., by raising the concentration (without causing molecular aggregation) or by increasing the volume of the sample detected. These are some of the strategies that can be implemented to improve the quality of NMR spectra (48).

2.5.2 Chemical shift

When a molecule containing the nucleus of interest is put in a magnetic field B_o, the electromagnetic theory dictates that the B_o field induces electrons in the molecule to orient themselves into a plane perpendicular to the applied magnetic field. The induced currents will then determine a small magnetic field that is opposed to the applied field. These partially cancel the applied field, thus shielding the nucleus. The resonant frequency at which a particular nucleus achieves resonance is determined by the effective magnetic field at the nucleus. The effective magnetic field is affected by electron shielding which in turn is derived from the surrounding chemical environment. Thus, information about the chemical environment of a nucleus can be obtained from its resonant frequency (v in Hz), called chemical shift (δ in ppm) when compared to a standard which is usually spiked into the sample of interest.

The chemical shift of any resonance is independent from the strength of the applied magnetic field. However, any factor which alters the electron density around the proton will affect the chemical shift, causing either shielding (up-field shift), or de-shielding (downfield shift in resonance). For example, the presence of α-electronegativity groups linked by covalent bonds, decreases the electron density surrounding the nucleus and reduces the shielding in the ^{1}H resonance. Other examples include noncovalent effects such as the presence of neighbouring π-bonds, called ring-current shift. The chemical shift is also affected by hybridization effects, by the solvent and H-bonding (49,50).

While chemical shifts for the resonances do not change with increasing field, the actual frequency differences do increase and therefore peaks are narrower at higher field strengths (50). Thus there is less risk of overlapping peaks which reduce S/N in NMR studies. For this reason, as well as the effect on the Boltzmann distribution mentioned above, there is a general interest in creating and making use of machines capable of generating ever more powerful electromagnetic fields. Experiments in this thesis were performed at 1H frequencies of 400 and 700 MHz.

There are additional methods in development attempting to overcome the low sensitivity of NMR, in particular Dynamic Nuclear Polarisation (DNP) NMR. DNP NMR is an exciting development that can hopefully increase the sensitivity of NMR experiments. In short, by irradiating the sample with microwaves, magnetisation transfer can occur between unpaired electrons to nuclei, increasing the nuclear signal (51). What is exciting about DNP NMR is that it can theoretically increase the sensitivity

of NMR experiments by a factor of 10^4 for ^{13}C experiments and 10^3 times for ^{1}H experiments (52). Although still in its infancy, initial work exploring how DNP NMR can be applied to metabolomics (53,54). Other experiments have been conducted using hyper-polarised metabolites to improve sensitivity in magnetic resonance imaging (55).

2.5.3 Solid-state NMR: dipolar coupling and magic angle spinning

Solid-state NMR spectroscopy is another available method to investigate biological samples and detect and quantify small molecule metabolites of a biological system of interest. The most visible difference between the NMR in solution and solid-state NMR is that in solid-state NMR transitions are broad, due to the full or partial effects of orientation-dependent interactions (anisotropy) being observed in the spectrum and shorter T_2 transverse relaxation times due to the restricted motion of the molecules(47). In solution, spectra consist of a series of sharp transitions because orientation dependent contributions are usually averaged out (56). Specifically, factors that determine line broadening and a loss of spectral resolution in solid-state NMR are heteronuclear and homonuclear dipolar coupling between neighbouring nuclei, the chemical shift anisotropy and, for nuclei with $I > \frac{1}{2}$, the electric quadrupole interaction (57).

The dipolar coupling comes from the interaction through space of one nuclear spin with a magnetic field generated by another nuclear spin, and vice versa. This coupling is stronger than spin-spin coupling, which instead is through bonds. The size of the interaction is related to: the inter-nuclear distance, inversely dependent on the distance between the nuclei; the gyromagnetic ratio of the nuclei; and the orientation of the inter-nuclear vector relative to the applied field Bo. In an isotropic liquid the molecular orientations are quickly changed by Brownian motion, thus averaged out and not observed. In crystals and solids molecular motion is restricted and this leads to NMR signals being split with a coupling constant (47).

Dipolar couplings can, to a certain extent, be removed in high-resolution solid-state NMR by rapidly rotating the sample about an axis oriented at an angle of 54.7356° degrees (the diagonal of a cube) with respect to the axis of the static magnetic field $\boldsymbol{B_o}$ (Figure 4). This is called the “magic angle” and therefore the technique is denoted magic-angle spinning (MAS). In the case of biological samples, the molecular motion within the semi-solid samples also partially removes some of the anisotropic interactions, as well as average out differences in magnet field inhomogeneity and magnetic susceptibility within a biological sample. Magnetic susceptibility is a dimensionless proportionality

constant that indicates the degree of magnetisation of a material in response to an applied magnetic field.

2.5.4 HR-MAS NMR

High-resolution Magic Angle Spinning solid-state NMR is a particular method of NMR that mechanically averages the anisotropic spin interactions by rotating a sample in a rotor. The rotor is set at the 'magic angle', which is 54.7356° with respect to the z axis of the static magnetic field. This is the angle that is made by the cross diagonal of a cube. Any point on this diagonal now has identical x, y, z coordinates and thus the anisotropic detail is lost (58). By increasing the spinning rate, the broad lines from the immobile sample become increasingly narrowed with a significant improvement in the signal amplitude and sensitivity. When the spinning rate is higher than the width of the anisotropically broadened NMR spectrum, the spectrum collapses to an isotropic-like spectrum (58). It should be noted however that these high spinning rates are only required to displace spinning side bands outside the spectral range of interest in metabolomics studies (59).

As conditions can be created with solids that generate NMR spectra similar to liquid state NMR, HR MAS-NMR can therefore be used as a highly versatile tool to analyse complex biological systems such as intact tissues and whole cell samples (60,61).

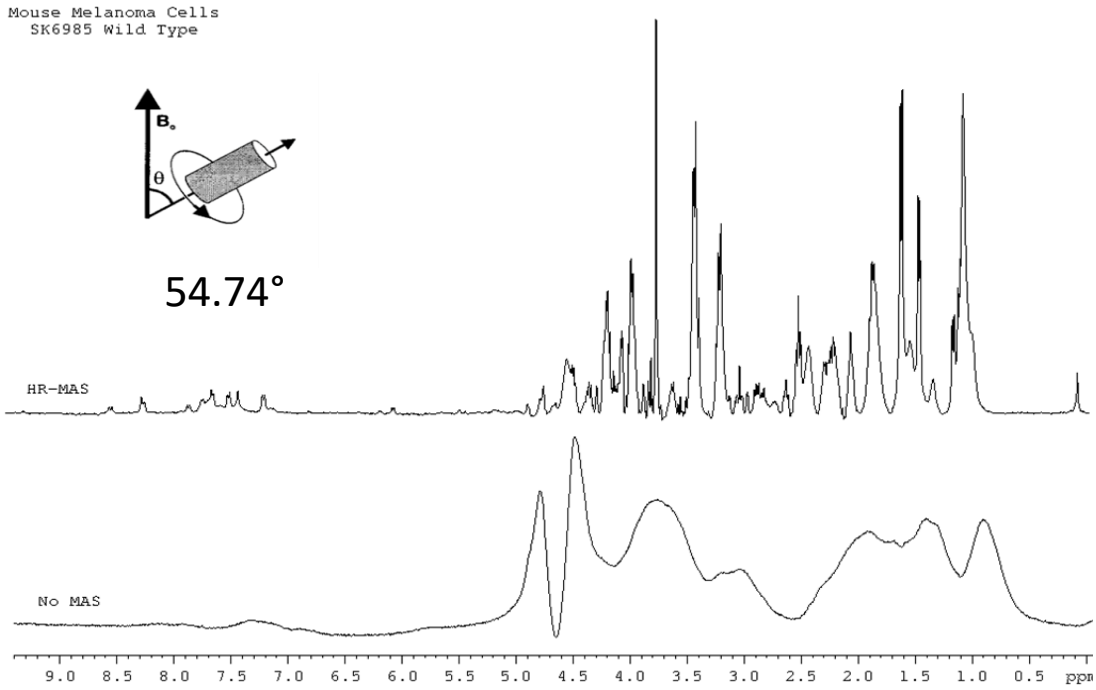

Figure 2.7. A Comparison of NMR spectra obtained on Mouse melanoma cells with (top) and without (bottom) MAS spinning. Tilting the samples at the 'magic angle' and spinning at high velocity narrows NMR peaks to become similar but not equal to those obtained in solution NMR. Spectra were obtained on a 400 MHz Bruker spectrometer.

The ability to study whole cells and tissues represents a major advantage of HR-MAS NMR over liquid state NMR, despite its inability to achieve the spectral resolution of liquid-state NMR. Another advantage to studying whole cells and tissues over liquid state NMR is that HR-MAS NMR does not require the extensive extraction protocols used in liquid state NMR. In addition, whole cells can be lyophilized and re-suspended directly in deuterium oxide before insertion into an NMR insert (Figure 6) significantly reducing the amount of residual water in the sample. This increases the reproducibility and reliability of the spectra obtained from HR-MAS NMR.

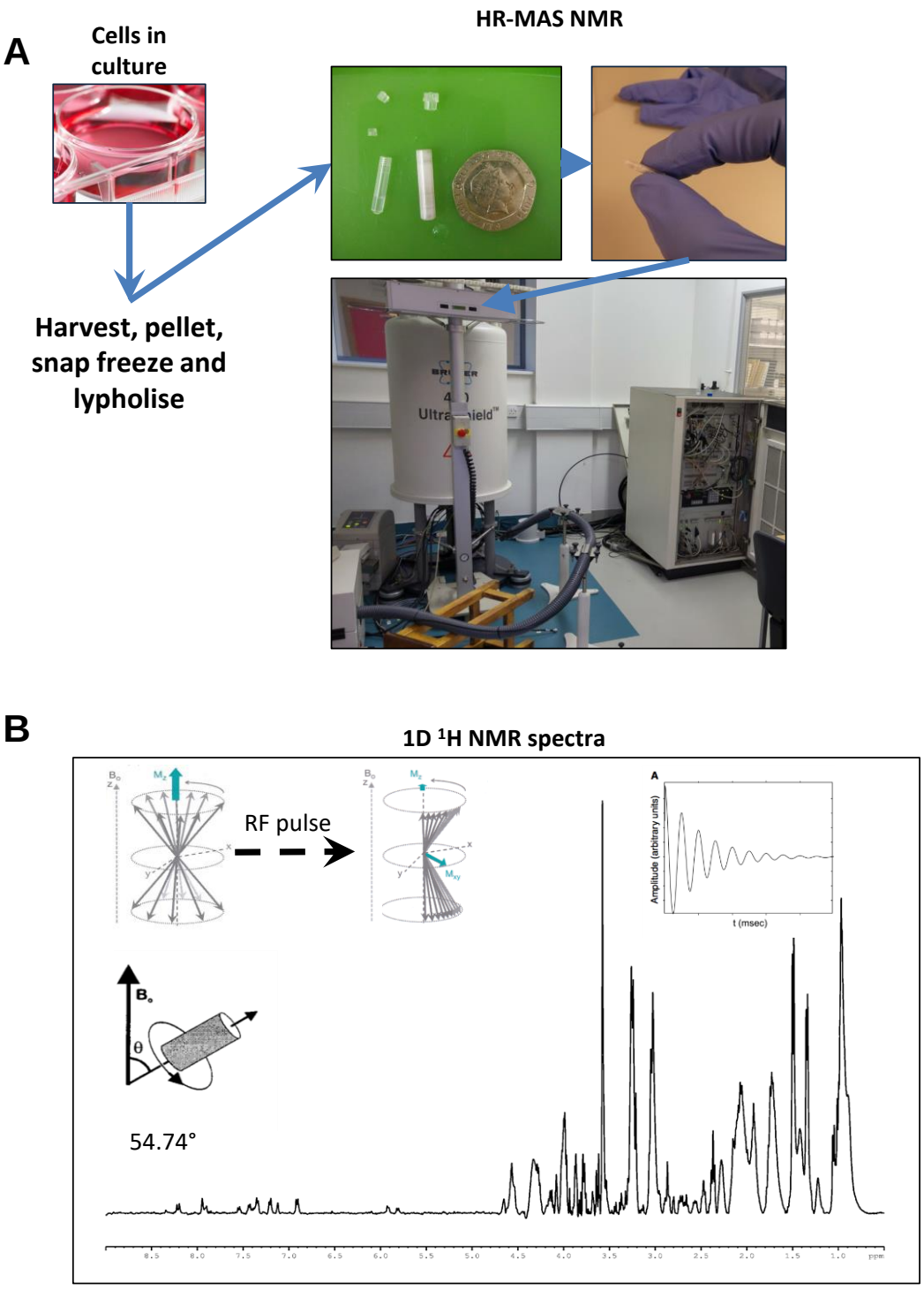

Figure 2.8. Workflow for *in vitro* whole cell HR-MAS NMR Metabolomics Studies. Whole cell studies remove the need for metabolite extraction protocols thus increasing reproducibility of experiments. A) Cells grown in culture are harvested, pelleted and snap frozen in liquid nitrogen. Pellets are then suspended in D_2O transferred to HR-MAS inserts and inserted into the NMR magnet. B) Once in the NMR magnet, the sample is tilted at the 'magic angle', 54.7356˚ and rotated a high velocity. The resulting NMR spectrum give high resolution data on the biological sample.

Liquid state NMR requires molecules to be in solution to obtain spectra of good resolution, therefore biological samples often require applying extraction protocols that will remove large macromolecules

that produce broad linewidths in the resulting NMR spectra. Additional methods can also separate polar and non-polar phases of the sample. These protocols add complexity to experimental set ups and often make use of carcinogenic chemicals such as chloroform, although alternatives are available, such as methyl-tert-butyl ether (MTBE). Each additional step of protocols also introduces the opportunity for human error in sample handling. A final challenge arises in the case of experiments with adherent cell lines as there is the concern for metabolite leakage when attempting to detach the cells from a plate(62). There are several studies that have investigated optimal methods for metabolite extraction (62,63), while other methods attempting to eliminate the solvent extraction steps have been proposed, instead making use of sonication of samples (63). In certain studies, HR-MAS has been shown to be preferable to solution state NMR as it also gives information on lipid profiles as well as information on small polar metabolites (64). Although it should be noted that issues with spectral peak overlap are an issue with HR-MAS NMR.

On the other hand, whole cell NMR means that there is potential for polar and nonpolar components of cells to overlap each other in the NMR spectra. This can become a problem as changes in metabolite concentrations can become masked by overlapping peaks. Extraction protocols can remove this issue as the different phases can be investigated separately, increasing the number of observed metabolites. These considerations must be taken into account when designing metabolomic studies.

The reliability of metabolite stability can be an issue with metabolomic work as several steps are taken

2.5.5 Pulse sequences

Methods for reducing the contributions of large macromolecules to NMR analysis have also been developed with alternative pulse sequences to the standard 1D NMR experiment. The most widely used is the Carr-Purcell-Meiboom-Gill sequence (CPMG). As mentioned earlier, large macromolecules have very short T_2 relaxation times due to restricted motion of molecules. This leads to broad lines that can overlap with other peaks, reducing the amount of information that can be obtained from an NMR spectrum Figure 2.9A.

The CPMG pulse sequence takes advantage of the phenomenon known as the Hahn echo. The pulse sequence is comprised of a 90˚ pulse, which forces the nuclei into the transverse plane, a 180˚ inversion pulse, which flips the nuclei vectors, and after time tau the Hahn echo appears, which is when the nuclei become perfectly phased again. This refocussing of the magnetisation vectors can improve the signal in the NMR spectra that can arise due to both inhomogeneity in the magnetic field as well as the short

T_2 relaxation times that arise due to large macromolecules in a sample (Figure 2.9B)(59), thus facilitating the observation of low molecular weight metabolites. If the 180˚ pulse is repeated multiple times, the echo can be repeated, however there is a loss of signal with each successive 180˚ due to T_2 relaxation. This phenomenon can be taken advantage of as one can thus repeat the 180˚ and only record once the initial signal from large macromolecules, which have very short T_2 relaxation times, is edited out.

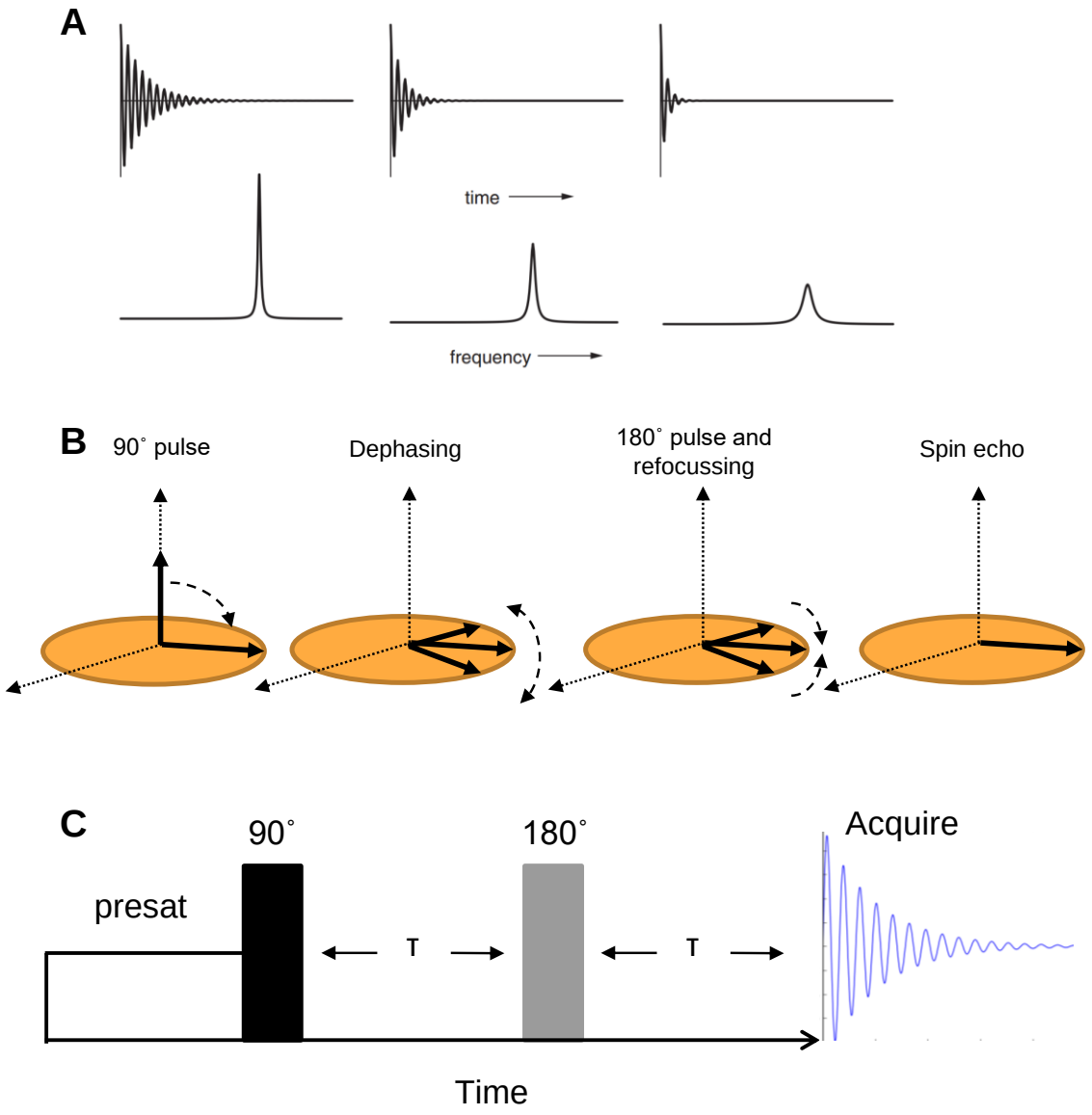

Figure 2.9. The Carr-Purcell-Meiboom-Gill (CPMG) pulse sequence can edit out broad peaks in NMR spectra through T_2filters. A) Large macromolecules have short T2 relaxation times which lead to broad signals in the Fourier transformed spectra. The contribution of these signals to the NMR spectrum can be edited out by taking advantage of the Hahn echo. B) When a 90-degree pulse is put onto a sample different nuclei relax at different rates, leading to a dephasing of the magnetisation vectors. The introduction of a 180-degree pulse allows the magnetisation vectors to refocus and leads to generation of the spin echo. The 180 degree pulses are repeated to filter out the fast T2 relaxation of large macromolecules so the resulting recorded FID contains only information on low molecular weight metabolites.

A final consideration has to be made for the large amount of water in biological samples. In HR-MAS NMR there is often a large amount of residual water in the sample that requires suppression. As stated previously water can be removed from the sample through lyophilisation, however it is nearly impossible to completely remove all water from a sample. In a standard CPMG experiment this is achieved through pre-saturation which is achieved by a long low pulse targeting the frequency of the solvent prior to the initial pulse sequence (Figure 2.9C) (36).

2.6 Data Processing in NMR Metabolomics

2.6.1 Data Pre-Processing

Once NMR data is collected, the spectra must be pre-processed prior to analysis to reduce as much as possible the entry of noise into the successive analysis. Spectra are base-line adjusted, phased, aligned and binned prior to analysis.

In this thesis, we make use of the software for NMR analysis developed in the Mason lab that have been previously published (65-68). There are several developments that have been added that should be considered. Those are the introduction of more advance alignment and binning algorithms into the analysis pipeline that hadn't previously been used. Previous work resorted to basic alignment methods and occasionally making use of correlation optimized warping (COW) algorithm (69) and manual bucketing methods.

Alignment of NMR spectra is important to ensure that pattern recognition methods used are not simply observing a change in pH as a signal in the analysis. There are several alignment algorithms available, reviewed by Vu and Laukens (70). Currently there is no accepted golden-standard method. The Correlation Optimised Warping (COW) algorithm has previously been used in the Mason group for spectral alignment, however it is very computational intensive and slows data processing considerably. For alignment of one dimensional NMR spectra we made use of the Icoshift algorithm (71) as it proves to be much faster computationally than COW and gives comparable results (70).

Binning allows a reduction in data size when analysing NMR spectra which can speed up analysis and further force spectra into alignment. However, it does not handle larger peak shifts, for example shifts caused by variation in pH between samples. The optimized bucketing algorithm (OBA)(72) allows the user to set the initial bucket size as well as the 'slackness' or the percentage of variability the algorithm is allowed when choosing the final bucket size in its search for local minima. Implementing these two features into our pre-processing pipeline has both greatly sped up pre-processing and increased the

reliability of the pre-processing compared to the previous manual bucketing and simple alignment tools used in previous publications of the Mason group.

2.6.2 Multivariate Analysis of NMR Data

Each one dimensional NMR spectrum is a collection of thousands to tens of thousands of data points. This increased complexity of the data requires specialised methods of data handling and multivariate statistical analyses to detect distinctions between groups of spectra depending on study design.

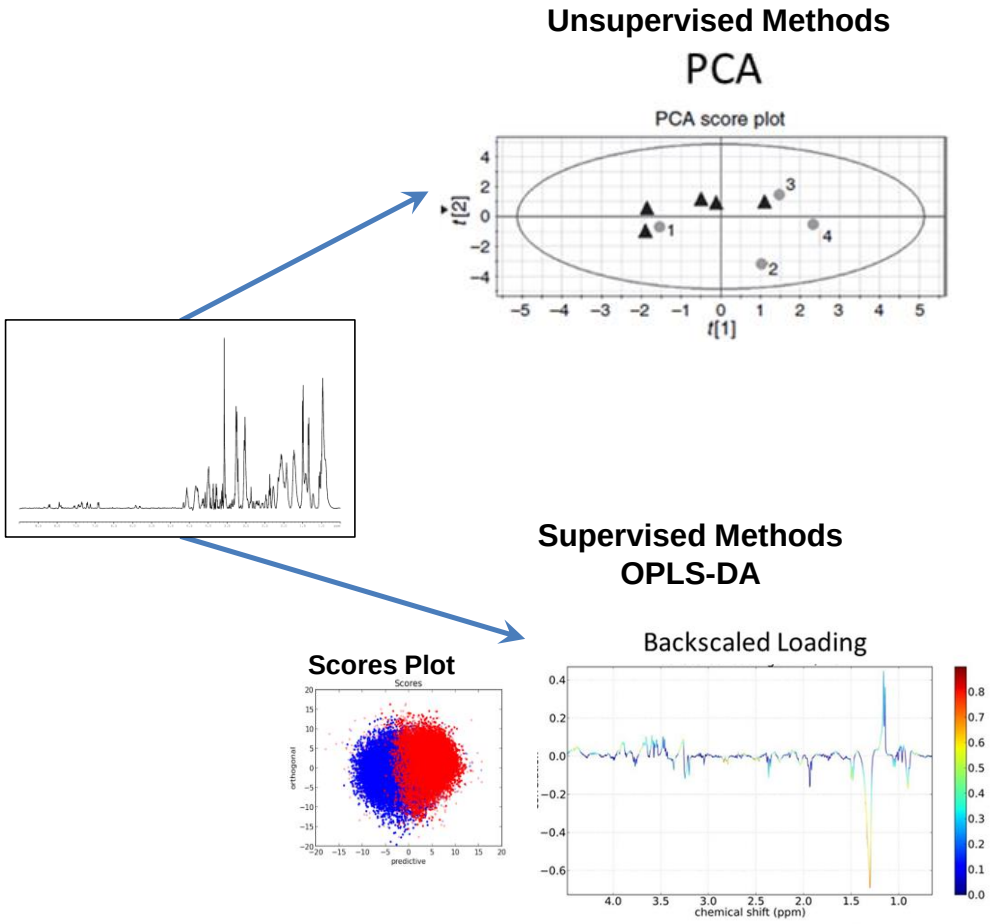

Figure 2.10. NMR metabolomic data multivariate statistics. NMR spectra represent tens of thousands of data points. Data reduction and multivariate models of the data can aid researcher to identify patterns in data sets and find discriminatory variables between groups. Unsupervised statistics such as principle component analysis (PCA, above) allow for initial visualisation of data and the identification of outliers. Supervised Discriminant Analysis, in this case Orthogonal Partial Least Squares-Discriminant Analysis (OPLS-DA) generates models of which features can be identified that discriminate between classes and traced back to the variables (metabolites) that are contributing to the separation between classes. This is visualised through the back-scaled loadings plot which is a pseudo-NMR spectrum showing which variables (chemical shifts) in the data sets correlate with a class (peak height) and if that correlation is highly weighted (colour of peak).

The statistical methods used in interpreting metabolomic data have been reviewed extensively (73). The standard, accepted techniques in use are Principle Component Analysis (PCA), Partial Least Squares Regression (PLS) and its variation Orthogonal Partial Least Squares Regression (O-PLS).

Metabolomic studies generate quite large datasets and as such many different algorithms and machine learning methods can and have been applied to analyse metabolomic data. Some of these other methods are support vector machines (74), artificial neural networks (75), and random forests (76). Each of these methods has its respective strengths and weaknesses. While some analytical methods may have more predictive power, there is a high barrier of entry for many non-expert researchers when applying more complex machine learning algorithms to metabolomic data. Currently the vast majority of metabolomics analyses make use of PCA and PLS.

Prior to multivariate analysis, data needs to be normalised and scaled to reduce variability between experiments as well as to avoid variables with highest signal intensity in dominating the data analysis. In addition, feature selection is an important aspect of data pre-processing to improve models generated in supervised machine learning algorithms. These pre-processing techniques will be discussed in chapter 3.

2.6.3 Principle Component Analysis (PCA)

PCA is an unsupervised algorithm that is used to reduce the number of dimensions of a given dataset to either increase computational speed or to more easily visualise high dimensional data. In PCA, the original variables are transformed into new variables called Principle Components which explain the largest possible amount of variation in the data. The data can be then plotted as points in a two or three dimensional space. This is known as the 'scores plot'. The individual principle components are uncorrelated and orthogonal to each other, therefore each principle component represents independent variation within the data.

Along with the scores plot of PCA, the contribution of individual variables to each principle component can also be visualised, this is called the 'loadings plot' and can give a picture of which original variables, or in this case which NMR resonances are contributing to the variation within the dataset.

PCA is principally used for initial analysis of the data, visualisation of clustering patterns within the data, and identification of outliers within the data. As stated above, the loadings can be used to identify which NMR resonances and thus metabolites are contributing to the variation in the dataset.

2.6.4 Partial Least Squares/ Projection onto Latent Structures (PLS)

PLS is a supervised machine learning algorithm that creates a linear regression model that projects predicted variables and observed variables into a new space. The underlying model of the PLS

algorithm uses the original data matrices X and Y Where X is a 2-dimensional matrix of dimensions of n samples and m predictors; Y is vector of dimensions *n* samples and *p* responses;

$$X = \begin{bmatrix} X_{1,1} & \cdots & X_{1,m} \\ \vdots & \ddots & \vdots \\ X_{n,1} & \cdots & X_{n,\boldsymbol{m}} \end{bmatrix}$$

$$Y = \begin{pmatrix} Y_{1,p} \\ \vdots \\ \vdots \\ Y_{n,\boldsymbol{p}} \end{pmatrix}$$

And is a decomposition of those matrices:

$$X = \boldsymbol{T}P^T + E$$

$$Y = \boldsymbol{U}Q^T + F$$

T and U are matrices that are projections of X and Y respectively, these are the 'scores'; P and Q are the orthogonal loading matrices, also known as the loadings when interpreting the data; E and F are the error terms. X and Y are decomposed to maximise the covariance between T and U. In 2002 the Orthogonal Projection on to Latent Structures, a variation of the PLS algorithm was proposed(77). In OPLS, variation in X that is not correlated to Y is removed. Thus the OPLS model is:

$$\boldsymbol{X = TP^T + t_1 p_1 + E}$$

$$\boldsymbol{Y = UQ^T + F}$$

Where t_1 and p_1 are the 'Y-orthogonal' projections of X that do not correlate with Y, while T and P are the Y-Predictive projections. Geometrically, this transformation can be imagined as rotating the data X to emphasize the variation in X that correlates with Y. This facilitates interpretability of the data; however, it does not improve the predictive ability of the algorithm.

PLS and OPLS can create linear regression models when working with continuous variables. In the case of discrete variables, such as group classifications or comparing two groups, Discriminant Analysis is applied to the PLS or OPLS algorithm, hence the final term of OPLS-DA. In the work presented in this thesis, OPLS-DA is the main algorithm used which is calculated using the non-linear iterative partial least squares (NIPALS) algorithm.

2.6.5 Cross Validation

Modelling high dimensional data is a very powerful method to get information from very large datasets. However, there is always the risk that the generated models explain the given data too well, and include

random noise into the model. This leads to a poorly generalised model that will not perform well to other datasets. This is known as 'over-fitting' a model. Over-fitting is especially an issue in -omics level biological research as in most cases the number of variables available to the research vastly out scale the number of biological samples available and so the risk of random noise being interpreted as signal is a major issue that needs to be addressed in the study design. Over-fitting can be addressed through cross-validation, or a model validation method where the model is tested against an independent set of data (78).

The standard method of cross validation is to split the available data into smaller subsets. Part of the data is used to generate the model and is known as the training set. Then the generated model is used to make predictions regarding the remaining data, known as the test set.

In our studies we use a double cross validation strategy (2CV) (79) whereby the training set is again split into its own training and test sets and undergoes a cross-validation process to select the optimal number of components to generate the model. This is followed by a model generation over the original training set and predictions on the original test set (Figure 2.11).

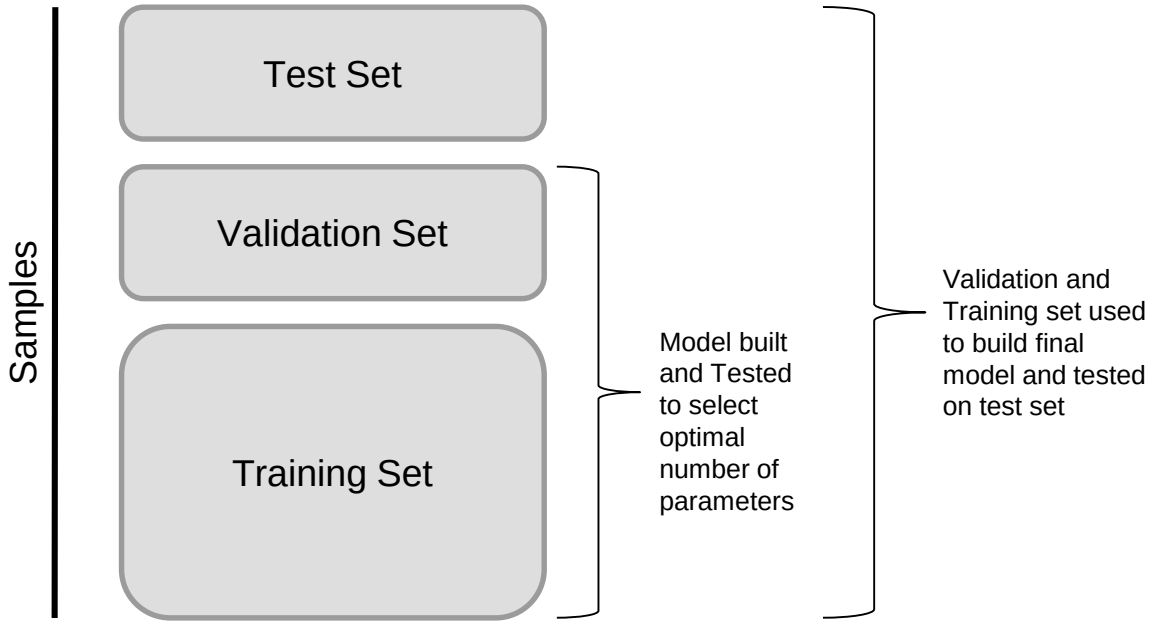

Figure 2.11. The double cross validation method (2CV). Samples in the dataset are randomly assigned to either a test, validation or training set. In a first step a model is created using the training set and is tested on the validation set to select the optimal number of parameters for model construction. Then the training and validation sets are combined and used to generate a final model which is the tested on the test set.

This process is repeated a few hundred or thousand times, and in each repeat samples are randomly assigned to the test, validation or training set. This strategy is preferred to an individual cross validation

strategy as in the 2CV method the model is constructed in absolute absence of the test set. It is also important to note that pre-processing steps such as normalisation and scaling are conducted separately on the training and test sets to ensure independence between the two sets of data. A representative cross validated OPLS-DA output is seen in Chapter 3.

2.7 Integration of -Omics data

The field of metabolomics has matured to a point where it is now being adopted to be used as a piece of larger studies of biological systems. While individual –omics studies are very powerful tools that can generate hypotheses that would otherwise be overlooked in traditional research, there is even more hope that running the same samples on several –omics platforms contemporaneously can exponentially increase the amount of available data of the biological system of interest. In an idealised example one could design an experiment which integrates genomic data on single nucleotide polymorphisms (SNPs) and merge them with transcriptome, proteome, phosphor-proteome and metabolome to reveal how SNPs effect the downstream biochemistry of a system. It should be obvious that increasing the amount of data to such a scale will bring up increased challenges in separating the signal from the noise and in quality control and assurance of the data generated from each platform. In addition, bioinformatics platforms have to be able to process with relative speed the enormous amount of generated data.

This field is very new and reviews on the topics are few. Cavill *et al* (80) suggest a theoretical framework on which the methods for multi-omics experiments can be conducted. They group the methods into three categories with differing levels of statistical power.

The ever increasing size of data generated in biological studies requires novel methods of analysis and data integration. Currently used methods are mainly conceptual, with statistical integration becoming more routine. The end goal would be to generate mathematical models of biological systems informed and refined by empirical evidence. The computational requirements for creating these models are currently unrealistic for most cases. Those methods are 1) Conceptual based integration 2) Statistical Based integration and 3) Model based integration (Figure 8). Conceptual based integration follows the more traditional path of scientific inquiry whereby datasets are analysed separately and hypotheses are made based on the data produced.

Statistical based integration makes use of different methods to find patterns between data blocks to generate novel hypothesis. A method of statistical based integration that has received quite a bit of attention in recent years is Metabolome Genome Wide Association Studies (mGWAS) which attempts

to identify genetic alterations that cause changes in the metabolism of the biological system of interest (81). In genome wide association studies large numbers of genomes are sequenced in an attempt to find statistically significant gene alterations, often SNPs. These types of studies fall into the conceptual and/or statistical based integration of –omics data. Often previous knowledge of metabolic networks is used to perform network analysis of the genomic and metabolomic data.

More powerful methods of statistical integration are the use of Multivariate models of multi-block datasets. Recent years have seen the development of computational methods allowing researchers to design studies that integrate different -omics techniques. A couple of examples of these methods are the Multi Block PLS algorithm (82) and the more recent consensus OPLS algorithm (83). Examples of the application of these statistical models are still few. As of May 2016 only five articles on PubMed cite the Consensus-OPLS algorithm.

The work presented in this thesis falls under a conceptual integration of -omics data whereby the metabolomic data generated will inform a bioinformatics screen of how metabolic related genes are expressed in a panel of melanoma patients. More advanced methods of -omics data integration fall outside the focus of this thesis, however, they will be discussed as future avenues of research in Chapter 7.

Finally, model based integration would aim to use generated data to build and refine mathematical models of biological systems of study. There is a growing field of research into whole cell modelling (84), bolstered by the rapidly growing field of synthetic biology. While historically these studies are mostly restricted to more simple systems of prokaryotes (85), there have been recent advances into the modelling of eukaryotic systems as well(86).

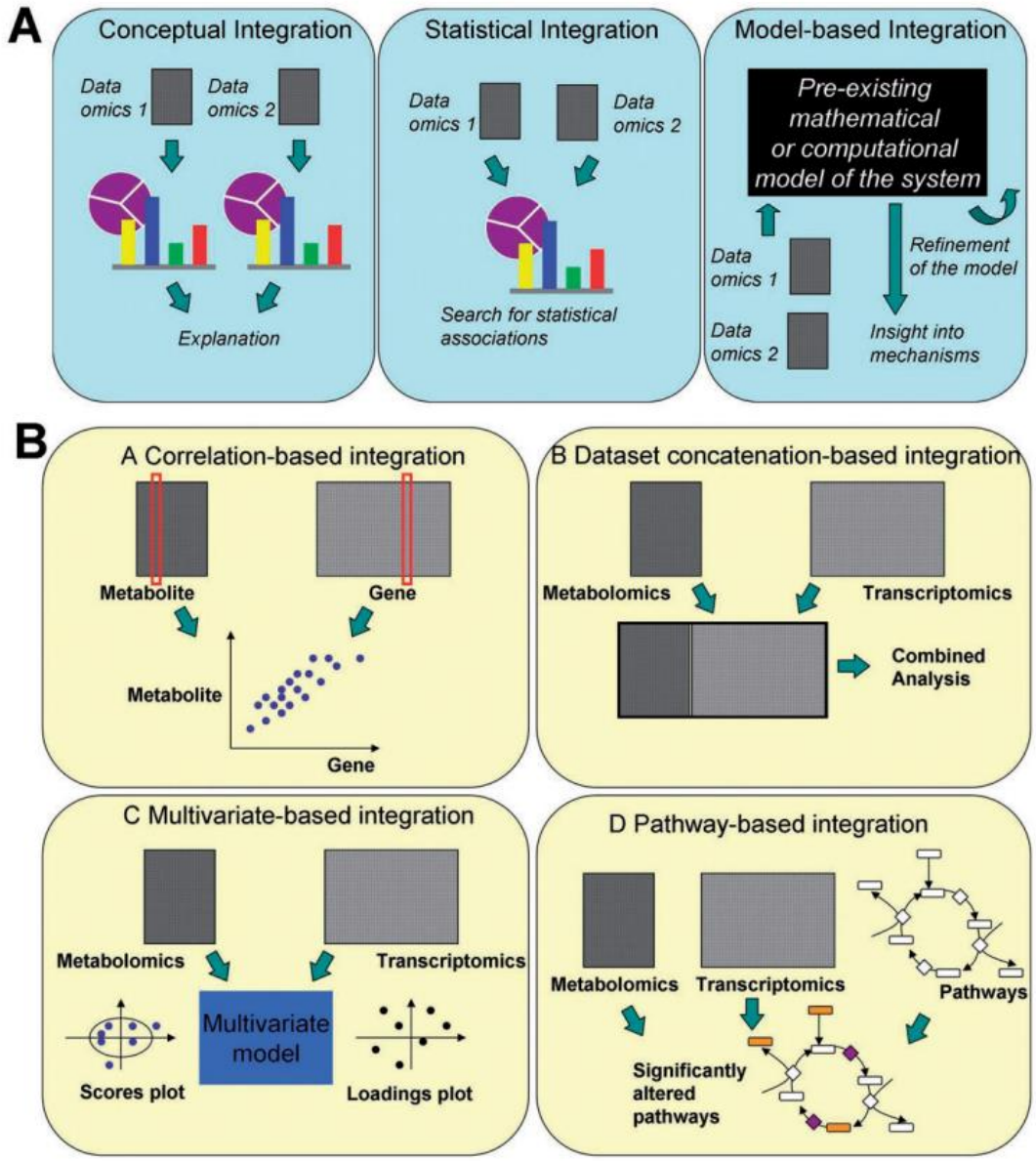

Cavill et al 2015

Figure 2.12. Integration of multiple -omics datasets can give greater information of a biological system than an individual dataset. A theoretical framework for –omics data block integration has been presented as follows: A) Conceptual integration of datasets where explanations of the observed phenomenon are given after analysing each dataset separately. In statistical integration associations between datasets can be found to explain a biological system. The optimal integration of -omics data would be to build mathematical models of systems that can explain biological phenomenon and used empirical data to refine the models. B) Statistical integration of diverse –omics datasets can be performed in four ways: 1) simple correlation based integration 2) Dataset concatenation-based integration 3) Multivariate-based integration 4) Pathway based integration. Figure reproduced with permission from (80).

2.8 Malignant Melanoma

We have spent time discussing cancer and metabolomics in a general sense. In the following sections we will discuss melanoma and melanoma therapy more specifically. There will also be a discussion of Rho and Rho Kinase (ROCK) as a novel therapeutic target of melanoma, particularly in the view of its potential role in regulating melanoma cell metabolism.

Melanomas are non-epithelial tumours arising from melanocytes, melanin-producing cells found predominantly in the epidermis. Melanocytes are derived from the neural crest during development and there is a growing body of work that links the stem cell properties of neural-crest derived melanocytes to the properties of malignant melanoma (87). This has been bolstered by the proposal that the cancer stem cell theory could apply to melanomas (88) although it remains debated as markers for melanoma cancer stem cells are still being discovered (89).

Approximately 90% of melanoma is a skin cutaneous melanoma. Traditionally the classification of primary melanomas has focused on the sites of origin, tumour thickness and histological subtype. Cutaneous melanomas have been classified into four major subtypes: superficial spreading, *lentigo maligna*, *acral lentiginous*, and *nodular*. Whilst these are clinically and histopathologically distinct, the most useful prognostic indicator is the Breslow depth which assesses the depth of tumour cell invasion (90).

50% of human melanomas harbour BRAF mutations, in particular the V600E mutation which drives oncogenesis (7). The *BRAF* gene encodes for the serine/threonine protein kinase BRAF. The RAF family of protein kinases was first linked with cancer in 1983 and its high mutation rate in human melanoma was first discovered in 2002 (91). In normal tissue, BRAF is involved in the RAS/MAPK pathway, which regulates response to growth signals in the cell (92). The V600E mutation leads to a much more catalytically active kinase than the wild type and its oncogenic power has been shown in several genetically engineered mouse models (91). Another 15-20% of melanomas have mutations in *NRAS* (93). Knowledge into these driving mutations of the disease have bolstered the study and design of small molecule inhibitors of oncogenes which have recently found their way into the clinic.

2.8.1 Melanoma Therapy

Although melanoma is the fifth most common cancer in the USA (94), it is much less common in the UK, accounting for only 4% of cancer diagnoses in the UK in 2013 (2). Nevertheless, incidence has increased 360% since 1970; In fact it is the most rapidly rising cancer in terms of incidence and

diagnosis, with over 75,000 cases in 2014 in the US and a steadily increasing average rate of 2.6% over the past 4 decades (94). Malignant melanoma is responsible for over 80% of all skin cancer related deaths (95).

Surgical resection of primary melanoma is an effective way to prevent disease progression. However if the patient is diagnosed with melanoma which has progressed to malignancy, median survival is less than 30% after five years(2). Novel clinical treatments have changed this statistic, but long term survival is only now being collected for patients given new treatments, discussed below.

Historically when treating cancer clinicians have used the 'cut, burn, and poison' strategy alluding to surgery, radiotherapy and chemotherapy respectively (96). While Early stage melanomas are relatively easily resected surgically, malignant and metastasized melanomas become difficult if not impossible to surgically remove. Chemotherapy has a success in late stage malignant melanoma of only 15-20% (97), therefore the need for better therapies has pushed research to develop targeted therapies of melanoma. The treatment of melanoma has been revolutionised in the past ten years with the emergence of immunotherapies and BRAF and MEK inhibitors. For example, Vermurafenib is a monoclonal antibody targeting the V600E BRAF mutant present in 50% of human melanomas. It was approved for use in the clinic by the FDA in 2011 and is currently the gold standard of treatment in the clinic (98).

There are many other treatments currently being tested pre-clinically and in clinical trials. Amongst these, immunotherapies and attenuated viruses are some of the most promising. Seven immunotherapies have been approved for use by the FDA since 2011. Anti-PDL1 and anti-CTL4 antibodies which help the host immune system to overcome the immune evasion of cancer cells have shown dramatic effects in patients (13). As these treatment have made their way into the clinic, chemotherapy is now seen as a second line treatment for malignant melanoma(98).

In 2015 the FDA approved a first in kind viral therapy to treat melanoma, Talimogene Laherparepvec (trademark name Imlygic) (99). The viral vector is a re-engineered Herpes Simplex virus (HSV-1) that is programmed to secrete the immune promoter Granulocyte macrophage colony-stimulating factor (GM-CSF). The mechanism of action of this treatment is still being elucidated, however it is suggested that the virus works in two phases. First, the virus itself can induce lysis in infected cells. Secondly, GM-CSF is a hematopoietic growth factor that is involved in the maturation of dendritic cells and the activation of T cells (100). Phase three clinical trials demonstrated that 16.3% of enrolled patients had

a ‘durable response rate’ (response that lasts more than 6 months) when compared to the 2.1% of patients with durable response when given GM-CSF only (99).

Despite the incredible progress seen in recent years, research into novel treatments is far from complete. Tumours that are initially sensitive to current treatments eventually develop resistance as shown by the median progression-free survival of 6-7 months (101). Long term clinical data for patients that have received newly developed drugs is only now being studied and published.

Patients who respond to vermurafenib show a 15.6 month median overall survival (102) and patients who continued vermurafenib after the initial local treatment showed a 20.6 month median overall survival (103). Puznov *et al* followed the analysis of the 48 patients from the phase 1 clinical trial of vermurafenib and 44 of the 48 patients presented with progressive disease. This highlights how understanding cells resistant to treatment is an important area of research and identifying different signalling pathways driving the disease could lead to improved outcomes in the clinic. It is understood that melanomas treated with vermurafenib eventually reactivate the MAPK pathway as well as upregulate PI3K/AKT signalling to overcome BRAF inhibition (104). Therefore, combination therapies are also being looked at to improve survival rates (101,105-108).

As stated earlier, 90% of cancer related deaths are due to the metastatic spread of cancers (6). All of the currently available targeted treatments are mainly designed to stop tumour cell proliferation or tumorigenesis and do not address the issue of metastasis (109). Part of the issue is that there is an added difficulty in designing clinical trials to assess metastatic spread (110). Looking at the metastatic cascade for possible therapeutic targets of disease represents an attractive strategy as there are multiple pathways that could eventually offer benefits for patients. Such pathways include angiogenesis (111,112), cancer cell dormancy (113), with immune evasion the area that has been addressed with the advent of immunotherapies for treating metastatic melanoma, discussed above. Another area that has received attention is tumour cell migration and invasion.

2.8.2 Cancer Proliferation and Metastasis

The process of cancer cells migrating and colonising a secondary site is known as metastatic cascade (114). This is a multi-stage process made up of (115):

- Invasion
- Intravasation in the circulatory system (Invasion basal membrane into the circulatory system)
- Survival in circulation
- Extravasation (anchoring onto the epithelium of the capillary and exiting circulation)
- Colonisation and proliferation in a secondary site

Each of these steps present cancer cells with different selective pressures, from surviving the shear stress of travelling in the circulatory system (116), to evading the immune response of the body (117), to colonising a secondary site which may have a very different physiological environment to that of the tissue of origin (115).

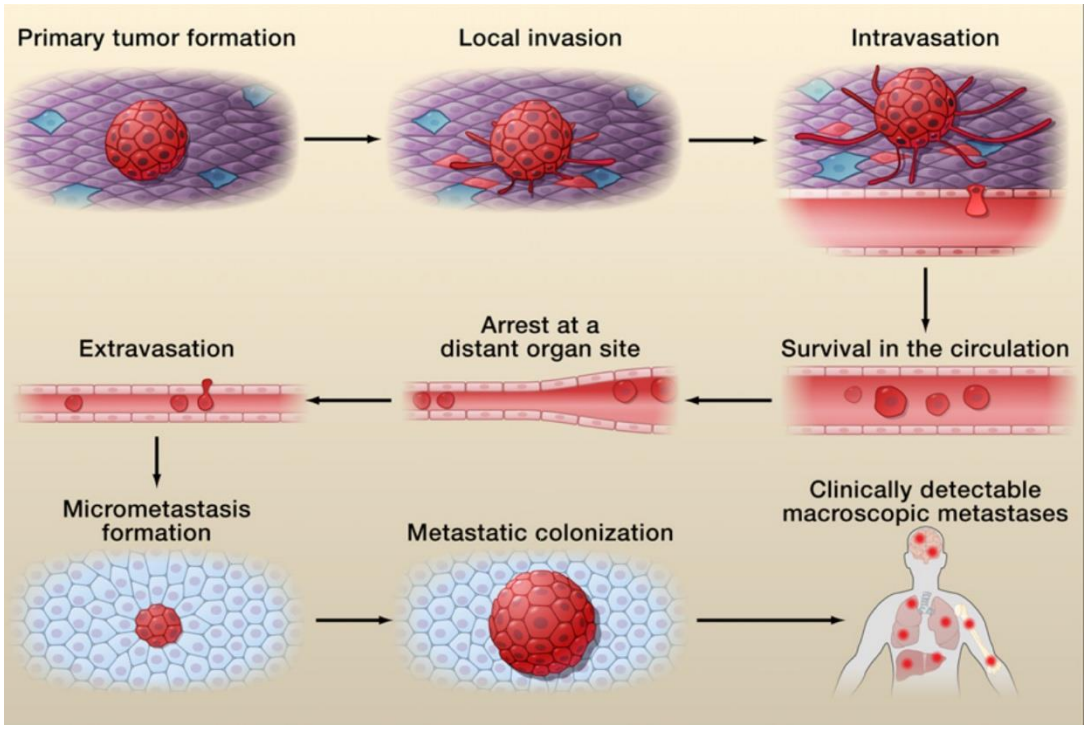

Figure 2.13. The metastatic cascade is comprised of five major steps. 1) Invasion 2) Intravasation 3) Survival in the Circulation 4) Extravasation 5) Metastatic colonisation. Each step presents evolutionary pressures on cancer cells before successful metastatic colonisation can occur. Figure reproduced with permission from (118).

2.8.3 Tumour Cell Plasticity

The ability to migrate is a fundamental aspect of many different stages of the metastatic cascade, from invading into local tissue, extravasation, intravasation and migrating through a secondary site (119). Cancer cells also maintain plasticity in their modes of migration in order to adapt to different environmental challenges (120). One illustration of this plasticity is in how cancer cells can migrate either collectively or as individual cells (121) (Figure 2.14). While it has been observed that cells can migrate collectively through the lymphatic system, only single cells are able to invade through the basement membrane, blood vessels and settle at distant sites (122). Within single cell migration, cells can be classified according to their mode of migration. There is the rounded-amoeboid mode characterised by membrane blebbing and low adhesion. The second mode is the elongated-mesenchymal mode of migration characterised by actin rich protrusions, an elongated morphology and high levels of adhesion (123).

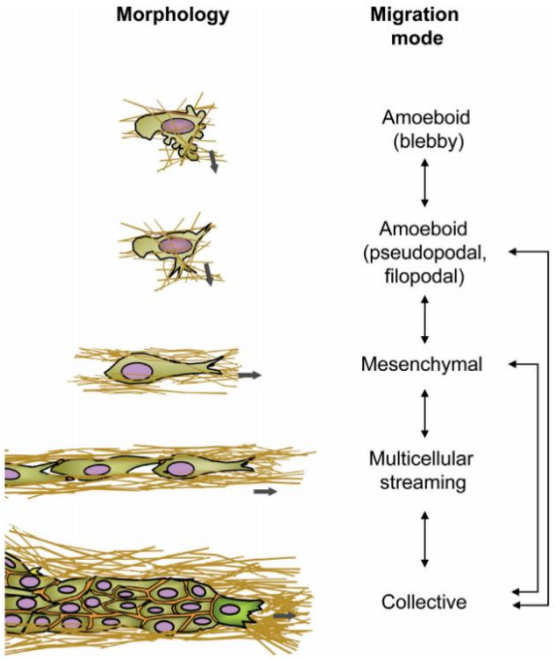

Figure 2.14. Cell Morphology and modes of migration. Cancer cells can invade and migrate either collectively or as individual cells and cellular morphology is connected to the mode of migration. Individual migration can be classified into elongated-mesenchymal type migration or rounded-amoeboid type of migration. Figure reproduced with permission from (120).

These modes of migration are promoted by Rho/Rock signalling (discussed below) and Rac signalling respectively and mutually supress each other (124). When thinking about targeting cell migration for therapies, one must consider that both amoeboid and mesenchymal migration require certain levels of actomyosin contractility, and simply targeting an individual mode of migration may not be sufficient to obtain a clinically relevant outcome. This is being addressed in current studies with the development of novel kinase inhibitors (3).

2.9 Rho GTPase/ROCK signalling

2.9.1 Rho GTPases

The Rho family of GTPases are small (~23KDa) monomeric G proteins that are part of the Ras superfamily of proteins. These proteins are known as ‘molecular switches’ that go from an inactive GDP (Guanosine Diphosphate) bound state to and Active GTP (Guanosine Triphosphate) bound state. They contain lipid modifications which target them to the cellular membrane. The binding of GTP and the successive hydrolysis of GTP to GDP are mediated by associated proteins Rho-Guanine Nucleotide Exchange Factors (Rho-GEFs) and Rho-GTPase Activating Proteins (Rho-GAPs) respectively (125).

In mammals there are 22 members of the Rho GTPase family, which are divided into 8 subclasses (126). The eights subclasses are: Cdc42, RhoUV, Rac, RhoBTB, RhoH, Rho, Rnd, and RhoF. The Rho subclass contains three members, RhoA, RhoB and RhoC.

After their initial discovery in 1985 (127), Rho GTPases were noted for their control of cellular morphology and the actin cytoskeleton. Since then a large body of research has grown to show their effects on cellular growth, proliferation and cell survival, all of which are of interest in cancer (125,128). The three best studied members of the Rho GTPases are Rac1, Cdc42 and RhoA. One of the major downstream targets of active RhoA and RhoC are the Rho Associated Protein Kinases (ROCK).

2.9.2 Rho Associated Kinase (ROCK)

ROCK is a family of serine threonine kinases with a molecular weight of about 160 kDa. The ROCK family of proteins comprises ROCK1 and ROCK2, which have a 62% sequence homology overall and 92% sequence homology in the kinase domain (129) (Figure 2.16). The kinase domain is located near the N-terminus of the protein sequence. Near the carboxyl terminus the Pleckstrin homology domain is located. These two regions are separated by a coiled coil region which contains the Rho binding domain (RBD) where RhoA binds, thus freeing the kinase domain and activating ROCK (130), #0}. When in monomer form, ROCK can be in an inactive form whereby the Pleckstrin domain and the RBD bind to the N-terminal Kinase domain, blocking it from activity. ROCK in solution is primarily a homodimer and dimerization occurs through the C-terminal domains and the coiled-coil region (131), which leaves the C-terminal Kinase domain free for catalytic activity. Other methods of activation in include the binding of Rho proteins to the coiled-coil region which blocks auto-inhibitory folding.

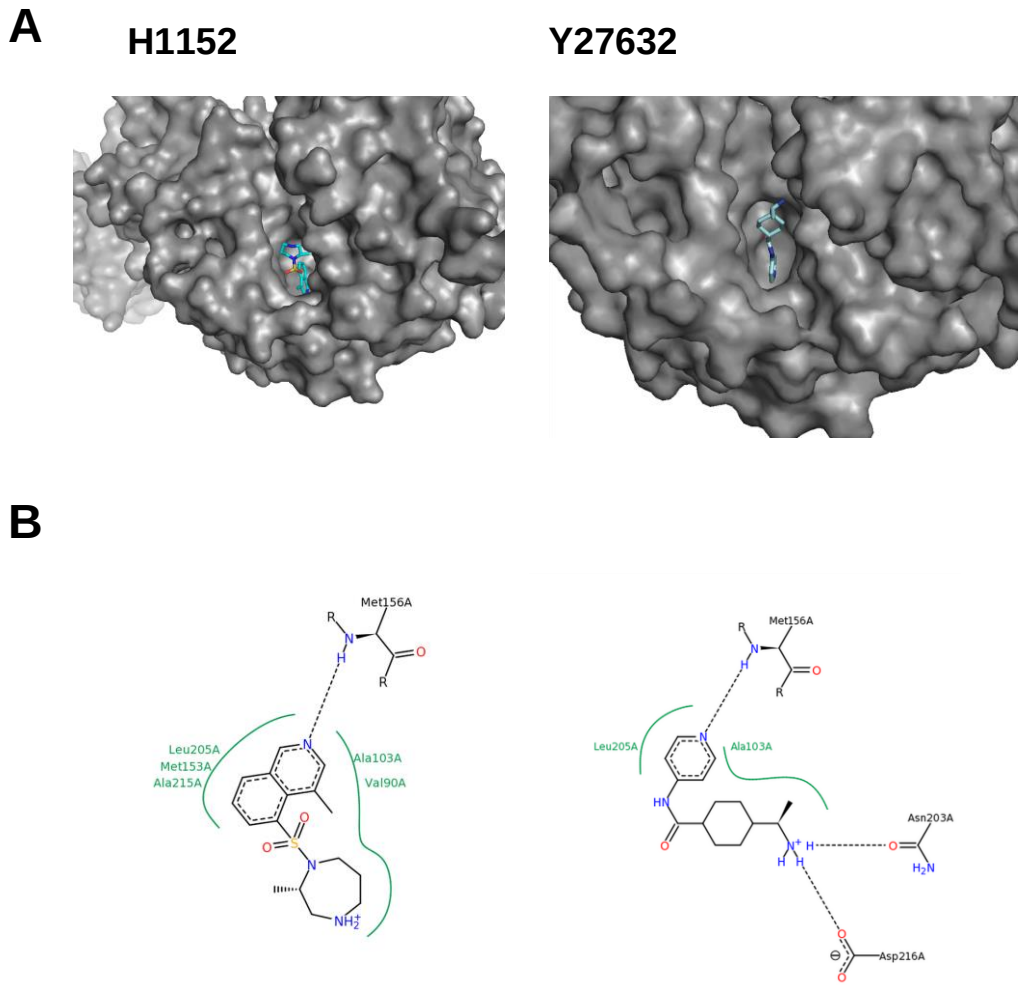

Figure 2.15. ROCK inhibitors are ATP competitors and H1152 forms more interactions with ROCK than Y27632 thanks to additional methyl groups, conferring higher binding affinity. A) Cartoon structures of H1152 (left) and Y27632 (right) bound to the catalytic pocket of ROCK1. B) Schematic illustration of H1152 (left) and Y27632 (right) and the interactions with ROCK1 residues. Figures in (A) generated in Pymol (132) and figures in (B) reproduced with permission from (131).

Most small molecule inhibitors of ROCK are ATP binding competitors (133) and several structures have been described showing the binding of the principle small molecule inhibitors of ROCK to the ATP binding pocket of the kinase domain of ROCK1 (133)(Figure 2.15A). Those inhibitors are H1152-p, Fasudil, and Y27632. In the study by Jacobs *et al* (131) they demonstrate that the higher affinity for ROCK of H1152 compared to other inhibitors such as Fasudil and Y27632 is due in part to the isoquinoline methyl group which limits the low energy conformations available to H1152, thus reducing the entropic cost of immobilising the rotatable bonds in binding to the protein (131) (Figure 2.15B).

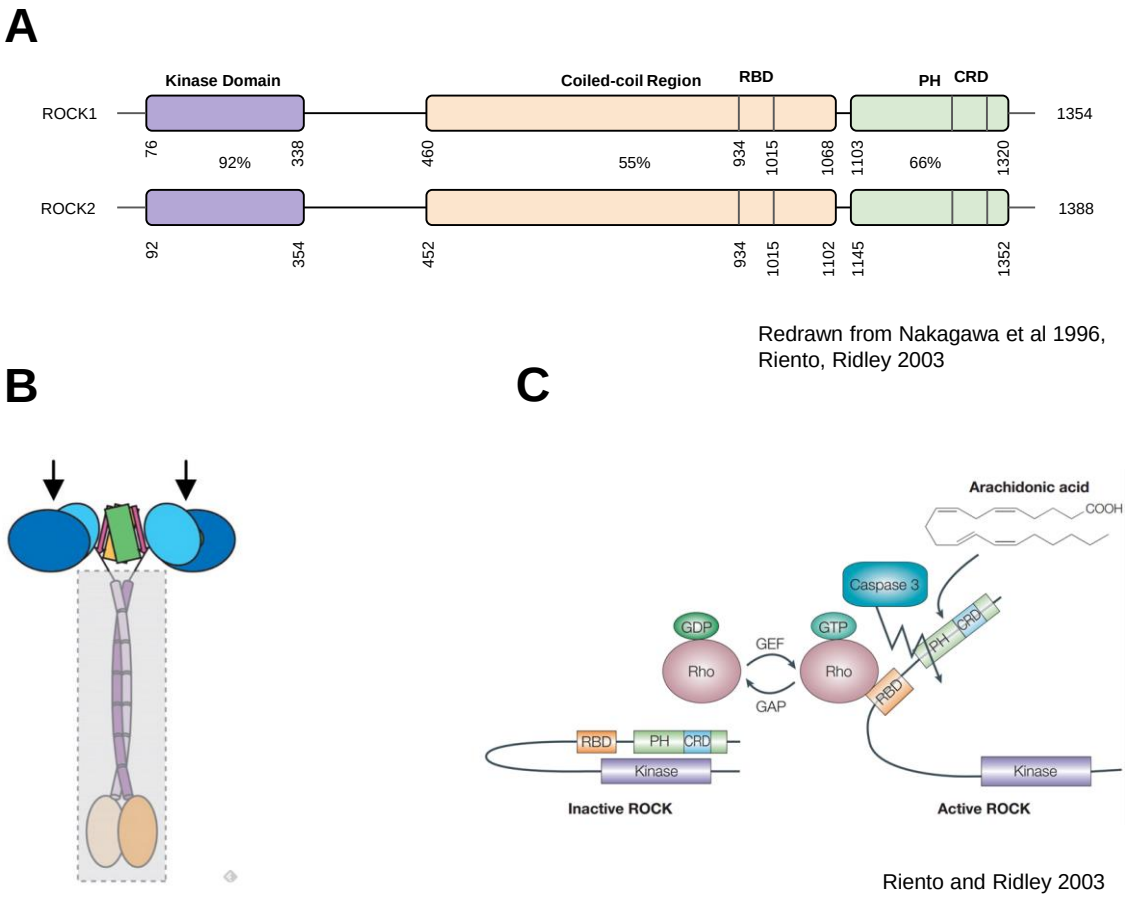

Figure 2.16. The Sequence, structure and activation of ROCK. A) The sequences and domains of ROCK. ROCK1 and ROCK2 are 92% similar in the Kinase Domain. B) ROCK can form homodimers via the coiled-coil region to release the kinase domain (in blue) from the auto-inhibition found in the monomeric form. C)ROCK can also be activated by binding of Rho GTPases to the Rho binding domain (RBS), exposing and thus activating the Kinase domain. Finally, ROCK can be activated by the cleavage of the inhibitory Pleckstrin Homology Domain by caspase 3, thus freeing the kinase domain for catalytic activity. Figures adapted and redrawn with permission from (130,134)

ROCK was first isolated and reported in 1995 (135) and in the following year shown to play a role in generating actin stress fibres in cells (136). Since then ROCK has been shown to play a fundamental role in regulating a wide variety of functions in the cell; from controlling the cells cycle (137,138), and in particular in controlling the cytoskeleton through its regulation of actomyosin contractility (136)(Figure 2.17). The control of the cytoskeleton gives ROCK a fundamental role in regulating modes of cell migration (139). In work by Sanz-Moreno *et al* (140), it has been seen that the rounded morphology of melanoma cells are observed in histopathological sections of both primary tumours and metastasised tumours. Cells found at the invasive front of primary tumours and cells comprising metastases have a more rounded morphology than tumour cells found at the core of primary tumours (Figure 2.18)(139).

The mechanism by which ROCK regulates actomyosin contractility is both by the phosphorylation of Myosin Light Chain 2 (141) which promotes actomyosin contractility and also by the inhibitory phosphorylation of Myosin phosphatase (142) which further increases levels of actomyosin contractility. Levels of phosphorylated Myosin Light Chain 2 can be measured via Western blot or confocal microscopy as a marker to determine ROCK activity (Figure 2.18).

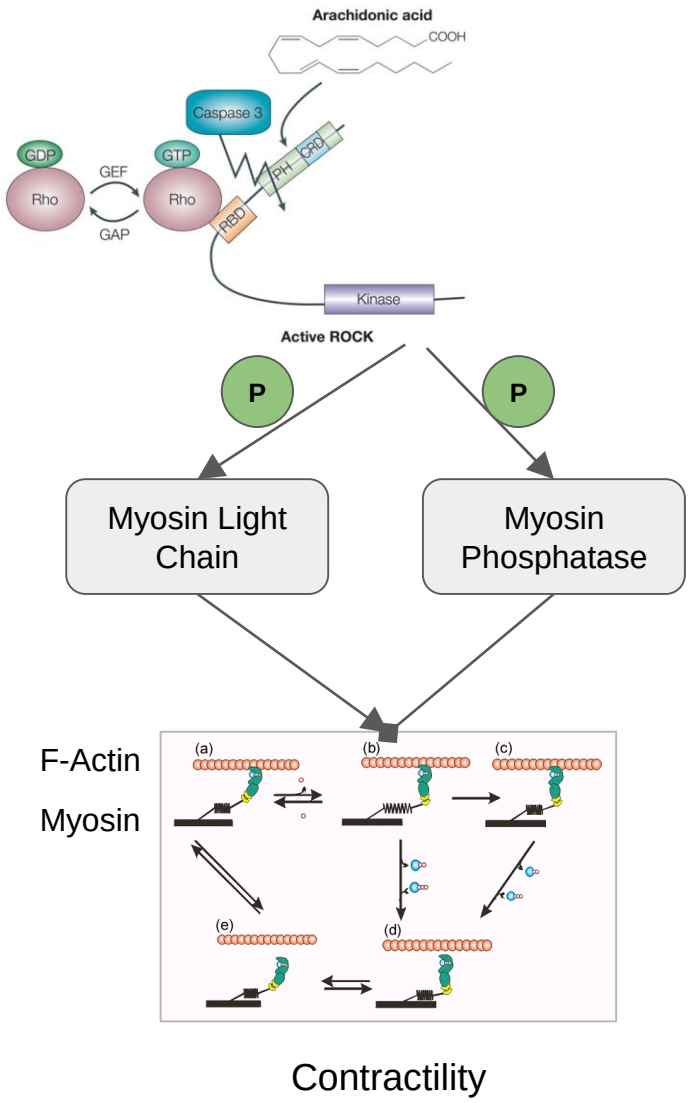

Figure 2.17. ROCK regulation of Cellular Contractility. When activated, ROCK phosphorylates both myosin light chain and myosin phosphatase. In this way ROCK promotes both contractility and inhibits inhibition of contractility. Thus, ROCK increases the amount of phosphorylated myosin light chain, which is then available for binding to F-actin and promoting actomyosin contractility.

2.9.3 Rho/ROCK signalling as a Therapeutic Target of Melanoma

The idea of targeting the Rho signalling pathway has been around for quite some time. The opportunities and challenges were reviewed by Eric Sahai and Chris Marshall in 2002 (125). As of 2015, there are over 2000 research papers focussed on Rho/ROCK function in cancer (143). Despite the

great interest in targeting the Rho signalling pathway, effective small molecule inhibitors of Rho were only first reported in 2012 (144). In this regard targeting the downstream kinase ROCK has been a much more viable option as kinase inhibitors are a much more developed field of research. As of March 2016, 27 kinase inhibitors have been approved for use by the FDA (145). This year, Feng *et al* reviewed 171 ROCK inhibitors (145) demonstrating the abundance of research into ROCK as a therapeutic target not only in cancer but also in ocular diseases such as glaucoma, psoriasis, systemic lupus erythematosus, idiopathic pulmonary fibrosis and graft-vs-host disease (145). ROCK inhibitors have also been suggested to have neuroprotective effects (146) and play a role in cardiac remodelling (147).

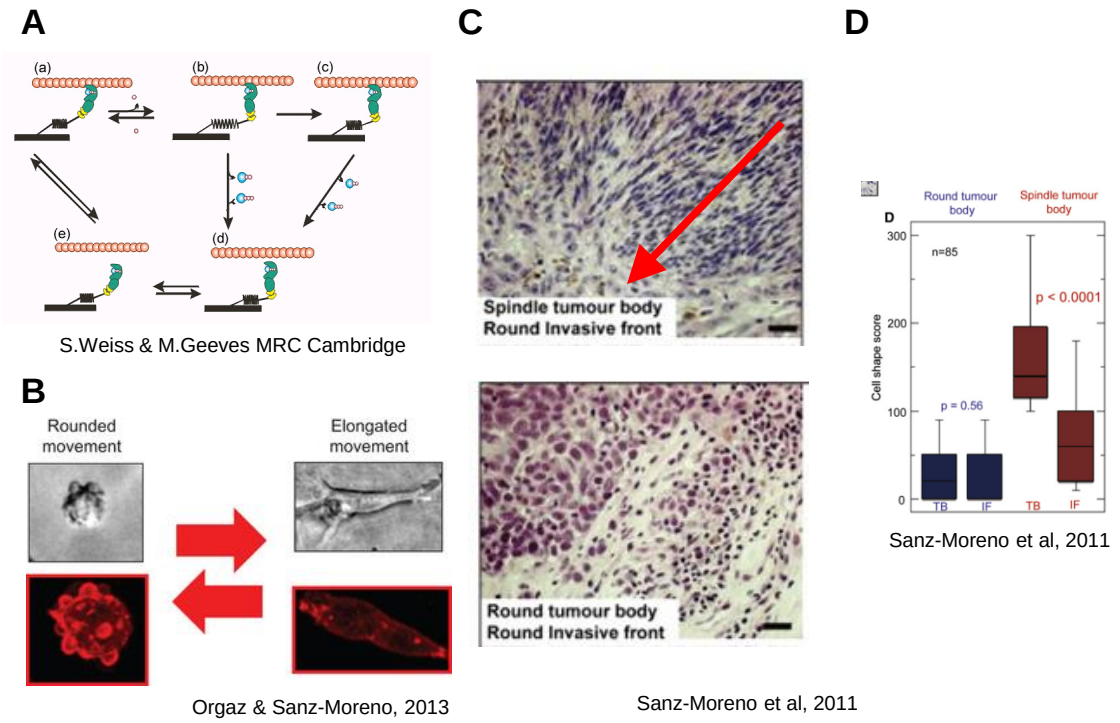

Figure 2.18. ROCK drives actomyosin contractility (A) and this can be observed *in vitro* through morphology in a rounded, amoeboid phenotype (B). C) In human melanomas tumour cells at the core of the primary tumour present mainly with and elongated phenotype, while at the invasive edge and at metastatic sites these cells present with a more rounded phenotype. The red arrow indicates the direction from the core of the primary tumour to the invasive front D) Quantification of data shown in (C). Cells in a spindle tumour body (TB) are more elongated than cells at the invasive front (IF). Images reproduced with permission from (95,140)

Over 600 somatic coding mutations in ROCK have been identified in human cancer genomes, either cell lines or primary tumours (143), and many of these mutations described in ROCK lead to a more active kinase as auto-inhibition is eliminated. RhoA or ROCK is often overexpressed in many tumour types (125,148), although this may not correlate with a more active kinase in itself.

Currently, the ROCK inhibitor Fasudil is approved for clinical treatment of cerebral vasospasm in Japan and China (149). However, it has not been approved for use in Europe or the US and, as its initial patent expires in 2016 (150), the financial incentive to invest into clinical trials for Fasudil is non-existent.

There are other examples of ROCK inhibitors being tested clinically. As the safety profiles of ROCK inhibitors are already established to a certain extent this makes it an attractive target for translation to other diseases such as cancer.

Inhibition of ROCK activity has been shown to slow or inhibit tumour growth in prostate, glioma and human papilloma virus positive tumours (97). Routhier *et al* first showed that inhibition of ROCK activity by systemic delivery of the ROCK inhibitor Y27632 in mice could reduce melanoma tumour volume (97). Chris Marshall's group in London has also shown that inhibition of ROCK can block melanoma cell migration and metastasis both *in vitro* and *in vitro* models of melanoma (3). In addition, they have also shown that ROCK1 and ROCK2 have redundant effects on melanoma growth *in vitro*. Kuemper *et al* demonstrated that the deletion of both *ROCK1* and *ROCK2* genes is required reduced cell proliferation and tumour growth *in vitro* (138). Individual knock-outs of either *ROCK1* or *ROCK2* did not lead to any significant reduction of tumour growth in their study.

In parallel to this, ROCK has been proposed as a potential combinatorial drug target. Smit *et al* from the Pepper lab first proposed ROCK as a potential combinatorial drugs target in melanoma in their 2014 paper (4). They show that a variety of BRAF inhibitor resistant cell lines became sensitised to BRAF inhibitors when used in combination with ROCK inhibitors. They also show that the proliferation of these resistant cells can be reduced just by using the ROCK inhibitors. They followed this study with another paper showing that inhibition of ROCK and MEK can also be effective with NRAS mutant melanomas (151).

Despite all the data supporting the idea of blocking ROCK activity to inhibit cancer progression, there are a couple of considerations that have to be made when thinking of ROCK as a therapeutic target. First, there have been examples of ROCK inhibition having pro-tumorigenic effects in other cancer cell types. As reviewed in Wei *et al* (143) pancreatic (152) and colon cancer cells (153) have been observed to increase in cell proliferation after treatment with the classic ROCK inhibitor Y27632. Further inspection of these studies points to gaps in their studies that deserve consideration. In the study by Nakashima *et al* in pancreatic cancer, Y27632 was used at concentrations of 3 μM. Y27632 is much less specific for ROCK than other inhibitors such as H1152, Fasudil and GSK269962A (Table 2). They

do not observe the effects of Y27632 at higher doses. Further in the study they use Fasudil to study the phosphorylation targets of ROCK in colon cancer, but never demonstrate what effects Fasudil have on cell proliferation in the study, which is a curious omission. In the other study by Nakashima *et al* in colon cancer cell lines, Y27632 is used at doses of 10 μM, which is the standard dose used in several other studies (154,155). Further work would be required to fully validate the claims of these two studies. Nonetheless, these studies point both to potential tissue specific effects of ROCK in regulating cell proliferation and the need for further studies to be conducted prior to using ROCK inhibitors clinically.

Secondly, as ROCK is a strong regulator of actomyosin and contractility in cells, one of the main side-effects of systemic ROCK inhibition would be a dramatic drop in blood pressure in patients. In the pharmaceutical industry this challenge has had two effects: on one hand, this has driven research into novel ROCK inhibitors with differing levels of specificity and potency aimed at addressing this negative effect in patients, on the other hand, it has also made ROCK inhibitors an attractive candidate for treating erectile dysfunction (145).

2.9.4 ROCK Regulation of Metabolism

Much attention has been paid to the role of ROCK in regulating actomyosin contractility, and thus its effects on the cytoskeleton, proliferation, division, cell cycle control, migration and invasion. However, little attention has been paid to its role in regulating cellular metabolism. It has often been assumed that any effect on cellular metabolism may be a secondary indirect effect of ROCK rather than a direct regulation. However, there is some evidence that ROCK could be altering cellular metabolism, either directly or through its regulation of the cytoskeleton. It has been observed in adipocytes and myoblasts that ROCK regulates the transport of the glucose transporter GLUT4 to the membrane through actin cytoskeleton regulation (156). ROCK has also been studied in its role of regulating both insulin signalling as well as leptin signalling in the brain through its interactions with the insulin receptor and JAK/STAT signalling pathway respectively (157).

There are currently only two published articles investigating the role Rho/ROCK signalling may have on cancer cell metabolism. The first, published by Zhang *et al* in 2010 (158), demonstrated how Rho dependent transformation of breast and lung cancer cells could be inhibited by blocking the mitochondrial glutaminase enzyme using their novel glutaminase inhibitor 968. They have recently followed up with a mechanistic explanation of the function of the 968 glutaminase inhibitor, which binds

to the monomeric form of mitochondrial glutaminase GAC, inhibiting the active glutaminase tetramer (159).

The second paper. by Zhang *et al* (155). is a much more comprehensive paper that demonstrates how, in a variety of lung and breast cancer cell lines, and within a gain of function mutant p53 background, Rho/ROCK signalling drives the Warburg effect by promoting the trafficking of the glucose transporter GLUT1 to the plasma membrane. In this study they interfered with ROCK activity with shRhoA stable knockdowns, siRNA transient knockdowns of ROCK1/2 and with 10 μM treatments of the ROCK inhibitor Y27632. They hypothesise that this trafficking is done via ROCK's promotion of actin filament formation, which allows GLUT1 to be trafficked to the plasma membrane. They also show that wild-type p53 represses the Warburg effect. Importantly it has been shown that loss of p53 promotes the Rho/ROCK dependent rounded-amoeboid type migration in A375P melanoma cells (160) and all of the work presented in this thesis has been performed in a p53 wildtype background. Secondly, they demonstrate these effects cell lines of epithelial origin, whereas melanomas are non-epithelial tumours. ROCK activity in metastatic melanoma has been shown to regulate a variety of cellular processes and to play a fundamental role in promoting melanoma proliferation and metastasis. The first part of this thesis aims to investigate how ROCK activity is affecting cellular metabolism.

2.10 Conclusion

This chapter set out to establish the background upon which this work is built. We have established that while clinically available treatments for melanoma have increased substantially in the last decade, there is still a great need to understand how melanomas metastasise in order to develop therapies for patients that either are non-responsive to currently available treatments or develop resistance to treatment. One approach to gain a deeper understanding of cancer metastasis is to study how cancer cells re-wire their metabolism. Metabolomic methods are now an established part of biomedical research and have come of age since the definition of the term metabolomics almost two decades ago (161). In particular, NMR metabolomics permits researchers to gain a broad biochemical understanding of the system of interest in a highly reproducible manner. The technical developments of mass spectrometry and NMR spectroscopy have resulted in a massive increase of data available to researchers, which has been accompanied by the development and application of multivariate statistics, pattern recognition and machine learning algorithms to make sense of the data. There is now a push to find methods to optimally integrate diverse -omics datasets through various statistical and mathematical modelling methods.

ROCK is a family of serine/threonine kinases that play an important role in regulating the actin cytoskeleton and thus cell growth, proliferation and migration, which comes with high energy demands. Recent pre-clinical data has suggested it may be a promising therapeutic target for metastatic melanoma and a phase one clinical trial targeting ROCK in metastatic melanoma is currently recruiting patients (clinical trial number: NCT01585701). While it is a thoroughly studied kinase, there is currently a gap in knowledge as to how it may regulate cancer cell metabolism. The work presented in this research project aims to address this gap in knowledge and conduct a 1D ^{1}HHR-MAS NMR study of metastatic melanoma cells *in vitro* after interfering with either ROCK activity or expression in both human and murine melanoma.

Chapter 3 : Materials and Methods

3.1 Cell Culture and Molecular Biology

3.1.1 Cell Culture

A375M2 were cultured in Dulbecco's Modified Media (DMEM from Sigma –Aldrich) supplemented with 10% Foetal Bovine Serum (FBS) and 1% penicillin/streptomycin (P/S). B16F10 cells were cultured in RPMI-1640 (Life Technologies) with the same supplements. Cells were incubated at 37ºC and at 10% CO_2. Cell culture media was replaced every other day and passaged when the cells reached 80% confluency. Frozen cells were stored by suspending 10^6 cells in a solution comprising 90% cell culture media and 10% DMSO. Cells were the transferred into cryo-vials and kept at -80 ºC for 24 hours. Cells were then transferred to liquid nitrogen storage. To thaw cells, cryo-vials were put at 37ºC and then 9 ml of cell culture media was added. The suspension was centrifuged at 1200 rpm for 5 min at room temperature. The supernatant was discarded and the pellet was re-suspended in 3 ml of media and then transferred into a T25 cell culture flask.

3.1.1.1 Cell Passage

Cells were passaged using the warm trypsinization technique. The medium was aspirated followed by two phosphate buffered saline (PBS) (without Ca^{2+} and Mg^{2+}) washes to remove any residual medium. Trypsin was added to the flasks (2 ml to the T75 flask and 5 ml to the T175 flask) containing the cells and incubated at 37ºC for 5 minutes. Following incubation flasks were gently shaken and cells were observed under the microscope to ensure cell detachment. Trypsinization was stopped by addition of media (3 times the volume of trypsin). The cells were transferred to a falcon tube and pelleted down by centrifugation at 1200 rpm for 4 minutes. The supernatant was aspirated and the pellet was then re-suspended in appropriate volume of fresh medium. 10 µl of the suspension was transferred to CASY counter and the number of cells/ml of the original suspension was determined. Cells were split 1/5 or 1/10 depending on speed of cell proliferation. The final volume was filled up to 8 ml for the 10 cm plates and to 2 ml for the 6-well plates by using fresh medium. All melanoma cells were passaged a maximum of six times to ensure homogeneity between experiments.

3.1.1.2 ROCK Knockout Mouse Melanoma sample preparation

Mouse melanoma samples were kindly provided by Dr. Sandra Kuemper (Marshall lab, ICR, London). The mouse melanoma model uses BrafV600E as an oncogene induced by Cre expression in melanocytes (using Tyr-Cre-ERT2). Mice were treated with tamoxifen which activates Cre in the cells where tyrosinase expressed as Cre is expressed under the tyrosinase promoter and held inactive.

Melanocytes become oncogenic and become melanomas after about 1-2 years (on a PTEN wildtype background). Cells from these primary tumours were cultured until melanoma cells grow out and fibroblasts in culture become senescent. Cells were then harvested for NMR experiments (described below) at passage number 4.

3.1.2 siRNA Knock Downs with LAH4-L1 or LADap(Me)6-L1 Peptides

Cells were seeded onto six-well plates at a concentration of 2×10^5 cells per well. 24 hours after seeding cells were transfected with siRNAs targeting the gene of interest. siRNAs were re-suspended to a final concentration of 20 μM according to manufacturer protocol. The ON-TARGETplus siControl non-Targeting siRNA (Dharmacon, GE) was used as mock control. LAH4-L1 peptide was purchased from Pepceuticals Ltd (Nottingham, UK), LADap(Me)6-L1 was synthesised in house (162).

Metabolomic experiments with siRNA knockdowns were performed with LAH4-L1 peptide transfections while siRNA screens were performed with LADap(ME)6-L1 peptide.

Peptide transfection was performed according to protocol (163). For transfections final siRNA concentrations in wells was 50nM. The amount of peptide used was a 1:10 siRNA/peptide weight ratio. For transfections in a 6 well plate, siRNA and peptide were diluted in separate 1.5 ml Eppendorf tube with 50 μl Opti-Mem media and left to resuspend for 5 min. They were then mixed and allowed to complex at room temperature for 30 min. The complex was then diluted with additional Opti-Mem to a final volume of 500ul per well. The cells were washed with PBS (without Ca^{2+} and Mg^{2+}) and the siRNA/peptide mixture was put into the wells. The cells were incubated with the siRNA/peptide complex at 37˚C for 4 hours. Opti-Mem was then aspirated from the wells and replaced with fresh cell culture media supplemented with 1% FBS.

For imaging and Western blotting 48 hours after transfection, cells were seeded onto collagen and after 24 hours the media was changed to 1% FBS in DMEM. After another 48 hours cells were lysed or fixed for Western blotting and microscopy respectively. For NMR experiments cells were treated in an

identical fashion but were seeded onto 10 cm plates at a concentration of 2 × 10^6 cells/plate. Transfection reagent volumes were multiplied 6 fold compared to transfection in a 6 well plate.

3.1.3 Western Blotting

3.1.3.1 Protein extraction for Western blotting

Molecular biology experiments: 200 µl of 1x Laemmli lysis buffer (with inhibitors: 1 µM DTT, 1 mM NaF, 100 µM β-Glycerol phosphate, 5 µM PMSF and Protease inhibitor cocktail tablet from Roche) were added to the cells into the 12-well plates, followed by occasional gentle shaking for 5 min. Lysates were then collected, and used for the Western blot analysis.

Metabolomics experiments: After scraping cells and transferring them into a 15ml tube, 1ml of suspension was transferred to a separate 1.5ml Eppendorf tube. The suspension was spun down at 1400 rpm for 4 min at room temperature. The supernatant was discarded and the resulting pellet was snap frozen in liquid nitrogen for 3 min and stored at -80˚C until protein extraction. 150 µl Laemmli lysis buffer was then added to the sample and the resulting lysates were treated as below.

The cell lysates obtained from the experiments performed on plastic and on collagen were thawed, boiled at 100°C for 5 min, sonicated for 15 seconds on ice (50% sonicator efficiency), centrifuged at 13,000 rpm for 30 min at 4°C, supernatants were collected and prepared with 4X LDS loading buffer (Invitrogen). The samples were resolved using with 8-10% acrylamide gels or premade Nu-PAGE™ 4-12% Bis-Tris gels (1.5 mm, Invitrogen) at 100V in MES running buffer (Invitrogen) for up to 2 hours at room temperature. The gels were then electrophoretically transferred onto a PVDF membrane (0.45 µm, Immobilion™) for 2 hours at 100V. Transfer tanks were surrounded by ice. Membranes were blocked with 5% BSA (PAA) in tris buffered saline containing 0.1% (v/v) Tween-20 (TBST) for 1 hours at room temperature. Membranes were then cut and incubated with primary antibodies diluted in 5% BSA-TBST overnight at 4°C. The next day membranes were washed for 3x 10 minutes in TBST, incubated with HRP (horseradish peroxidase) conjugated secondary antibody for 1 hour and then washed again with TBST for 3x 10 min. They were developed by using ECL or ECL Prime western blotting detection reagents (Amersham) and exposed to X-ray film in a dark room. Images were analysed with ImageJ. Briefly, a box was drawn around the bands of interest using the “rectangular selection” tools, the intensity profile of the bands was drawn (“Analyse” → “Gels” → “Plot lanes”) and

the intensity of each peak (corresponding to a band) was measured using the “Wand” tool. Data was collected and figures were made by using Excel, R, or OriginPro.

3.1.4 Experiments on collagen

3.1.4.1 Collagen 1 preparation

Bovine skin collagen type I (PureCol, Nutacon BV, 5005-B, pepsinised, telopeptide free) was prepared to a final concentration of 1.8 mg/ml in 5x-DMEM (phenol red and serum free, from ICR) as per the following recipe (for 1 ml): 55.56% collagen, 20% 5 x DMEM, 21.35% H_2O (MilliQ, sterile and filtered) and 3% 0.1M NaOH. Following degassing in a vacuum, 700 µl/well was placed in 12-well plates, 300 µl/well in 24-well plates and 100 µl/well in a 96 well plate. Collagen was polymerised for 4 h at 37°C, 10% CO_2. Cells were seeded on top of the matrix in media (DMEM with 10% FBS and 1% Penn/S) at concentration of 8,000 cells/well in 96 well plates, 10,000 cell/well for 24-wells plate and 100,000 cell/well for 12 well plates.

3.1.4.2 Light microscope morphology assessment

The 24-well plates were subjected to a wash with 1 ml of PBS (with Ca^{2+} and Mg^{2+}) to each well, addition of 600 µl of 4 % formaldehyde. After 15 min, 1 ml of PBS (with Ca^{2+} and Mg^{2+}) was added to each well, aspirated and added for the second time. Next, three pictures for each well were taken by QC Capture and the quantification of % elongation was conducted by using ImageJ.

3.1.4.3 RNA extraction for qPCR

RNA extraction was done by adding 900 µl Trizol (Invitrogen) per well for 5 minutes at room temperature. Lysates were then transferred to an Eppendorf tube and mixed with 200 µl chloroform for 10 min at room temperature. Samples were then centrifuged at 12,000 rpm at 4 ºC for 15 min to separate RNA from the protein containing phase. The RNA containing phase presents as the aqueous phase in the upper part of the Eppendorf tube. The RNA containing phase was carefully transferred to a new tube to not disturb the opaque protein containing phase. 400 µl isopropanol was then added and the sample was spun at 12,000 rpm at 4 ºC for 10 min. The supernatant was then discarded and 400 µl 75% ethanol in RNAse free water was added to the tube and spun at 12,000 rpm at 4 ºC for 10 min. the supernatant was discarded and the remaining pellet was dried for 10-30 min at room temperature followed by resuspension in 30 µl RNAse free water. The sample was then further purified from DNA by using the DNAse removal kit according to manufacturer’s instructions.

3.1.5 Quantitative Real Time Polymerase Chain Reaction (qRT-PCR)

For qPCR experiments cells were seeded either onto bovine collagen 1 or plastic at concentration of 40,000 cells/well in a 6 well plate. 24 hours after seeding cells were treated either with mock DMSO or ROCK inhibitor (5 µM H1152) for 24 or 48 hours.

Quantitech Primer assay qPCR mRNA primers (Qiagen) were purchased for the respective genes. Primer sequences are proprietary information and so are not listed here. Primers were used at approximately 10 µM qPCR was performed using one-step Brilliant II SYBR Green qPCR kit (Agilent Technologies) and Stratagene MX 3005x qPCR system with MxPro software. RNA concentration was adjusted to 100 ng RNA/well for all samples: in addition, GAPDH was used as a loading control. Samples were loaded in qPCR plates and sealed with qPCR strips. Each sample was run in duplicate or triplicate. qPCR data was considered reliable if GAPDH measurements were between 15-20 cycles. Individual gene measurements were expected to fall between 15-30 cycles and measurements greater than 30 cycles were considered unreliable. Data was exported from the MxPro application as a text file containing the number of cycles for each well. Data from all the replicates was then analysed using the delta/delta method and normalised to GAPDH using Microsoft Excel.

3.1.6 Light microscopy Morphology assessment

Fibrillar bovine dermal collagen was prepared at 1.7 mg/ml according to the manufacturer's protocol at 100 ml/well in T96 plates and 300ml/well in T24 plates. Cells were seeded on top at 7×10^3 cells/well in T96 plates and at 30×10^3 cells/well in T24 plates in 10% FBS medium. Cells were allowed to adhere for 24h and the medium was changed to 1% serum. Cells were subsequently imaged 24h. Cells were imaged with QImaging O1Q1 Click FM12 camera and Q-imaging software. The calculation of the number of elongated cells was carried out with ImageJ. For this calculation, cells were classified into two categories, ‘rounded’ or ‘elongated’ according to their morphology.

3.1.7 Immunohistochemistry

3.1.7.1 Sample preparation

A375M2 human melanoma cells were seeded onto a thick layer of collagen in 96 well plates at 10,000 cells/well. B16F10 mouse melanoma cells were plated onto a glass coverslip for microscopy.

At the conclusion of the experiment, cells were washed 3 times with PBS (with Ca^{2+} and Mg^{2+}), fixed in 5% PFA for 10 min at room temperature, and permeabilised in 0.3% Triton in 4% BSA/PBS for 20

min at room temperature. Non-specific binding was blocked in 4% BSA/PBS for 1 hour at room temperature. Cells were then incubated overnight at 4℃ with primary antibody (see table below) diluted in 4% BSA/PBS. The next day cells were washed three times in PBS (with Ca^{2+} and Mg^{2+}) and subsequently incubated at room temperature for 2h in secondary antibody (concentration 1:300) in 4% BSA/PBS. Cells were then washed and stained with Phalloidin 546 (Invitrogen) (1:200) and Hoechst 0.5% for 5 min at room temperature. Finally, cells were washed with PBS and stored in PBS at 4˚C until imaging. For cells seeded onto a glass coverslip, DAKO was used to mount the coverslips onto glass slides for imaging.

For imaging with collagen 1, the collagen was removed with tweezers and placed upside down on a glass bottom culture dish to ensure the cells at the top of the collagen layer were in close proximity to the microscope. Imaging was done with a LSM5 10META Zeiss confocal microscope and Zen software. Images were analysed with Zen software. Indirect quantification of immunofluorescence intensity was carried out with ImageJ. A perimeter was drawn around individual cells and the 'measure' (ctrl+m) function was used. The Raw integrated density was normalised by dividing by the area of the selected region.

3.1.7.2 Image Capture and Morphology Analysis

Cells were washed once with PBS followed by fixing in 4% paraformaldehyde (PFA) for 15 min. Cells were imaged at 40x magnification and images were counted and analysed with ImageJ. Cell rounding was assessed by manually tracing the perimeter of each cell and then calculating the ratio of the largest and smallest diameter. Therefore, a perfect circle would have a roundness index of 1.0 while a straight line would have a roundness index of 0.0. Data was collected analysed and visualised with Microsoft Excel (Microsoft), SPSS 20 (IBM), Graphpad Prism (Graphpad Software Inc.) and R with 'ggplot2' visualisation library.

3.1.8 Statistics

For pairwise comparisons, students t-test was performed. Multivariate analysis was performed with 1-way ANOVA. Statistics were calculated used Excel (Microsoft), SPSS, and R.

3.2 Metabolomics

3.2.1 NMR samples preparation

At the end of the experimental procedure cells were washed with 5 ml cold fresh 1x PBS (with Ca^{2+} and Mg^{2+}). The wash was followed by addition of 6 ml of the same cold fresh 1x PBS (with $Mg^{2+}Ca^{2+}$). For metabolomics experiments trypsin-EDTA was not used to avoid potential leakage of metabolites (164). The cells were then mechanically scraped from the plates, transferred to a 15 ml Falcon tube and pelleted at 1400 rpm for 4 min at room temperature. The supernatant was discarded and cells were re-suspended in 500 µl PBS (with $Mg^{2+}Ca^{2+}$) and transferred to 1.5 ml Eppendorf tubes and spun down at 0.2 g for 5 min at 4ºC. The supernatant was aspirated and the pellets were snap frozen by immersion in liquid nitrogen for 3 minutes. The samples were then lyophilized overnight and kept at -80°C until further use.

The reliability of sample preparation for NMR metabolomics studies have previously been studied. In the Mason group, previous work has shown that the current method results in good quality spectra(65). Cells were mechanically scraped from the plate as trypsinisation has shown to lead to metabolite leakage that is an unacceptable loss for metabolomics studies (164). Additionally, it was chosen to snap-freeze cells in order to rupture 100% of the cell membranes. Other methods that do not rupture all cell membranes can lead to varying lipid profiles due to sample handling or spinning by MAS. This snap-freezing step in liquid nitrogen also serves to quench metabolism and preserve the metabolic state. A drawback is the matter that the cells are effectively washed in PBS three times prior to the snap-freezing step, which may be a source of metabolite leakage.

For liquid state NMR, 1.5 ml of spent media was collected and transferred to an Eppendorf tube. Samples were centrifuged at 1400 rpm for 5 min to precipitate any debris and the spent media was transferred to a new Eppendorf tube. Samples were then lyophilised at -58 ºC overnight, and stored at -80°C. Prior to NMR acquisition, samples were re-suspended in 600 µl D_2O.

3.2.1.1 NMR spectra acquisition

The lyophilized cell pellets were re-suspended in Kel-F inserts (Bruker, Rheinstetten, Germany with 30 µl D_2O (Sigma-Aldrich, St Louis, MO, USA) at room temperature 2 hours before the acquisition to provide a lock signal. This step was performed as shorter rehydration times lead to larger spectral linewidths. A potential downside to this rehydration step is the possibility of metabolite degradation during rehydration and during spinning, especially 2D NMR experiments which last several hours.

Figure 3.1 demonstrates an example of a ^{1}H 1D NMR spectra acquired from A375 M2 human melanoma cells at the beginning and end of spinning for 2 hours at 298˚K. The metabolic profile is fairly stable, with decreases in the signal from lipid components, such as the CH2-CH2 resonance of lipids and phosphocholine, possibly due to degradation over time. There is also and a shift in the formic acid peak, which could be attributable to a change in pH over time. This highlights the need to handle the samples with very similar time frames to reduce the chance for the inclusion of variability in obtained data.

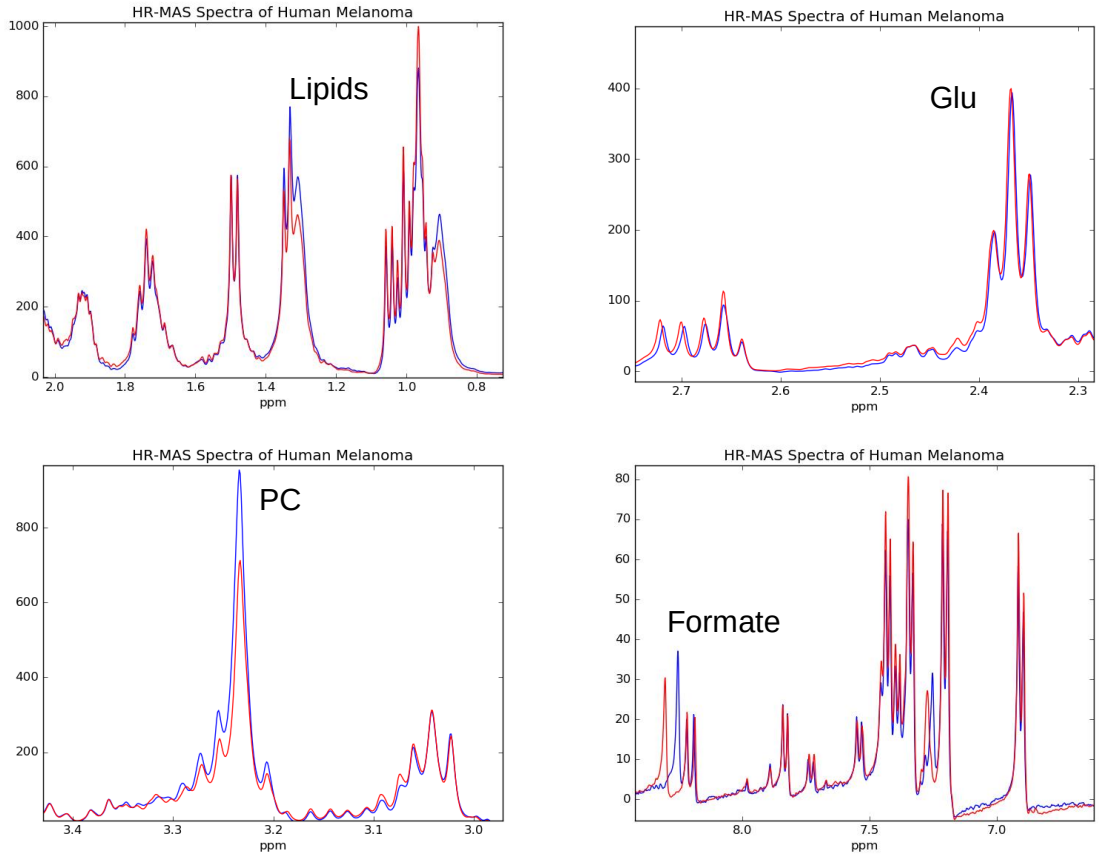

Figure 3.1. The lipid profiles of human melanoma cells change over time with MAS. Representative 1D spectra of A375 M2 human melanoma cells at the beginning (blue) and end (red) of 2 hours spinning at 298˚K 5 kHz. Spectral regions shown highlight the lipid region (top left), glutamate (top right), choline bodes (bottom left) and aromatic regions (bottom right).

Subsequently, the samples were placed in 4 mm Zirconia Magic Angle Spinning (MAS) rotor and preserved with Kel-F cap. For HR-MAS NMR, an Advance ^{1}H 400 MHz spectrometer equipped with a 4 mm ^{1}H/^{13}C HR-MAS probe (Bruker UK Limited, Coventry, UK) was used. 1D spectra were recorded using a standard a Carr-Purcell-Meiboom-Gill (CPMG) spin echo pulse of 190 µs with water pre-saturation during recycle delay of 1 second. The spectral width was 16.02 ppm and ^{1}H 90 pulse length was 7.81 µs. Two dummy scans were performed before recording acquisition data. Total acquisition time was 2.5 seconds and a pre-scan delay of 6.5 µsec. Tau delay (d20) was 200 µsec. There was an

additional 1 sec delay between scans. The number of complex points recorded was 32048 data points. Other experimental parameters were 4096 receiver gain, with a total recording time of 7 min 55 s and total of 128 scans were acquired. To achieve sufficient statistical power 9 samples were collected and recorded for each tested condition. The 9 samples were comprised of three experimental replicates and each experimental replicate was composed of three technical replicates. All the spectra were recorded at 310°K and the magic angle spinning frequency was 5000 Hz. 2D ^{1}H-^{1}H correlation spectroscopy (COSY), J-resolved and ^{1}H-^{13}C-Heteronuclear Single Quantum Correlation (HSQC) experiments were performed on a representative sample for each tested condition, using standard Bruker settings.

For liquid state NMR, ^{1}H NMR spectra were acquired under automation at 298 K and 700 MHz on a Bruker Advance II 700 NMR spectrometer (Bruker Biospin, Coventry, UK) equipped with a 5 mm QCI helium-cooled cryoprobe and a cooled SampleJet sample changer. The temperature was allowed to stabilise for 3 min after insertion into the magnet. Tuning, matching and shimming was performed for each sample and the ^{1}H pulse length was calibrated on each sample and was typically around 12 µs. 1D CPMG-presat (cpmgpr1d) experiments were acquired with 128 transients, a spectral width of 20.5 ppm, 64 K data points, a mixing time of 10 ms, a relaxation delay of 4 s and a total echo delay of 78.7 ms. 1D NOESY-presat (noesygppr1d) were also acquired, but with 32 transients. Free induction decays were multiplied with an exponential function (line broadening of 0.3 Hz), Fourier transformed and calibrated to a 2,2,3,3,-D4-3-(trimethylsilyl) propionic acid (TSP) reference signal at 0.0 ppm.

The spectra were Fourier transformed, manually phased and automatically baseline corrected using standard Bruker commands to remove NMR artefacts and then calibrated with 2,2,3,3-D4-3(Trimethylsilyl) propionic acid sodium salt (TMSP-2,2,3,3-D4) with reference signal at 0 ppm by using Bruker Topspin 3.0 Software. Occasionally manual baseline correction was performed in Topspin 3.0 by defining baseline points and correcting the baseline using cubic spline.

3.2.2 Data Analysis

3.2.3 Data pre-processing and Software

Spectral pre-processing, and the cross-validation and multivariate analysis were conducted using a combination of software developed in our laboratory for a previous study by Dr Louic Vermeer and the MVAPACK, an open source Octave library for NMR metabolomic data processing and analysis.

The in-house script uses Python 2.7, a programming language which allows efficient integration of systems (Python™ 2013) with the mathematical Numpy and SciPy extension, and Matplotlib to visualise

PCA and OPLS plots (65). The pre-processing methods were used to modify NMR spectra and reduce the variances and influences which are not of interest and might interfere during the data analysis. Therefore, the spectral regions below 0.58 ppm, between 4.70-4.53 ppm and above 8.63 ppm were excluded as these regions contained respectively the TSP reference peak, residual water peak or noise, which are not useful regions.

Data was then exported from the in house software into the MVAPACK software as a .csv file.

Spectral alignment and binning was done in the octave environment using the Icoshift alignment algorithm and the optimized binning algorithm respectively. Data was then transferred again into the Python environment.

Data was normalized using probabilistic quotient normalization (PQN), based on the assumption that changes in concentrations of single analytes only influence sections of spectra, while overall concentrations dominate the influences on the complete spectrum (165). PQN normalisation is calculated in the following manger: first an initial integral normalisation of each spectrum is conducted. Then a reference spectrum is calculated (such as an average spectra). Then a for each variable the quotient between the test spectrum and reference spectrum is calculated. Once all the quotients are calculated the median quotient is estimated. Finally, each data point is divided by the median quotient(166).

Pareto-scaling of the spectra was adopted to assign equal significance to both small and large peaks, leading to the amplification of low intensity signals. In pareto-scaling, individual data points are mean cantered and then divided by the square root of the standard deviation. This decreases the impact that large fold changes have on the dataset.

3.2.4 Metabolomics analysis development

The Mason lab has been making use of an in-house metabolomic data processing and analysis package developed by Louic Vermeer. It has been featured in several publications in the last five years (65,67,68). ‘Louic’s Metabolomics Thingy’ was developed using Python 2.7 programming language using the Scipy, Numpy, and Matplotlib packages. It is equipped with the PyQT front end Graphical User interface (GUI) that facilitates metabolomic data processing and analysis to non-experts. It allows users to do an entire metabolomic workflow, from importing raw NMR Bruker data to the final PCA and OPLS-DA analysis.

Additional pre-processing and analyses were performed using MVAPACK (167) which is an open source software package developed by Worley and Powers at the University of Nebraska. It is built on Octave GNU, an open source mathematical programming language based on Matlab, to offer an exhaustive list of functions to streamline NMR metabolomic data processing and analysis. Once parameters and scripts are established, it can also handle the entire metabolomic analytical workflow with a few keystrokes.

To facilitate data processing and analysis in our study we have used the icoshift and optimised binning algorithms available in the MVA pack toolbox to improve and accelerate our NMR data analysis (71,72).

Multivariate pattern Analysis

Spectra were analysed initially by principal component analysis (PCA) to identify clustering of spectra into groups and to identify potential outliers from experimental variability in the dataset. For this analysis, after normalization pareto-scaling was applied, where the mean-centered data is divided by the square root of the standard deviation.

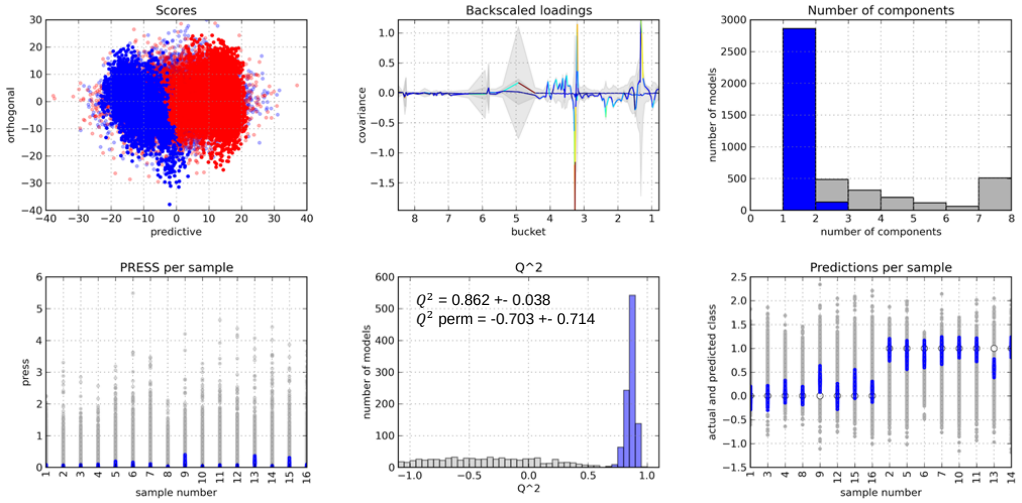

Figure 3.2. Representative cross-validated OPLS-DA output. Sample data is plotted in blue and permutated data where class labels are randomly assigned are plotted in grey. Data is taken from lentiviral stable knockdown of fatty acid synthase in PC3 human prostate cancer cell line. Top left: Scores plot from 2CV strategy. Individual points represent individual NMR samples and are potted according to their score of the predictive component (x-axis) and orthogonal component (y-axis). This plot visualises the separation between classes when using features that can distinguish between classes. Control class is plotted in blue and treatment class is plotted in red. Top middle: Back scaled loading plot: the OPLS-DA data is back-scaled to the original variables (NMR ppm/hertz) and plotted according to the covariance associated with the class (y-axis) as well as the correlation weights, visualised by colour. This plot allows easy visualisation of which variables in the data have discriminatory importance in the data. Top right: histogram of the number of components used to create the OPLS-DA model with each iteration of cross-validation. Bottom left: Predicted Residual Sum of Squares (PRESS) dot-plot for sample and permutated data each samples in the dataset. Bottom middle: Q^2 histogram of generated OPLS-DA models comparing sample data (purple) and permutated data (grey). This allows for a comparison of OPLS-DA models of the data and random noise. Bottom Right: Predictions made per sample. This allows for easy visualisation of outlier samples and give a general overview of the predictive ability of the OPLS-DA models.

In order to provide a robust statistical analysis and assess the predictability of the OPLS-DA, a double cross validation strategy was used (79). A representative visual output of OPLS-DA cross-validation data is shown in Figure 3.2. 4-fold cross-validation was performed using Leave-One-Out Cross-Validation (LOOCV), where one sample is left out of the training set and is used as the validation data (168). 75% of samples were used as a training set and the remaining 25% of the samples were used as a test set. This ensured that the number of samples in the test set was proportional to the total number of samples from each class (65). The training set was then used to obtain a classification model, and this model was then used to predict the classes of the samples in the test set. This analysis was repeated for each sample in the data set. At the end the cross-validation is given as a Q^2 value.

The maximum number of components for the model was between 6 and 10 and the component selection was selected by which model gave the best F1-score. Each of these models leads to a point on the scores plot while loadings and weights are presented as averages over all the models. The procedure was repeated 200-2000 times with randomly chosen samples in the training and test sets, this was to prevent bias due to an unlucky choice of validation. to assess whether the differences between classes occurred by chance as well as to give a reference value for Q^2. In total 4 × 2000 models was generated. In addition to the Q^2 histogram, the data were plotted into the back-scaled loadings, the principal components histogram, the predicted residual error sum of squares (PRESS)/sample and the predictions per sample plots.

3.2.5 Qualitative and Quantitative Metabolic Analysis

Metabolite assignment was done by comparing peak chemical shifts to those found in the literature (60) and in metabolomic database: Human Metabolome Database (HMDB) (169), and Biological Magnetic Resonance Data Bank (BMRB) (170) and Chenomx Software. Representative 2D spectra were also obtained to support the assignment. The 2D experiments conducted were Heteronuclear single quantum coherence spectroscopy (HSQC), homonuclear correlation spectroscopy (COSY), and homonuclear J-resolved spectroscopy (J-RES) experiments were conducted. Representative figures of 2D spectra with partial assignments and 1D assignment with Chenomx are shown in Appendix B.

MultiExperiment Viewer (MeV) which is a part of the TM4 Microarray Software Suite (171) was used to quantify the variations in metabolite concentrations and generation of heat maps and Hierarchical cluster analysis (HCL). The Euclidian distance algorithm was used to compute the differences between

metabolite level changes and the average linkage method was used to define the distances. Additional Heat map generation and analysis was performed in R using the Heatmap2 library.

The online software MetaboAnalyst 2.0 (172) and 3.0 (173) was to identify the metabolic pathways most likely to be involved in the treatment effects. The list of relevant metabolites was uploaded into the Pathway Analysis and human pathway library was selected. Hypergeometric test was used to determine whether a metabolite occurred more than by chance in a compound list, and relative-betweenness centrality was selected for metabolite importance determination by measuring in a graph network the number of shortest paths going through the node.

3.3 Bioinformatics

3.3.1 GSEA (Gene Set Enrichment Analysis)

Gene Set Enrichment Analysis is a computational method that determine whether a pre-defined set of genes shows significant expression enrichment between two biological states. The sets of genes used with GSEA software are derived from a collection of annotated gene sets known as the Molecular Signatures Database (MSigDB). It is also possible to create gene sets for analysis. For statistical purposes GSEA compares the expression of the given gene set to a random walk. Shortly, the gene set enrichment analysis uses a given set of gene expression data and examines its overall correlation with a phenotype by progressing or 'walking down' the gene list. The Enrichment Score (ES) starts at zero and decreases gradually, when it encounters a gene expression correlates with the phenotype, the ES is increased proportional to the correlation between the individual gene and the phenotype. In this way a curve is obtained (seen in green in Figure 3.3). Statistical significance is determined by comparing curve obtained to a permutated dataset.

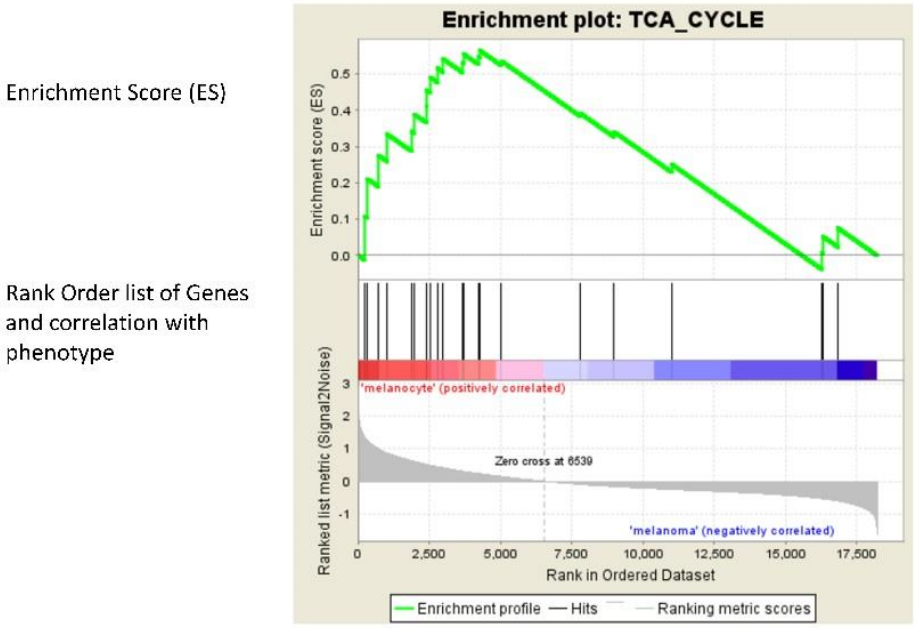

Figure 3.3. A Representative GSEA output. GSEA calculates the enrichment score (ES) by progressing or 'walking down' a ranked list of given genes in a gene set (represented by black lines in figure). As the algorithm progresses, the ES decreases gradually. When a gene in the set correlates with the phenotype in question, the ES (shown as a green line) increases proportional to the correlation of the gene expression with the phenotype. Statistical significance is then determined by comparing the obtained ES to a permutated dataset which is used as the null-hypothesis (174).

3.3.2 Analysis of gene expression from human databases

Gene expression data of human melanoma samples from published microarray studies was used to analyse gene expression in melanoma progression as in (154).

3.3.3 Gene Expression Omnibus (GEO)

The National Center for Biotechnology Information's (NCBI) Gene Expression Omnibus (GEO) - a public, international repository of, amongst other datasets, gene expression profiles - was accessed as the source of five MIAME-compliant transcriptomic databases. These databases, signified by their GEO accession number, were: GSE29359; GSE3189; GSE8401; GSE46517; GSE7553 (supplementary to, respectively: Avery-Kiejda *et al.*, 2011 (175); Talantov *et al.*, 2005 (176); Xu *et al.*, 2008 (177); Kabbarah *et al.*, 2010 (178); Riker *et al.*, 2008 (179)). Avery-Kiejda *et al.* focussed on a comparison of gene expression profiles between 'melanocytes' and 'melanoma' cells (n=8, n=92, respectively), whilst Talantov *et al.* focussed on a comparison between 'normal' and 'malignant' cells (n=7, n=45, respectively). Hereafter, these two comparative conditions will be defined as a comparison between 'normal' cells (non-tumorous) and 'primary' cells (tumorous, non-metastatic). Xu *et al.*, Kabbarah *et al.*

and Riker *et al.* each analysed ‘primary’ and ‘metastatic’ cells (n=31 and n=52; n=31 and n=73; n=14 and n=40, respectively).

Gene expression data was extracted from each of the 5 databases for the genes of interest. In each of these databases, initial gene selection for subsequent experimental analysis was based upon the exclusion criteria that the gene exhibited a significant ($p<0.05$) fold-change expression of 1.5 or greater in primary or metastatic cells with regards to normal or primary cells, respectively. This was determined by means of performing an unpaired *t* test for each of the comparisons for each gene. In the case that multiple primers were used for individual gene expression analyses in a single microarray, the datum representing the greatest fold-change expression was selected.

3.3.4 The Cancer Genome Atlas (TCGA) and Survival Analysis

Data from The Cancer Genome Atlas (TCGA) – a joint effort of the National Cancer Institute (NCI) and the National Human Genome Research Institute (NHGRI); both part of the US National Institutes of Health (NIH) which comprehensively catalogues a broad spectrum of expression profiles and tumorigenic mutations – was accessed from the cBioPortal for Cancer Genomics (180,181). In particular, data was obtained from the supplementary work of (182), detailing expression profiles in 257 Skin Cutaneous Melanoma (SKCM) patients with complete sequencing and copy number alteration (CNA) data, from a total patient database of 470.

Gene expression and patient survival data was extracted for the 94 genes previously detailed. Since individual survival times, both censored and uncensored were available for each patient, we utilised the Kaplan-Meier method of cumulative group survival determination. The Kaplan-Meier survival estimate of each of the genes was determined from survival curves using IBM SPSS Statistics 22 and Graphpad Prism 6. The vital statistic of each patient was defined and limited by an absolute time-frame of 10 years following initial diagnosis.

gene exhibited a significant ($p<0.05$) association with negative prognosis in patients over the 10-year period of observation.

3.3.5 Heatmap Generation

Heatmaps were generated using the open source Multiple Experiment Viewer (MEV) software. Loading data from OPLS-DA models were used for Heatmap data at buckets selected for identified metabolites. To generate the heatmaps Euclidean distance was calculated with average linkage clustering. Both sample tree and metabolite trees were generated.

3.4 Reagents

Reagent	Supplier
4-12% Bis-Tris polyacrylamide precast gels NuPage	Invitrogen
AlexaFluor ® Phalloidin 546	Life Technologies
Amersham ECL Prime	GE Healthcare
Amersham ECL Western Blotting Detection Reagent	GE Healthcare
Amersham Hyperfilm ECL	GE Healthcare
Amersham rainbow protein molecular marker	GE Healthcare
Atelopeptide bovine collagen I, PureCol	Advanced BioMatrix
Bis – acrylamide 29:1 40% solution	Fisher Scientific
Cassettes 1.5 mm	Life technologies
Complete EDTA-free protease inhibitor cocktail tablets	ROCHE
Dimethyl sulfoxide (DMSO)	Sigma
Dulbecco's Modified Eagle Medium (DMEM)	Life Technologies
Dulbecco's Phosphate Buffered Saline (PBS)	Life Technologies
Glass bottom culture dish (35mm dish, 14 mm well)	MatTek
H1152	Calbiochem
Hoescht 33258 Pentahydrate	Invitrogen
MOPS SDS running buffer	Invitrogen
NUPAGE ® LDS sample buffer	Life Technologies
NUPAGE® MES SDS running buffer	Life Technologies
Opti-MEM reduced serum media	Life Technologies
PCR microplate Thermo-Fast 96 well non-skirted white	Thermo Scientific
Penicillin – Streptomycin	Life Technologies
RPMI Medium 1640	Life Technologies
Serum	Sigma
Tetramethylethylenediamine (TEMED)	Sigma

Tripsin 0.05% EDTA	Life technologies
Trizol	Life technologies
Ultra-clear cap strips from PCR microplates	Thermo Scientific
Water resistant marker pen	DAKO
Whatman 3MM chromatography paper	Whatman
Xylene	Sigma
Y27632	Tocris Bioscience
CFM-2	
MK-801 (Diclozipine)	
GSK269962A	Axon Medchem
GYKI-52466	
Memantine	

3.5 Kits

Kit	Supplier
Brilliant III SYBR Green QRT-PCR kit	Agilent
DNA-free™ DNA Removal Kit	Life technologies

3.6 Buffers and solutions

Solution	Composition
Fixation solution (immunohistochemistry)	4% Formaldehyde
Laemli buffer	0 .1 mM DTT + 1M glycerol phosphate + 0.5M sodium fluoride + 100 mM Sodium Vanadate + 0.1 PMSF + phosphatase inhibitors
PVDF membrane stripping solution	0.1M Guanadine hydrochloride pH 2.5
Transfer buffer	100 ml TrisGlycine + 200 ml methanol + 700 ml H20
Acrylamide gel	10% gel: 2.5 ml 40% acrylamide + 2.5 ml TrisHcl pH 8.8 + 5 ml H2O + 66.7 µl APS + 13.3 TEMED
Acrylamide stacking gel	0.98 ml 40% acrylamide + 2.5 ml Tris HCl pH 6.8 + 6.4 ml H2O + 100 µl APS + 20 µl TEMED

3.7 Antibodies

Antibody	Species and concentration	Use	Supplier
GAPDH	Mouse, 1:10,000	WB	Abcam (MAB374)
MLC2	Rabbit, 1:500	WB	Santa Cruz (sc-15370)
GRIK2	Rabbit 1:100	WB	Abcam (ab66440)
ROCK1	Rabbit 1:1,200	WB	BD Transduction Laboratories
ROCK2	Rabbit 1:500	WB	Abcam

pThr18/Ser19-MLC2	Rabbit, 1:500	WB	Cell Signalling (#3674)
pSer19-MLC2	Rabbit, 1:50	IF	Cell Signalling (#3671)
Mouse Igg Hrp-Linked Whole Antibody	Secondary antibody 1:10,000	WB	VWR International (NA931)
Rabbit Igg Hrp-Linked Whole Antibody	Secondary antibody 1:10,000	WB	VWR International (NA934)
Anti-rabbit Igg secondary antibody Alexa Fluor® 488 conjugate	Secondary antibody 1:100	IF	ThermoFisher Scientific (ab150077)
Anti-rabbit Igg secondary antibody Alexa Fluor® 647 conjugate	Secondary antibody 1:100	IF	ThermoFisher Scientific (ab150075)

3.8 siRNAs

siRNAs were purchased from Dharmacon (GE Healthcare). Genes and respective siRNA sequences are as follows:

Gene	Sequence
ACO2	CAAUCUAGCUGAUGAAUUC
	CCACUUCCGUGUUCCCUUA
	GCAGUGCCCUCAACAGAAU
	GGACGGCUAUGCACAGAUC
ENO1	GAACGUCACAGAACAAGAG
	GAUAAGACUCGCUAUAUGG
	AAUGAUAAGACUCGCUAUA
	AUAAGGUGGUCAUCGGCAU
ENO2	CUGAACGUCUGGCUAAAUA
	GGACAUAACUUCCGUAAUC
	CCACUGAUCCUUCCCGAUA
	CCUCAGAGUUUUAUCGUGA
EPRS	GUAAAUCUCUGUAUGAUGA
	GAAGAAAGCUCCAGUUCAU
	GAAGAGGGAUGACAGUUGA
	GGAAACUGAUCAUGAGAUU
FOLH1	GAUAGCAGCUGGAGAGGAA
	GCACAGAAGCUCCUAGAAA
	GCAGAGCACGGUAUACUAA
	AAACAAAUUCAGCGGCUAU
GLS1	AGACAUGGUUGGUAUAUUA
	UGAAUAAGAUGGCUGGUAA
	GGUGGUUUCUGCCCAAUUA
	GAAUAACACUCCCAUGGAU
GLS2	GCUGAAGCAGUGCGCAACA
	CGAGACUGCAUGAGCGAGA
	ACCGAGAUCUCUUCCGAAA
	GAAUUAUGCCAUCGGCUAU
GOT1	GAGCAUAUCGCACGGAUGA
	UUAAAGACAUUCGGUCCUA
	UAGCCUAAAUCACGAGUAU

	GAACAGGUGCACUUCGAAU
GOT2	GCAUGCAGCUACAAGGUUA
	AACAUGGGCUUAUAUGGUG
	CUUGAAGAGUGGCCGGUUU
	UGAGAAACAGCACACGUUA
GPI	GGAAAUACAUCACCAAAUC
	CAACCAAAGUGAAGGAGUU
	GAUGAUACCCUGUGACUUC
	UCACGACGCUUCUACCAAU
GRIA1	GAACAUACAUCGUCACAAC
	GCAGAGAAUUGAUAUAUCU
	GGACAUUGACUUAAACAAA
	GGUAGUAGGUGCCAAUUUC
GRIK2	UGACUCUGCUGAUGAUUUA
	GUAAAGAAACCAUGGCAUA
	GAUAGAAUAUGGAGCAGUA
	GCACUGGUCUCAUUCGUUU
GRIK2 (mouse)	GCAGAUUGGUGGCCUUAUA
	GCAAUGCAAUCGACACAAA
	GGAAUCUUCUAUUUGGUUA
	GUUUAUGACUCUUGGAAUA
GRIN3A	UCACAUGGGUUUAUGGAUA
	CGACGGAAAUACAUCUUUA
	GAAGAUCUAUGAAGAGCUU
	GGACAAAGCCCUUCUGGAU
HK3	GGAAUGCGAUGUCUCCUUA
	GCAGUUGACUCGUGUCUGA
	GACAGGAGCACCCUCAUUU
	UCACGUUCCUGCAGUCAGA
IDH3A	GCAGAAAGCUGUAAAGAUA
	GAACGUCACUGCCAUUCAA
	GGAAAGAGCUUGACAAAAG
	GCUAAAGAGUCCAUGGAUA
IDH3B	UGAAGAAGGUGAUCAAAGU
	GCAUCUUAAUCUUGAGUAU
	GCAGUGGGCAGGAAUAUAG

	UUGAGACAAUGAUCAUAGA
IDH3G	GCAAGAGUAUCGCCAAUAA
	GGACAUAGACAUCCUCAUU
	GCACGUGAGUUCCAAUGCU
	GAACACAGAGGGCGAGUAC
MDH1	CAAAGGAACUGACAGAAGA
	CAUCAAGGCUCGAAAACUA
	GUUGAAGGUCUCCCUAUUA
	AAGGUGAAAUUGCAAGGAA
OGDH	GCUAGGACAUUUCAACAGA
	CAGACAAACUUGGGUUCUA
	UCUAGAAGGCUGCGAGGUA
	CUGAUGAGGGCUCCGGAGA
PPAT	GAAAUGGUCUGGAAUGUUU
	GGUAAAUGCUGCUCGAUUA
	GGGAAUGGGUCUUGUAAAU
	GAAUGGGUCUUGUAAAUCA
ROCK1	CUACAAGUGUUGCUAGUUU
	UAGCAAUCGUAGAUACUUA
	CCAGGAAGGUAUAUGCUAU
	GCCAAUGACUUACUUAGGA
ROCK1 (mouse)	UGUCGAAGAUGCCAUGUUA
	GCGGUUAGAACAAGAAGUA
	GCACCAAUCUAUCGAAGAG
	GACCUUCAAGCACGAAUUA
ROCK2	GCAACUGGCUCGUUCAAUU
	UAGAAUAUGUGGCCUAGAA
	GAAACUAAUAGGACACUAA
	CAAACUUGGUAAAGAAUUG
ROCK2 (mouse)	GAGAUUACCUUACGGAAAA
	GGACAUGAGUUUAUUCCUA
	GCAAUGAAGCUUCUUAGUA
	CACAACAGAUGAUCAAAUA
SLC1A5	GGAUGUGGGUUUACUCUUU
	GUUCUGGUCUCCUGGAUCA
	GAGAGGAAUAUCACCGGAA

	CAGUCAACCUCCCGGUCGA
SLC38A1	GAACUACCCUCUGCCAUAA
	AAACAGAAAUGUACAGGAU
	GAUGUUAGGUCGAAUUUAA
	CAAAAGUGGACUCGAAUUA
SLC3A2	AGAAUGGUCUGGUGAAGAU
	GAAGAAUGGUCUGGUGAAG
	UCACGGGCCUGUCCAAGGA
	GAGCAUCCGUGUCAUUCUG
SLC5A3	GCCAAAGGCUCUACUCUUA
	GAAGAGACUCGGCAAGUUA
	GCAAACUGGCCGUCGGUAA
	AGAUAAUGUGCUCGAGUAA
SLC6A19	GAGAAGGACUCGGUGAUUG
	UCUGUGCUCUUCUUCAUUA
	GAACAUGGAGGGCGUCGUU
	GAUCAUGUGGUACUUAUUC
SLC7A5	GAUCCCAACUUCUCAUUUG
	UGACCAACCUGGCCUACUU
	GUGAACUGCUACAGCGUGA
	UGAAAACUCUGGUACGAAU
SLC7A8	GGACAGAGGAGGCUAAUGA
	UCAACUACCUCUUCUAUGG
	CCACGAAGGACAAGGACGU
	UGGCCAUGAUCCACGUGAA
SLC7A11	GGAAGUCUUUGGUCCAUUA
	GGAGUUAUGCAGCUAAUUA
	GGGAACAACUAUAAAGAAA
	UGACAAAUGUGGCCUACUU
TGM2	GAACAUGGGCAGUGACUUU
	CCGAGGAGCUGGUCUUAGA
	GCAACCUUCUCAUCGAGUA
	GGUCAAUGCCGACGUGGUA
TPI1	GCAAGGUCGUCCUGGCCUA
	GCUCAGAGCACCCGUAUCA
	AGAGAGAAGGCAUGUCUUU

	GAUCAAAGACUGCGGAGCC

Chapter 4 : A Metabolomic Investigation of Rho/ROCK Signalling in Metastatic Melanoma

4.1 Introduction

Melanomas are the deadliest form of skin cancer and despite great advances in the treatment of malignancy, there is still a need for alternative targeted therapies of disease that can address non-response and resistance that arises in patients after receiving currently available therapies (183). Rho Kinase (ROCK) is an attractive target to treat metastatic melanoma as it has been shown to regulate both melanoma proliferation and the formation of metastasis *in vitro* models of melanoma (3,5). Targeting cancer metabolism represents another attractive area of research into potential cancer therapies as cancer cells often present with re-wired metabolism that allows for increased proliferation, resistance to apoptosis, and metabolic signalling (16). ROCK is principally studied for its role in regulating the actin cytoskeleton by promoting high levels of actomyosin contractility. ROCK has been shown to regulate cellular metabolism in non-cancer cells and its role in insulin response has been well established (130,157). There is also some evidence that ROCK may play a role in promoting altered metabolism in cancer cells (155,158,184), however, these studies are few relative to the interest that ROCK has received in recent years with regards to melanoma. ROCK may re-wire cellular metabolism to sustain high levels of cellular contractility along with proliferative and invasive potential. In this section of the thesis we aim to address this gap in knowledge by studying the metabolic profile of human and murine melanoma cells when ROCK activity or expression is ablated.

4.1.1 Study Design

We hypothesize that ROCK activity regulates melanoma cell metabolism and our principle objective is to investigate how ROCK activity and expression is regulating cellular metabolism. An introduction to the study design follows.

4.1.2 *In vitro* models of metastatic melanoma

One of the principle functions of ROCK is to regulate the actin cytoskeleton and increase cellular contractility by phosphorylating myosin light chain (141). These effects are best measured *in vitro* with what is called a '2 ½ D' cell culture system by which cultured cells are placed atop a thick layer of collagen 1, either bovine or rat tail (140,185). Cells can then be measured phenotypically by microscopic imaging measuring the 'roundness index' of the cells which is the ratio between the largest and smallest diameter. Cellular contractility is then measured biochemically by quantifying the amount of phosphorylated myosin light chain 2 (p-MLC). This can be done by Western blot, calculating the ratio

between p-MLC to total-MLC. Otherwise, contractility can be measured by immunohistochemistry and confocal imaging of fixed cells stained for p-MLC.

For this thesis we principally use the A375M2 human metastatic melanoma cell line. This cell line is a derivative of the original A375 parental cell line, initially derived from a 54 year old female (186). The M2 variant was produced by two rounds of injection of A375P cells into the tail vein of mice, extracting and culturing the lung metastases. A375M2 cells have much higher levels of p-MLC compared to the parental cells and when cultured onto a thick collagen-1 layer present with 95% rounded cells when compared to the 50/50 round/elongated phenotype displayed by the A375P cells (154) (Figure 4.1).

We also use the B16F10 mouse melanoma cells line which is a variant of the B16F0 cell line. B16F10 cells were generated in a similar fashion to the A375M2 cells however with ten rounds of harvesting lung metastases (187) as opposed to the two rounds of A375M2 cells.

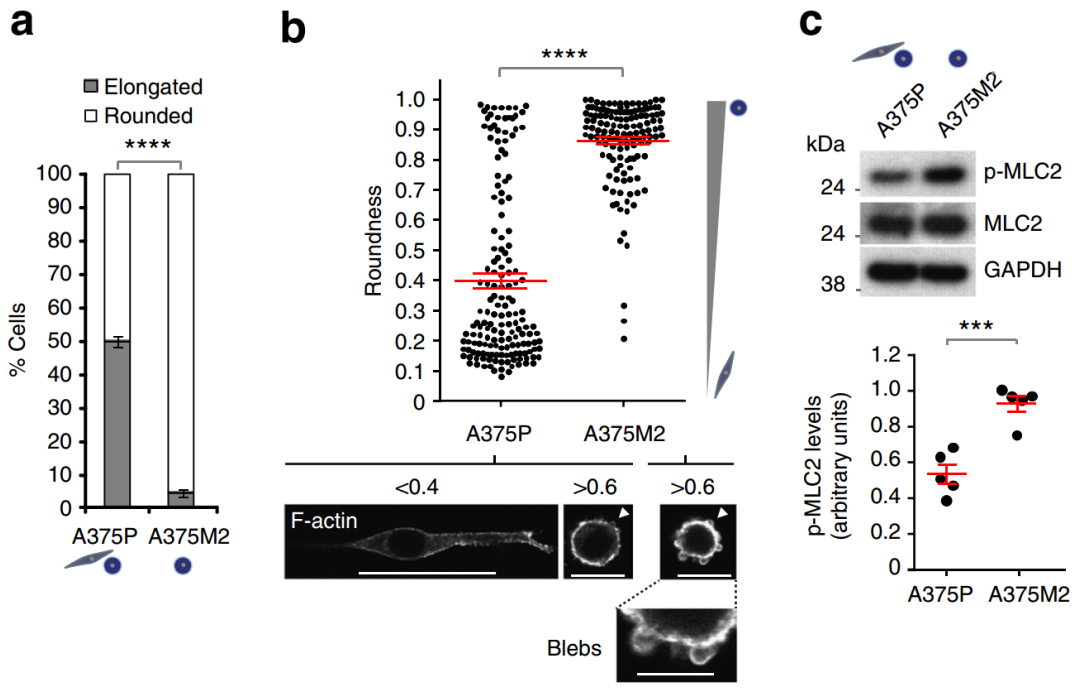

Figure 4.1. A375M2 Human Melanoma Cells as an *in vitro* model of metastatic melanoma with high levels of actomyosin contractility and Rho/ROCK signalling. A) Cells are classified into binary categories of 'round' or 'elongated'. A375M2 cells are 95% rounded when seeded on a collagen 1 matrix compared to the 50/50 rounded/elongated of A375 Parental cells. B) Roundness can also be quantified by finding the roundness index; the ratio between the largest diameter and the shortest diameter, where a perfect circle is 1 and a straight line is 0. Cells with high roundness levels also present with blebbing. C) A375M2 cells have high levels of actomyosin contractility, seen by increased levels of double phosphorylated myosin light chain 2 (p-MLC) show in western blot. Figure adapted from (154).

In this chapter, we have chosen to interfere with ROCK activity using three different strategies. They are: 1) small molecule inhibition of ROCK, 2) interference of ROCK expression by use of small interfering RNAs (siRNA) technology, 3) genetic knock out (KO) of ROCK in a murine model of malignant melanoma.

Each method proposed has its advantages and disadvantages when it comes to targeting ROCK. Small molecules have a very rapid mode of action and can take effect within very small time frames. However, kinases are inherently very similar topologically and therefore small molecules looking to block the kinase activity can have off-target effects by blocking alternative kinases. It is known that ROCK inhibitors can bind to a variety of other kinases, such as AKT2, PKA, PKC, PKG, CAMK2 and MLCK (Table 2).

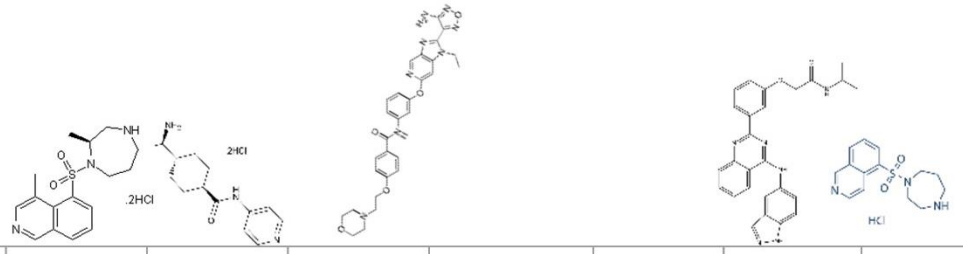

IC50 Drug / Protein	H1152P	Y27632	GSK269	CCT129254/ CCT54	AT13148/ AT48	SLx-2119	Fasudil
ROCK1	12 nM	140-220 nM	1.6 nM	214 nM	6nM	24 uM	330 nM
ROCK2		300 nM	6 nM	141 nM	4nM	105 nM	
AKT2			1.35 uM	2.2 nM	402 nM		
PKA	745 nM	25 uM					1.6 uM
PKC	3.03 uM	73 uM					3.3 uM
PKG	360 nM						1.6 uM
CAMK2	180 nM						
MLCK		>250uM					36 uM

Table 2. ROCK inhibitors and binding specificities. There are hundreds of ROCK inhibitors available for research however few have been used *in vitro*. Here listed are the ROCK inhibitors most widely used. The specificity of ROCK inhibitors are vastly different and have binding specificities for other kinases as well. Fasudil is the only ROCK inhibitor currently approved for clinical use.

For our study we have chosen to test three ROCK inhibitors. We make use of two classic inhibitors, H1152-p and Y27632, which are well evaluated in the literature (3,95,140,184). In addition, we make use of a newer generation of ROCK inhibitor, GSK269962A (GSK269), first developed in 2007(188). GSK269 has more than double the binding affinity to ROCK2 compared to H1152 and more than 7-fold increased binding affinity to ROCK1 compared to H1152 (Table 2).

For our studies we will be using H1152 at a concentration of 5 µM and Y27632 at concentrations of 10 and 20 µM. These concentrations were chosen to allow us to compare our results to those from previous studies in the Sanz-Moreno group (140,154,184,189). GSK269 will be used at a concentration of 0.1 µM, as it has been previously shown that 0.1 µM GSK269 is sufficient to induce significant morphological changes in A375M2 cells similar to H1152 (Francesca DiGiuseppe, personal communication, Figure 4.2).

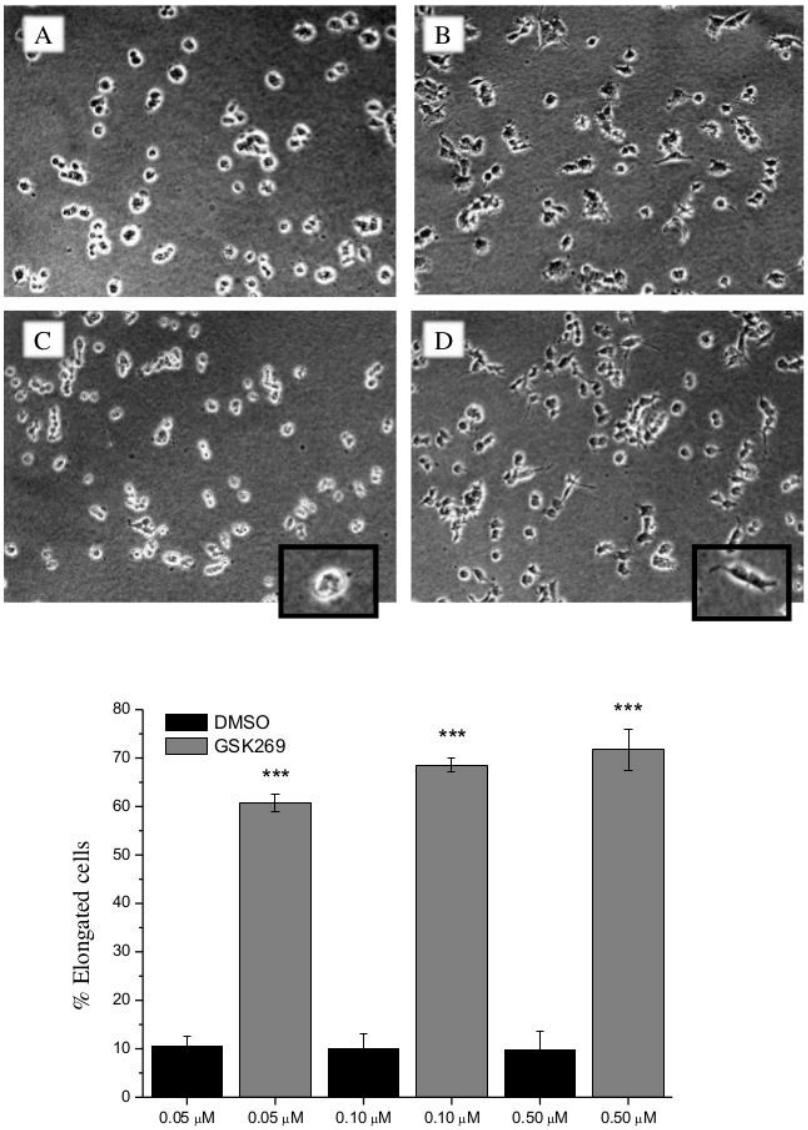

Figure 4.2. 0.1 μM GSK269 is sufficient to significantly alter A375M2 human melanoma cell morphology. A-D) Light microscopy images of A375M2 cells seeded onto collagen 1 show that 0.1 μM GSK269 is sufficient to induce an elongated phenotype. A) 5 μM DMSO control treated cells B) 5 μM H1152 treated cells C) 0.1 μM DMSO control treated cells D) 0.1 μM GSK269 treated cells. Below: quantification of the percentage of elongated cells after treatment with 0.05, 0.1, and 0.5 μM GSK269. *** -p<0.001. Data and figure generated by Francesca Di Giuseppe.

To address the potential off target effects, from ROCK inhibitors of varying specificity, that could impact this study we will also make use of siRNA targeting *ROCK1* and *ROCK2*. Gene silencing is a more specific way to target individual genes and observe their effects on the system, however it is rare if not impossible to obtain a full knockdown of gene expression by siRNA. Additionally, the full effects of the knockdown take several days to materialise. There is the additional challenge that we will need to deliver twice as many oligonucleotides to knockdown the expression of two genes simultaneously.

Finally, we have been graciously provided cultured murine melanoma cells where ROCK is genetically deleted from Dr. Sandra Kuemper in Chris Marshall's lab. These cells were generated from a spontaneous murine model of melanoma where the *ROCK* genes were knocked out by Cre-Lox Recombinase technology (Dr. Sandra Kuemper, Personal communication, Figure 4.3, Figure 4.4). This strategy has the additional strength of being a sustained knockdown of gene expression. On the other hand, as these samples are of a different species care must be taken not to over interpret results.

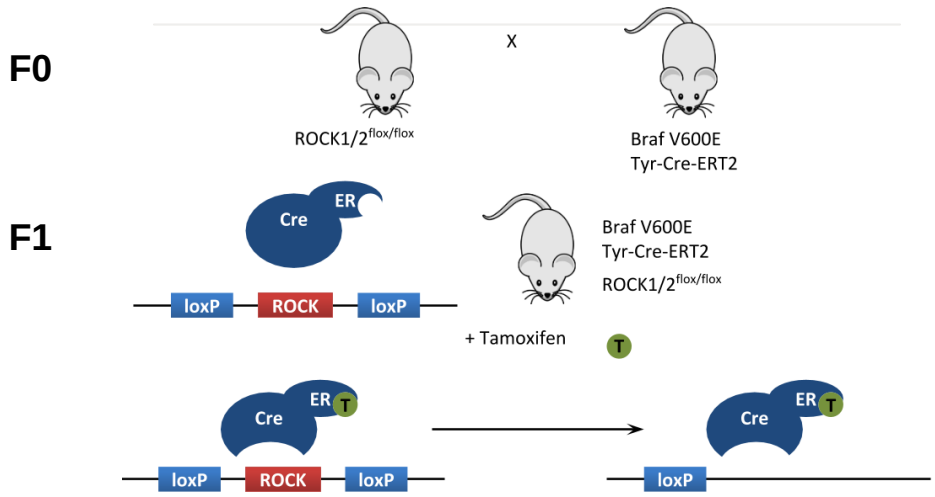

Figure 4.3. Schematic of Murine melanoma model generation. Mice harbouring the V600E BRAF mutation and the CRE recombinase gene spontaneously generate melanomas. These mice are bred with mice with ROCK1 and/or ROCK2 genes surrounded by flox/flox sites. 25% of the progeny of these mice contain all three mutations. When the F1 are administered tamoxifen, the expressed CRE-recombinase is activated and cuts out the ROCK genes.

It is hoped that with three different strategies of targeting ROCK activity we may be able to identify common features correlating with ROCK activity that can be used as a platform for further investigation. ROCK activity and expression will be altered by small molecule inhibition, siRNAs targeting *ROCK* and in a murine model of melanoma where the *ROCK* genes are knocked out (KO).

In our studies, the metabolomes of these cells will be studied with HR-MAS NMR, which is a highly reproducible metabolomic method that removes the need for labour intensive extraction protocols. Liquid NMR metabolomics will also be conducted to study how melanoma cells consume and secrete metabolites in control settings and after interfering with ROCK activity/expression. Finally, network analysis will be conducted to identify metabolic pathways that are potentially regulated by ROCK activity.

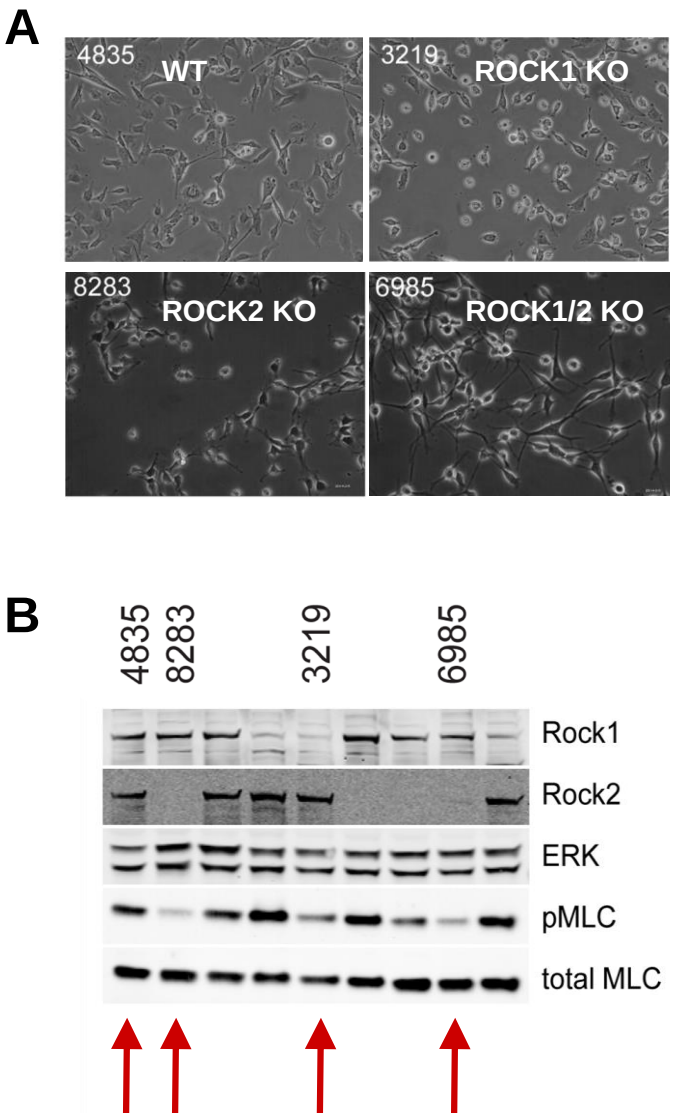

Figure 4.4. Cultured murine melanoma cells of with ROCK knocked out (KO) show a more elongated phenotype compared to wild type cells. A) Light microscopy images of wild-type, ROCK1 KO, ROCK2 KO and double KO melanoma cells. B) Western blot confirming KO and lowered levels of p-MLC compared to total-MLC. As double ROCK KO mice did not develop melanomas, the other isoform was knocked down *in vitro* for our studies. Figures provided by Dr. Sandra Kuemper.

4.2 Results

4.2.1 Small molecule inhibition of ROCK decreases actomyosin contractility and Cell Roundness

When seeded onto a thick layer of bovine collagen 1 and treated with ROCK inhibitors H1152-p, Y27632 or GSK269, melanoma cells elongate significantly (Figure 4.5A) and have a reduction in p-MLC (Figure 4.5B). H1152 showed mean 86% reduction in p-MLC compared to control while Y27632 at 10 µM showed a 75% reduction in p-MLC (Figure 4.5C).

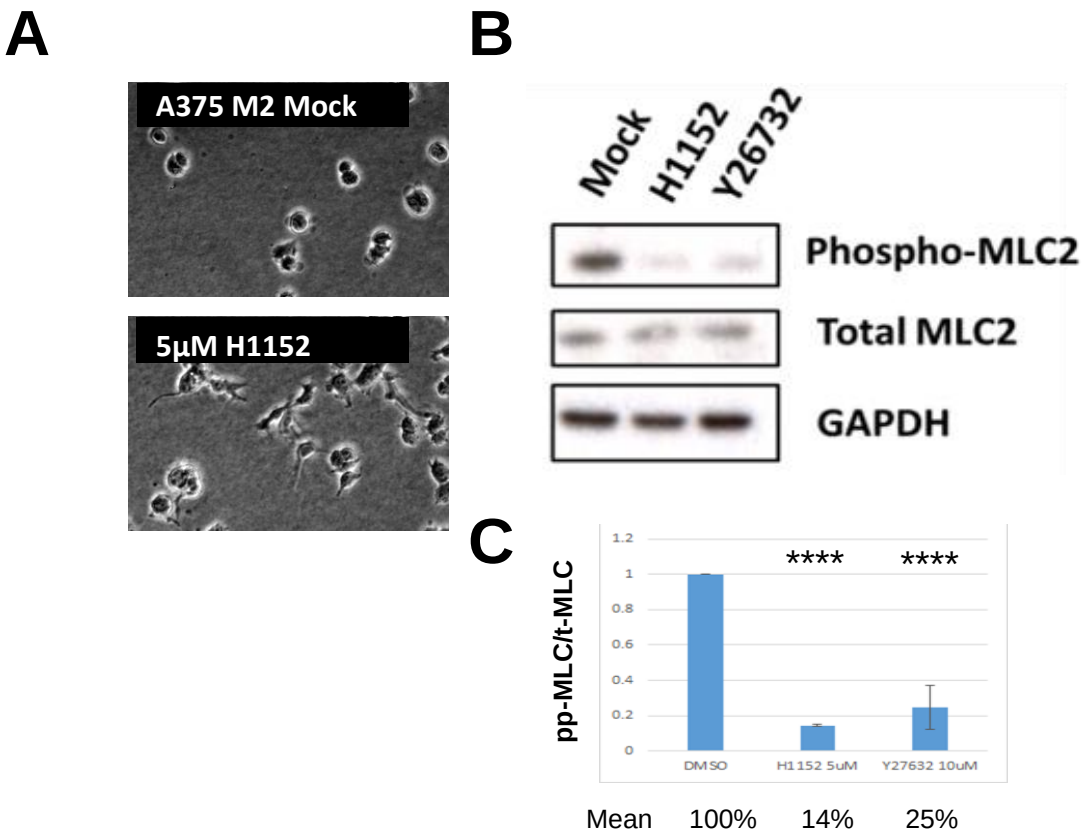

Figure 4.5.ROCK inhibition regulates phosphorylated-myosin light chain and cell morphology. A) Representative light microscopy images of A375M2 human melanoma cells seeded on a collagen 1 matrix treated with DMSO as control or H1152 ROCK inhibitor. B) Western Blot showing double phosphorylated myosin light chain 2 (pp-MLC) (pT18, pS19) compared to total myosin light chain 2 (t-MLC). GAPDH used as loading control. C)Quantification of pp-MLC/t-MLC by western blot (n=3). Bar chart shows mean +/- SEM error bars. **** -p<0.0001.

4.2.2 ROCK knockdown decreases actomyosin contractility in mouse melanoma cell line B16F10 and decreases proliferation *in vitro*.

Additional work was conducted with a murine melanoma cell line B16F10. Treating B16F10 mouse melanoma cells with the ROCK inhibitor H1152 at 5 µM led to a large decrease in contractility seen through a reduction in p-MLC (Figure 4.6A). We could also confirm that ROCK inhibition blocked cell proliferation in murine melanoma cells (Figure 4.6B).

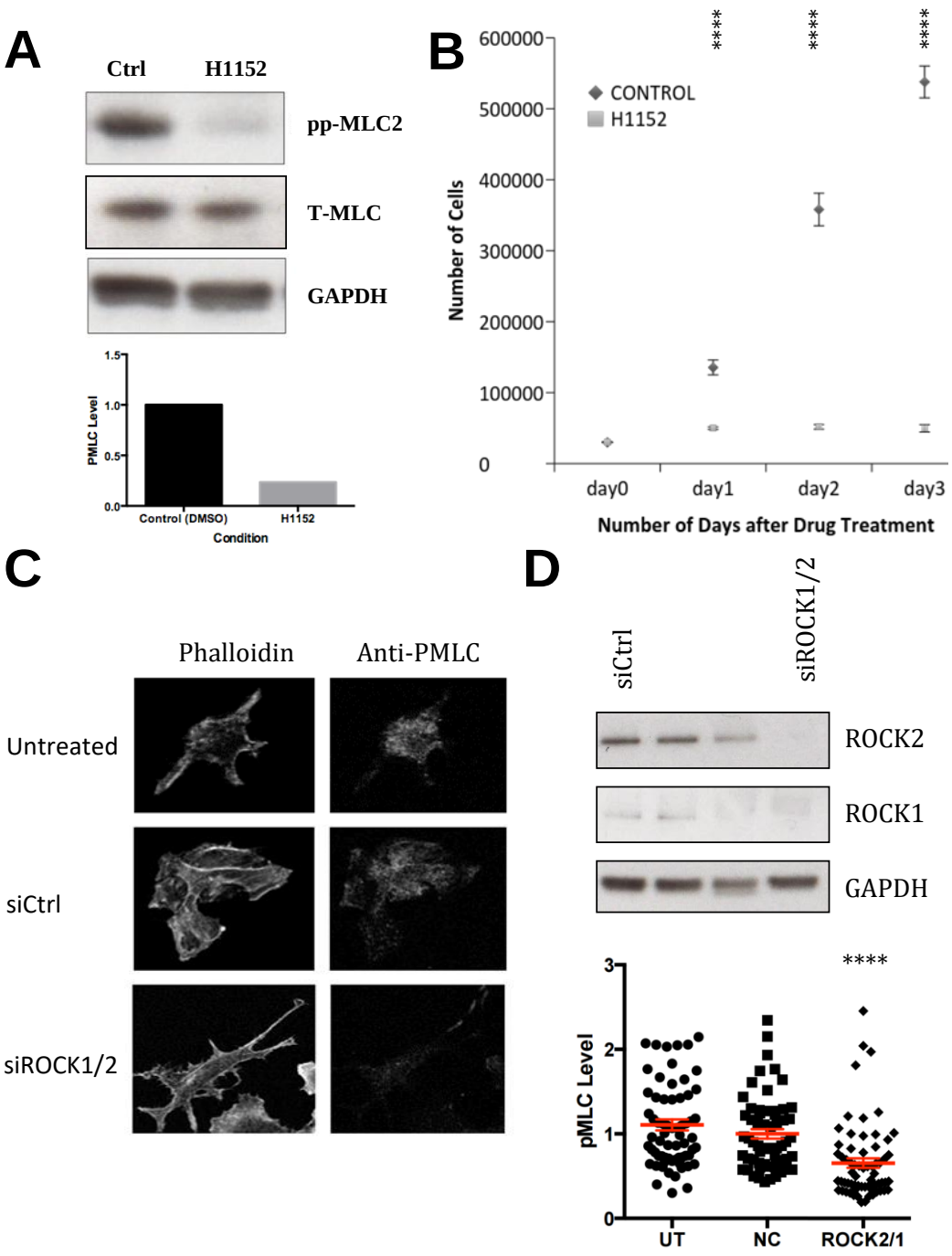

Figure 4.6. Inhibiting ROCK activity and Expression in B16F10 melanoma cells reduces cellular contractility and cell proliferation. A) Western blot and quantification of p-MLC levels after rock inhibition with H1152. B) Cell proliferation assay of B16F10 murine melanoma cells after rock inhibition. C) immunostaining and confocal imaging of B16F10 cells after rock knockdown show increased number of protrusions and lower p-MLC levels. D) Western blot confirming knockdown of ROCK2 and ROCK1 in B16F10 cells and quantification of p-MLC levels from confocal imaging. Error bars show mean +/- SEM. **** -p<0.0001. UT – Untreated NC – Negative Control/ non-targeting siRNA

When blocking *ROCK* expression *in vitro* we again observed that transient siRNA knockdowns of *ROCK1* and *ROCK2* simultaneously led to a reduction in contractility measured by p-MLC (Figure 4.6A) and cell morphology where more long actin protrusions were present (Figure 4.6C).

4.2.3 ^{1}H HR-MAS NMR spectra of the human melanoma cell line A375M2

Figure 4.7 shows mean normalised HR-MAS NMR spectra of control A375M2 cells (blue) and cells treated with 5 µM H1152 for 24 hours (red). Spectra were obtained on a 400 MHz NMR spectrometer. Assignments of metabolites associated with peaks are also showed in Figure 4.7 and can be used as a reference for the back scaled loadings and NMR spectra shown in this work. 24 individual metabolites were confidently assigned. In the HR-MAS spectra, the amino acids valine, leucine, isoleucine, glutamate, glutamine, alanine, tyrosine, phenylalanine was identifiable. Glutamine and glutamate were individually identifiable by their resonances at 2.36 ppm and 2.46 ppm respectively. Lipid components such as CH2-CH2 and CH3 groups were observable in HR-MAS spectra, choline, phosphocholine and glycerophosphocholine were also distinguishable. At higher regions, cytidine, uracil, adenine, inosine and uracil were observed. Taurine and creatine and *myo*-inositol were also observable. Residual DMSO was visible in the spectra from drug treated cells as the ROCK inhibitors were dissolved in DMSO.

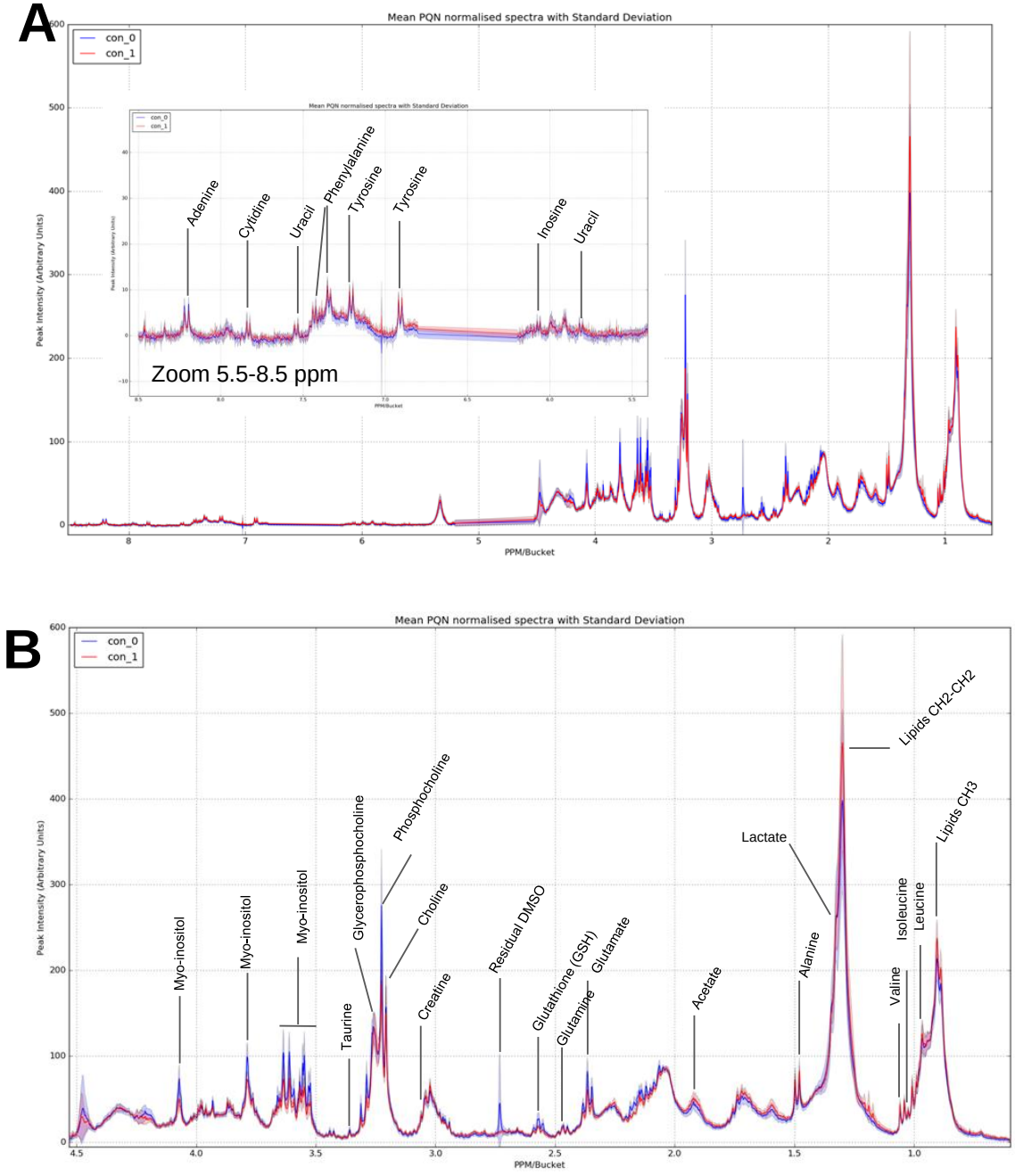

Figure 4.7. Mean PQN Normalised HR-MAS NMR spectra of whole A375M2 Cells treated with DMSO control (blue) and 5 µM H1152-p (red) for 24 hours. Averaged spectra are composed of 9 samples each. Spectra were recorded on a 400 MHz Bruker Magnet. Identified metabolites are assigned in figure. A) Full spectrum with zoomed inset of high ppm region. B) zoom of low ppm region with assigned metabolites. The water region between 4.5 and 5.2 ppm was excluded along with a noise region between 6.2 and 6.8 ppm. A table of assignments can be found in Appendix B.

4.2.4 Small Molecule Inhibition of ROCK alters the cellular metabolome

Each treatment of ROCK inhibitors led to a significant shift in the cellular metabolome of A375M2 cells (Figure 4.9). H1152 showed a shifted in metabolism at concentrations of 5 µM (Q^2 =0.246) while Y27632 was tested at both 10 µM (Q^2 =0.156) and 20 µM (Q^2 =0.193). With regards to GSK269, cells were tested with both 0.1 µM and 5 µM concentrations (Q^2 = 0.607 and Q^2 = 0.521 respectively). This was done as initially 0.1 µM GSK269 was seen to be sufficient induce morphological changes in A375M2 cells (Figure 4.2). Further work was performed with 5 µM doses to observe the metabolic profile of cells concentrations that induced anti-proliferative effects similar to those seen with H1152 and Y27362 (Figure 4.8). In both cases significant changes in metabolic profiles and 0.1 µM was sufficient to see a large significant change in the metabolome.

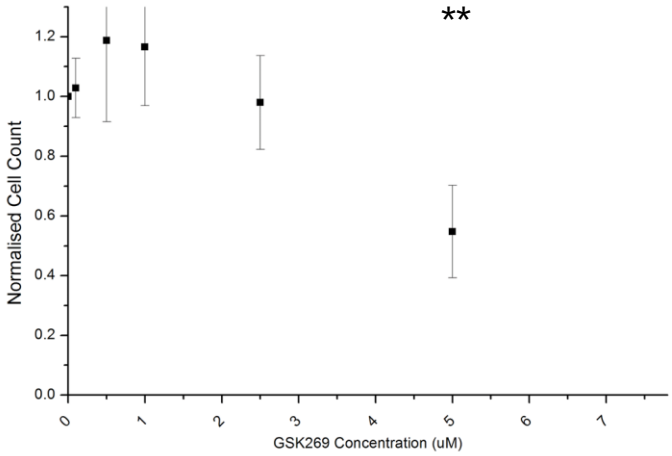

Figure 4.8. 5uM GSK269 is required for anti-proliferative effects in A375M2 human melanoma. A375M2 cells were treated with different doses of GSK269 for 48 hours and then cells were counted. Doses used were 0.5 µM, 1 µM, 2.5 µM and 5 µM. Data points show mean values +/- SEM (n=4). One-way ANOVA with Tukey's post-hoc test. ** $p<0.01$

This data suggests ROCK play a significant role in rewiring the cellular metabolome. We observed significant metabolic changes at doses of ROCK inhibitors that do no limit cell proliferation, suggesting these changes may be independent of the anti-proliferative effects and may be tied to the morphological effects. The performance of the OPLS-DA models also suggests that the stronger binding affinities of GSK269 when compared to H1152 and Y27632 lead to larger changes in metabolome than the other inhibitors.

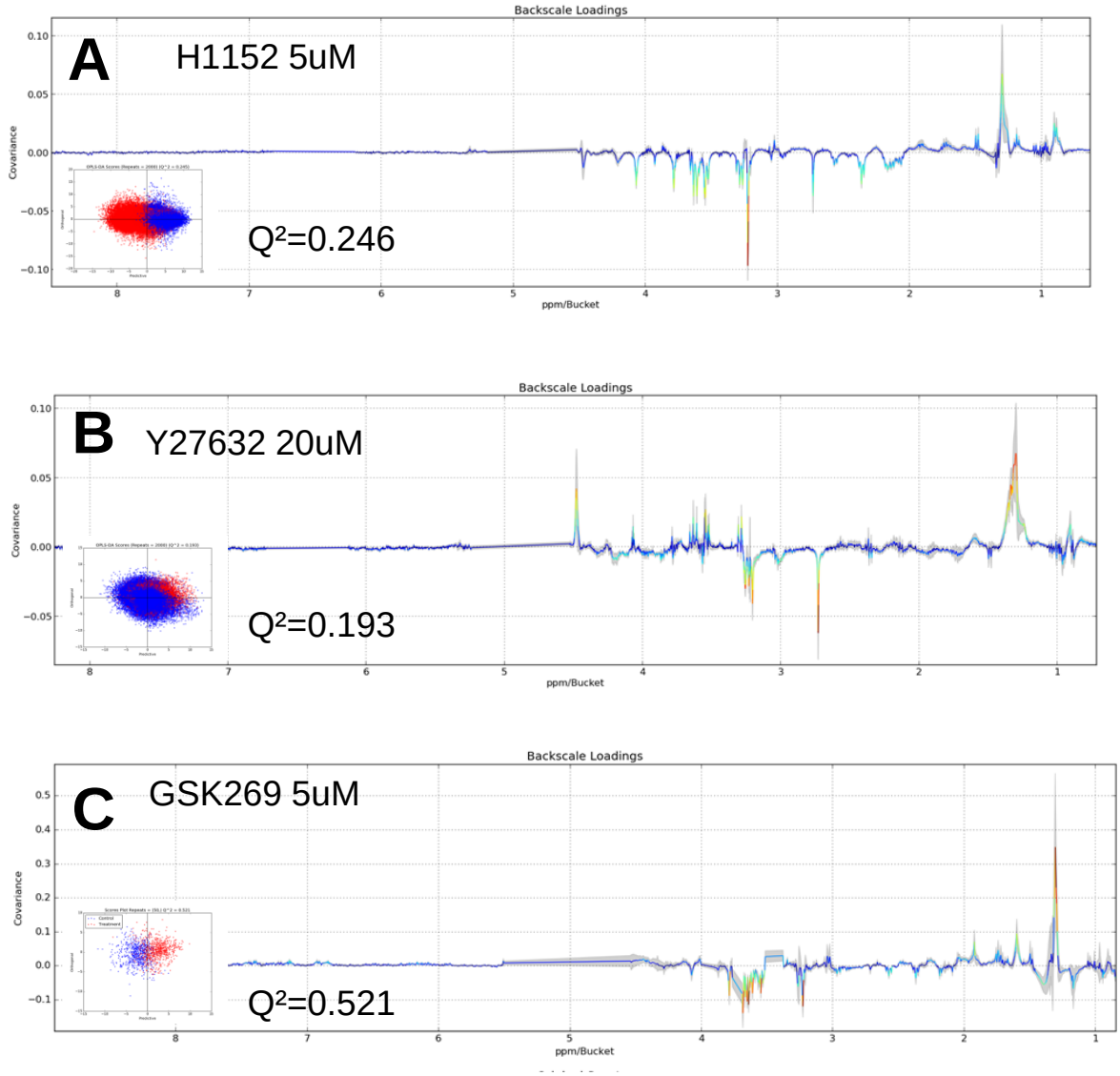

Figure 4.9. ROCK inhibition significantly alters the metabolic profiles of A375M2 human melanoma cells. A,B,C) Scores plots, back scaled loadings and mean PQN normalised spectra of HR-MAS NMR data from small molecule inhibition of ROCK. A) H1152 5 μM B) Y27362 at 20 μM C) GSK269 5 μM. Every experiment was conducted n=3 times, and each experimental replicate containing three technical replicates, for a total of 9 samples per experimental condition.

Hierarchical clustering of the NMR data of assigned metabolites also suggest that specificity of ROCK inhibitors can be reflected phenotypically in the cellular metabolome. Euclidean distance mapping show that the metabolic profiles induced by H1152 and GSK269 cluster more closely than Y27632 (Figure 4.9, Figure 4.18).

There were several consistent metabolic changes observed across treatments. We observed significant increases in CH2-CH2 bonds of lipids and methyl groups in lipids across treatments. As ROCK plays a

large role in regulating cell morphology, it would be interesting for future work to study the fluidity of melanoma cell membranes after ROCK inhibition.

There were also significant decreases in choline, glycerophosphocholine, phosphocholine and glutamate. *Myo*-inositol decreased sharply in H1152 and GSK269 treated cells however increased in Y27632 treated cells.

4.2.5 Glutamine, glutamate and glutathione are initially depleted in melanoma cells treated with GSK269 followed by recovery at 24 hours

It has previously been observed that small molecule inhibition of ROCK leads to changes in the cytoskeleton within a few hours of treatment. Therefore, we were interested in understanding how the cellular metabolome may be changing within a shorter time frame than in previous experiments. Cells were treated with 5 µM GSK269 and harvested at 4, 8 and 24 hours. It was seen that after 4 hours there was already an observable change in the metabolome (Q^2 =0.298) which then became much larger at 8 hours (Q^2 =0.761) (Figure 4.10B, C, Figure 4.11A). It seems the cells attempt to recover the initial challenge which is reflected in the smaller separation between classes at 24 hours (Q^2 =0.521) (Figure 4.10D, Figure 4.11A).

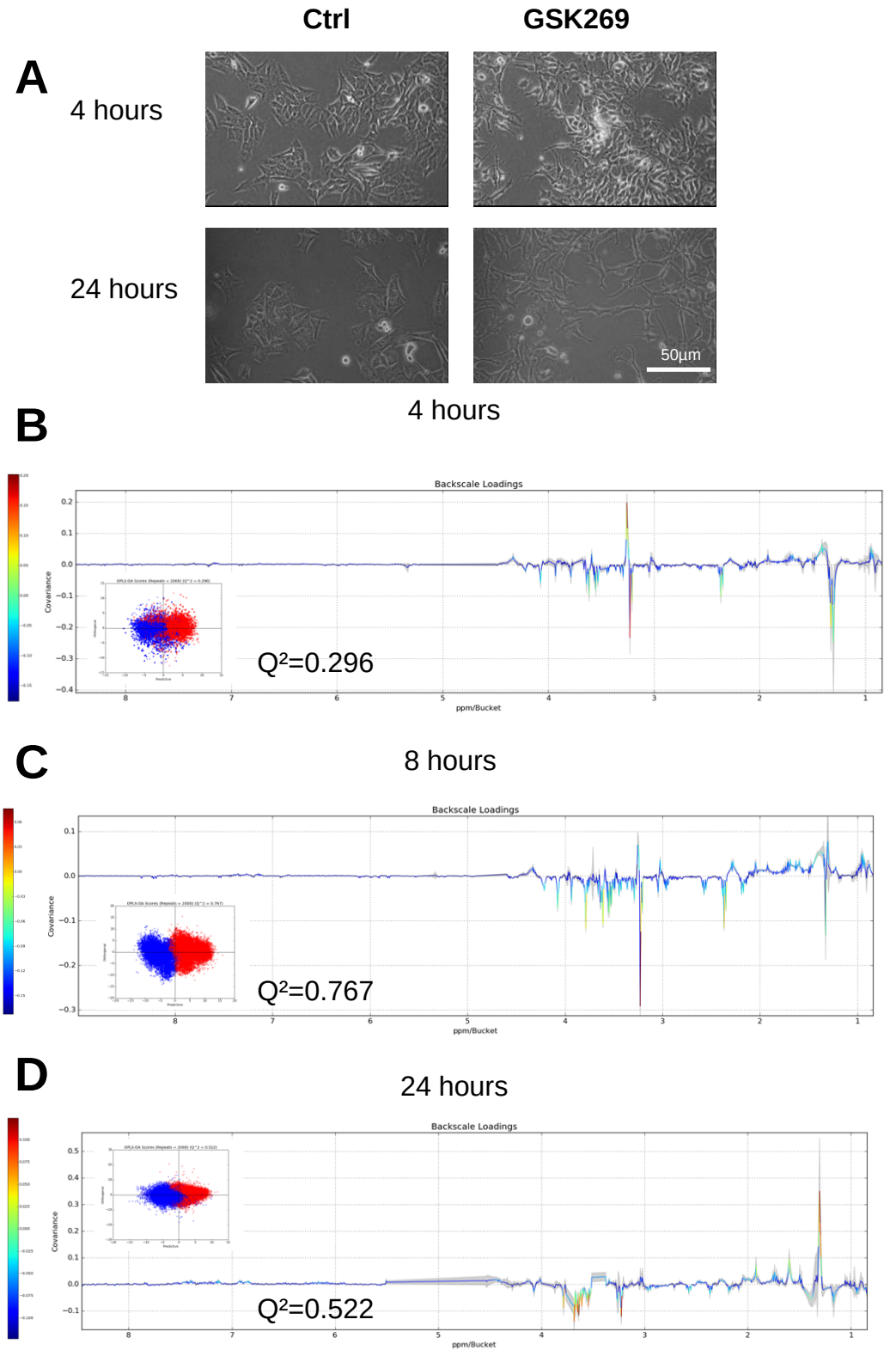

Figure 4.10. GSK269 alters melanoma metabolism within 4 hours and has sustained effects on metabolism at 24 hours. A) Addition of the ROCK inhibitor GSK269 leads to increased number of protrusions and elongated phenotype of A375M2 cells on plastic. Representative light microscopy images of A375M2 cells on plastic at 4 and 24 hours treatment of 5 µM GSK269. B,C,D) Scores plots, Q^2 values and Back-scaled loadings of OPLS-DA models at 4,8 and 24-hour time points. Every experiment was conducted n=3 times, and each experimental replicate containing three technical replicates, for a total of 9 samples per experimental condition.

An initial decreased in saturated lipids at 4 hours was observed, however, it reversed into an increase in at 8 hours that was sustained after 24 hours (Figure 4.10C, D, Figure 4.11A). The decreases in choline and phosphocholine are already observable at 4 hours and are sustained at 24 hours while glycerophosphocholine increases up to 8 hours and is then decreased at 24 hours.

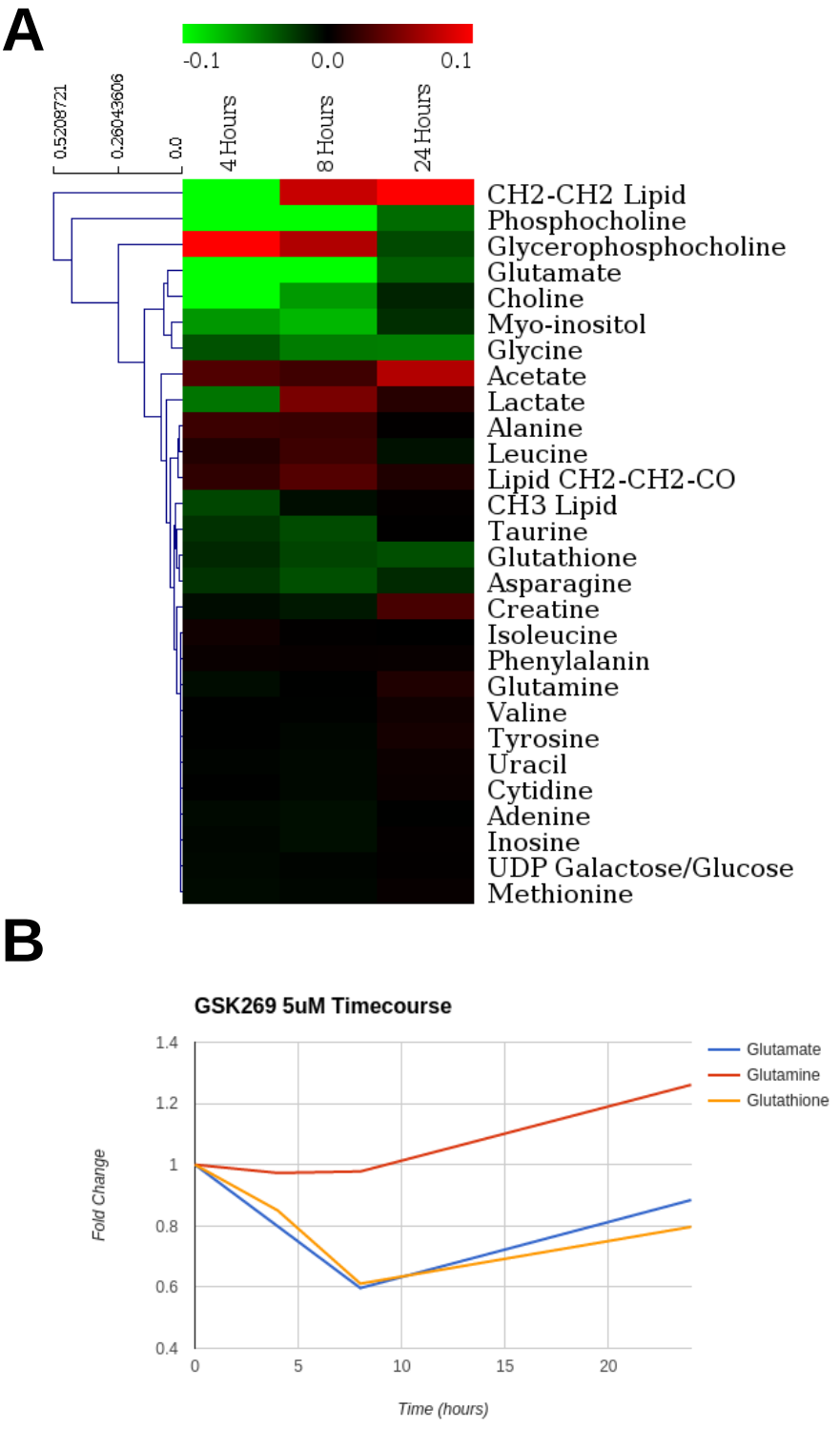

Figure 4.11. Time-course analysis with 5uM GSK269 at 4, 8 and 24hours. A) Heat map of A375M2 cells treated with 5μM GSK269 for 4, 8 and 24 hours. Hierarchical clustering was performed calculating Euclidean distance and average linkage. Colours represent covariance associated with treatment with lower covariance in green and higher covariance in red. B) Line chart showing fold change of glutamine, glutamate and glutathione at different time-points. Data presented is fold-change of GSK269 treated samples compared to control and zero-time point.

Glutamate and Glutathione decreased steadily until 8 hours and then recover slightly at 24 hours (Figure 4.10C, D, Figure 4.11B). Glutathione is the major antioxidant in cells and it is known that high levels of ROCK signalling can inhibit reactive oxygen species (184). It could be explained that initial ROCK inhibition leads to a depletion of glutathione as cells respond to oxidative stress. In longer time points, cells start to replenish glutathione by switching on synthetic pathways.

4.2.6 Sequential Knockdown of ROCK2 then ROCK1 gives optimal gene silencing

Silencing ROCK expression with siRNAs will reveal which metabolic changes observed in the small molecule experiments are specific to ROCK and could identify which effects are due to off target effects of the small molecule inhibitors. Work was conducted to achieve an optimal silencing of ROCK with consideration to the added difficult of silencing two genes at once. The standard protocol (163) was conducted simultaneously delivering *ROCK1* and *ROCK2* siRNA (2 µl *ROCK1* and 2 µl *ROCK2* siRNA complexed with 3.5 µl LAH4-L1 peptide). The 'Double' protocol saw 4 µl *ROCK1* and 4 µl *ROCK2* siRNA complexed with 3.5 µl peptide followed by simultaneous delivery. Sequential knockdowns were also tested, with either siROCK1 or siROCK2 being delivered on the first day and siROCK2 or siROCk1 respectively being delivered after 24 hours.

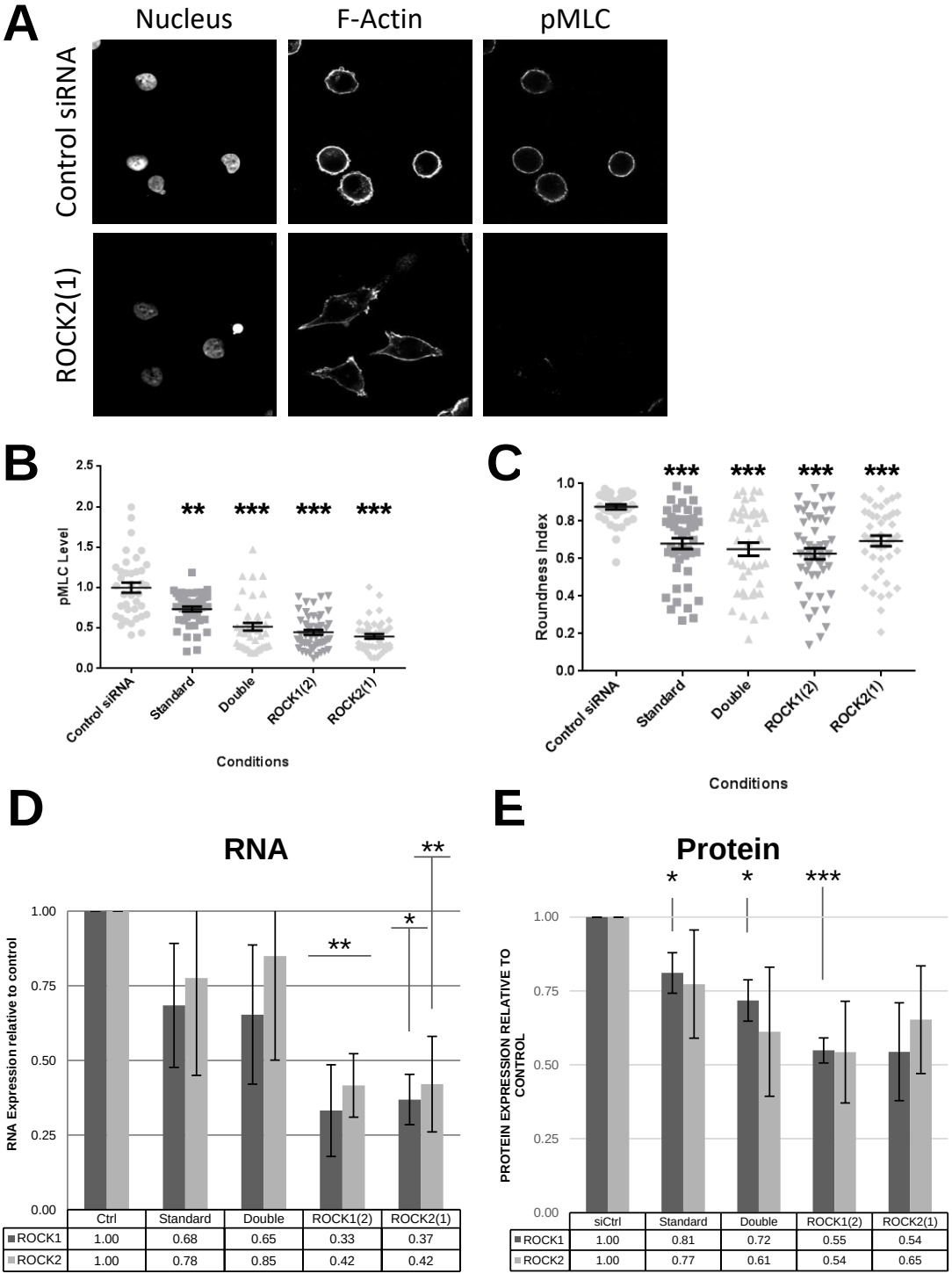

Figure 4.12. Optimisation of siRNA knockdowns of ROCK1 and ROCK2 in A37M2 cells. A) Representative Immunostaining and confocal imaging of A375M2 human melanoma cells after sequential knockdown of first ROCK2 then ROCK1. B) Quantification of p-MLC levels from confocal imaging data C) Quantification of roundness of melanoma cells after rock knockdowns with different siRNA delivery strategies D) validation of knockdown of ROCK by qPCR E) Validation of knockdown of ROCK by western blot. Bar charts show mean value and error bars represent standard error of the mean. All experiments are n=3. * p<0.05, ** p<0.01 ***p<0.001.

The sequential knockdown of *ROCK2* then *ROCK1* was observed to give the most efficient knockdown when checking p-MLC levels in immunofluorescence (Figure 4.12B). It was also similar to the *ROCK1* then *ROCK2* sequential knockdown in terms of RNA and Protein levels (Figure 4.12D, E). The sequential knockdown of *ROCK2* then *ROCK1* was also significantly more effective than the standard protocol showing a 33.9% +/- 5.6% less p-MLC (Figure 4.12C). For these reasons, the sequential knockdown of *ROCK2* then *ROCK1* was chosen as the protocol used for treating cells prior to NMR analysis.

4.2.7 Effects of the delivery peptide LAH4-1 on cellular metabolism

Challenging cells with a peptide/RNA complex could in itself alter the cellular metabolome and induce different stress responses. It has been shown previously that choline containing metabolites increase after transfection, probably due to membrane disruption during siRNA delivery(190). Delivery of other nanoparticles has also been observed to induce stress responses in cells(191). Metabolomic studies were conducted and OPLS-DA was performed between untreated A375M2 cells and those treated with non-targeting siRNA. A significant shift in the metabolome of the cells was observed (Q^2 = 0.795 vs random Q^2 =-0.405) (Figure 4.13A). There is a decrease of the methyl groups of lipids in the cells accompanied by an increase in unsaturated lipids (Figure 4.13B). We also observed an increase in glutamate, glutamine and glutathione. Finally, there was an increase in phosphocholine while choline and glycerophosphocholine decreased slightly. These observed changes are in accordance with previous observations(190) and demonstrate how not only DNA plasmid transfection but siRNA oligonucleotides can disrupt the cell membrane. This also demonstrates the importance of using non-targeting control siRNA as a control for future experiments.

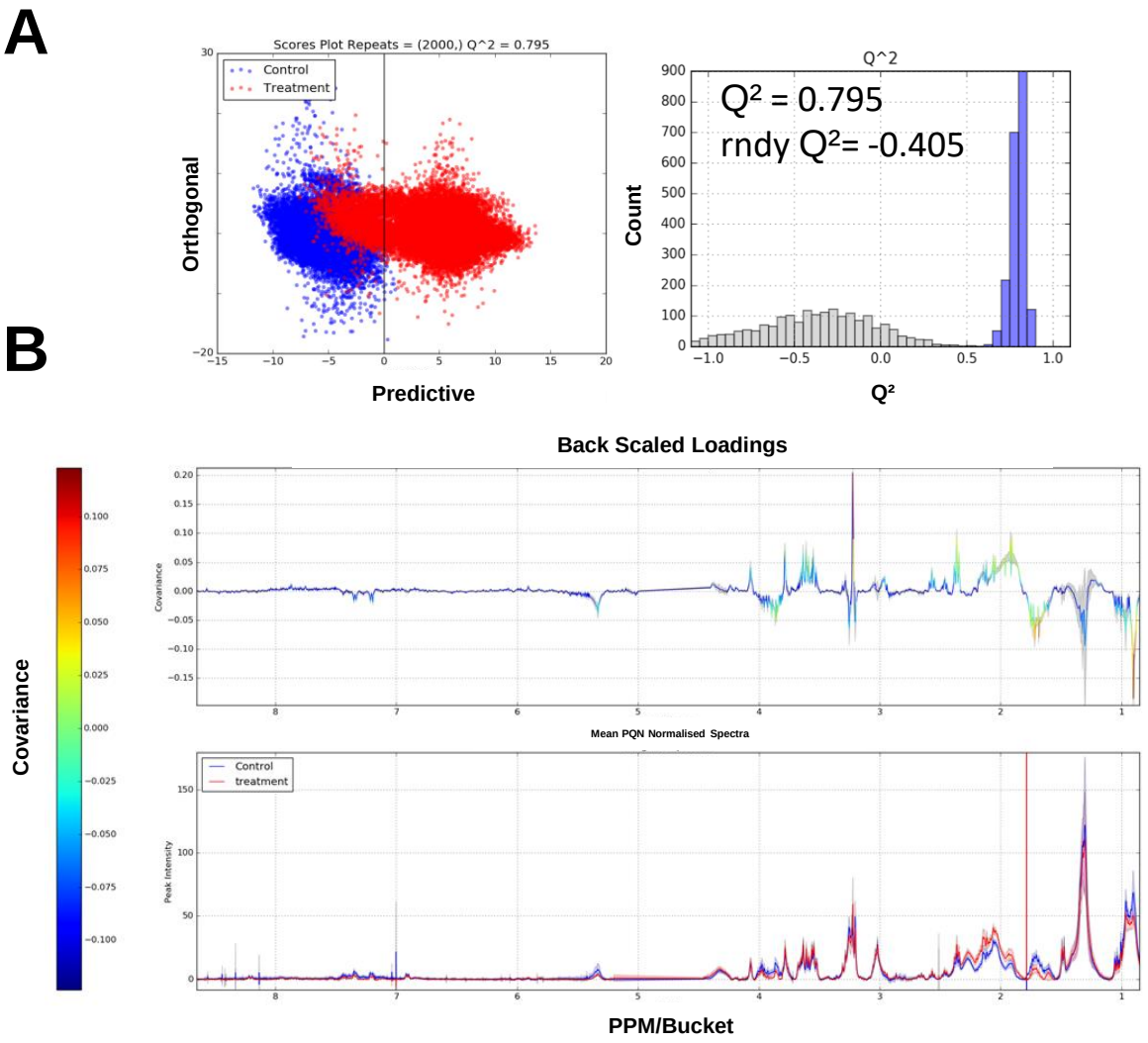

Figure 4.13. Metabolomic changes observed in A375M2 cells after transfection with LAH4-L1 Peptide/siRNA complex. A) scores plot showing statistical separation between treatment (blue) and control (red). Q^2 histogram showing Q^2 distribution of OPLS-DA models (blue) and OPLS-DA models of data with permutated classes (grey). B) back scale loadings plot and mean normalised HR-MAS NMR spectra illustrating difference in metabolome after treatment with peptide/RNA complex. Experiments were conducted n=3 times, and each experimental replicate containing three technical replicates, for a total of 9 samples per experimental condition.

4.2.8 ROCK1/2 Knockdown significantly alters Cellular metabolism

A clear separation between cell treated with non-targeting siRNA and cells treated with *ROCK* double knockdown was observed (Q^2 =0.747 vs. random Q^2 =-0.293, Figure 4.14A).

Increases in the CH2-CH2 bonds of lipids was observed, similar to that seen in the small molecule treatments. This was accompanied by a decrease in unsaturated lipids as well as decreases in glutamate and glutathione, which is also consistent with the small molecule treatments (Figure 4.14B). An increase in *myo*-inositol was observed in the siRNA treatments which is opposite when compared to the drug treatments.

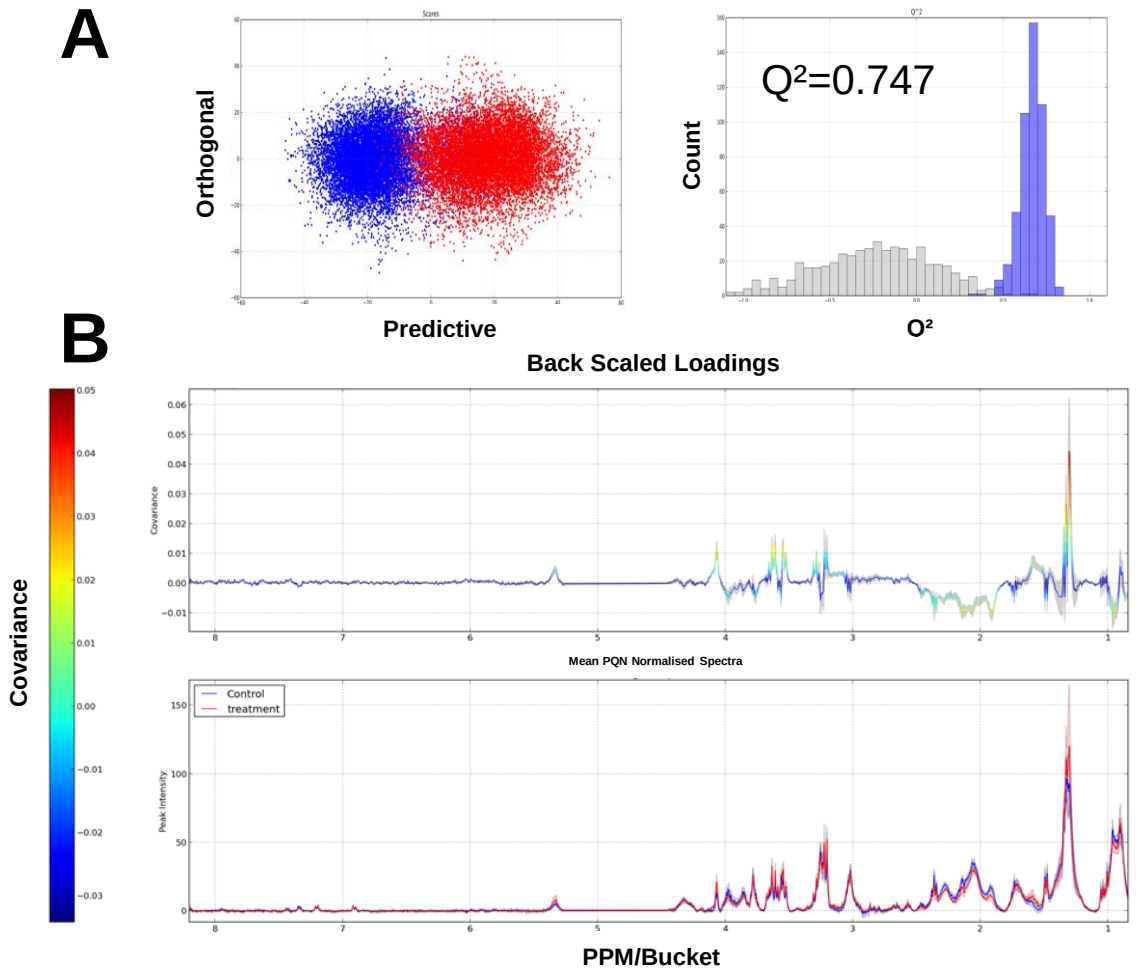

Figure 4.14. Metabolic changes observed in A375M2 cells after silencing ROCK1 and ROCK2 when compared to non-targeting siRNA. A) scores plot showing statistical separation between treatment (blue) and control (red). Q^2 histogram showing Q^2 distribution of OPLS-DA models (blue) and OPLS-DA models of data with permutated classes (grey). B) Back scaled loadings and mean normalised spectra highlighting differences between siCtrl treated A375M2 cells and siROCK treated cells. Experiments were conducted n=3 times, and each experimental replicate containing three technical replicates, for a total of 9 samples per experimental condition.

4.2.9 Cultured Melanomas Extracted from *ROCK* KO mice reveal differing metabolic profiles between *ROCK1* and *ROCK2* single KOs and *ROCK1/2* KO mice.

In this section we study an ex vivo model of murine melanoma where *ROCK* is genetically deleted. Murine melanoma samples were generated, profiled and provided for metabolomic studies by Dr. Sandra Kuemper. Previously reported data demonstrate that ROCK1 and ROCK2 play redundant roles in sustaining melanoma proliferation (5) and to stop proliferation both isoforms must be knocked out.

As discussed in the introduction of this chapter, murine melanoma samples where *ROCK* was knocked out either individually or together, were compared to wild-type melanomas (Figure 4.3). ROCK KOs show increased elongation and number of protrusions (Figure 4.4A) along with decreased levels of p-

MLC (Figure 4.4B). Knock out of both ROCKs in the murine model lead to no melanoma formation, therefore to study the metabolome of a double ROCK depletion individual ROCK KO melanomas were extracted, cultured and the other isoform of ROCK was knocked out *in vitro*. In every studied case significant changes in the metabolome were seen (ROCK1 $Q^2 = 0.628$, ROCK2 $Q^2 = 0.779$, ROCK1/2 $Q^2 = 0.678$) (Figure 4.15).

Individual KOs of ROCK show distinct metabolic profiles. ROCK1 KO melanomas showed increases in the CH2-CH2 bonds of lipids and phosphocholine while there was a decrease in alanine and *myo*-inositol (Figure 4.15A, Figure 4.16). ROCK2 KO had increases in valine, alanine, glutamine, *myo*-inositol and the methyl groups of lipids (Figure 4.15B, Figure 4.16). There was a decrease in choline and glycerophosphocholine while there was a slight increase in phosphocholine.

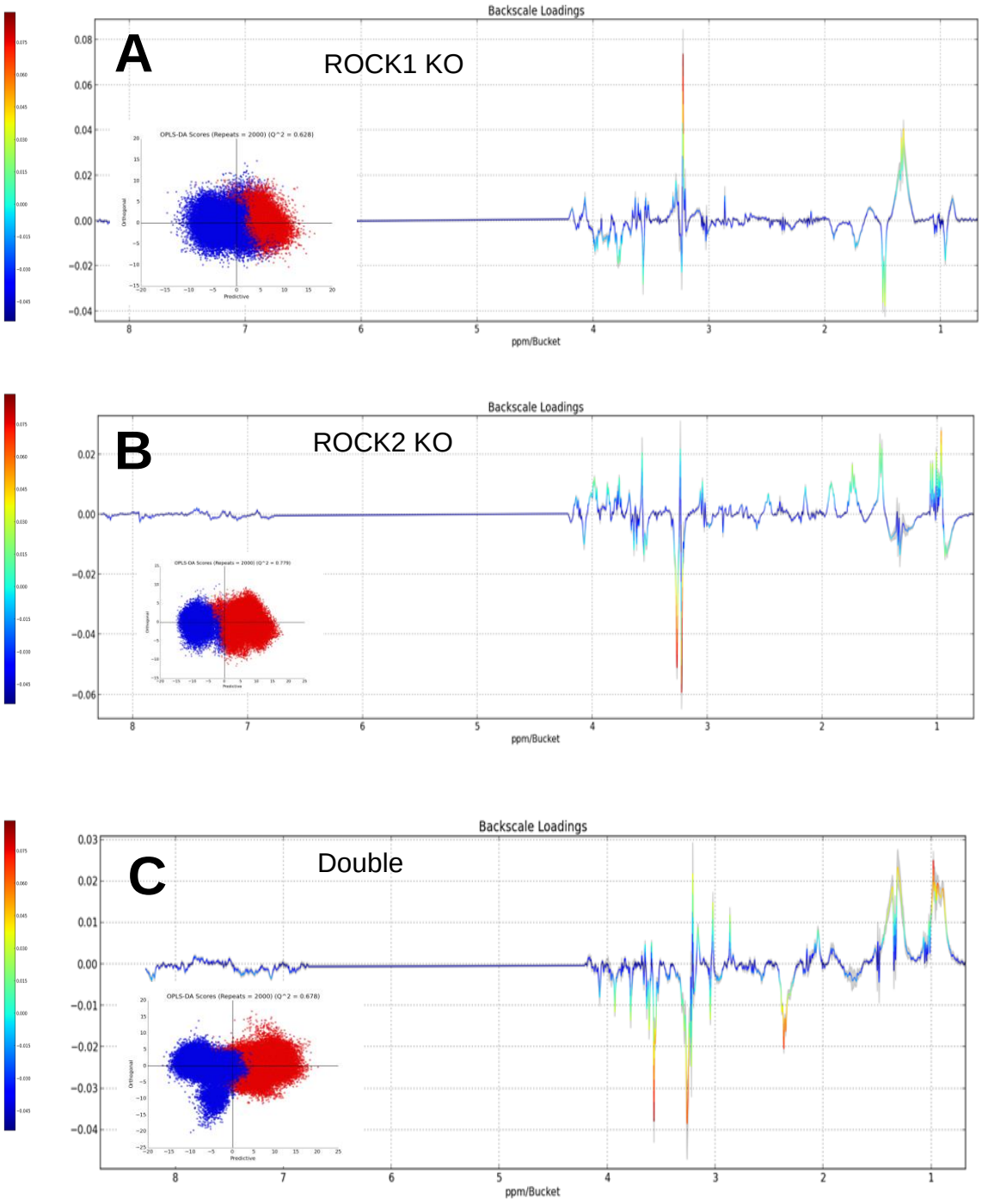

Figure 4.15. Back scale loadings plots with scores plots in-set of ROCK knocked murine melanomas. A) ROCK1 KO B) ROCK2 KO B) ROCK1/ROCK2 double KO Experiments were conducted n=3 times, and each experimental replicate containing three technical replicates, for a total of 9 samples per experimental condition.

The Double ROCK KO showed large increases in the methyl resonance of lipids and the CH2-CH2 resonance of lipids which is similar to that seen in the small molecule treatments and siRNA treated cells (Figure 4.15C, Figure 4.16). There was an increase in choline and a decrease in phosphocholine and glycerophosphocholine. The decrease in glutamate observed in the previous experiments targeting *ROCK* was only observed in the double KO and was not present in the single KO. This suggests that

ROCKs play redundant roles in glutamate metabolism (Figure 4.16). There was also an increase in creatine in the double KO not observed in the individual KOs

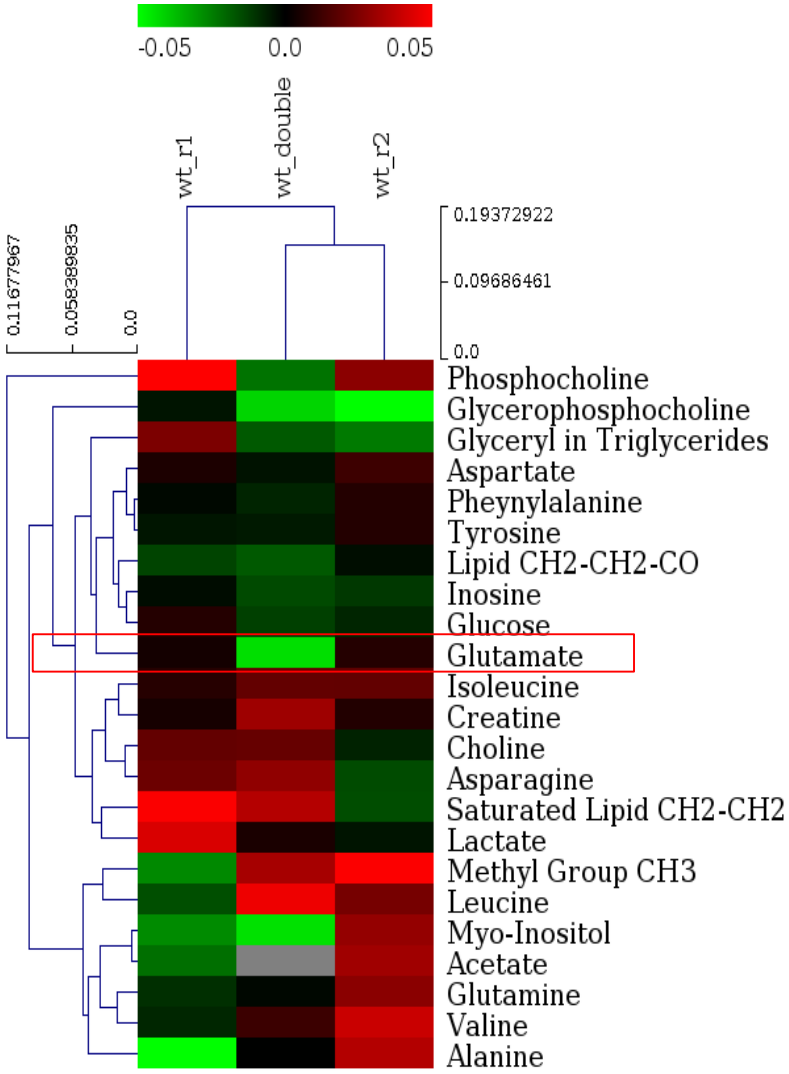

Figure 4.16. Heatmap of Mouse melanoma metabolic profiles. Hierarchical clustering of both metabolites and treatments was performed calculating Euclidean distance and average linkage. Colours represent covariance associated with treatment with lower covariance in green and higher covariance in red. Glutamate is circled in red to show functional redundancy of ROCk1 and ROCK2 in regulating intracellular glutamate levels. In the single KOs there is no change in glutamate, however in the double KO there is a reduction in glutamate levels.

There was an observed decrease glutamine and alanine in the ROCK1 KO while they were increased in the *ROCK2* KO. In the double *ROCK* KO there is no change in either glutamine or alanine compared to wild-type (Figure 4.16). This suggests that ROCK1 and ROCK2 play opposing roles in regulating glutamine and alanine metabolism. However, as glutamine and glutamate are so tightly intertwined in their metabolic regulation these findings will have to be further explored. Alanine is also tied to glutamine metabolism, it has been shown in glioblastoma that 60% of glutamine is secreted as lactate and alanine

(192). Future work could further investigate glutamine utilisation in melanomas using labelled metabolites.

ROCKs play redundant roles in regulating melanoma proliferation(5). How the individual isoforms regulate metabolism may shed light into potential mechanisms ROCK dependent regulation of proliferation. Metabolites that have subtle changes in individual KO while having larger changes in the double KO may suggest metabolic pathways that are redundantly regulated by both isoforms and suggest pathways critical to sustain melanoma proliferation. On the other hand, metabolites that show large changes in the individual KO suggest metabolites and pathways that are not critical to melanoma proliferation. In this set of experiments, glutamate stands out as there is no observed change in glutamate concentrations in the individual KO while in the double KO there is a large decrease in intracellular glutamate.

Condition	Q^2	Permutated Q^2
H1152 5 μM	0.246	-0.500
Y27632 10 μM	0.156	-0.487
Y27632 20 μM	0.193	-0.474
GSK269 0.1 μM	0.607	-0.355
GSK269 5 μM	0.554	-0.660
siROCK1/2	0.747	-0.476
ROCK1/2 Double KO	0.678	-0.486

Table 3. Q^2 values of Metabolomics Experiments presented in this chapter.

4.2.10 Silencing of *ROCK1* and *ROCK2* in A375M2 melanoma cells show similar metabolic profiles

Based on the results from the murine models of ROCK KO melanomas (Figure 4.15, Figure 4.16), similar experiments were conducted in A375M2 human melanomas to see if results could be replicated in a model of human melanoma. ROCK1 or ROCK2 expression was transiently silenced with siRNA and their metabolic profiles were studied.

It was observed that the individual knockdowns of ROCK1 and ROCK2 both had good separation of metabolic profiles when compared to siCtrl treated A375M2 cells (siROCK1 Q^2 = 0.679, siROCK2 Q^2 =0.535). Both conditions had very similar metabolic profiles to each other when compared to non-targeting siRNA treated cells (Figure 4.17A, B). In both comparisons, the majority of the separation between classes seems to be attributed to a reduction the CH2-CH2 and CH3 resonances of lipids. Other changes were quite subtle, with a possible increase in phosphocholine in both conditions.

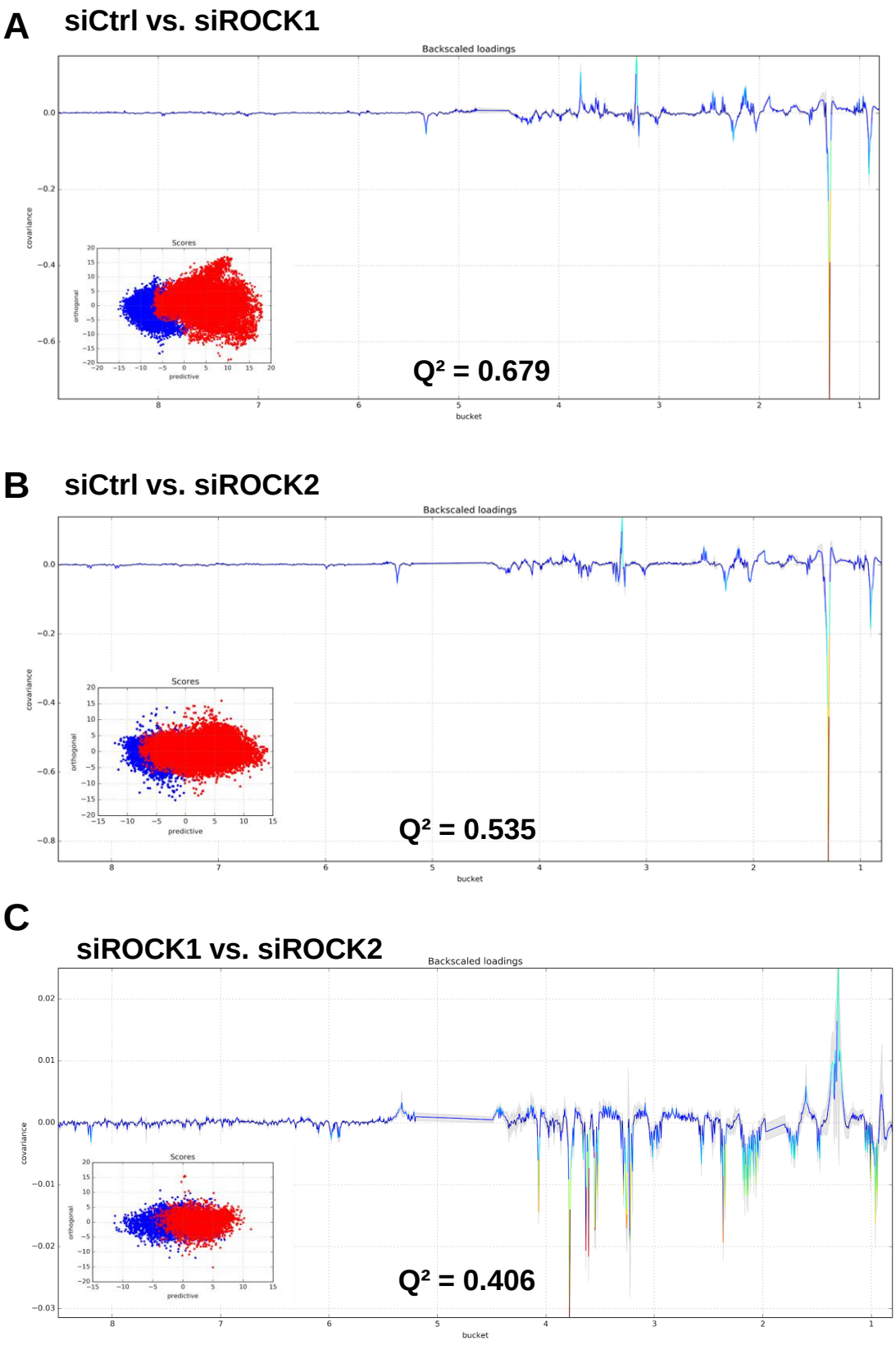

Figure 4.17. Back scaled loadings plots with scores plots and mean Q² values inset of OPLS-DA models of (A) siCtrl vs. siROCK1 (B) siCtrl vs. siROCK2 and (C) siROCK1 vs. siROCK2 A375M2 melanoma cells. Experiments were conducted n=3 times, and each experimental replicate containing three technical replicates, for a total of 9 samples per experimental condition.

A comparison between siROCK1 treated cells and siROCK2 treated cells was also performed and showed separation between classes (Q^2 = 0.406). The back scaled loading plot from this comparison shows a decrease in most metabolites in the siROCK2 condition compared to the siROCK1 condition with the exception of saturated lipids (Figure 4.17C). The data suggests that in A375M2 cells the changes in metabolism responsible by ROCK are mainly a factor of magnitude rather than of differential regulation of metabolism, with ROCK1 being more responsible for saturated lipids while ROCK2 driving increases in most other metabolites. This observation is partially consistent with what was observe in the murine models of *ROCK* KO melanoma. In those experiments it was seen that *ROCK1* KO led to increases in saturated lipids while *ROCK2* KO had no change in saturated lipids. The difference is that these changes in CH2-CH2 bonds of lipids were observed in the comparison with wild type melanomas while the changes observed in this section only became apparent when comparing siROCK1 and siROCK2 treated melanoma cells. In the comparison with siCtrl treated cells, there was a general decrease in lipids.

When comparing siROCK1 and siROCK2 treated human melanoma cells, we still observed a significant difference in the metabolic profiles (Figure 4.17C). This is very different to the effects observed in the murine model shown in section 4.2.9 (Figure 4.15, Figure 4.16), where we observed that individual KOs of ROCK in the murine models led to very different metabolic profiles. Compared to wild-type melanoma.

The difference between results could be due to weak silencing of *ROCK1* and *ROCK2* expression; data validating the knockdown of *ROCK1* and *ROCK2* are not currently available. It could also be explained by the very different systems of murine melanomas and human melanoma cells lines used.

4.2.11 Hierarchical clustering of metabolomics data strongly correlates with IC50 data of ROCK SMI

Hierarchical cluster analysis of the generated metabolomic data show that the metabolic profile of the cells treated with the more specific ROCK inhibitor GSK269, clusters more closely to the genetic alterations of ROCK than the metabolic profile of cells treated with the less specific inhibitors H1152 and Y27362 (Figure 4.18). The siRNA *ROCK* treatment clustered closest with the GSK269 treatment. Together they then formed a cluster with the *ROCK* double KO in the murine melanoma cells. It is interesting to note that the metabolic profiles of the treatments correlate so closely despite coming from different species. Finally, H1152 and Y27362 clustered furthest from the other treatments which is in agreement with the smaller metabolic changes observed in the OPLS-DA comparisons.

Studying the ratios of some critical metabolites can also reveal information about the underlying biology taking place in the cells. For example, the alanine/lactate (ala/lac) ratio is known as a marker for the redox state of cells as both alanine and lactate are produced form pyruvate and are coupled with NAD^+ and NADH (193). From our data, only H1152 alters ala/lac (Figure 7.5 in Appendix B).

Another example is the glycerophosphocholine/phosphocholine (GPC/PC) ratio, which uses the knowledge that malignant tissues contain more phosphocholine with an accompanying decrease in (194). From our studies, we did not observe great changes in GPC/PC after ROCK inhibitor treatments, however there was a decrease in GPC/PC in mouse melanoma cells were ROCK was knocked out (Figure 7.6 in Appendix B). In the time course experiments with GSK269, we observed there was an initial increase of GPC and decrease of PC at 4 and 8 hours, while at 24 hours this change had stabilised (Figure 4.11). These changes in GPC and PC after ROCK inhibition on a short time scale are consistent with the hypothesis that ROCK activity is tied to a malignant phenotype. The fact that this is not observed at 24 hours in the time-course experiments with GSK269 could also explain the lack of changes in GPC/PC observed in other ROCK inhibitors experiments at 24 hours.

From Figure 4.18 we can observe that most conditions correlated with a decrease in glutamate concentrations, which becomes the rationale for further investigation into glutamine and glutamate metabolism in melanoma in the following chapters. Full spectral overlays of the NMR spectra of glutamine, glutamate and glutathione can be found in Appendix B (Figure 7.7).

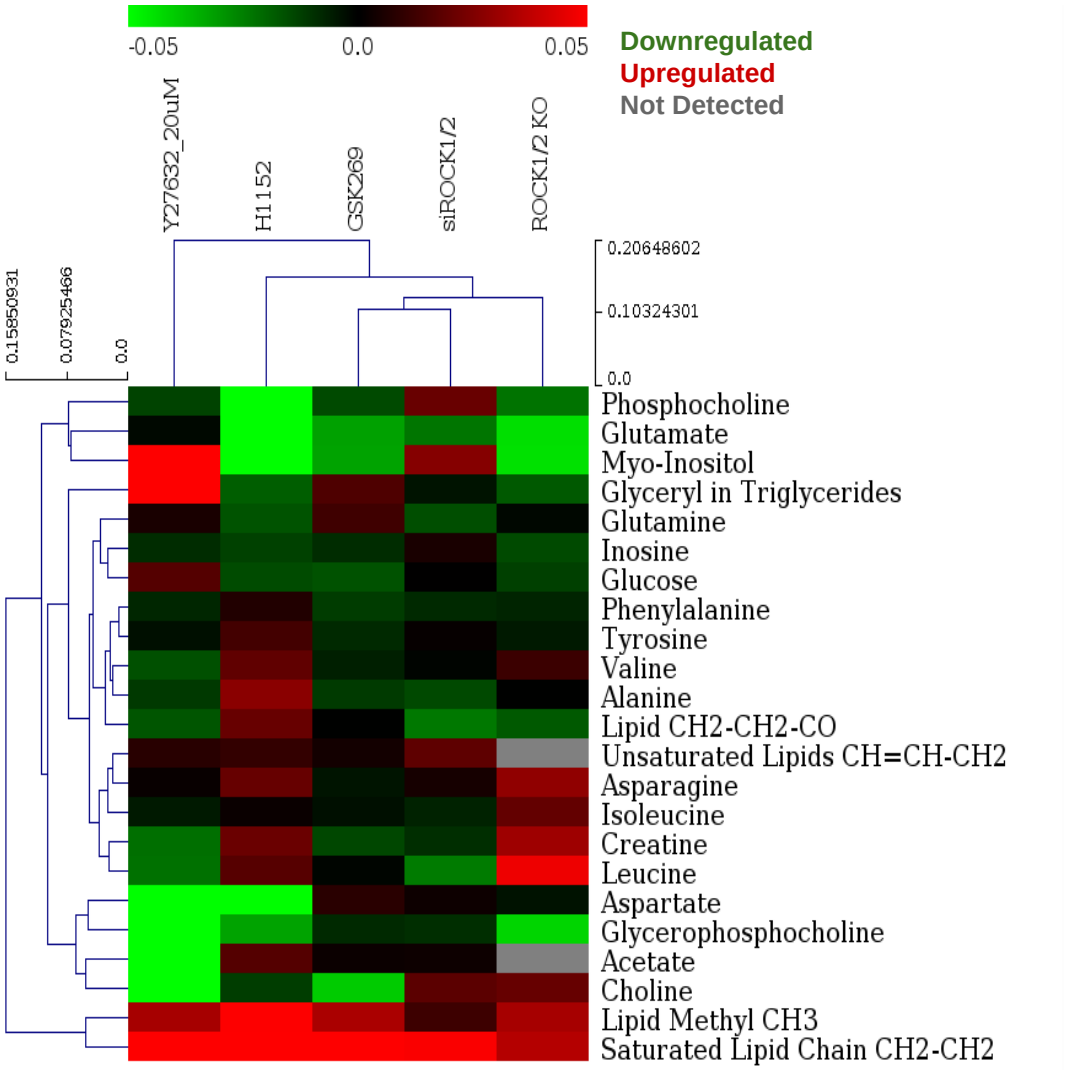

Figure 4.18. Heat map of all ROCK cellular metabolomic data with hierarchical clustering. Hierarchical clustering of both metabolites and treatments was performed calculating Euclidean distance and average linkage.

4.2.12 Metabolomics of Spent media reveal Consumption patterns of melanoma cells in culture

Thus far, work has been conducted looking solely at the intracellular metabolites. We observed significant and consistent changes in metabolism of melanoma cells after altering ROCK activity and expression. To gain a broader picture of the metabolism of the cells we studied the spent media of A375M2 cells after ROCK inhibition or silencing. Work was conducted aiming to understand how ROCK activity might affect how melanoma cells are using the cell culture media and secreting metabolites into the spent media. It has been seen that melanomas secrete glutamate into the tumour microenvironment (195-197) and the Warburg effect is observed in many tumour types (16).

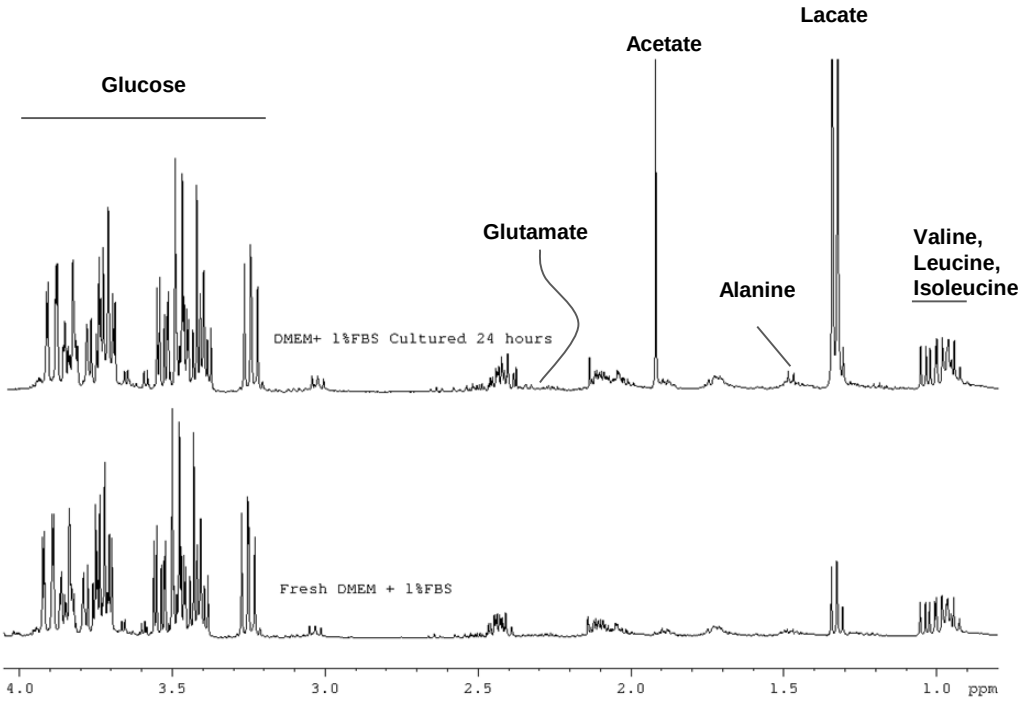

Figure 4.19. Representative NMR Spectra comparing fresh and spent cell culture media after siRNA transfection. Top) Spent DMEM cell culture media from A375M2 human melanoma cells after transfection. The large acetate peak is due to the counter-ion from the cationic peptide transfection vector used in the transfection process. Bottom) Fresh DMEM cell culture media.

4.2.13 Melanoma Cells consume more glucose, secrete more lactate and secrete less glutamate after ROCK inhibition

An initial observation of the NMR spectra generated from fresh cell culture media compared to spent cell culture media reveal that A375M2 melanoma cells secrete large amounts of lactic acid, and to a lesser extent alanine and glutamate (Figure 4.19). In the figure there is a substantial acetate peak which is a residual from the transfection protocol. The transfection vector LAH4-L1 is dissolved in acetic acid to displace trifluoroacetic acid as a counter ion priori to lyophilisation and the acetate is present in solution when the peptide-siRNA complexes are produced.

An issue that becomes apparent when working with spent cell culture media is that glutamine cyclises into pyroglutamate. This has been reported in other metabolomic work with blood serum (198) and has been suggested to be due to as of yet unidentified factors in serum. The reasons for this phenomenon has not been explained as of yet. The cell culture media used in these studies contained between 1%-10% FBS. To compensate for the effects of glutamine cyclisation of glutamine in NMR studies Nagana Gowda *et al* (198) suggest summing the peak intensities for both glutamine and pyroglutamate to give

a fair view on glutamine levels in the presence of serum. In this work this step has not been taken with the spent media studies, however this phenomenon is taken into account when discussing future results. Analysis of fresh media used in our experiments showed that there was 0.39 mM pyroglutamate present in the media before starting experiments. This demonstrates the need in future work to add fresh glutamine just prior to experiments in the cell culture experiments rather than relying on media supplemented with glutamine. A table of assignments made from the cell culture NMR spectra can be found in Appendix B.

For more in depth statistical analysis of the metabolites consumed as well as secreted, nine replicates from cells treated with DMSO and cells treated with GSK269 at 5 µM were collected and analysed by ^{1}H 1D liquid NMR.

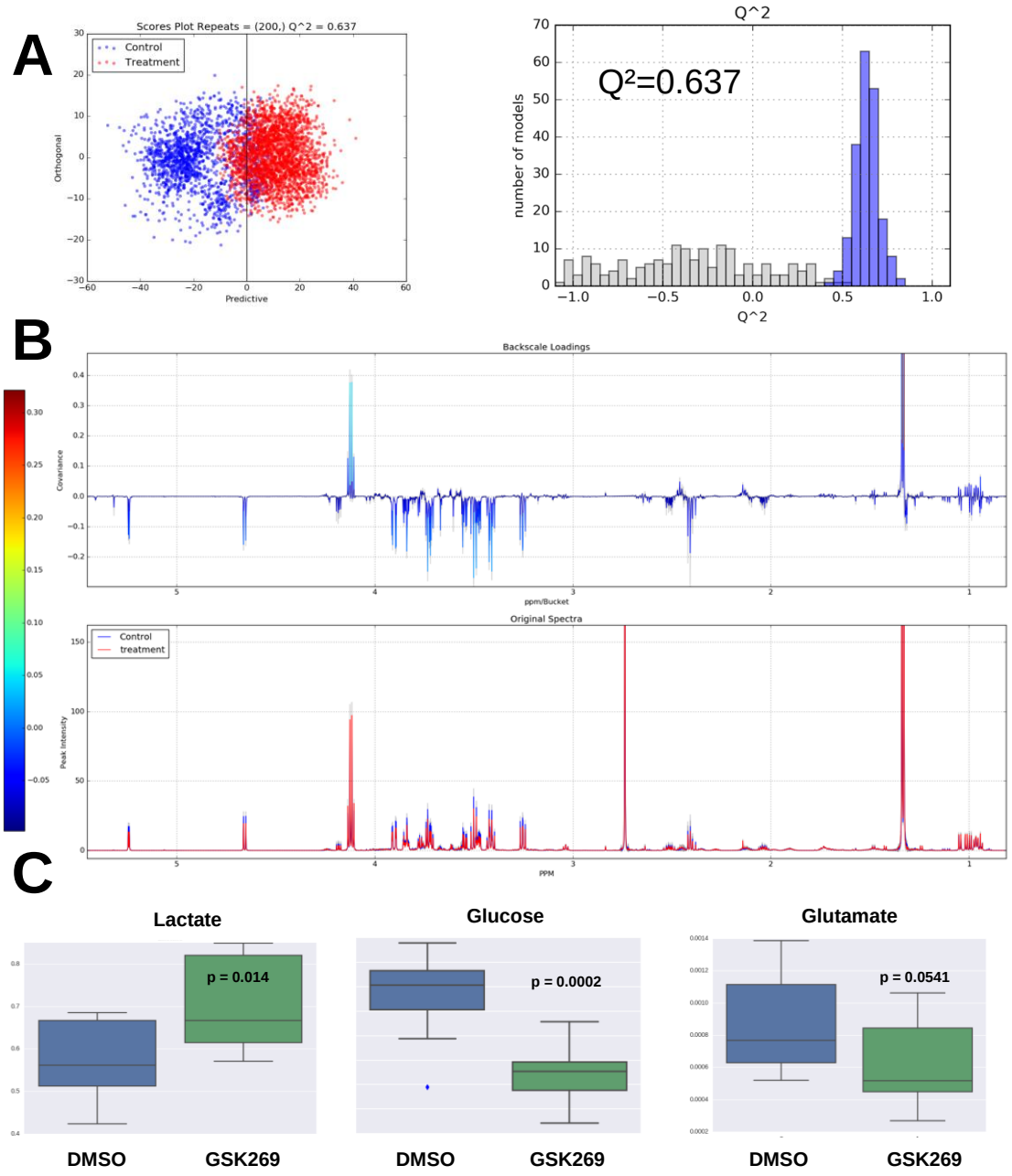

Figure 4.20. NMR Metabolomics of spent cell culture media shows the ROCK inhibitor GSK269 induces significant changes in glucose and glutamate metabolism in A375M2 cells. OPLS-DA of spent 1% FBS DMEM cell culture media after ROCK inhibition with GSK269. A) Scores plot and Q² histogram of OPLS-DA models of spent media comparing control to GSK269 treated cells. B) back scale loadings plot and mean normalised spectra C) box plots for the median normalised peak intensity of select metabolites (Lactate, Glucose and Glutamate) showing significant changes in metabolite consumption and secretion patterns. Experiments were conducted n=3 times, and each experimental replicate containing three technical replicates, for a total of 9 samples per experimental condition.

OPLS-DA of Spent media from cells treated with DMSO vehicle control and ROCK inhibitor GSK269 5 μM for 24 hours showed that there is a clear separation between the two treatments (Q^2 = 0.637 Figure 4.20A, B). There was a residual DMSO peak present in the NMR spectra at 2.71 ppm as GSK269 is dissolved in DMSO. The residual peak was excluded from the analysis along with the residual water peak. ROCK inhibition led to an increase in the amount of secreted lactic acid as well as a decrease in

glucose, meaning the cells were taking up more glucose after ROCK inhibition. There was also a reduction in the amount of glutamate present in the spectra (Figure 4.20C). Univariate analysis of the peak intensity corresponding to glucose, lactate and glutamate respectively show a mean 20.68% decrease, 26.49% increase and 27.5% decrease (Figure 4.20C). There is a 3-fold increase in the lactate/glucose ratio of GSK269 treated cells compared to control (mean lac/glc ratio control = 4.99, GSK269 = 14.54).

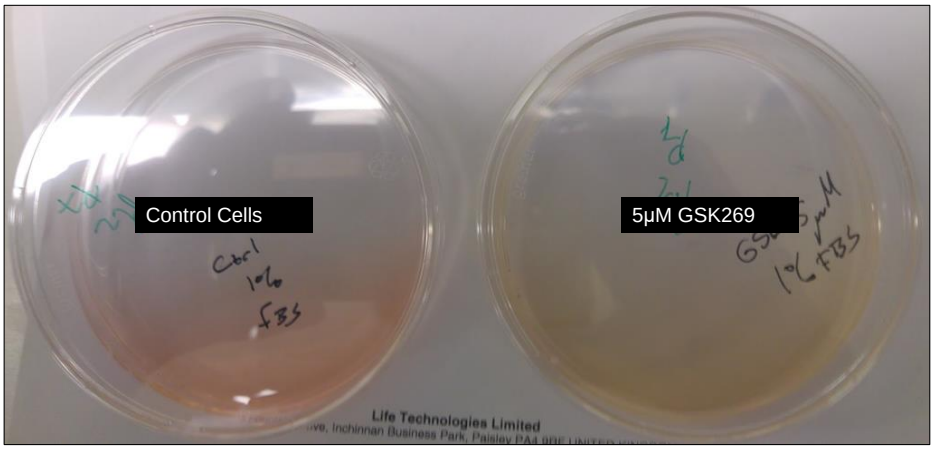

Figure 4.21. Melanoma cells treated with ROCK inhibitors secrete more lactic acid. Cell culture plates containing A375M2 cells after 24-hour treatment of either DMSO control (left) or 5 μM GSK269 (right). The pH sensor Phenol red turns yellow in acidic environments and it is seen that the cell culture media of ROCK inhibitor treated cells is a markedly different colour from control cells.

These are striking findings as the proliferative potential of melanoma cells are blocked by ROCK inhibition, yet they are upregulating their dependence on glucose fermentation as an energy source compared to control cells. These findings were also confirmed as the pH of the spent cell culture media was reduced due to the increased secretion of lactic acid (Figure 4.21). This could be a part of the response to ROCK inhibition. The reduction in the amount of glutamate in the media is more difficult to justify. It is borderline significant ($p = 0.0541$) and the change in glutamate could be explained either as an effect of ROCK inhibition or could simply be due to the reduced cell number seen after 24 hours of ROCK inhibition (Figure 4.24A).

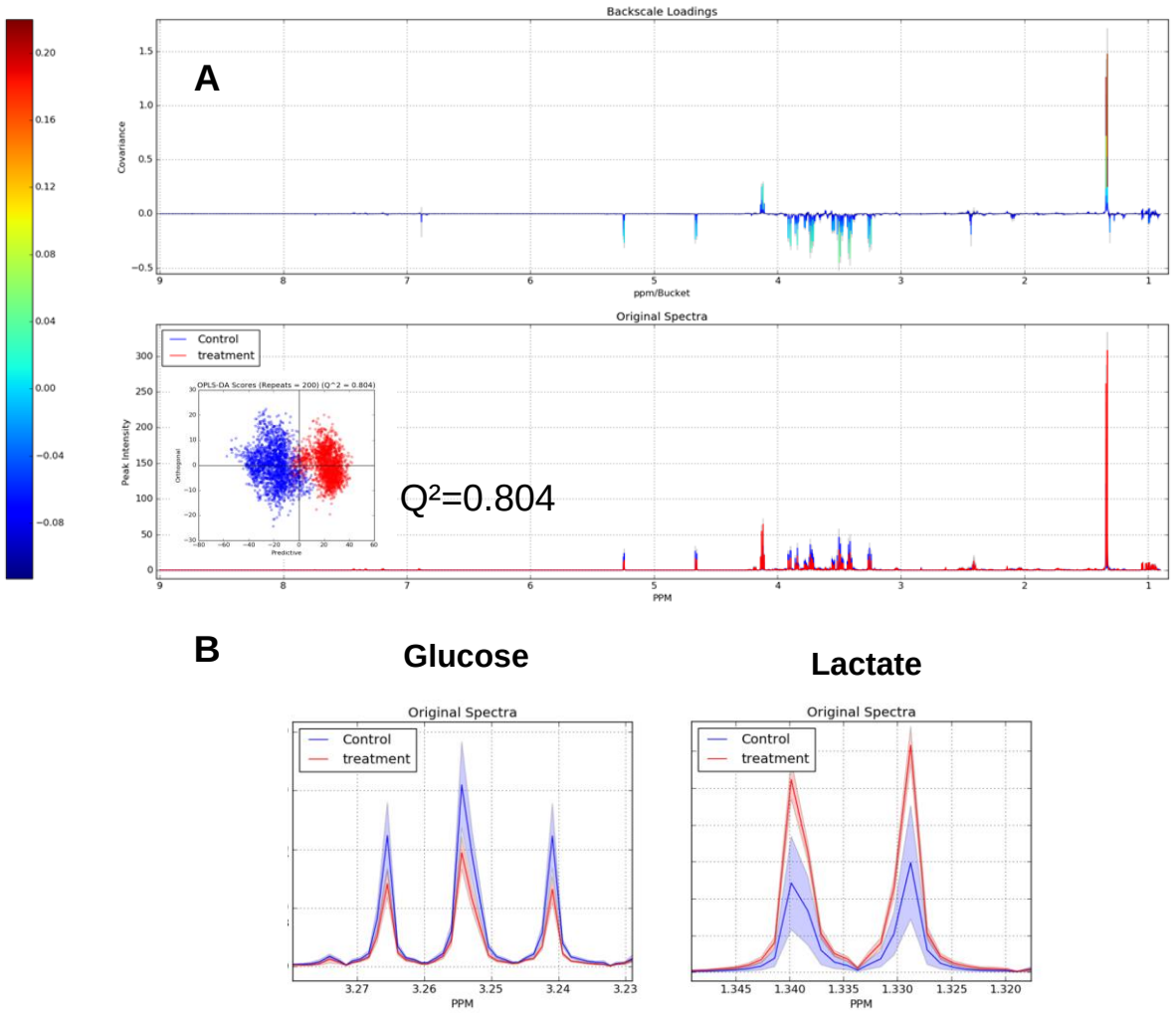

Figure 4.22. Spent cell culture media experiments were repeated at high growth conditions of 10% FBS and show similar findings to 1% FBS conditions. OPLS-DA of spent 10% FBS DMEM cell culture media after ROCK inhibition with GSK269. A) back scale loadings plot and mean PQN normalised spectra with the OPLS-DA scores plot inlayed. B) Zoom of mean normalised spectra on the resonances of Glucose (left) and lactate (right). Mean spectra (average spectra) with standard deviation (shaded) is plotted for DMSO treated cells (blue) compared to GSK269 treated cells (red). Experiments were conducted n=3 times, and each experimental replicate containing three technical replicates, for a total of 9 samples per experimental condition.

NMR metabolomics were repeated at the higher growth condition of 10% FBS (Figure 4.22) and showed that at high growth conditions this pattern was even greater than experiments conducted at 1% FBS conditions. We again observed increased consumption of glucose and increased secretion of lactate into the spent cell culture media in GSK269 treated cells compared to DMSO control treated cells (Figure 4.22B). Estimations of the concentrations of lactate and glucose in the spent media performed with Chenomx showed an average of 5.82 mM glucose in control conditions compared to 3.71 mM glucose in GSK269 treated conditions, a 36.3% reduction in the uptake of glucose. Likewise, there were 11.76 mM lactate in control conditions compared to 27.90 mM lactate in GSK269 treated conditions, an effective increase of 2.3-fold increase of lactate. The media used for all experiments contains 10 mM

glucose and 1 mM glutamine. The mean lactate/glucose ratio in control conditions was 2.67 while in GSK269 treated conditions mean lac/glc was 7.73. Additionally, the relative rate of lactate production over glucose consumption ([Lactate]/([Glucose in fresh media] –[Final Glucose]) was 2.81 for control treated cells and increased 1.5-fold in GSK treated cells to 4.44. This again points to a shift in the Warburg effect after ROCK inhibition.

4.2.14 Network Analysis of NMR metabolomics and transcriptome data suggest Glutamine/Glutamate pathways as most significantly regulated by ROCK activity

To conclude this section of work and to generate a hypothesis for future work, we aimed to understand which metabolic pathways were most altered based on the data collected thus far. We were aided by the data presented in the study by Sanz-Moreno *et al* (140). In this work they performed a microarray analysis of A375M2 cells seeded onto a thick collagen matrix and studied the transcriptomic profile of cells after ROCK inhibition by H1152 for 16 hours. To obtain a deeper understanding of the cross-talk between metabolism and gene expression in our systems we made use of the publicly available data (GSM586484–GSM586501) to integrate transcriptome data with the generated NMR metabolomic data.

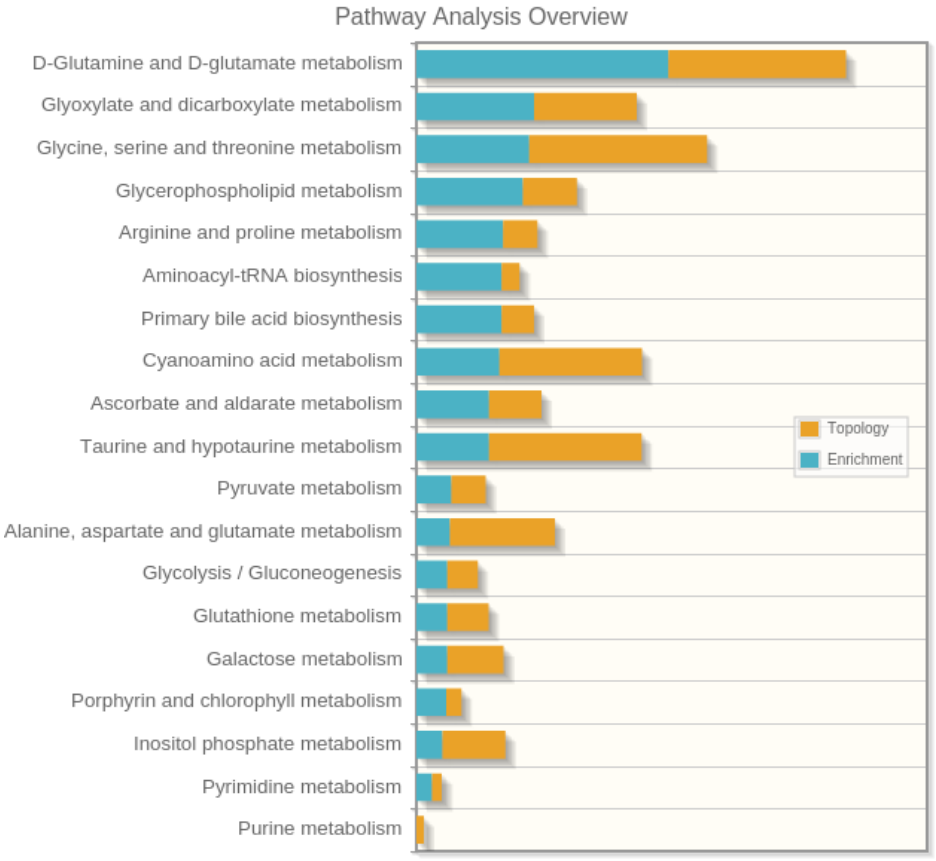

Figure 4.23. Pathway Analysis of metabolic pathways most regulated by ROCK activity from metabolomic and transcriptomic data. Pathways are ranked in descending order by enrichment score shown in blue. Also shown is the topology score of each pathway in yellow. Pathway analysis was performed in Metaboanalyst 3.0 web service.

Integrated pathway analysis was performed using the Metaboanalyst 3.0 web tool (173)(Figure 4.23). All genes that were downregulated after H1152 treatment along with downregulated metabolites after treatment in the same conditions were used for analysis. Metabolites were selected from the OPLS-DA back-scaled loadings plot The metabolites selected for pathway analysis were Aspartate, Choline, Glucose, Glutamate, Glutamine, Glycerophosphocholine, Inosine, *Myo*-inositol, Phosphocholine, and Isoleucine. Glyceryl in Triglycerides, which was also downregulated in after H1152 treatment, was not recognised in Metaboanalyst and was thus excluded from pathway analysis.

The hypergeometric test and degree centrality analysis was selected for enrichment analysis and topology analysis respectively.

Pathway analysis reveal that glutamine/glutamate metabolism was the most regulated metabolic pathway by ROCK activity from our dataset. This was followed by glyoxylate and dicarboxylate metabolism, glycine, serine and threonine metabolism, glycerophsopholipid metabolism and arginine and proline metabolism (Figure 4.23). This suggested to use that glutamine/glutamate metabolism is the most regulated metabolic pathway by ROCK activity and formed the hypothesis upon which future work was based.

4.2.15 ROCK activity and exogenous glutamine is required for melanoma cell proliferation in human and mouse melanoma

With the information that ROCK could be regulating glutamine and glutamate metabolism we then studied how A375M2 human melanoma cells proliferate in absence of exogenous glutamine. It was seen that after 24 hours there is already a trend of less proliferation which becomes more pronounced at 48 hours (Figure 4.24). It was seen that melanoma cells cannot proliferate in absence of glutamine.

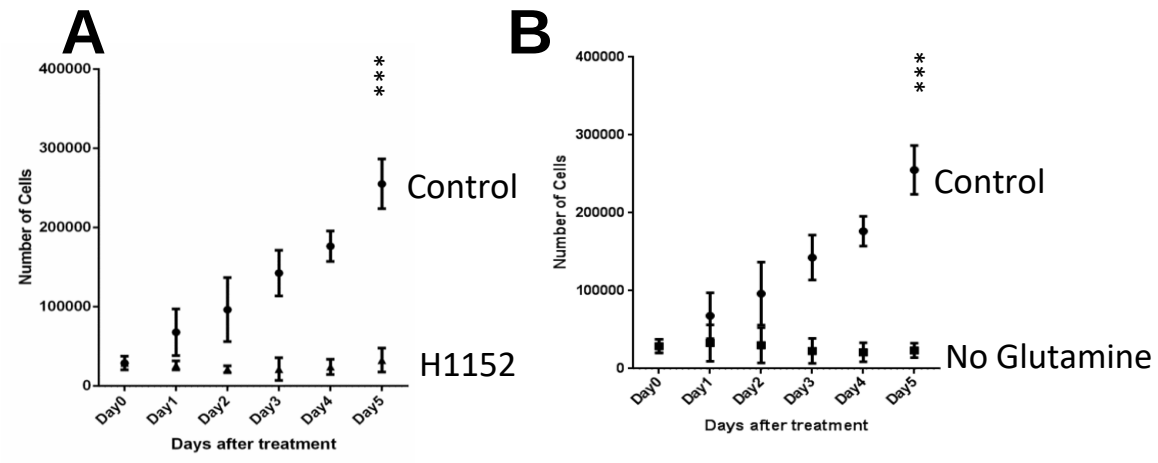

Figure 4.24. ROCK and exogenous glutamine are required for A375M2 melanoma proliferation *in vitro*. A) A375M2 cells treated every 24 hours with 5 μM H1152 over 5 days show near complete termination of proliferation. B) Cells cultured in glutamine free media also completely halt proliferation. experiments done in triplicate. data points are mean cell number and error bars represent Standard error of the mean. Student's t-test, *** $p<0.001$. Experiments are n=3.

4.3 Discussion

In this chapter we aimed to understand if and how ROCK regulates melanoma cell metabolism. We studied the metabolic profiles of cells after interfering with ROCK activity or expression in human and mouse melanomas. We observe that ROCK does alter the metabolic profiles of cells in each condition studied. There were many metabolic changes observed ranging from lipid metabolism, amino acid metabolism and carbohydrate metabolism. In this section we will discuss the presented data, aiming to give context to our findings and suggest future research directions.

4.3.1 ROCK as a therapeutic target of melanoma

In recent years ROCK has been suggested to be a potential therapeutic target for malignant melanoma either alone or in combination with currently available treatments such as BRAF inhibitors (3,4,199). Interfering with ROCK activity has been shown to block melanoma proliferation (5) and metastasis in *in vitro* models of melanoma (3). While there are a couple of studies implicating Rho/ROCK signalling in cellular metabolism (156) and cell transformation (158), to date there has been no -omic level study as to whether ROCK regulates melanoma metabolism.

In this chapter we sought to investigate if and how ROCK re-wires cellular metabolism. We designed our study to investigate the cellular metabolome using three different strategies in order to account for short-comings with each experimental system such as off target effects of small molecule inhibitors and of genetic alterations of *ROCK* expression by siRNA (200,201). Understanding the differences between targeting strategies could also have implications for future studies. Additionally, transient knockdowns by siRNA do not perfectly ablate protein expression and therefore phenotypic studies must be taken with caution. Studies were also conducted on genetic KOs of *ROCK* in models of spontaneously developed murine melanomas. The data collected from this study show surprisingly similar results to those found in the transient knockdowns in A375M2 human melanoma cell line. Hierarchical clustering of the data demonstrates it clustering more closely to GSK269 and the siRNA knockdown than the data from older ROCK inhibitors (Figure 4.18).

In all cases studied where ROCK activity or expression was blocked we observed significant changes in the metabolic profile of melanoma cells. Consistent changes observed in each experimental set up were increases in the CH2-CH2 bonds of lipids, and decreases in the intracellular concentrations of glutamate.

Gaining a deeper understanding of the biochemistry of melanoma cells driven by Rho/ROCK signalling can point to additional opportunities in terms of designing therapies for melanoma. In particular glutamine and glutamate metabolism may be an attractive target for future cancer therapies.

4.3.2 Glutamine/glutamate metabolism

Pathway and network analysis from our studies suggest that glutamine/glutamate metabolism is the metabolic pathway most affected by ROCK. This was demonstrated both when analysing metabolomic data alone and when integrated with transcriptomic data from experiments in similar conditions. Glutamine is generally a non-essential amino-acid although in various cancer types a requirement for exogenous glutamine to sustain proliferation has been observed. This phenomenon is call 'glutamine addiction' (22,202) and has been established for a variety of cancer types, including melanoma (203). Glutamine is the key nitrogen donor for the de-novo synthesis of a variety of macromolecules, such as most amino-acids excluding proline (Figure 4.25). It has also been suggested that reliance on glutamine may serve as a mechanism for acid-resistance in the case of increased lactate secretion seen in cancer cells displaying the Warburg effect (204). Glutamine addiction in melanomas was investigated by Ratnikov *et al* (195) who demonstrated that melanomas mainly used glutamine through the TCA cycle and produced aspartate as melanoma had limited ability to use exogenous aspartate. In addition, melanocytes could grow without exogenous glutamine.

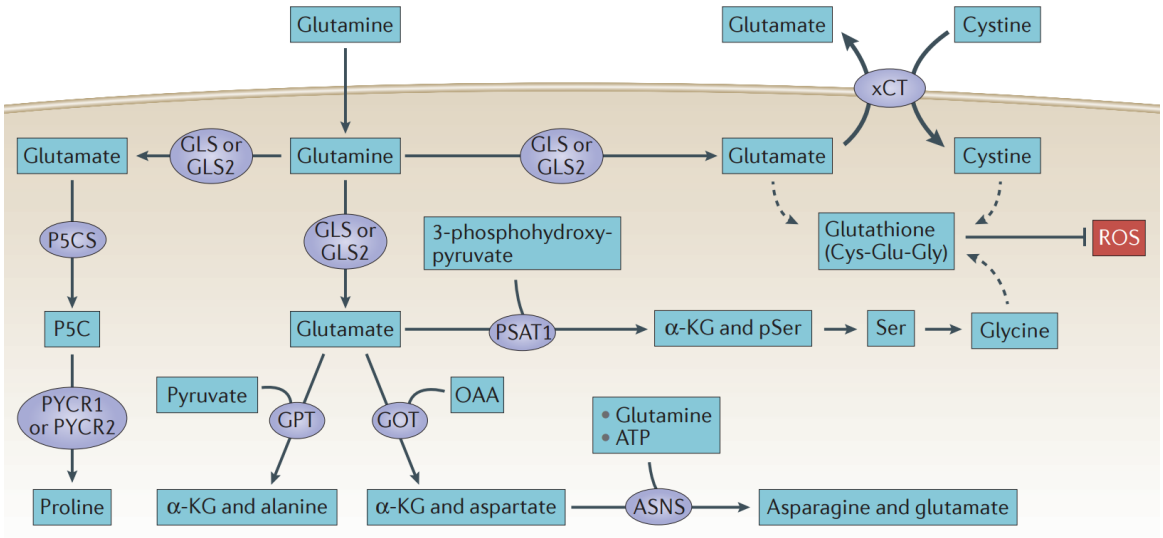

Figure 4.25. Glutamine metabolism in cancer and its role in maintaining amino acid pools and antioxidant homeostasis. Exogenous glutamine is essential for many cancer cells to sustain growth and proliferation. Figure reproduced with permission from (205)

Rho signalling has already been linked to glutamine metabolism as Rho dependent transformation of fibroblasts and the growth of breast and B cell lymphomas(158), however a mechanism was never proposed.

There is some evidence that metabolites may influence not only cell proliferation but morphology and migration as well. Fu *et al* (206) studied how amino acid restriction of melanoma cell lines affect cell attachment and actin cytoskeletal remodelling. They observed in A375 human melanoma cells that restriction of glutamine did not affect attachment, while restriction of phenylalanine (Phe) or tyrosine (Tyr) significantly reduced cell attachment to laminin and fibronectin. They also observed that cell morphology was affected by Gln/Phe/Tyr restriction by affecting the expression of Integrin α5.

In our work we saw that intracellular glutamate was consistently regulated by ROCK, in addition, we observed that glutamate was secreted by melanoma cells into the extracellular environment. In the murine melanomas cells studied, we observed that glutamate was unchanged in the individual KOs while having dramatic changes in the double KO. This suggests that glutamate is redundantly regulated by the different ROCK isoforms and could play an important role in proliferation. Glutamate is also a very important signalling molecule and both glutamine and glutamate are also essential precursors to glutathione synthesis which is discussed below.

4.3.3 Glutamate Signalling in Melanoma?

Glutamate has been observed to be altered by ROCK activity both in our whole cell studies as well as in the spent media studies. Glutamate is not only an essential part of the process of using glutamine as an energy source but is a very important signalling molecule as well. Cancer cell metabolism has also been known to use metabolites such as glutamate and lactate for paracrine or autocrine signalling (16,207). Glutamate is the primary excitatory neurotransmitter involved in a variety of neural functions such as memory and synaptic plasticity (208).

Glutamate signalling is mediated by transmembrane proteins known as glutamate receptors (208) (Figure 4.26).

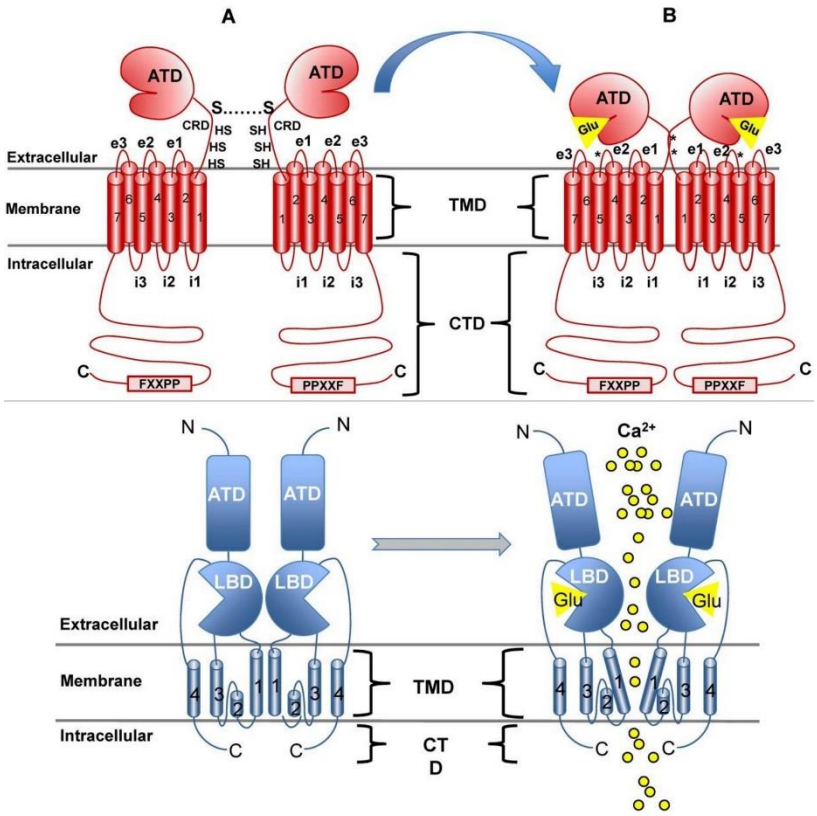

Figure 4.26. Structure and function of glutamate receptors. Top – metabotropic glutamate receptors are G-protein coupled receptors activated by glutamate binding. Activation by glutamate leads to downstream signalling. Bottom – ionotropic glutamate receptors are ion channels activated by glutamate. They are classically known to be involved in calcium signalling. Figure adapted from (208) under the Creative Commons Attribution (CC-BY-NC) License.

External glutamate binds to these receptors and induces downstream signalling. Glutamate receptors are divided into two major classes according to their signalling pathways. Metabotropic glutamate receptors (mGluRs), are G-protein coupled receptors while Ionotropic glutamate receptors (iGlurRs). mGluRs are ion channels (Figure 4.27).Ionotropic receptors are subdivided into three groups according to the original agonists that were found to have specific binding (209): NMDA, AMPA and kainate. AMPA and NMDA receptors are better understood while less is known about kainate receptors (210).

There is strong evidence that glutamate signalling may play a role in melanomas and other cancers. Metabotropic glutamate receptors were the first to be identified as potential therapeutic targets in cancer. The *GRM1* gene, which codes for metabotropic glutamate receptor subtype 1 (mGluR-1) has been shown to be essential for the growth and migration of murine and human melanoma (211,212), it has been seen that mice with *GRM1* overexpression spontaneously develop melanoma (213) and there has even been an initial clinical trial investigating the feasibility of using a glutamate activated sodium channel blocker (Riuzole) in patients with resectable stage 3 and 4 melanoma (214). The

expression of *GRM5*, another metabotropic glutamate receptor, has also been observed to lead to the development of melanoma in mice (215).

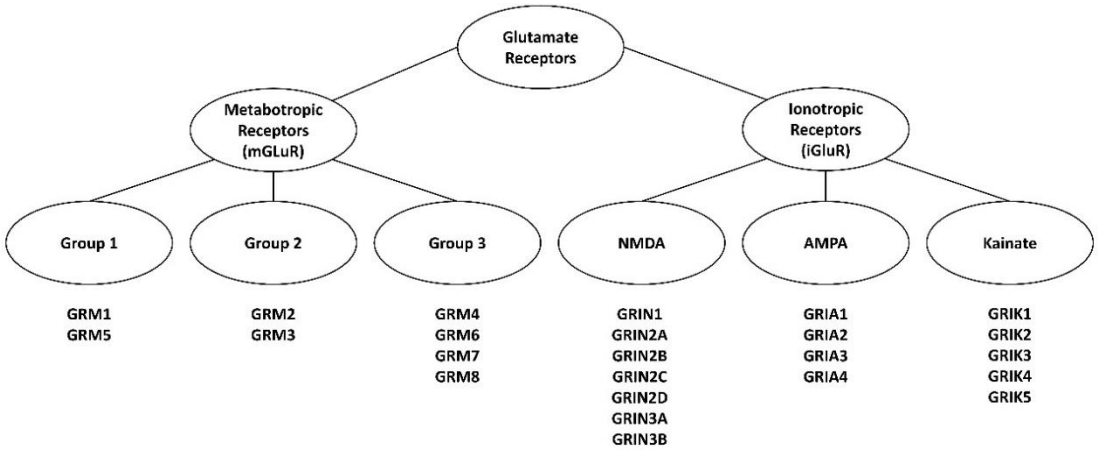

Figure 4.27. Glutamate receptor families. Glutamate receptors are divided into metabotropic receptors, which are g-protein coupled receptors, and ionotropic receptors which are ion channels. both metabotropic and ionotropic glutamate receptors are subdivided into three sub-groups; group 1, group 2, group 3 for metabotropic receptors and NMDA, AMPA and kainate receptors for ionotropic receptors.

Studies into the role of ionotropic receptors have mainly been focussed on their role in glioma as glutamate receptors play an important role in synaptic signalling in the CNS. It has been seen that blockage of AMPA receptors (*GRIA* family of genes), which reduces calcium permeability in cells, reduced migration and induced apoptosis in human glioblastoma (216) and later that AMPA receptors also regulate growth of human glioblastoma via Akt (217). There is evidence also that the expression of AMPA receptors allows glioblastoma to survive in a glutamate-rich environment which is otherwise cytotoxic (218). Building on this idea, Beretta *et al* demonstrated that GRIA2 is more expressed in slow growing and low grade tumours while less expressed in fast growing tumours (219). Piao *et al* showed that overexpression of *GRIA1* enhanced glioma cell migration by increasing beta-1 integrin surface expression and thus increasing the number of focal adhesions.

Outside of the brain, *GRIA3* (AMPA type receptor) expression has been shown to be correlated with pancreatic cancer cell proliferation and migration while inversely correlated with apoptosis (220). Very recently the NMDA receptor antagonist MK-801 has also been shown to be effective at reducing cell proliferation in combination with tamoxifen *in vitro* (221). Kainate receptors to date have been overlooked at potential therapeutic targets, partially due to the lack of sufficiently specific drugs.

Glutamate receptors have been shown to play an important role in melanoma genesis. The NMDA type receptor *GRIN2A* has been suggested to have a tumour suppressive role in melanoma (222), Depletion of endogenous wild-type *GRIN2A* lead to an increase in proliferation and migration in melanoma cell

lines. In other studies, overexpression of the metabotropic glutamate receptor *GRM1* in mice was sufficient for the spontaneous generation of uveal melanomas (223,224) and promotes pro-angiogenic signalling in melanoma (225). *GRM5* glutamate receptor over-expression was also sufficient to induce melanomas in mice(226), and it seems that *GRM1* and *GRM5* can act independently of each other to induce melanomas(227).

In the next chapters, we will examine how glutamate receptors may play a role in melanomas and if altering glutamate signalling can regulate cell proliferation and morphology in our system.

4.3.4 Increased Warburg effect after ROCK inhibition

A375M2 melanoma cells where ROCK was inhibited showed significant alterations in the consumption and secretion patterns when compared to control cells. Principally we observed that cells increase the consumption rate of glucose and secretion of lactic acid after 24 hours. The real effect is probably even more drastic as there are fewer cells following ROCK inhibition cells compared with the control.

This is an interesting finding as we know that ROCK is essential for melanoma proliferation both from published data (97,138) and from our data (Figure 4.24). Additionally, both exogenous glucose and glutamine are essential to sustain melanoma proliferation. This upregulation of the Warburg effect after ROCK inhibition may be a stress response to ROCK inhibition or attempt of the cells to compensate for the challenge. It has been proposed that the Warburg effect can play a role in balancing oxidative stress (228,229). It has already been shown that inhibition of ROCK in melanomas leads to increase levels of ROS (184). Therefore, it would be reasonable to assume that during ROCK inhibition melanoma cells may upregulate the Warburg effect as a response to the increased oxidative stress. This would also help to explain how our results contradict those found in Zhang *et al*'s work which explores how mutant p53 drives the Warburg effect via Rho/ROCK signalling (155). They found that in H1299 lung cancer cells, SKBR3 and MDA-MB-463 breast cancer cells ROCK inhibition with Y27632 led to a reduction of the Warburg effect. There are additional possible explanations for this discrepancy. The GOF mutant p53 studied in their paper led to increased levels of RhoA and thus ROCK activity background while A375M2 cells used in our system are wild-type p53 but still have relatively high levels of Rho/ROCK signalling. Finally, it may be a tissue specific effect as Zhang *et al* saw the opposite effects in two breast cancer cell lines (SKBR3 and MDA-MB0463), and one lung cancer cell line (H1299), all of which are of epithelial origin. Our work was performed in malignant melanomas which are of neural crest origin and not of epithelial origin. The study of spent media should be replicated in a tumour of epithelial origin to

see if the work of Zhang *et al* can be replicated. Our study of spent media was replicated at both 1% FBS and 10% FBS conditions to show different levels of growth factor stimulation and in both situations we saw an almost identical metabolic profile of the spent media.

Our findings should also be viewed within the context of recently published data investigating BRAF mutant melanoma, BRAF inhibitor resistant melanomas and combinatorial therapies of melanoma. Baenke *et al* (230) recently demonstrated that melanomas resistant to BRAF inhibition switch to mitochondrial oxidative metabolism, produce less lactic acid and become more dependent on exogenous glutamine than melanomas sensitive to BRAF inhibition. They also demonstrate that blocking glutaminase activity with BPTES can re-sensitise melanomas to BRAF inhibition. Additionally, it has been shown that inhibition of ROCK activity can re-sensitise resistant melanomas to BRAF inhibitors (4). One possible explanation could be that ROCK inhibition in BRAF inhibitor resistant melanomas could also be switching these cells from the TCA cycle and forcing them back into a glycolytic state. Studying the metabolism of BRAF resistant melanomas after ROCK inhibition would be another avenue of research worth pursuing and may shed new light into how ROCK activity drive melanoma metabolism, proliferation, and drug resistance.

There are also many potential indirect ways of ROCK regulating metabolism. ROCK has multiple confirmed and proposed downstream targets. Many of these targets related to cytoskeletal functions, such as Lim Kinase (LIMK), Adducin, ERM, NHE1, CRMP2, Vimentin (130). There have recently been phosphor-proteomic studies proposing more than 100 potential substrates for ROCK (231). Among the proposed targets of ROCK, Nishioka *et al* observed binding between ROCK and 6-phosphofructo-2-kinase (PFKFB2) peptide, again suggesting a role in the regulation of glucose metabolism by ROCK. While in this study they observed binding between ROCK and PFKFB2, they did not confirm a direct phosphorylation, so this data still needs confirmation.

4.3.5 Glutathione and ROS in melanoma

Glutathione is the main anti-oxidant present in mammalian cells to counter-act the damage that reactive oxygen species can cause to cells, namely DNA damage that leads to oncogenic mutations. It has commonly been thought that anti-oxidant treatment could be used as a preventative measure for cancer (232) or as a cancer treatment (233), although this view is currently being challenged (184,234,235). As reviewed in (234) several groups have demonstrated that anti-oxidants can actually favour tumorigenesis and metastasis. Herraiz *et al* (184) demonstrated that inhibition of ROCK activity and

actomyosin contractility led to an increase in intracellular ROS and an increase in RAC1 activity. RAC1 then led to an increased expression of the tumour-suppressor TP53, which can in turn promote pro-apoptotic pathways.

In our study we have observed that inhibition of ROCK activity leads to an initial decrease of glutathione in A375M2 melanoma cells, this could be explained by how in the short term ROCK inhibition leads to an increase in intracellular ROS which consumes the available GSH in the cells. At 24 hours we observe that GSH concentrations start to recover. This data is consistent with ^{13}C flux GC-MS studies currently being conducted in the Sanz-Moreno group (unpublished Data) as well as previously published work showing that ROCK inhibition leads to increased DNA damage in melanomas via reactive oxygen species(184). Future work should also elucidate the long term effects of ROCK inhibition on anti-oxidant levels in melanomas.

4.3.6 *Myo*-inositol

Myo-inositol was observed to decrease in all the small molecule treatments, however we observed an increase in *myo*-inositol concentrations in the siROCK treated cells. In the KO model of *ROCK* in melanoma, we observed that *myo*-inositol was decreased in the double *ROCK* KO only.

myo-inositol is an extremely important signalling molecule, with a diverse set of phosphates and lipids added to the *myo*-inositol building block to form a series of second messenger (236), that have been shown to regulate metabolism, aging, oxidative stress, DNA repair, and autophagy/cell death (237).

Myo-inositol has previously been implicated as a biomarker for prostate cancer (238) On the other hand, dietary supplements of *myo*-inositol been seen to reduce tumour growth in murine models of mammary gland, colon and lung cancer (239,240) and has even been tested in humans as a potential chemo preventative agent for lung cancer (241). In primary glioblastoma multiform (GBM) patients, proton MR spectroscopy of the affected hemisphere revealed an increase in the concentrations of *myo*-inositol and glutamine, relative to control subjects. *Myo*-inositol has been characterized as a specific marker of astrocytes in the adult brain, providing preliminary evidence of the abnormally higher astrocytic cell density in GBM (242). Furthermore, *myo*-inositol has been reported to increase in colon adenocarcinoma, schwannomas, ovarian carcinoma, astrocytoma and endometrial cells (243) and decrease in breast tumours (244). This suggests it may play very different roles in cancers dependent on the tissue of origin. We have observed high levels of *myo*-inositol in melanomas. Melanomas originate from melanocytes which are neural crest derivatives. One could hypothesise that melanomas

might have similarities with glioblastomas, compared to cancers of epithelial origin such as breast cancers. In work not presented in this thesis, MCF7 breast cancer cells had a very low or absent signal for *myo*-inositol.

In melanomas it was observed that supplementing B16 mouse melanoma cells with m*yo*-inositol partially reversed the anti-proliferative effects of lithium chloride, suggesting LiCl affects phosphatidylinositol metabolism in melanomas (245). The fact that we observed certain alterations of ROCK activity in melanoma also regulated m*yo*-inositol levels suggests ROCK could also be affecting these pathways.

4.3.7 Lipids/Choline

It is well established that cancer cells have drastically different lipid profiles to normal tissue (246,247). The understanding of lipid metabolism in cancer has reached the point where real-time analysis of tissue lipid profiles are being tested clinically to aid surgeons in the resection of tumours (248). In our studies we have observed that there is a consistent increase in CH2-CH2 bonds of lipid chains after ROCK inhibition/ablation. ROCK is an important regulator of cell morphology so it is not surprising that we observe changes in the lipid profiles of cells after ROCK inhibition. Cells with high ROCK signalling are much more contractile and rounded when in a three dimensional environment. ROCK can also be activated by binding to lipids such as arachidonic acid (148). We observed that in short time scales saturated lipids decrease initially at 4 hours before increasing at 8 hours and this increase is sustained at 24 hours.

Observations of changes in Choline metabolism has been a staple of metabolomic studies and has been correlated with malignant progression in a large number of studies as reviewed by Griffin and Shockor(249). In our work we observed that small molecule inhibition of ROCK in melanomas led to a decrease in choline while silencing through siRNA or genetic KOs led to an increase in choline. This could be explained either through off-target effects of either treatment or due to the very different timescale of each experiment. Drug treatments studies were halted after 24 hours while the siRNA knockdowns were conducted over 96 hours. In the *ROCK* KOs of murine melanoma cells were passaged five times after extraction from mice to allow senescence of fibroblasts to take place. These factors could contribute to the differences observed between different experimental procedures.

4.3.8 Different Roles for ROCK1 and ROCK2 in regulating melanoma metabolism?

We observed that individual KOs of *ROCK1* or *ROCK2* led to distinct metabolic profiles and suggest they play different roles in regulating cellular metabolism. We observed that in amino acid metabolism (leucine, glutamine, valine and alanine) ROCK1 promotes increases in concentration while ROCK2 decreases concentration in *ROCK* KO models of murine melanoma. When we examined ROCK1 and ROCK2 in the human melanoma cells A375M2 we also observed slight differences in metabolism between *ROCK1* and *ROCK2* knockdowns. The data suggested to us that changes in metabolism responsible by ROCK1 and ROCK2 are mainly a factor of magnitude rather than of differential regulation of metabolism. It appears ROCK1 is responsible for saturated lipids while ROCK2 drives an increase in most other metabolites. Further experiments should be conducted to further understand not just the differences between ROCK isoforms but also to understand the differences between the two models of melanoma to better understand how to advance research of ROCK driven melanoma metabolism.

ROCK1 and ROCK2 are very similar and it has been demonstrated that ROCKs play redundant roles in sustaining melanoma proliferation (5). There are studies into differential effects they may have on cellular function. It has been seen that ROCK1 and ROCK2 play different roles in keratinocyte differentiation (250), myosin 2 activity (251), leukocyte recruitment (252) and cell detachment (253). Related to cell metabolism, however it has been shown in adipocytes and myoblasts that ROCK1 and not ROCK2 regulated glucose transport and insulin response (156). Further work could be conducted to investigate how the individual isoforms of ROCK regulate metabolism and whether metabolite restriction differentially affect isoform specific KOs.

4.3.9 ROCK promoting stem cell like features in melanoma metabolism?

Melanomas are derived from melanocytes, which are themselves neural-crest derived cells in embryo development. This has led several groups to consider the theory that melanoma behaviour could be explained through the view of the cancer stem cell theory (88,89,254,255). It has also been shown that cells with high ROCK signalling and demonstrate amoeboid-like features are associated with stem-likes features of melanoma cells (256). In our work we have described the metabolic profiles of cells displaying amoeboid like features. One possible avenue for further research is into glutamate as a signalling molecule that promotes contractility. It could be that these neural crest derived cells maybe rewiring themselves to take advantage of the glutamate signalling pathways that are often used in

neural tissue. There is evidence that glutamate signalling may play an important role in melanoma proliferation and migration as discussed in section 1154.3.3 and will be explored further in the following chapters.

4.3.10 Limitations of study

The limitations of this study range from the limitations of the sampling, experimental and analytical methods.

The sample preparation methods the metabolomic studies required long time periods of 10-15 min per sample, which is a long time for metabolomic studies. This was addressed by mechanical detachment of cells from plates, however other methods of quenching, such as cold methanol may be preferable for future work.

While HR-MAS NMR allows a removal of the extraction steps in most metabolomic experiments, there downside is the decreased resolution of the NMR spectra due to overlapping signals from polar and non-polar compounds.

Spectra were allowed to suspend at room temperature for 2 hours prior to insertion into the magnet and were then heated to 310˚K and kept at temperature for several minutes to stabilise. There is the probability of sample degradation during this timeframe which would influence the data obtained. Further work should address these experimental limitations.

While much work on cell morphology was conducted on a thick collagen 1 layer, it was impossible to create experimental conditions NMR metabolomics in a collagen environment. Therefore, all NMR metabolomic experiments were conducted on plastic. It is well known that the matrix on which cells are cultured can significantly alter the transcriptomic profile of cells (257). In addition, our studies were conducted over very different time-scales due to the requirements of each experimental system. Drug treatments were conducted at 24-hour time points while siRNA silencing was done at 96 hours and the murine melanoma cells were passaged four times in culture after extraction to allow fibroblasts to senesce. While this can be seen as a shortcoming, it also demonstrates that the metabolic changes observed are sustained over time. In our studies we conducted transient knock-downs to study gene expression. Other available gene editing methods such as short-hairpin RNAs or CRISPR/Cas9 could be implemented in the future to study long term silencing of ROCK expression.

4.4 Conclusion

In this chapter we aimed to study how ROCK activity and expression may rewire the metabolic profiles of melanoma cells. We have demonstrated through whole cell HR-MAS NMR melanoma cells with high ROCK activity is correlated with increased levels of glutamate and m*yo*-inositol. Network analysis suggests that glutamine/glutamate metabolism is the pathway most regulated by ROCK activity. Cells with high ROCK activity and thus a rounded morphology have decreased levels of saturated lipids. These observations offer interesting starting points for future research and should be further characterised in future work.

We have also demonstrated with 1D liquid NMR that melanoma cells where ROCK activity was inhibited switched increased the rate of glycolysis. Increased consumption of glucose and increased secretion of lactate after ROCK inhibition suggest cells become more dependent on glucose for their energy demands despite the anti-proliferative effects of ROCK inhibitors.

Examining the effects of ROCK inhibitors over shorter time frames also revealed that glutathione is initially depleted and then starts to recover after 24 hours. This fits data published in the literature that ROCK inhibitors cause increased oxidative stress in melanoma cells (184).

Finally, we observed that individual KOs of *ROCK* have distinct metabolic profiles suggesting they have distinct roles in regulating cellular metabolism. This does not lead to a difference in proliferative ability, and therefore suggests that only certain metabolites, such as glutamate is much more important in sustaining proliferation.

Further work in this thesis will attempt to further characterise glutamine and glutamate metabolism in melanoma along with its association with ROCK activity.

Chapter 5 : A BIOINFORMATICS INVESTIGATION OF GLUTAMINE AND GLUTAMATE METABOLISM AND SIGNALLING IN HUMAN MELANOMA

5.1 Introduction

In the previous chapter the metabolic profiles of melanoma cells were studied while perturbing either ROCK activity or expression. It was seen that glutamine/glutamate metabolism was the most consistently regulated metabolic pathway by ROCK. Other major changes observed were in glutathione, *myo*-inositol and lipid metabolism. In the exometabolome it was seen that ROCK inhibition led to increased Warburg effect. It was also seen that melanoma cell secrete glutamate, suggesting a role for glutamate signalling in melanoma.

This work was performed with several melanoma cell lines; the A375M2 human melanoma cell line, the B16F10 mouse melanoma cell line, and a murine model of melanoma in which the *ROCK* genes were deleted. *In vitro* studies with cell lines are powerful models to study disease as it allows researchers to conduct experiments on genetically identical systems in controlled experimental environments where senescence is not an issue(258). However, the strictly controlled nature of cell lines can be a great weakness as well. Human tumours are very heterogeneous and also exhibit intra-tumoral heterogeneity that cannot be replicated with individual cell lines (259). Interactions between the stroma and tumours are not taken into account in research using only cell lines (260). Even more importantly the interactions between tumours and the immune system, which have proved to provide clinical benefit when targeted, require more sophisticated models than most *in vitro* work provides(261). For these reasons, among others, cell line experiments run the risk of being poorly generalisable to a clinical setting. This issue has arisen as some cell lines are better models of disease than others along with issues of the cell culture environment, namely growing cells on plastic in highly oxygenated environments, selects for vastly different subpopulations of cells compared to tumours grown *in vitro* (262).

In our studies we have attempted to address these issues by studying the role of ROCK in several models of metastatic melanoma. We have used the A375M2 human melanoma cell line as opposed to the parental A375P cell line. A375M2 cells were chosen due to their high metastatic potential along with increased expression of RhoC/ROCK signalling compared to A375P cells (154). This decision was made due to our interest in metastatic melanoma. They have also been used in key studies making the foundation of this thesis (3,140,184,263). In this chapter we make use of microarray data from (140). In that study, A375M2 human melanoma cells were treated with ROCK inhibitors to identify genes whose expression was correlated with ROCK activity and thus rounded-amoeboid type migration. In this

chapter we make use of this data set to analyse the expression of metabolic genes in the context of ROCK activity.

While *in vitro* studies of metastatic melanoma cell lines are important models enabling the role of ROCK to be more accurately defined, it is important to understand what relevance these findings have to the wider melanoma patient population. We can then understand whether future interventions can be developed from our *in vitro* studies and be applicable in the much more heterogeneous environment of the clinical setting. Consequently, in this chapter we have conducted a bioinformatics screen of genes related to glutamine/glutamate metabolism and glutamate signalling. By harnessing publicly available gene expression data of patients at different stages of disease, metabolic targets of disease associated with disease progression may be identified, related to our experimental findings described in the previous chapter. This information can then fed be back into *in vitro* studies of melanoma in an attempt to gain further mechanistic insight.

It is fairly well established that glutamine metabolism is important for sustaining melanoma proliferation (3-5,97) and the link with ROCK signalling, described in the previous chapter, adds a new perspective on the potential mechanisms of how ROCK regulates melanoma proliferation and metastasis. An additional question is how glutamine and glutamate metabolism may support not only melanoma proliferation but metastatic potential as well. We also observed that ROCK may supress the Warburg effect in melanoma, or possibly that ROCK inhibition may lead to an upregulation in Warburg effect to counteract an increase in oxidative stress.

The first aim of this chapter therefore is to investigate whether there is any evidence in publicly accessible databases of increased glutamine/glutamate metabolism and/or suppressed Warburg effect in metastatic as opposed to non-metastatic melanomas.

The second aim is to identify whether increased or decreased expression of any genes is associated with the expression of *ROCK1* and/or *ROCK2* and whether these genes may be related to glutamine/glutamate metabolism or suppression of the Warburg effect. A short discussion on glutamine and glutamate metabolism follows.

Glucose and glutamine are the essential sources of carbon for many cancer types and this holds true for melanomas. Ratnikov *et al* demonstrated that all of the 9 melanoma cell lines investigated were dependent on at least 1 mM glutamine in the cell culture media to sustain proliferation (195). The findings in this study led to a review by Ratnikov *et al* (264) where they discuss the roles glucose and

glutamine metabolism play in melanoma progression (Figure 5.1). Glutamine is the most abundant amino acid present in serum and the phenomenon of glutamine addiction in many cancer types has been described in the literature (22,23,202,205,264-266) and observed in our experimental system. Glutamine is a major precursor for the TCA/Krebs cycle. It is converted to glutamate and subsequently α-ketoglutarate which then feeds into to the TCA cycle, eventually leading to the generation of ATP via oxidative phosphorylation. The first catabolic step in glutamine metabolism (glutaminolysis) is the reaction catalysed by the glutaminase enzyme (GLS) which generates glutamate from glutamine. Glutamine is also a major source of nitrogen source for the synthesis of most other amino acids. It is also essential for the production of glutathione, which is the most abundant anti-oxidant molecule that plays a crucial role in cell survival in the face of oxidative stress. (205,264), Figure 5.1*)*.

Several aspects of glutamine/glutamate metabolism have been implicated as potential therapeutic targets in melanoma. One example is glutaminase: Inhibition of glutaminase via small molecule inhibitors has been shown to inhibit RhoA dependent transformation in fibroblasts (158) and has also been suggested to be a potential treatment for melanomas resistant to BRAF inhibitors (230).

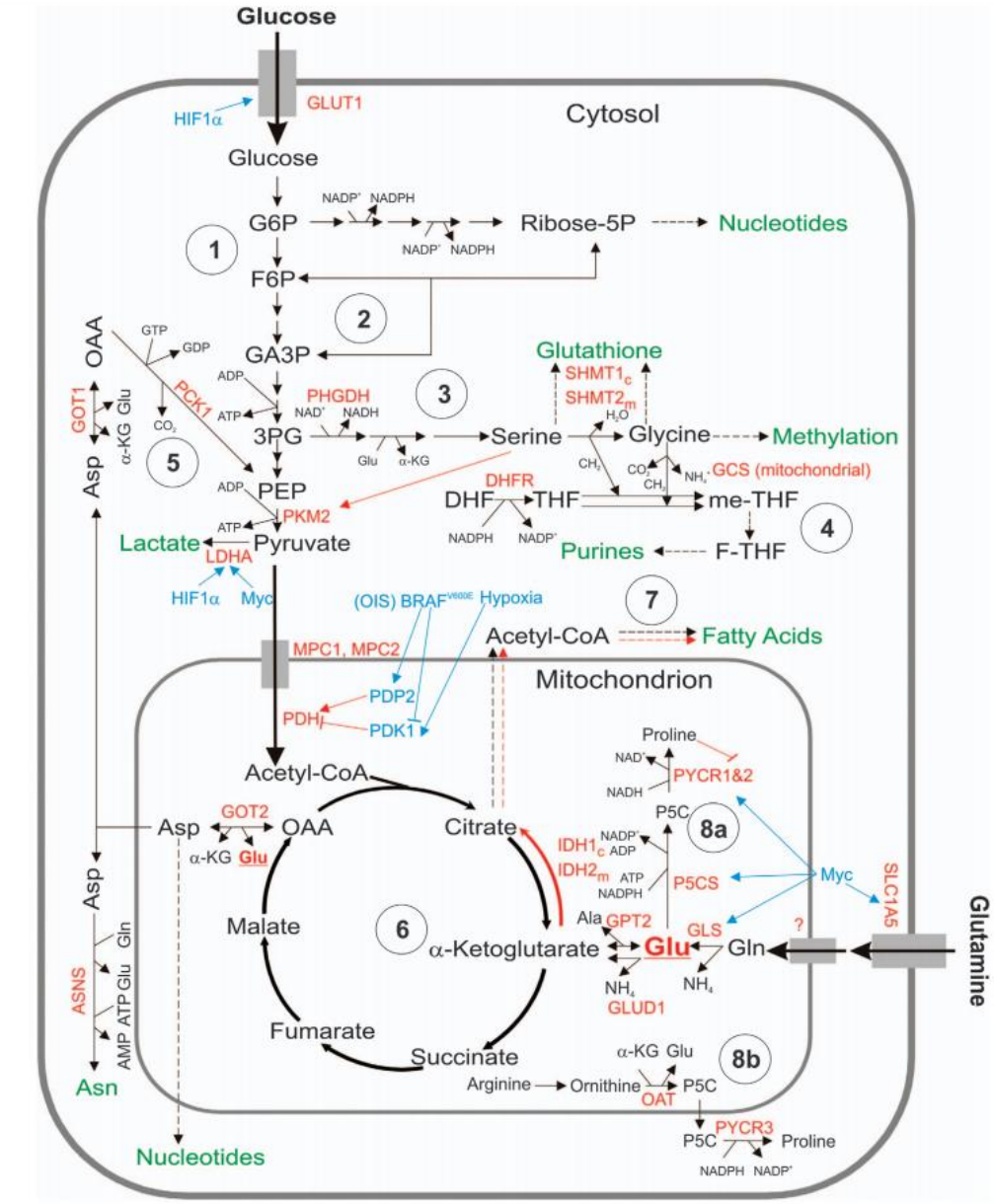

Figure 5.1. Glutamine and Glucose Metabolism are re-wired in melanoma. Melanomas are dependent on exogenous glutamine and glutamine metabolism can be re-wired by oncogenes such as Myc and mutated BRAF to drive increased glutamine transport and glutamine metabolism. Figure adapted from.(264).

Another example are the solute carriers responsible for glutamine and glutamate transport as melanomas require exogenous glutamine to grow and proliferate. The study of solute carriers, the family of proteins responsible for amino acid transport has been understudied (161,267), showing the importance of further research.

Glutamate is also another area of interest for targeted therapies. Glutamate is not only a major metabolite involved in the various cellular processes described above, but it is a major signalling molecule as discussed in Chapter 4. We observed that A375M2 cells secrete glutamate and it has also been observed in the literature. For example, Ratnikov *et al* showed not only that melanomas secrete

glutamate, but also that 30-50% of the glutamate secreted from the 9 melanoma cell lines studied were derived from the TCA cycle in their $^{13}\mathbf{C}$ tracer studies of glutamine metabolism in melanoma (195).

Glucose metabolism is also another attractive therapeutic target in cancer (268) and the Warburg effect was the first metabolic rewiring observed in cancers (20). In our studies in the previous chapter we observed that inhibition of ROCK activity led to an increase in the Warburg effect. This could either be a compensatory mechanism to reduced proliferation or to increase lactate production as a response to increased oxidative stress. Several studies have shown that melanomas make use of both glucose and glutamine as energy sources to maintain flexibility in sustaining proliferation (269). However, *Ratnikov et al* showed that 8 of the 9 melanoma cell lines studied could sustain proliferation without glucose (195). Additionally, it has recently been shown that melanomas resistant to BRAF inhibition with vermurafenib, the current first line treatment for BRAF mutant melanomas, switch to glutamine dependence (230,270) rather than glucose. This suggests that while glucose and glutamine are both important for melanomas, they may become more dependent on glutamine at later stages of the disease. In unpublished work by the Sanz-Moreno group, it has been seen that A375M2 cells require glucose to sustain proliferation.

In this chapter we aim to identify potential therapeutic targets of malignant melanoma involved in glutamine/glutamate metabolism and glutamate signalling based on the metabolomic pathway analysis conducted in the previous chapter. The study proposed here is a conceptual level of -omic data integration discussed in chapter 1, namely we aim to use the generated metabolomic data to inform our studies of gene expression in a panel of melanoma patients. The data shown in the previous chapter identified that glutamine/glutamate metabolism is significantly altered after interfering with ROCK signalling. We will now investigate if these findings related to glutamine, glutamate and ROCK have broader applications to clinical data.

Genes related to glutamine, glutamate and glucose transport and metabolism as well as glutamate signalling will be identified. We will explore the regulation of these genes through post-hoc analysis of a previously published microarray study in A375M2 human melanoma cells where ROCK activity was inhibited with the small molecule inhibitors H1152 and Y27632 for 16 hours (140). This may give an indication if the expression of the genes of interest are under control of ROCK.

Additionally, six publically available databases containing microarray data of melanoma patients at different stages of disease are also identified and the change in expression of these genes will be

studied by comparing both primary melanoma against normal tissue and comparing metastatic melanomas to primary melanomas. This will allow us to identify if any genes of interest may be more broadly implicated in melanoma clinically. Where available survival analysis based on these genes expression will also be studied to find if any genes may have prognostic value.

We will be looking at several melanoma databases and there is a large heterogeneity between studies and individual patients, therefore, we will be looking for qualitative indications that metabolic pathways may be altered in primary melanomas and metastatic melanomas through gene set enrichment analysis (GSEA).

A next step will be to investigate if ROCK signalling regulates these candidate targets. This could shed light mechanistically as to how ROCK regulates cellular metabolism seen in the previous chapter. Linear correlations of the expression of ROCK and candidate genes will be explored through post-hoc analyses of publicly available databases of melanoma patient microarrays containing data about both primary and metastasized melanomas.

We will conclude this chapter by returning to *in vitro* studies to examine the findings from our bioinformatics work. We will select a sample of the genes studied and confirm if ROCK activity regulates gene expression by RT-qPCR. Finally, an siRNA screen of a selection of genes from each metabolic pathway studied will investigate the effects of these genes on proliferation and cell morphology on collagen. This will bring the clinical data collected in this chapter back into an *in vitro* setting where we can build an understand of how these genes are promote an invasive phenotype in metastatic melanoma.

5.2 Methods

5.2.1 Initial gene selection

The identification of candidate genes takes two different strategies. One is searching of the Human Metabolome Database (HMDB) for candidate genes using the keyword 'glut*'. This strategy will allow identification of targets not just for glutamine and glutamate, but also include terms such as glutathione. The downside is this may identify genes not of interest to our pathways and thus depower our study.

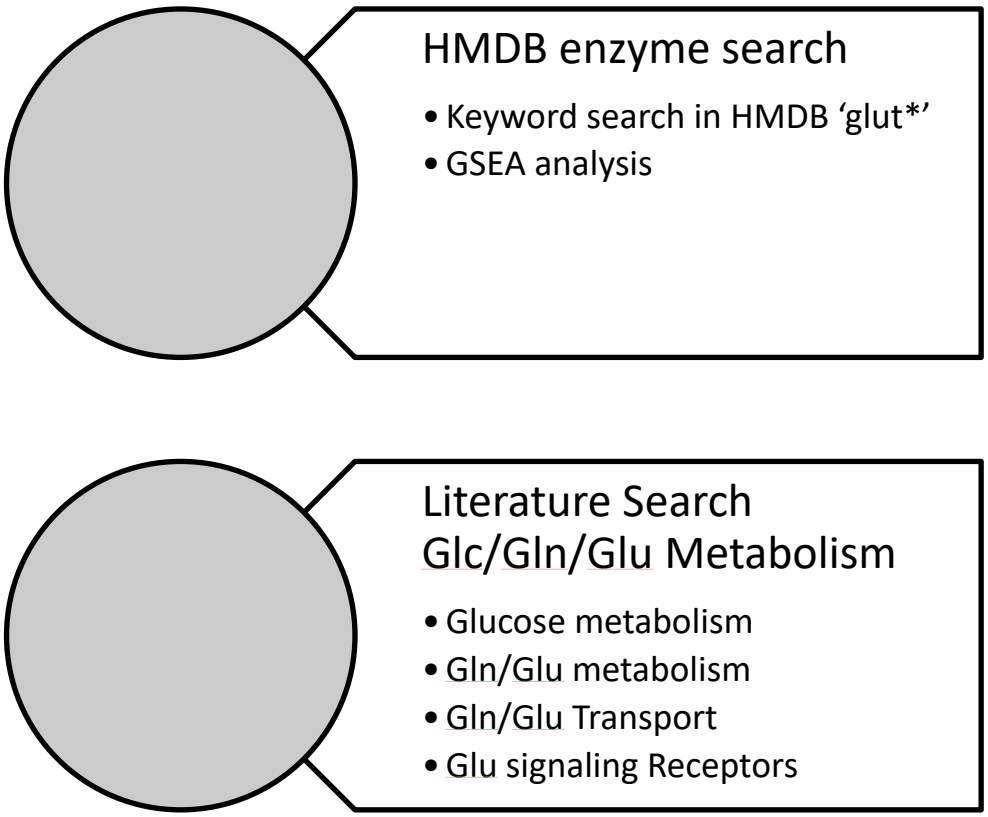

Figure 5.2. Search Strategy for Candidate Genes from Glutamine and Glutamate related genes. The Genes were searched for in an un-biased manner through keyword search for genes was conducted by both searching in the Human Metabolome Database for (HMDB). This search was then supplemented with manually searching other databases and the keyword glut* as well as a literature search, KEGG for genes belonging to different metabolic pathways, and wikipathways databases for genes involved in glucose metabolism, glutamine, glutamate metabolism, glucose and glutamine transport and glutamate receptor signalling.

To supplement this strategy, we are also including a literature and database search of candidate genes involved in glucose, glutamine and glutamate metabolism, transport, and glutamate signalling.

5.2.2 Generation of candidate library

Searching the HMDB for genes and descriptors including the search term 'glut*' gave a list of 106 genes (listed in Appendix A) in November 2013. Genes found in the HMDB search were integrated with genes selected through literature search and KEGG pathways databases. Genes included for analysis were involved in glutaminolysis, TCA cycle, glycolysis, glutamine/glutamate transport and glutamate

receptors. Searches were conducted in the literature KEGG pathways and wikipathways databases leading to a final library of 181 unique genes. The genes and their pathways are detailed in Table 4. Whole gene lists can be seen in Appendix A.

Gene Set	HMDB search	Glycolysis and glucose transport	Glutaminolysis and TCA cycle	Glutamate signalling	Gln/glu Transport	Total Unique Genes
Number of Genes	106	31	30	26	21	181

Table 4. Metabolic pathways and search terms used to select genes for screening.

5.2.3 A375 Melanoma microarray

The data generated by Sanz-Moreno *et al* (2011)(140) (accession numbers GSM586484–GSM586501) was selected for analysis in this chapter. In this study, they conducted a transcriptome analysis of A375 and A375M2 human melanoma cells seeded on a thick collagen 1 layer and observed the transcriptome changes after ROCK inhibition with H1152 and Y27632.

5.2.4 Analysis of gene expression from human databases

Publicly available melanoma patient transcriptome databases that comply with the minimum information about a microarray experiment (MIAME) standards (271) were searched for in the The National Center for Biotechnology Information's (NCBI) Gene Expression Omnibus (GEO), as performed in (154). The GEO-NCBI is a public international repository of, amongst other datasets, gene expression profiles.

Databases selected for post-hoc analysis were selected for having high sample purity (>95% melanocytic cells), enough patient samples to perform statistical comparisons (n>40) and include normal tissue samples. Samples from these studies were reported to have >95% melanocytic/melanoma cells and no mixed histology.

These databases, signified by their GEO accession number, were: GSE29359; GSE3189; GSE8401; GSE46517; GSE7553 corresponding to the following publications: Avery-Kiejda *et al*, (2011)(175); Talantov *et al*, (2005)(176); Xu *et al*, (2008)(177); Kabbarah *et al*, (2010); Riker *et al*, (2008)(179). The databases and number of samples are shown in Table 5. Avery-Kiejda *et al* focussed on a comparison of gene expression profiles between 'melanocytes' and 'melanoma' cells (n=8, n=92, respectively), whilst Talantov *et al* focussed on a comparison between 'nevus' and 'malignant' cells (n=7, n=45, respectively). These two conditions will be defined as a comparison between 'normal' cells (non-tumorous) and 'primary' cells (tumorous, non-metastatic). Xu *et al*, Kabbarah *et al* and Riker *et al* each

analysed ‘primary’ and ‘metastatic’ melanoma cells (n=31 and n=52; n=31 and n=73; n=14 and n=40, respectively) (Table 5). Gene expression data was extracted from each of the 5 databases for the 181 genes previously detailed. In the case of more than one primer being present in the microarray data, the primer with highest mean expression was selected.

Data set	Avery	Talantov	Kabbarah	Riker	Xu	TCGA
Sample Description	Melanocyte (n=8) vs. Melanoma (n=92)	Normal (n=7) vs. Malignant (n=45)	Primary (n=31) vs. Metastasis (n=73)	Primary (n=14) vs. Metastasis (n=40)	Primary (n=31) vs. Metastasis (n=52)	Primary (n=58) vs. Metastasis (n= 296)

Table 5. Melanoma databases used in study and number of samples in each study.

A final data set was obtained from The Cancer Genome Atlas (TCGA), which is a collaboration between the National Cancer Institute (NCI) and the National Human Genome Research Institute (NHGRI); both part of the US National Institutes of Health (NIH). It aims to comprehensively catalogue a broad spectrum of expression profiles and tumorigenic mutations. Data was accessed from the cBioPortal for Cancer Genomics (180,181). In particular, data was obtained from the supplementary work of Guan *et al* (2015)(182), detailing expression profiles in 354 Skin Cutaneous Melanoma (SKCM) patients with complete sequencing and copy number alteration (CNA) data, from a total patient database of 470.

5.2.5 Data Analysis

In each of these databases, initial gene selection for subsequent experimental analysis was based upon the exclusion criteria that the gene exhibited a significant (FDR adjusted p value<0.05) and a fold-change expression >1.5 or a fold-change expression < 0.66 in primary or metastatic cells with regards to normal or primary cells, respectively.

5.2.6 GSEA (Gene Set Enrichment Analysis)

GSEA is a computational method that determine whether a pre-defined set of genes shows significant expression enrichment between two biological states (174). The sets of genes used with GSEA software are derived from a collection of annotated gene sets known as the Molecular Signatures Database (MSigDB). It is also possible to create *ad hoc* gene sets for analysis.

The statistical test given in GSEA is the ‘enrichment score’ (ES). This is calculated by ‘walking down’ a rank ordered list of genes within the gene set and incrementing the ES according to how much a gene’s

expression correlates with the given phenotype (Figure 3.3). Significance tests are then run against a permutated dataset used as the null hypothesis and nominal p-values are false-discovery rate (FDR) adjusted as the multiple test correction (174). GSEA was performed using the desktop app available from the Broad Institute website. A representative output of GSEA is visualised in Figure 3.3.

Seven gene sets were constructed based on metabolic pathways of interest. These are:

- Glycolysis
- TCA Cycle
- Glutaminolysis
- Gln/Glu transport
- Ionotropic Glu Receptors
- Metabotropic Glu Receptors
- Glucose Transport

Full gene lists can be seen in Appendix A.

5.2.7 Survival Analysis

Survival analysis is the statistical estimation of the time taken until an event. In the case of this work, the event is death. Survival analysis was performed in R using the '*survival', 'ggplot2',* and '*ggsurv'* packages in the R Studio interactive development environment (IDE). Z-score normalised gene expression data was used for the analysis. and patients were divided into 'low' and 'high' expression groups according to a cut-off of z-score =0. The z-score is the number of standard deviations a measurement is from the mean value and is calculated with the equation:

$$\boldsymbol{z = \frac{X - \mu}{\sigma}}$$

Where X Is the original expression value, $\boldsymbol{\mu}$ is the mean expression for the gene of interest, and $\boldsymbol{\sigma}$ is the standard deviation of the gene of interest. The cut-off was selected as the z-score is the number of standard deviations from the mean, therefore z =0 is the mean expression value for the gene of interest. Kaplan Meier plots were generated for each gene of interest using the *'ggsurv'* R package, which is built using both the *'survival'* and the '*ggplot2*' package in R. Log-rank tests were performed for each gene of interest and nominal p-values were FDR adjusted for multiple-test corrections.

5.2.8 Gene Expression Correlations

Gene expression networks are highly variable, non-linear and complex. While advanced network-based differential gene analysis tools are available (272-275), they fall outside the scope of this work. Correlations between gene expressions were analysed to reveal patterns between ROCK expression

and the expression of metabolic genes. Expression data over the five databases was normalised by calculating the z-scores each gene in each database. This gave a final dataset comprised of 804 melanoma patients. Spearman rank correlations were calculated for the 181 genes of interest and both ROCKs. The Spearman rank correlation was chosen instead of the Pearson correlation because we are not assuming a normal distribution of gene expression. Only genes that had a Spearman $R^2 > 0.25$ or $R^2 < -0.25$ were considered. p-values were FDR adjusted to account for multiple testing.

Data was processed and analysed in python 3.5 using the numpy, scipy.stats, *statsmodels* and *pandas* packages. Data was visualised using *matplotlib, pandas, and seaborn.*

5.2.9 RT-qPCR

RT-qPCR was performed as described in chapter 2.

5.3 Results

A summary of the genes that passed the exclusion criteria is show in Table 6. The full list of genes that passed exclusion criteria is shown in Appendix A. The diverse data sets showed very different numbers of genes that passed the exclusion criteria, with the Talantov data set having 48 of the 150 examined genes pass the exclusion criteria while on the other end the Riker dataset only had 3 of the 172 genes examined pass exclusion criteria. This cannot be explained by the total number of patients enrolled in the studies as Talantov contained 52 total samples while Riker contained 54 total samples. It can be explained however by the number of samples per group. The Talantov data set only contained 7 normal tissue samples, while Riker had double the number of primary samples. The small sample size of normal tissue in Talantov could enhance be attributed to the large number of genes that passed the exclusion criteria. This highlights the need for multiple data sets to increase confidence in our analysis.

	NORMAL VS. PRIMARY		**METATASIS VS. PRIMARY MELANOMA**			
	Avery	Talantov	Kabbarah	Riker	Xu	TCGA
INITIAL GENE SELECTION	181	181	181	181	181	181
GENES FOUND IN ARRAY	164	150	150	172	150	177
GENES PASSING SIGNIFICANCE THRESHOLD	15	76	38	4	63	10
GENES PASSING FOLD CHANGE THRESHOLD	15	48	14	3	32	7
GENES WITH HIGHER EXPRESSION	1	29	8	0	22	4
GENES WITH LOWER EXPRESSION	14	26	6	2	10	3

Table 6. Number of Genes that pass the exclusion criteria of >1.5-fold change in expression or <0.66-fold change in expression in each of the six melanoma patient databases. A full list of the genes that were up- or down-regulated in each database can be seen in Appendix A.

5.3.1 *SLC2A3* (GLUT3) is overexpressed in primary melanomas

In both databases (Avery and Talantov) where comparisons were made between normal tissue/nevi and primary melanomas only *SLC2A3* was observed to be overexpressed (Figure 5.3A, C). The *SLC2A3* gene codes for the GLUT3 glucose transporter. It has been shown to be involved in promoting epithelial to mesenchymal transition in non-small cell lung cancer (276), proliferation of breast cancer (277), and is correlated with increased aerobic glycolysis in colon cancer (278). There were no other

genes that were found to be overexpressed in the Avery data set however the Talantov data set showed 28 other genes that were overexpressed in primary melanomas (Table 6, Figure 5.3A). Among these there were genes involved in glycolysis (*ENO1, ENO2, OGDH, PFKL, PFKP, TPI1*) additionally supporting the role of increased glycolysis in primary tumours. Glutamine transporters (*SLC1A5, SLC7A5*) and glutamate receptors (*GRIK1, GRIK2, GRIN2D*) were also seen to be overexpressed in primary tumours.

Ornithine aminotransferase (*OAT*) and Phosphoserine aminotransferase (*PSAT1*) were observed to be less expressed in primary melanomas compared to normal tissue in both data sets (Figure 5.3B). OAT functions within the pathway that converts arginine and ornithine into glutamate and GABA. It has also been shown to be under-expressed in prostate cancer (279) which leads to an accumulation of putrescine. *PSAT1* encodes for an aminotransferase which is part of the serine biosynthesis pathway, it catalyses a reaction which consumes α-ketoglutarate and produces glutamate as a by-product hence its inclusion in our studies. *PSAT1* has previously been shown to be overexpressed in colon cancers and overexpression in SW480 human colon cancer cells increased cell proliferation and chemoresistance (280).

In individual data sets it was seen that several genes involved in the glutaminolysis and the TCA cycle were under-expressed in primary tumours (*CS, IDH1, SDH1, SDHC, ACO1, GLS2, GLUD2, IDH2, ME1, ME2*), while only a few glycolysis genes were under expressed (*PKFM, GAPDHS, GPT, GCLM*) (Figure 5.3B). Finally, several transglutaminases were also observed to be under-expressed in primary melanomas. *TGM7* was seen in Avery while *TGM1*, *TGM3* and *TGM5* were seen in Talantov (Figure 5.3B).

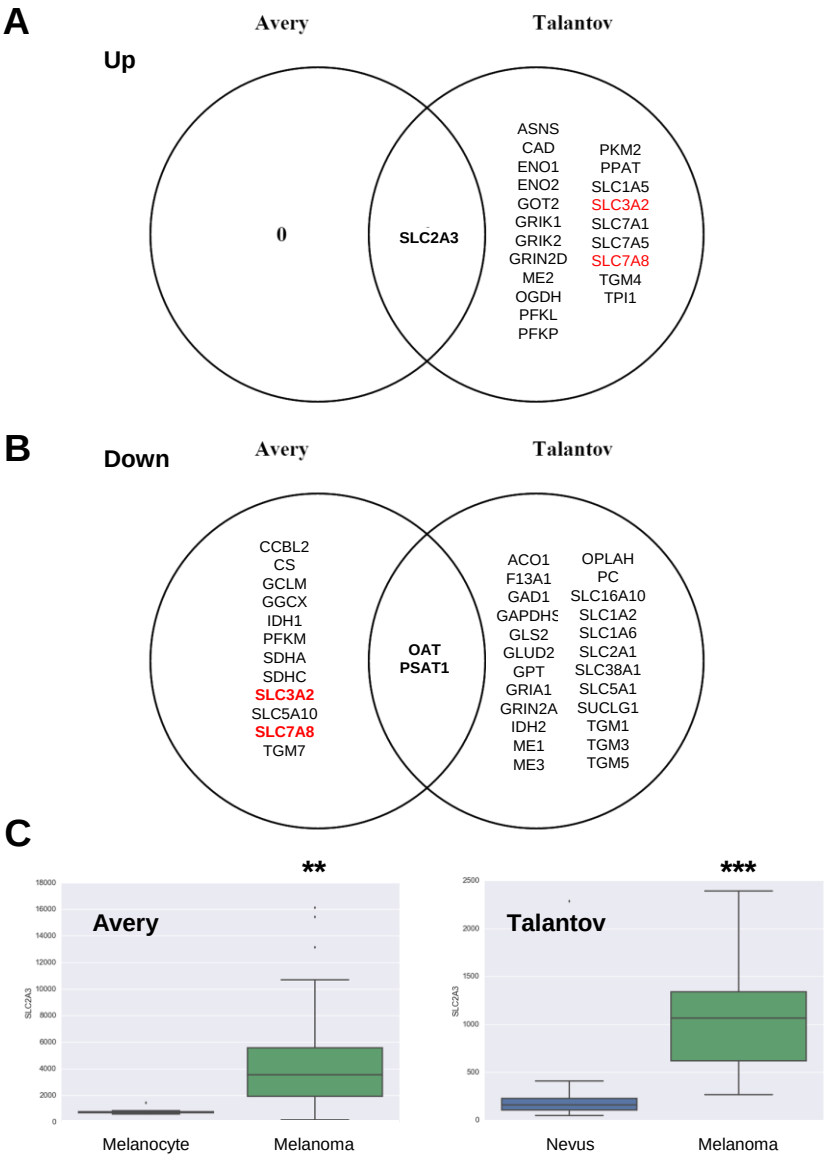

SLC2A3	Fold Change	FDR adjusted p-value
Avery	5.26	0.002
Talantov	3.68	<0.0001

Figure 5.3. *SLC2A3* is overexpressed in Primary Melanoma Samples. A) Only *SLC2A3* was observed to be significantly overexpressed in both datasets with normal tissue vs. primary melanoma samples. Venn diagram of the two databases with metastatic and primary melanoma samples. Genes shown passed criteria of having fold change expression <1.5 and FDR adjusted p <0.05 B) *OAT* and *PSAT1* are less expressed in primary melanomas compared to normal tissue. Venn diagram of the two databases with metastatic and primary melanoma samples. Genes shown passed criteria of having fold change expression <0.66 and FDR adjusted p <0.05. Highlighted in red are genes that show to be both overexpressed and under expressed in databases. C) Box and whisker plots *SLC2A3* expression in the Avery and Talantov Databases. Boxplots show median expression along with upper and lower quartiles. Whiskers show 95% confidence interval. ** p<0.01 ***p<0.001 and Fold Change in Expression and FDR adjusted p-values for fold change in expression between primary melanoma samples and Nevus or Melanocyte samples in the respective databases.

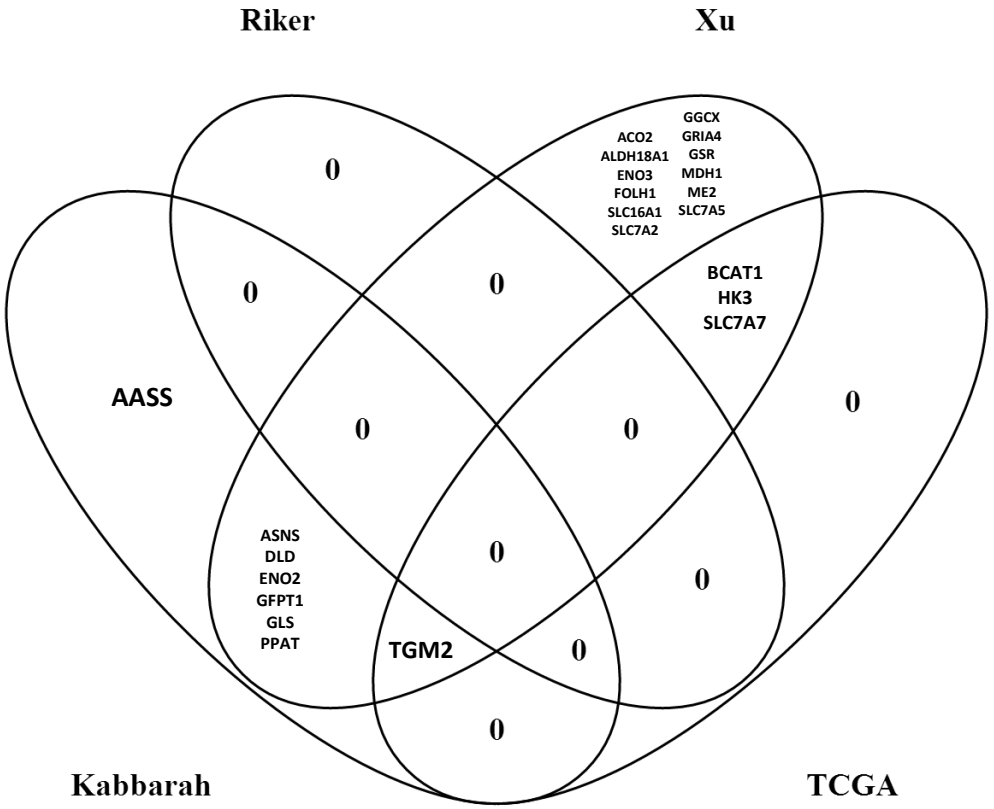

Figure 5.4. The transglutaminase *TGM2* is more expressed in metastatic melanomas compared to primary melanomas. Venn diagram of the four databases with metastatic and primary melanoma samples. Genes shown passed criteria of having fold change expression <0.66 and FDR adjusted p <0.05. Figure generated with VENNY(281).

5.3.2 *TGM2* is overexpressed in metastatic melanoma samples compared to primary melanoma samples while *TGM1* expression is down regulated in metastatic samples compared to primary melanomas

Transglutaminase 2 (*TGM2*) is more highly expressed in all the databases analysed comparing metastatic melanoma samples compared to primary melanoma samples. *TGM2* was included in the screen not only for its catalytic activity as a transglutaminase, but it has also been shown to regulate RhoA signalling. Transglutaminase binds to an transamidates RhoA which leads to a constitutively active GTPase. This can then lead to increased activity of ROCK(282-284). Across the four databases examined, it showed a mean 3.35-fold increase in expression in metastatic samples vs. primary samples and had a significant change in three of the four databases (Figure 5.4). In the Riker database the change in expression was not statistically significant ($p = 0.19$), however the trend is consistent with the other databases as a 2.05-fold increase in expression was observed (Figure 5.5). *TGM2* encodes for the protein tissue transglutaminase TG2. Its main function is to crosslink proteins between the ε-

amino group of a lysine residue and a γ-carboxamide group of a glutamine residue. It can be found both intracellularly and in the extracellular matrix (285).

A

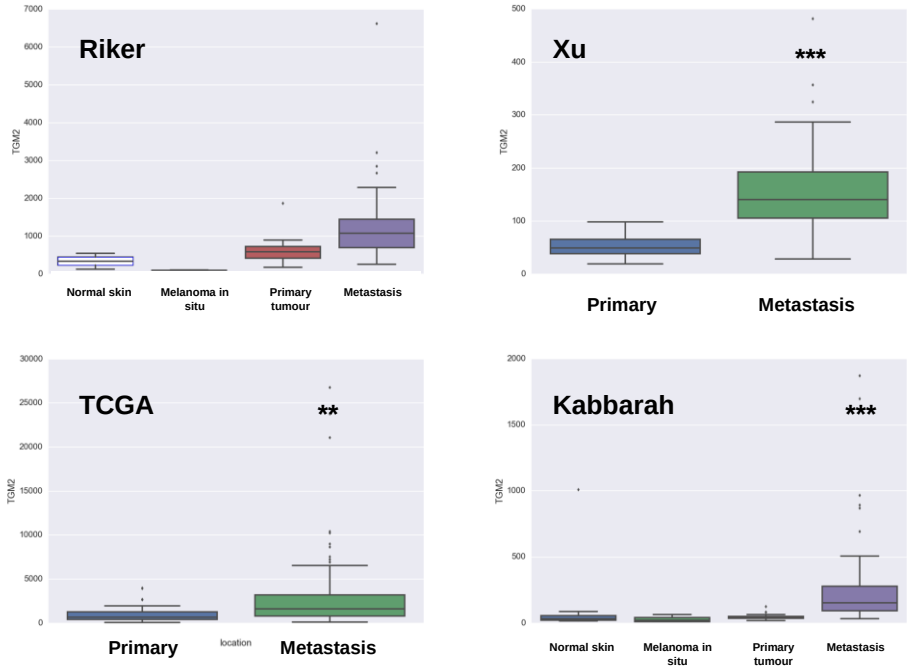

B

Data Set	Fold change	FDR adjusted p-value
Riker	2.05	0.19
Xu	3.03	<0.0001
TCGA	2.59	0.005
Kabbarah	5.75	<0.0001

Figure 5.5. *TGM2* is overexpressed in metastatic melanoma compared to primary melanomas. A) box and whisker plots illustrating the expression of *TGM2* in the datasets analysed. Boxplots show median expression along with upper and lower quartiles. Whiskers show 95% confidence interval. ** p<0.01 ***p<0.001 B) Table of fold change in expression in metastatic melanoma samples compared to primary melanoma samples along with FDR adjusted p-values.

TGM1 and other transglutaminases such as *TGM3* and *TGM5* showed lower expression when comparing expression between metastatic samples compare to primary samples (Figure 5.6A). *TGM1* was found to be less expressed in metastatic melanomas compared to primary melanomas in all four databases (Figure 5.6B).

A

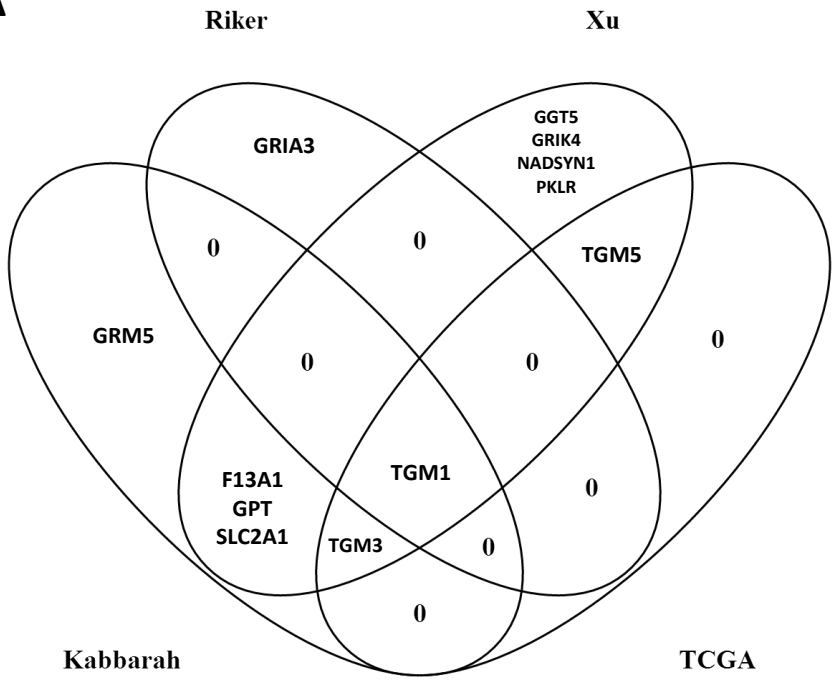

B

TGM1 Expression
Metastatic vs. Primary

Database	Fold Change Expression	FDR adjusted p-value
Kabbarah	0.449	<0.0001
Riker	0.104	0.0167
TCGA	0.040	<0.0001
Xu	0.109	<0.0001

Figure 5.6. Several Transglutaminase family members are less expressed in metastatic melanomas compared to primary melanomas. Venn diagram of the four databases with metastatic and primary melanoma samples. Genes shown passed criteria of having fold change expression <0.66 and FDR adjusted p <0.05. Figure generated with VENNY (281).

5.3.3 GSEA reveal melanomas upregulate glycolysis and downregulate the TCA cycle in tumorigenesis while switching to glutamine metabolism in metastasis

Gene Set Enrichment Analysis is a computational tool to assess whether a set or group of genes is overrepresented in a disease state. This non-threshold bioinformatics technique can reveal if a set of genes is being globally regulated, in this case in metastatic melanoma or in ROCK inhibition. The genes comprising the gene sets can be seen in Appendix A. Gene sets that were selected (Table 4) were run through GSEA against each database.

In terms of Primary melanomas, The TCA cycle gene set was found to be significantly overexpressed in melanocytes when compared to melanomas in the Avery dataset (Nominal p-value = 0.036, FDR q-value = 0.0098, Figure 5.7). This suggests that melanomas switch from aerobic respiration to anaerobic

respiration during tumorigenesis, consistent with the Warburg effect observed in melanomas. GSEA analysis of the Talantov dataset shows that Gln/Glu transporters and glycolysis are significantly overexpressed in melanomas when compared to benign nevi (FDR q-value = 0.021 and 0.041 respectively, Figure 5.7).

When comparing metastatic melanomas to primary melanomas, there was a trend for the Gln/Glut transport gene set being overexpressed in metastatic melanomas compared to primary melanomas in the Kabbarah dataset (nominal p= 0.038, FDR q-value = 0.132, Figure 5.7). In the Xu dataset there was a trend for the TCA cycle gene set being overexpressed in metastatic samples when compared to primary samples (nominal p-value = 0.036, FDR q-value = 0.098, Figure 5.7).

This data presented here suggests that in tumorigenesis cancer cells switch away from aerobic respiration and upregulated glycolysis while in metastasis they may upregulate glutamine metabolism and aerobic respiration to adapt to new environmental pressures.

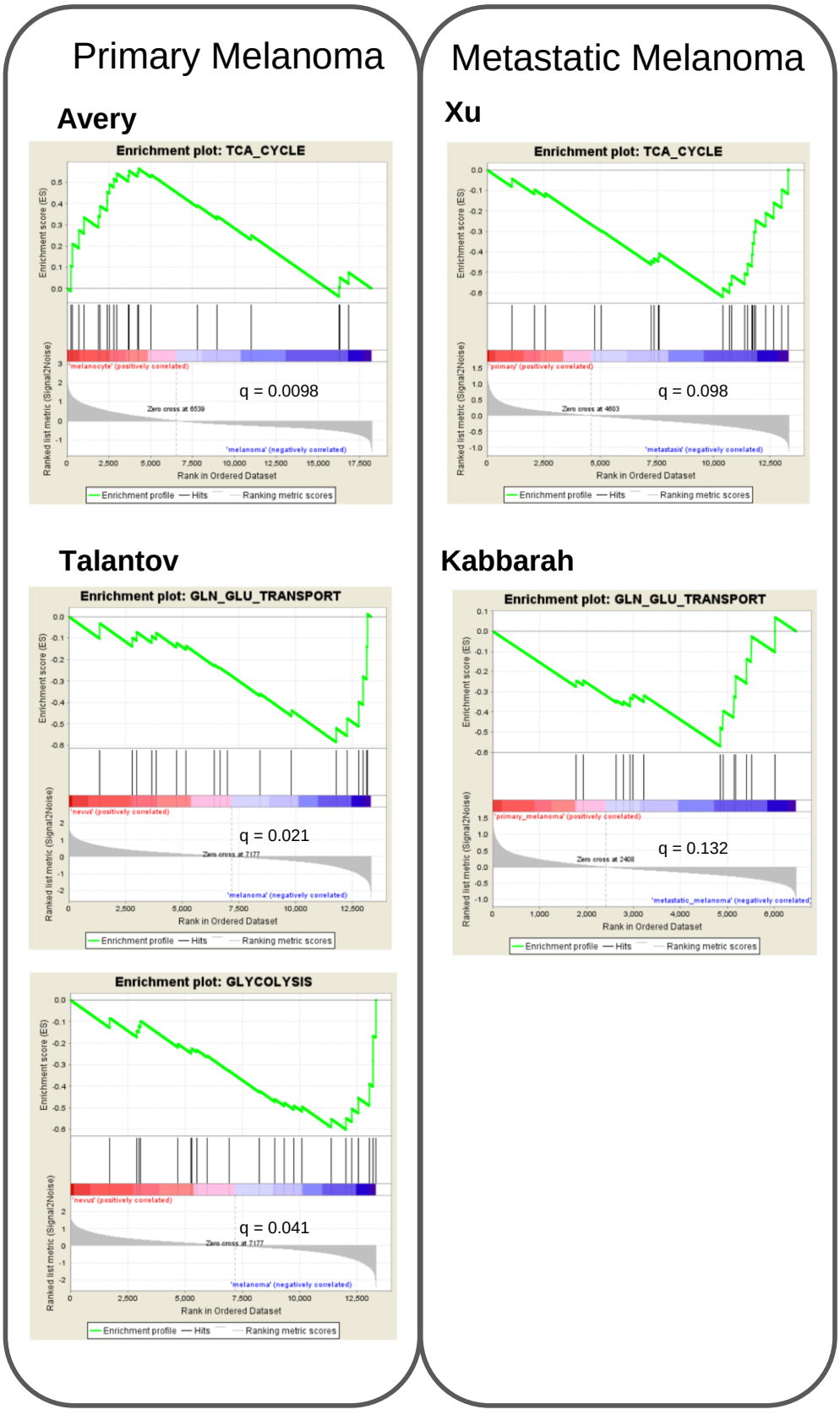

Figure 5.7. Melanoma cells upregulate glycolysis and downregulate aerobic respiration in tumorigenesis and switch to glutamine metabolism during metastasis. GSEA data from Analysis of patient databases. Gene sets were made for diverse metabolic pathways involved in glutamine/glutamate metabolism. Full gene sets are shown in the Appendix A.

5.3.4 *ROCK* expression positively correlates with glutamine metabolism and the TCA cycle while it negatively correlates with glycolysis

It was observed that *ROCK* expression is not normally distributed in melanoma patients, *ROCK1* shows expression that is left-skewed (Figure 5.8A), with most patients having expression below the median. *ROCK2* shows a potential bimodal distribution (Figure 5.8A). While beyond the scope of this work, future work studying the subpopulations of patients expressing different levels of *ROCK* may reveal other factors regulating tumour progression in melanomas.

Linear correlations of the metabolic genes analysed show that genes involved in glutamine metabolism are positively correlated with *ROCK* expression (*GLS1, SUCLG2, ME2, and SDHD.* Table 7). This supports the hypothesis that ROCK can regulate glutamine/glutamate metabolism and the TCA cycle such as. The correlation between *ROCK1* and Glutaminase 1 (*GLS1*) is shown in Figure 5.8B as an illustration.

ROCK expression is also positively correlated with genes involved in glutathione synthesis such as, *GCLC* and *GCLM* (Table 7). This also suggests *ROCK* plays a role in supressing reactive oxygen species by promoting anti-oxidant synthesis.

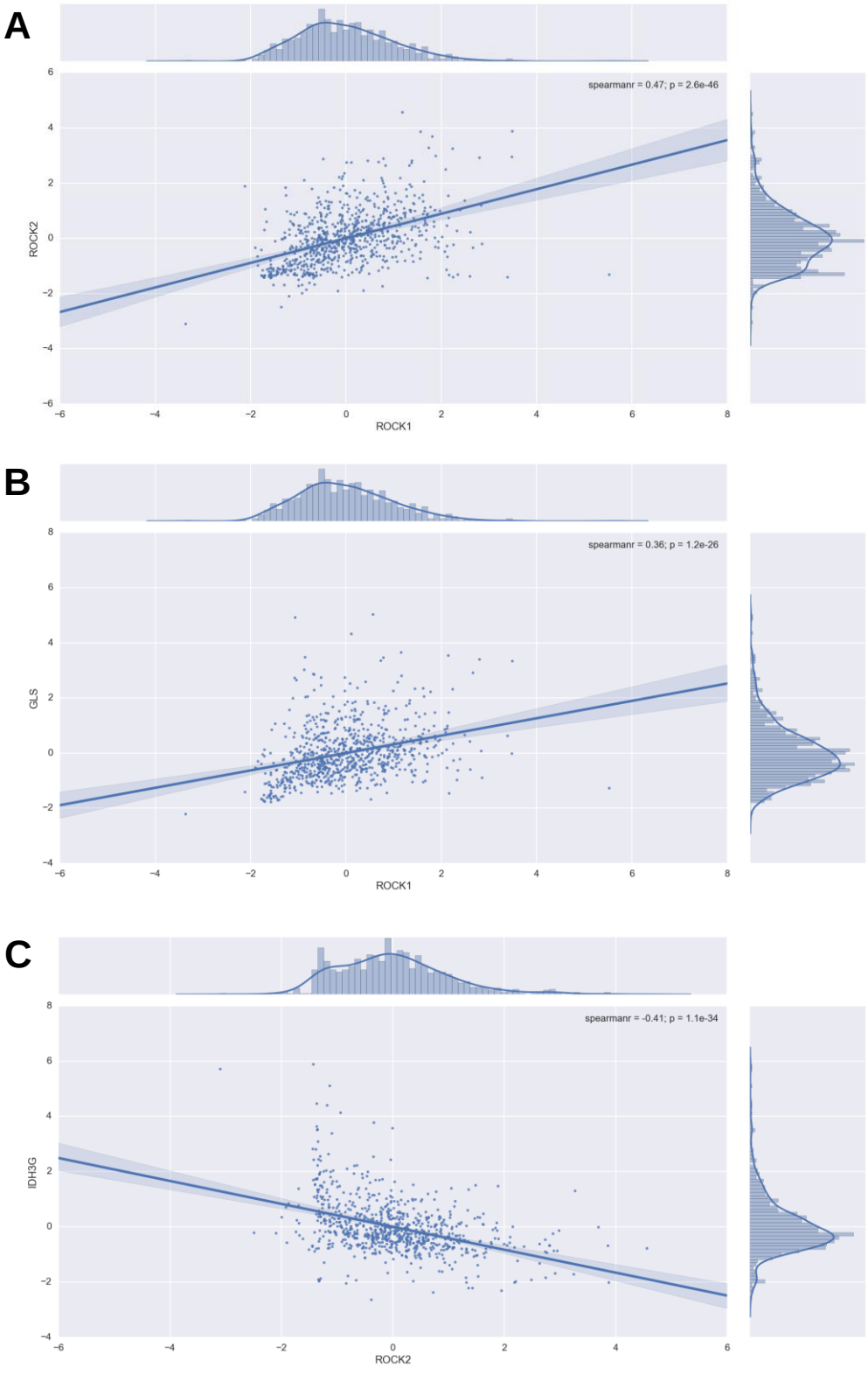

Figure 5.8. Linear regression between z-scores of A) *ROCK1* and *ROCK2* B) *ROCK1* and *GLS1* and C) *ROCK2* and *IDH3G* across the five human melanoma databases (n=804). Covariance test is Spearman's rank correlation and 95% confidence interval is imaged around the linear fit. The margins of the scatter plots show histograms of the distribution of expression of the genes of interest.

Linear correlation analysis of *ROCK* expression show that *ROCK* expression is negatively correlated with a range of glycolysis genes such as *PFKL, TPI1, PKM, PFKL*, and *GAPDH* (Table 8). It has been seen that cells with inhibited ROCK have increased Warburg effect and this supports the data found in the previous chapter. However, it should be noted that there are TCA cycle genes that also negatively correlate with *ROCK*, such as *IDH3G* and *PC*.

5.3.5 *ROCK1* correlates with different metabolic enzymes compared to *ROCK2*

An interesting pattern appears when looking at the genes that pass the cut-off criteria. While *ROCK1* and *ROCK2* expression are strongly correlated (Spearman r = 0.4744, Table 7), there is a difference in which other genes their expression correlates. *ROCK1* expression positively correlates with several TCA cycle genes while *ROCK2* does not (Table 7). On the other hand, both *ROCK1* and *ROCK2* expression is positively correlated with genes involved in glutathione synthesis and nucleotide synthesis (*PPAT*) (Table 7).

ROCK1	**Pathway**	**SpearmanR**	**ROCK2**	**Pathway**	**SpearmanR**
ROCK2	Rho/ROCK	0.4745	ROCK1	Rho/ROCK	0.4745
GLS	Glutaminolysis	0.3646	GFPT1	Glutamate Metabolism	0.2832
SUCLG2	TCA Cycle	0.3518	EPRS	t-RNA synthesis	0.2817
ME2	TCA Cycle	0.3441	PPAT	Purine synthesis	0.2590
GCLM	Glutathione Synthesis	0.3129	ENPEP	Renin-angiotensin system	0.2589
PPAT	Purine synthesis	0.2989	GCLC	Glutathione Synthesis	0.2526
GCLC	Glutathione Synthesis	0.2974	AASS	Lysine Degradation	0.2524
SDHD	TCA Cycle	0.2943	RIMKLB	Glutathione Synthesis	0.2500
GFPT1	Glutamate metabolism	0.2781			
EPRS	t-RNA synthesis	0.2779			

Table 7. Genes involved in the TCA cycle and glutamine synthesis positively correlated with *ROCK* expression. Genes, metabolic pathways and Spearman rank correlations shown for genes where $\boldsymbol{R^2 > 0.25}$

ROCK2 is positively correlated with genes involved in the TCA cycle (*ACO1*, *SUCLG2*) and glutamate synthesis (*ENPEP*). It is negatively correlated with glutamine secretion (*SLC7A5*, *SLC3A2*), and individual genes in the TCA cycle and glycolysis (*IDH3G* and *PFKL* respectively).

Both *SLC3A2* and *SLC7A5* are genes that are involved in glutamine transport. *SLC3A2* codes for the 42F cell-surface antigen heavy chain protein (4F2HC) while *SLC7A5* codes for the Large neutral amino acids transporter small subunit1 (LAT1). When *SLC3A2* and *SLC7A5* associate they form the heterodimer CD98, also called LAT1. LAT1 is involved in the transport of not only glutamine, but also

branch-chained amino acids such as valine, leucine, isoleucine as well as aromatic amino acids like tryptophan and tyrosine.

While *ROCK1* and *ROCK2* expression positively correlate together (Spearman r = 0.4744, Table 7) it is interesting to find that they still correlate a few different genes. This data connects with the results shown in the previous chapter; we observed that *ROCK1* and *ROCK2* have different metabolic profiles in murine models of melanoma where *ROCK* is knocked out. It was suggested that individual isoforms of ROCK redundantly regulate glutamate concentrations. From the expression correlation analysis, we could suggest further that ROCK1 promotes the processing of glutamine/glutamate through the TCA cycle while ROCK2 may play a lesser role in promoting oxidative phosphorylation. ROCK may also suppress the expression of glycolytic enzymes, which is supported by our data showing that inhibiting ROCK activity leads to increased glycolysis in melanoma in the previous chapter.

ROCK1	**Pathway**	**SpearmanR**	**ROCK2**	**Pathway**	**SpearmanR**
IDH3G	TCA Cycle	-0.4799	IDH3G	TCA Cycle	-0.4144
PFKL	Glycolysis	-0.4090	GATB	t-RNA synthesis	-0.3608
GSS	Glutathione Synthesis	-0.3712	*SLC3A2*	Glutamine Transport	-0.3440
OGDH	Glycolysis	-0.3450	PFKL	Glycolysis	-0.3381
SLC3A2	Glutamine Transport	-0.3445	*SLC7A5*	Glutamine Transport	-0.3198
BCAT2	Branched chain amino acid synthesis	-0.3439	PKM	Glycolysis	-0.2995
TPI1	Glycolysis	-0.3334	GOT2	Glutaminolysis	-0.2647
PKM	Glycolysis	-0.3300			
PC	TCA cycle	-0.3266			
ALDH4A1	Glutamate synthesis	-0.3104			
GATB	t-RNA synthesis	-0.2960			
QARS	t-RNA synthesis	-0.2904			
GAPDH	Glycolysis	-0.2871			
SLC7A5	Glutamine Transport	-0.2849			
SLC25A22	Mitochondrial glutamate transport	-0.2676			
EARS2	t-RNA synthesis	-0.2523			

Table 8. Genes involved in glycolysis and glutamine efflux negatively correlated with *ROCK* expression. Genes, metabolic pathways and Spearman rank correlations shown for genes where $\boldsymbol{R^2 > 0.25}$

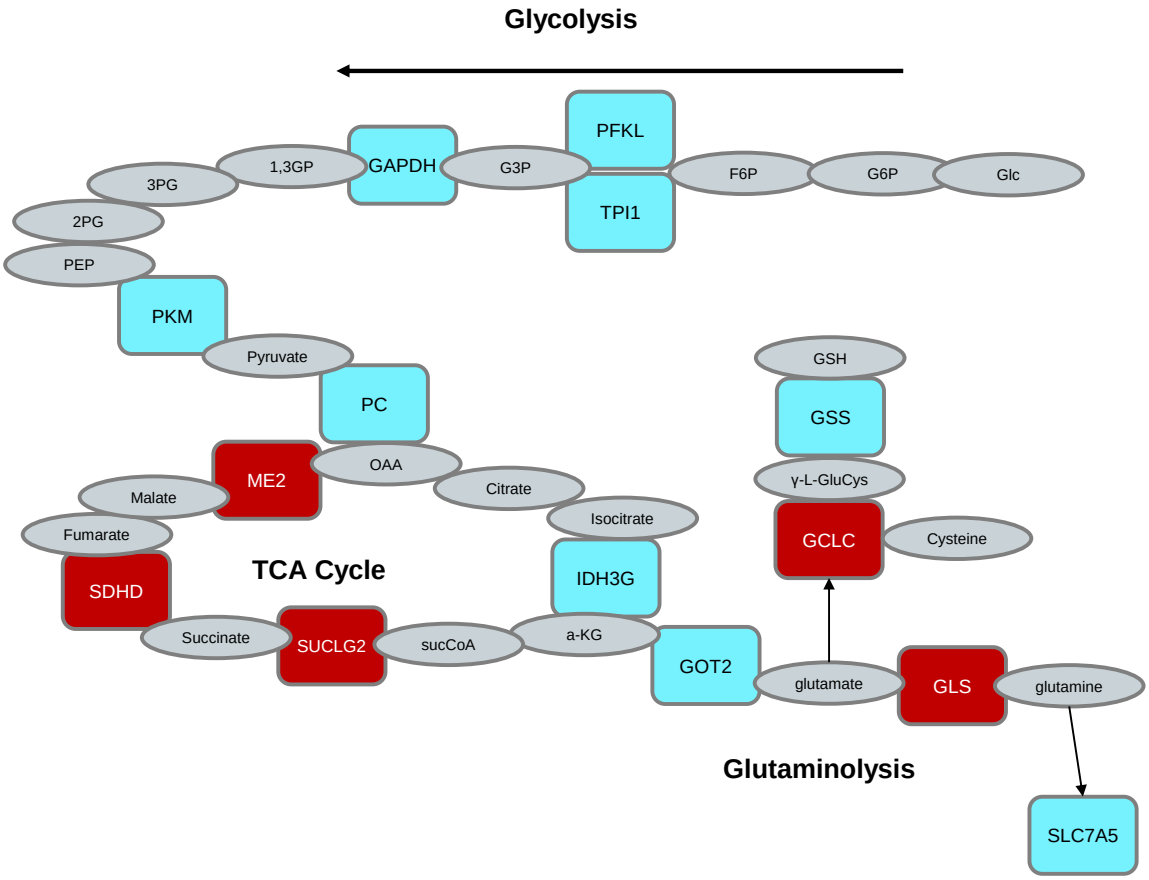

Figure 5.9. *ROCK* expression is positively correlated with glutamine metabolism and the TCA cycle while negatively correlated with glycolysis. Representative figure demonstrating metabolic pathways where *ROCK* expression was positively correlated (red) and negatively correlated (blue) with genes. Metabolites are shown in grey. Genes that did not pass threshold criteria are excluded for illustrative purpose.

The picture that forms from this analysis is that *ROCK* expression is positively correlated with glutamine metabolism and part of the TCA cycle while it is negatively correlated with glycolysis and the release of glutamine via *SLC7A5* (Figure 5.9).

5.3.6 Genes from several metabolic pathways correlated with patient outcomes

The TCGA dataset had the added benefit of having overall survival data along with RNA-set gene expression data which allowed an investigation of how gene expression correlates with patient outcomes. This survival dataset contains a majority of patient data from metastatic melanomas (296 of 354 samples) and therefore is highly biased toward poor prognosis in patients. Despite this, survival analysis of this dataset may reveal patterns within patients that present with metastatic melanomas.

A

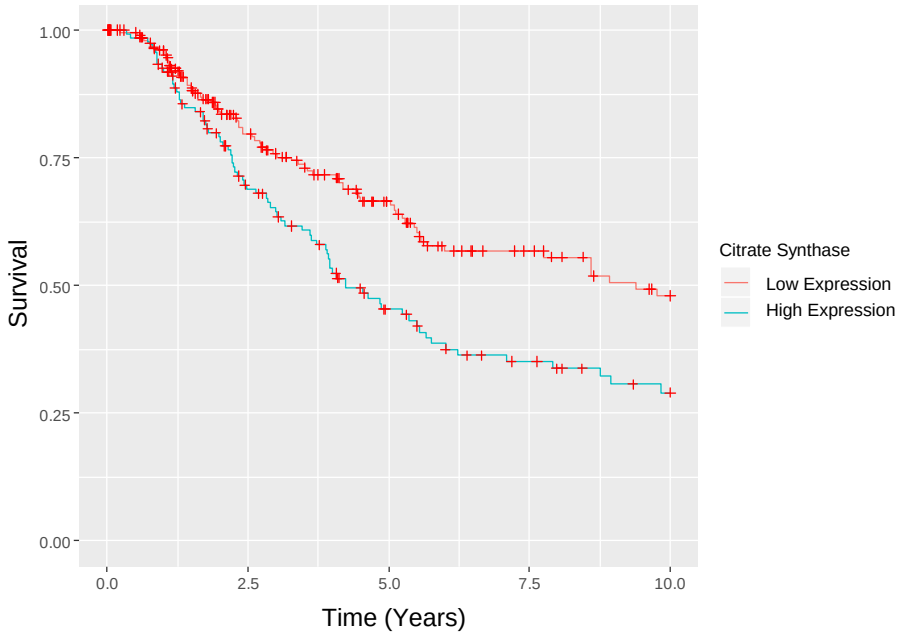

B

Gene	Pathway	q-value	Diff Median OS (Years)
CS	TCA Cycle	0.0262	-5.14
PGAM1	Glycolysis	0.0262	-4.95
GOT2	Glutaminolysis	0.0100	-4.75
CTPS1	Phospholipid and nucleic acid synthesis	0.0140	-4.72
PFAS	Purine synthesis	0.0054	-4.72
GGT6	Glutathione synthesis	0.0155	-3.71
GRIN3A	Glutamate Receptor	0.0054	3.16

Figure 5.10.Survival Analysis of TCGA melanoma data show several genes correlate with overall survival (OS) at 10 years. A) Representative Kaplan-Meier survival curve of Citrate Synthase (CS) demonstrating lower survival of patients with expression of *CS* higher than median expression. CS curve shown for illustrative purposes. B) Table of genes that showed significant correlation with patient outcomes after multiple test corrections.

After False Discovery Rate (FDR, Benjamini-Hochberg method (286)) multiple test correction, seven genes were significantly correlated with better or poorer patient outcomes (Figure 5.10B). *GRIN3A* correlated with better prognosis in patients. *GRIN3A* encodes for the glutamate receptor NMDA type subunit 3A. The other six genes (*PFAS, GOT2, CTPS1, GGT6, PGAM1* and *CS*) all correlated with poor prognosis (Figure 5.10B). The genes that correlated with poor prognosis are genes involved in the TCA cycle, glycolysis, glutaminolysis, and both lipid and nucleotide synthesis. There does not seem to be a clear pattern from this data; it may suggest that highly energetic melanoma cells that cause poor

prognosis and require increased expression of metabolic genes. *ROCK1* and *ROCK2* were also tested and did not correlate with patient outcomes. However, as noted in section 5.3.4, the expression of *ROCK* is non-normally distributed. Future work would look sub-groups of patients with different expression profiles of *ROCK*. This shows that the relevance of ROCK in metastatic melanoma may go beyond expression and instead is related to its activities.

5.3.7 Summary of bioinformatics

To summarize the analysis done in this chapter; we aimed to assess if the metabolomic findings in chapter 4 could be more broadly applicable to clinical data of melanoma patients. 181 genes related to glucose transport/metabolism, glutamine/glutamate transport/metabolism, TCA cycle and Glutamate signalling were selected to analyse gene expression at different stages of melanoma, correlations with *ROCK* expression and correlations with patient prognosis. Univariate analysis was performed to understand the change in expression of these genes in primary melanomas and in metastasized melanomas. It was seen that expression of the glucose transporter *SLC2A3* was upregulated in primary tumour samples while the transglutaminase *TGM2* was upregulated in metastatic samples. This supports the hypothesis that the Warburg effect is important in primary tumour formation and is partially replaced by glutamine metabolism in the metastatic disease. Gene set enrichment analysis was also performed, suggesting that melanomas upregulate glycolysis and downregulate the TCA cycle in primary tumour formation while switching to glutamine metabolism during metastasis. Correlations of gene expression were analysed compared with *ROCK* and it was seen that *ROCK* is negatively correlated with a number of genes responsible for glycolytic enzymes while being positively correlated with a number of TCA cycle genes. This further supports a role for *ROCK* in promoting metastasis via its regulation of metabolism. The glutamate receptor *GRIN3A* correlated with better patient prognosis while a number of genes involved in a variety of pathways such as glutaminolysis, glutathione synthesis, glycolysis and the TCA cycle correlated with poor prognosis.

It was also observed that *ROCK* expression is not normally distributed which would suggest that future analysis of gene expression and patient data should take into account the bimodal distribution *ROCK2* expression. This may reveal additional information on gene expression patterns and potentially prognosis in sub-groups of melanoma patients.

5.3.8 qPCR validation of genes identified from microarray

Thus far analyse have been conducted in patient databases of melanomas. We were further interested in examining the microarray data presented by Sanz-Moreno *et al* (140) from the view of glutamine/glutamate metabolism because their study closely resembles the experimental conditions conducted in our *in vitro* work.

Microarray data on A375M2 cells treated with the ROCK inhibitor H1152 for 16 hours was obtained from (140). The largest change in gene expression observed from the microarray was that the expression of glutaminase (*GLS1*) decreased 8.2% after treatment with H1152 compared to control (FDR adjusted p value = 0.0012). interestingly, there is also a 13.4% reduction in *GLS1* expression in A375 parental cells compared to A375M2, which further suggests that glutamine metabolism may be important in promoting metastatic potential in melanoma. However, this suggests that the gene expression changes observed from this microarray are quite subtle.

As a final part of this work, we aimed to identify potential gene targets in related to glutamine and glutamate metabolism in A375M2 to then further study their roles in cell proliferation and morphology. We used the 106 genes taken from the HMDB gene set described in Figure 5.2 and looked at expression of these genes in the microarray data. The top 20 genes that appeared to be positively regulated by ROCK activity the microarray were then selected to further validate if their expression is regulated by ROCK activity. Primers were validated and optimised (Figure 5.11) prior to gene expression analysis by qPCR. The titration curves for *TGM2* are shown in Figure 5.11A as an illustration. Primers were optimised in A375M2 cells seeded on bovine collagen 1 using 100, 10, 1 and 0 ng of extracted RNA (Figure 5.11B). From the optimisation it was decided that 100 ng of RNA would be used per qPCR well.

Several genes showed very low expression and ct values were not distinguishable between wells with 100 ng RNA and those without cellular RNA. This made quantification by qPCR impossible for genes such as *GRIA1*, *SLC25A18*, and *GRIK1* (Figure 5.12). Other genes showed relatively high expression in A375M2 cells and gave confidence to studies in the transcriptional regulation of these genes during ROCK inhibition.

A Titration curves qPCR - TGM2

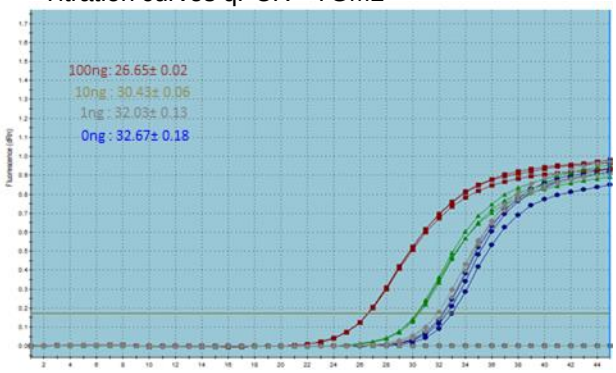

B

Gene	ct_100ng	ct_10ng	ct_1ng	ct_0ng
GAPDH	12.72	15.45	18.47	29.33
GRIK2	18.64	24.14	27.01	34.54
GFPT1	19.09	22.01	25.4	31.58
EPRS	19.55	22.4	25.69	32.42
PPAT	19.91	23.15	26.61	34.33
GCLC	19.96	23.17	26.47	31.34
SLC7A11	20.23	23.05	26.24	34.9
GLUD1	20.5	23.48	26.86	32.37
GLS1	21.09	27.36	31.33	32.05
GLUD2	21.63	22.68	25.19	28.66
OAT	21.83	24.96	28.43	36.69
AASS	24.41	27.71	31.11	36.83
ABAT	25.79	28.31	31.64	36.11
SLC1A1	26.03	28.77	30.31	30.79
SLC7A8	26.41	29.42	32.91	36.99
TGM2	26.65	30.43	32.03	32.67
GLUL	26.84	31.56	35.72	37.18
NAGS	27.92	28.3	30.73	32.72
GRIA1	29.29	30.32	31.99	32.87
SLC25A18	29.79	32.45	34.42	35.82
FOLH1	29.96	31.14	33.83	39.64
GRIK1	31.61	31.51	30.99	30.89

Figure 5.11. Titration of qPCR primers from metabolic genes of interest. A) Representative plot of curves generated from the primer targeting *TGM2*. B) Table of mean ct values for the primers tested at 0, 1, 10, and 100ng. RNA was taken from A375M2 cells seeded onto Collagen 1 for 24 hours at 1% FBS supplemented media.

The expression of the 20 genes was assessed by qPCR. RNA from A375M2 cells plated on collagen 1 was extracted and quantified for the 20 genes of interest. It was seen that there are several genes with relatively high expression compared to *GAPDH*. *PPAT*, *SLC7A11*, *OAT*, *GRIK2*, and *GLS1* were the

most expressed genes from this screen. Of the 20 genes tested, *PPAT* and *SLC7A11* showed the highest expression, with an expression level ~40% that of *GAPDH* (Figure 5.12A). *PPAT* encodes for Phosphoribosyl Pyrophosphate Amidotransferase (PUR1 at protein level) which is the enzyme involved in the first step of *de novo* purine synthesis (287). *SLC7A11* encodes for the glutamate-cysteine exchange transporter protein xCT. It will be further studied in the next chapter due to its relevance to glutamate transport and high expression levels in A375M2 cells. The ionotropic glutamate receptor GRIK2 was also relatively highly expressed in A375M2 cells, with even higher expression glutaminolytic genes such as *GLS1* and *GLUD1* (Figure 5.12B). These findings also suggest that glutamate secretion via *SLC7A11* and glutamate signalling by *GRIK2* may be important in metastatic melanoma.

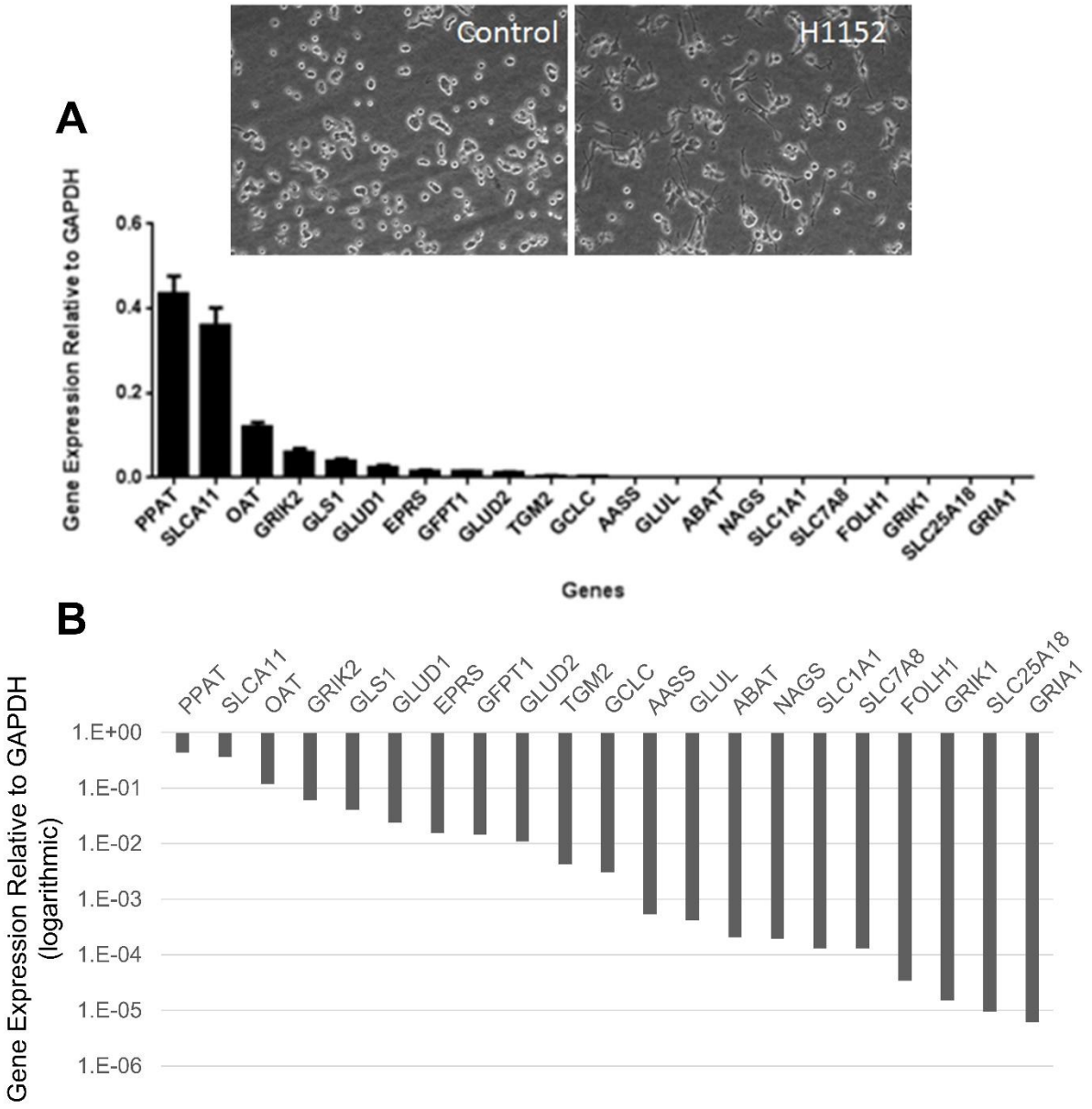

Figure 5.12. Expression of select metabolic genes in A375M2 human melanoma cells. A) Representative images of selected genes in A375M2 human melanoma cells and quantification of gene expression relative to GAPDH of A375M2 cells when seeded on collagen 1. Genes shown in descending order. B) Quantification of gene expression by qPCR relative to GAPDH shown on a Log 10 scale.

We then assessed if the expression of these genes is regulated by ROCK activity as was observed by the previous microarray. Cells plated on collagen were treated with DMSO as control or H1152 for 24 hours. RNA from these cells was extracted and gene expression was quantified by qPCR. The results show that many of the genes did not have a strong regulation of expression by ROCK activity. Initially *TGM2*, *FOLH1* and *GFPT1* RNA levels appeared to decrease after ROCK inhibition (Figure 5.13A). Additional repeats show *TGM2* expression is significantly regulated by ROCK activity (Figure 5.13B). Replicates however showed this effect was much less stated (Figure 5.13B). This is particularly

interesting as we observed in 5.3.2 that *TGM2* is overexpressed in metastatic melanomas when compared to primary melanomas. This points to the possibility that ROCK activity is regulating *TGM2* expression in metastatic melanoma.

The results suggest that only *TGM2* expression is regulated by ROCK activity from the 20 genes initially selected for analysis. This also suggested that the microarray used was not sufficient to draw any conclusions regarding the control of metabolic genes expression by ROCK.

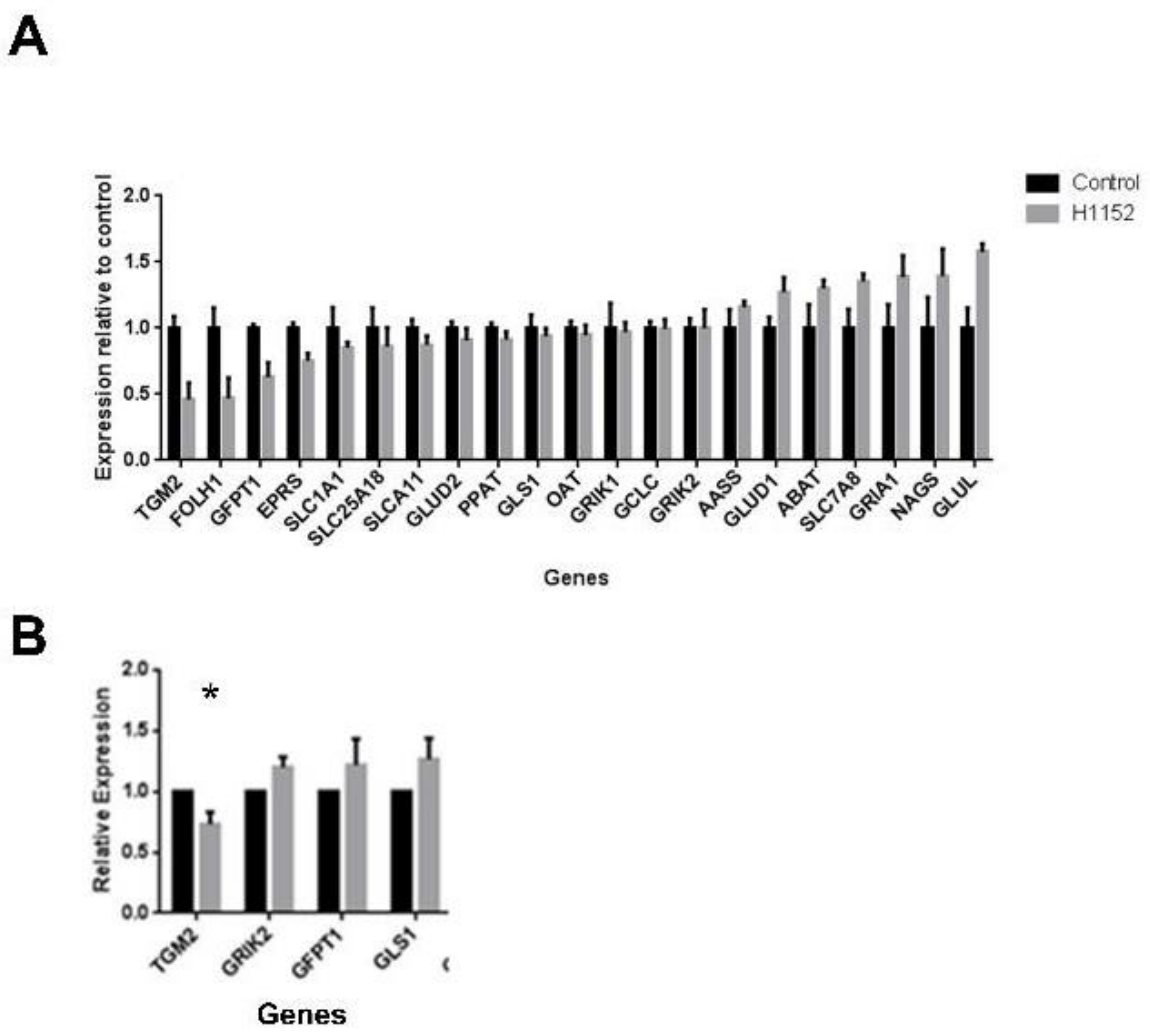

Figure 5.13. *TGM2* expression is regulated by ROCK activity. Gene expression after 24h ROCK inhibition. A) n=1 screen of gene expression of A375M2 cells on collagen 1 treated with DMSO control and H1152 ROCK inhibitor for 24 hours. Genes shown in ascending order of expression after ROCK inhibition. Each sample was tested in triplicate B) Based on initial screen genes were selected for repeat screens. Gene expression relative to control after 24 hours H1152 n=4.

5.3.9 *In vitro* Screens of metabolic targets reveal differential regulation of melanoma morphology and cell proliferation

The candidate did not generate the following data shown in this section. Data presented here was generated by Dr. Eva Crosas-Molit from the Sanz-Moreno group and Ms. Beatriz Padilla from the Mason group. It is presented here to help create a larger context for discussion.

Data generated from the metabolomic data in the previous chapter along with the bioinformatics analysis of glucose metabolism, glutamine metabolism and glutamate signalling was used to inform the generation of a candidate library with which to perform and *in vitro* screen of how these pathways contribute to melanoma proliferation and cell morphology. A total of 21 genes were selected for screening. These were:

- 5 TCA cycle genes (IDH3A, IDH3B, IDH3G, MDH1)
- 4 glutaminolysis genes (GOT1, GOT2, GLS1, SLC7A8)
- 7 glycolytic genes (OGDH, GPI, HK3, ACO2, ENO1, ENO2)
- 2 glutamate receptors (GRIN3A, GRIK2)
- 4 genes identified from the HMDB search which had potential regulation by ROCK. (TGM2, FOLH1, PPAT, EPRS)
- 1 gene regulating m*yo*-inositol transport (SLC5A3)

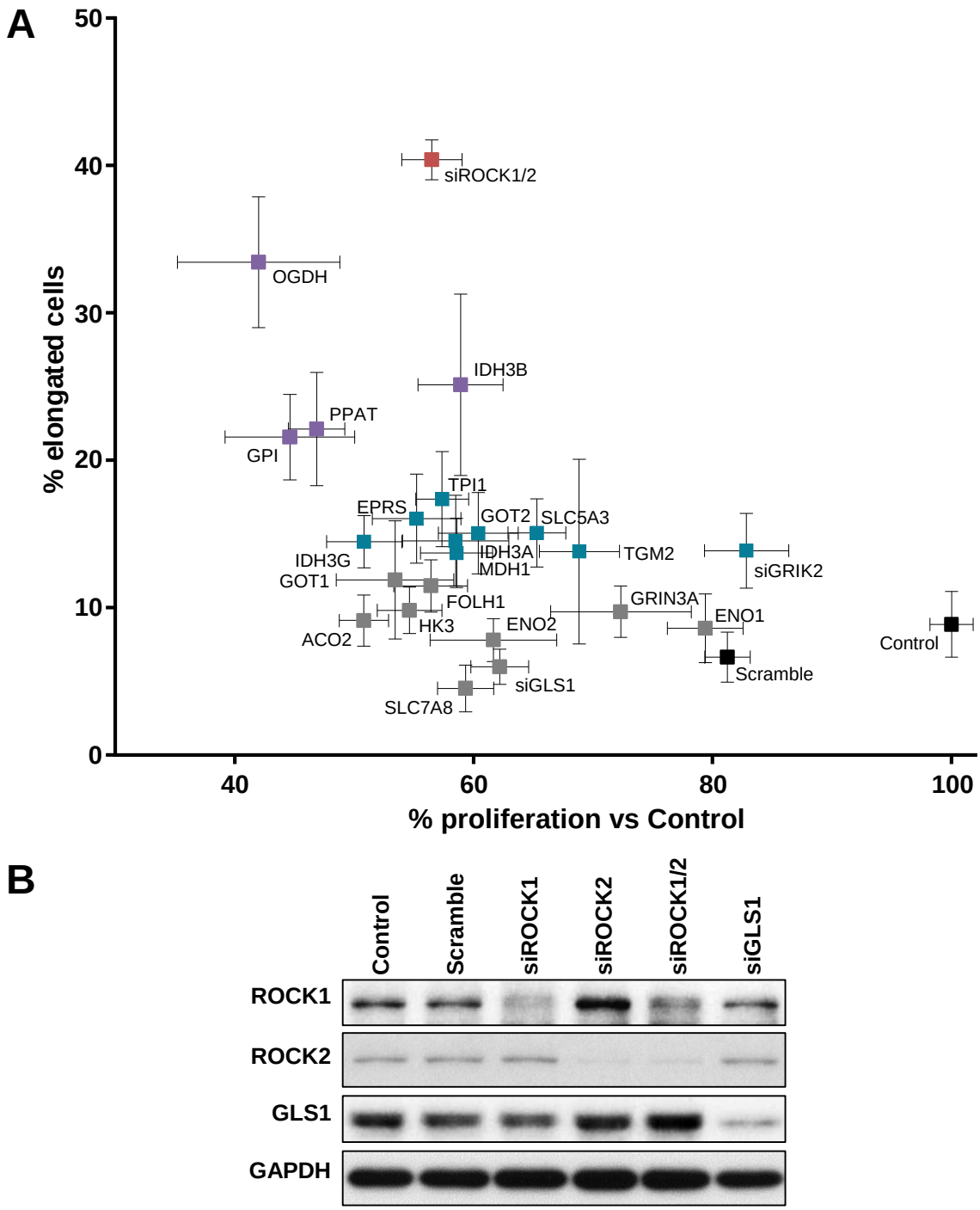

Figure 5.14. Screen of metabolic enzymes show glutamine and glycolysis are required for both cell proliferation and amoeboid phenotype. A) siROCK1/2 is shown in red as a positive control for both cell proliferation and cell morphology. Genes that were selected as have 'strong' regulation of morphology coloured in purple. Other genes with significant regulation of cell morphology are coloured in blue. All experiments were n=3, plots show mean +/- SEM of measured values. B) Representative Western Blot Confirming Knockdowns of genes from screen. Data and figures generated by Dr. Eva Crosas Molist and Ms. Beatriz Padilla

In the screen it was observed that blocking glycolysis (*GPI*, *OGDH*), the TCA cycle (*IDH3B*), or nucleotide synthesis (*PPAT*) led to a significant decrease in proliferation in melanoma cells, similar to or even exceeding that found in the *ROCK1/2* knockdown. In addition, it was seen that knockdown of these gene led to a significant elongation of cells, comparable but less pronounced than those found in ROCK knockdowns.

The results from this screen demonstrate that melanoma cells require both glycolysis and oxidative respiration to sustain both proliferation and a rounded morphology. It is sufficient to block one pathway to see a reduced ability of these cells to sustain proliferation and morphology.

Among other targets selected in the bioinformatics screen, *TGM2* was studied in the first screen and the knockdown a non-significant elongation of cells and a significant reduction in proliferation, however not to the extent of the principle hits found above. Genes involved in glutamine metabolism and transport, such as *GLS1* and *SLC7A8*, had no on cell morphology while leading to a considerable reduction in cell proliferation.

Interestingly, among the three isoforms of Isocitrate dehydrogenase 3 (*IDH3*) studied, *IDH3B* showed to have the largest effect on cell morphology while *IDH3G* had the largest effect on cell proliferation. *IDH3G* was also observe to be negatively correlated with ROCK expression. *IDH3* catalyses the enzymatic reaction of isocitrate to α-ketoglutarate in the TCA cycle. It could be assumed that the isoforms could compensate for the depletion of one isoform, however it was observed that it was sufficient to target an individual isoform to reduce cell proliferation. IDH1 and IDH2 have been extensively implicated in cancer (288) and while no mutations of *IDH3* have been observed in cancer (289) aberrant signalling of IDH3A via HIF1α has recently been seen to promote proliferation in lung cancer cell lines (290).

Two glutamate receptors were also screened, the NMDA receptor *GRIN3A* and the kainate receptor *GRIK2*. Silencing *GRIN3A* had no significant effects on either cell proliferation or morphology while *GRIK2* had a significant effect on cell morphology while having no effect on cell proliferation. This contrasts with the vast majority of genes silenced in the screen and shows it is possible to alter morphology without impacting on proliferation.

5.4 Discussion

This chapter builds upon the metabolomic work in Chapter 4 by investigating the role of glucose/glutamine/glutamate metabolism, transport and signalling in melanoma metastasis in a large set of melanoma patient transcriptome data. This was done to determine whether the experimental data found in chapter 4 is more broadly applicable to a clinical setting.

Gene expression at different disease stages was analysed suggesting differing roles for glycolysis and the TCA cycle in melanoma tumorigenesis and progression respectively. Gene expression was investigated both at an individual level and at the level of gene sets. Glycolysis and in particular *SLC2A3* was seen to be overexpressed in the process of primary tumour formation while the TCA cycle was seen to be downregulated in primary tumour samples when compared normal skin/melanocyte. Several genes were found to have potential therapeutic value as their expression was correlated with poor prognosis in patients.

Finally, the link between ROCK and these metabolic pathways was further investigated by examining the correlation in expression between ROCK and the metabolic genes. It was seen that *ROCK1* expression positively correlates with TCA cycle genes and negatively correlates with a number of glycolytic enzymes. In the previous chapter we observed that inhibition of ROCK activity led to increases in the consumption of glucose and lactate production. It has also been shown that ROCK1 regulates the trafficking of the glucose transporter GLUT3 to the plasma membrane (156). It may be that, in future, this link could be further established at a transcriptional level for both ROCK signalling and glycolysis.

Post-hoc analysis of previously published micro-array data (140) suggested several metabolic enzymes that may be transcriptionally regulated by ROCK signalling. Further investigation of the micro-array data along with validation of these results by qPCR demonstrate the difficulty observing relatively small changes in gene expression.

5.4.1 Transglutaminases are differentially expressed in melanomas

Tissue transglutaminase 2 (*TGM2*) was observed to be significantly overexpressed in three of the four patient databases examined comparing metastatic melanoma samples to primary melanoma samples (Figure 5.5) but that this expression pattern does not correlate with either ROCK1 or ROCK2. Nevertheless, we observed *in vitro* that *TGM2* expression was modestly but significantly downregulated after ROCK inhibition (Figure 5.13B). This data points to *TGM2* playing an important role in melanoma

metastasis and could be directly regulated by ROCK activity. Furthermore, knockdown of *TGM2* had a modest but significant effect on both melanoma cell proliferation and morphology (Figure 5.14). in contrast, *TGM1* was seen to be less expressed in all four of the databases (Figure 5.6) while *TGM3* and *TGM5* we also observed to be less expressed in metastatic melanomas; again this pattern did not correlate with *ROCK1* or *ROCK2* expression. As briefly touched upon in the results section (5.3.2), transglutaminases have been shown to regulate the activity of both RhoA (284)and ROCK2 (283). It has been seen that transglutaminases can transamidate RhoA which leads to a constitutively active GTPase which can then lead to increased activity of ROCK. It is interesting that we observe a regulation of *TGM2* expression by ROCK as this suggest a regulatory loop between *TGM2* and ROCK.

TG2 is a complex and multifunctional enzyme involved in catalysing the formation of an isopeptide bond between a free amine group and acyl group, peptide cross-linking and post-translational modifying transamidation, deamidation, as well as a host of other functions such as the ability to serve as a kinase and atypical ATP/GTPase. These numerous roles within the cell have implicated *TGM2* in cellular adhesion, migration, growth and survival as well as regulating apoptosis, differentiation, and ECM organization. As a result of these processes, *TGM2* is associated with not only tumour growth and metastasis, but wound healing, inflammation, neurodegeneration and tissue fibrosis (285). However, the particular role played by *TGM2* in tumorigenesis and metastasis is not well defined and appears likely to be influenced and altered by a number of factors. *TGM2* has been shown to have opposing effects in anti- and pro-apoptotic effects on cancer cells depending on its multifunctional activity and conformational changes dependent on the local environment, in addition to the genetic background of the system of study(291).

In the context of metastasis, it has been shown that both the absence of *TGM2* in secondary site cells and overexpression in primary site cells is essential for successful melanoma metastasis (292). Further complicating the matter, melanoma tumour growth and invasion has been shown to be inhibited by an atypical GPCR, GPR56, of which TG2 is a major binding partner (293). Nevertheless, there does appear to be ample reason to believe that *TGM2* plays a tangible role in tumour development and metastasis in renal cell carcinoma (294), colorectal cancer (295) and breast cancer (296). It seems highly likely that the particular function and potential pathogenicity of *TGM2* is highly tissue-dependent (297,298). Our data supports not only the idea that *TGM2* could promote metastasis, but that changes in ROCK activity could be regulating *TGM2* expression.

We also observed that other members of the transglutaminase family such as *TGM1* and *TGM5* were downregulated both in primary melanomas and in metastatic melanoma. There is much less literature available regarding other the other transglutaminase family members observed in our study. *TGM1* has been shown to stabilise endothelial and keratinocyte cell junctions (299) therefore it would be possible that invading cancer cells would downregulate *TGM1*. *TGM5* also seems to play a role in maintaining the structural integrity of the epidermis; mutations in *TGM5* lead to acral peeling skin syndrome, a rare autosomal recessive disorder which is characterised by blistering and peeling of the skin (300). This will present challenges for further research as it will be important to understand if *TGM2* has a role in promoting metastasis. Further work should be conducted to understand to what extent ROCK is regulating *TGM2* expression and/or activity.

5.4.2 Glutamine/glutamate transporters

5.4.2.1 *SLC1A5* and *SLC7A5*

We observed that *ROCK2* expression is negatively correlated with *SLC3A2* and *SLC7A5*. *SLC3A2* (CD98hc) and *SLC7A5* (LAT1) dimerize to form the active amino acid transporter LAT1 (301). *SLC3A2* is of particular interest as it is required for the active transporters not only of LAT1, but of several other amino acid transporters such as LAT2 glutamine transporter (*SLC7A8*) and xCT (*SLC7A11*) glutamate/cysteine exchange (302). This fits well with the data presented in Chapter 4 as the LAT1 heterodimer is involved in glutamine efflux coupled with leucine intake (303). In the study by Nicklin *et al (303)*, they demonstrated that *SCL7A5* (LAT1) is coupled to *SLC1A5* (ASCT2) in activating the mTOR pathway as ASCT2 regulates glutamine uptake coupled with sodium efflux while LAT1 then exchanges intracellular glutamine for extracellular leucine. While in our work we have focussed on glutamine and glutamate, it should be noted that leucine also regulates melanoma proliferation and autophagy via mTORC signalling (303). Autophagy is a self-destructive process which allows cells to adapt to nutrient deprivation (304). It has been shown that under low pH conditions, melanomas undergo autophagy as a protective mechanism (305). More recently, Jewell *et al* showed that depriving melanomas of leucine inhibited autophagy and lead to apoptosis in four melanoma cell lines(306). This suggests that LAT1 could potentially play a role in these pathways as it is also involved in leucine uptake. In our studies we observed that when ROCK is inhibited, melanoma cells secrete lactate, which would thus reduce the pH of the microenvironment. This adds acid stress to melanoma cells, and thus cells would require

more leucine to support autophagy. This could partially explain the inverse correlation in expression between *ROCK2* and *SLC3A2*/*SLC7A5*.

Additionally, CD98hc (*SLC3A2*) has been shown to bind and regulate β1 Integrin, which itself is responsible for regulating Rac, PI3K and AKT signalling (307,308), suggesting a role for amino acid transporters not only in direct metabolism, but also in signalling pathways involved in cell proliferation and migration.

ASCT2 and LAT1 are the two most well studied glutamine transporters. ASCT2 has been shown to play a role in sustaining the proliferation of cervical cancer, osteosarcoma, clear-cell renal carcinoma, triple negative breast cancer, non-small cell lung cancer, prostate cancers, colorectal cancers, and hepatomas (309-319). With regards to melanoma, *SLC7A5* has already been proposed to be an independent prognostic marker for melanoma in a study of 30 melanoma patients (318). In a study by Wang *et al*, targeting ASCT2 reduced proliferation, however targeting LAT1 with the small molecule inhibitor BCH did not reduce melanoma proliferation (203). As has been previously suggested, this could be explained by the opposing but coupled roles of ASCT2 and LAT1 in regulating glutamine transport.

5.4.2.2 SLC7A8

Data from this chapter points to *SLC7A5* as being of particular importance in melanoma patients. Additionally, there was some initial indication that *SLC7A8* may also be of interest as in the microarray data in the previous chapter we observed that *SLC7A8* expression could be regulated by ROCK activity. However, further work showed it is very weakly expressed in A375M2 cells and there was no observed regulation of *SLC7A8* by ROCK activity. Furthermore, it was observed to be both over and under expressed in primary melanomas compared to normal tissue and it was not seen to be overexpressed in metastatic melanomas.

SLC7A5 and *SLC7A8* are both members of the cationic amino acid transporter/glycoprotein associated family of solute carriers (SLC). Both of these light chain subunits associate with *SLC3A2* (4F2hc/CD98), the heavy chain subunit, to form functional channels, LAT1 and LAT2 respectively. Each are associated with the transport of large, neutral amino acids, or in the case of LAT2, occasionally various cationic amino acids. LAT1 preferentially transports large neutral amino acids, for instance, L-phenylalanine, L-tryptophan, L-leucine and L-tyrosine. The selectivity of LAT2 appears to be broader whilst the affinity towards each is generally lower, excluding alanine, which only the latter is capable of transporting at

physiological concentrations (320). LAT2 has been implicated in arginine/glutamine exchange, with glutamine influx being heavily favoured over efflux (321). The transport of amino-acids is essential for a variety of nutrient-based cellular functions such as growth, proliferation and cell integrity and maintenance.

While *SLC7A5* expression has been consistently associated with a number of cancerous conditions, *SLC7A8* has rarely been observed in tumour cells, whilst shown to be ubiquitously expressed in non-tumour cells. Thakkar and colleagues (322) demonstrated activation of *SLC7A8* in breast cancer cell lines overexpressing the oestrogen receptor, suggesting its involvement in mitogenic signalling. Expression of *SLC7A8* in ovarian cancer has shown to be unchanged while *SLC7A5* was overexpressed (323), or even negatively associated with tumorigenesis (324). Expression of *SLC7A5* was associated with the development of malignant glioma (325), breast cancer (320), colorectal adenocarcinoma (326) and gastric carcinoma (327). On the other hand, the expression and activity of SLC7A8 in each of these cancers was either unchanged or negatively correlated. Furthermore, *SLC7A5* was found to be associated with tumorigenesis, migration, invasion and metastasis in renal cell carcinoma (328) and cholangiocarcinoma (329). Again in these studies the impact of *SLC7A8* was seen to be non-significant.

It is well established that melanoma is a highly plastic cancer and can shift between different invasive phenotypes with rapid succession. In some systems such as astrocytes LAT2 *(SLC7A8)* rather than LAT1 (*SLC7A5*) is the principle transporter of glutamine and is primarily involved in its influx (330). It does not appear to play an important role in melanomas or other tumour types however and *SLC7A5* is taking a more central role in sustaining tumour proliferation and invasion.

5.4.2.3 *SLC7A11*

SLC7A11 encodes for the xCT protein and is a cysteine/glutamate exchange transporter which in principally known for importing extracellular cysteine while exporting glutamate. We observed that *SLC7A11* is highly expressed in A375M2 human melanoma cells. The importance of xCT has typically been thought to be the import of cysteine whose presence is the rate limiting amino acid in the synthesis of glutathione (331,332). It has been suggested to be a useful target for cancer therapy since 2005 (332). Its additional role in glutamate release, also makes it an attractive target. As stated earlier, glutamate is both an important signalling molecule and can create excitotoxicity for surrounding tissue.

Glutamate signalling has been shown to promote glioma cell invasion (333), decrease cell adhesion in melanocytes (334), and promote invasion in bone metastasis (197). It has been suggested to be a therapeutic target in triple negative breast cancer (335) and targeting xCT has shown to induce tumour regression in HIV-associated lymphoma (336,337). It binds to CD44, an important antigen that regulates cell migration and adhesion (338). *SLC7A11* expression correlates with patient prognosis in glioblastoma (339), hepatocellular carcinoma(340), squamous cell carcinoma (341) and malignant gliomas (342), suggesting its importance in a variety of cancer types.

5.4.3 Glutamate Receptors

Glutamate receptors play an important role in pre- and post-synaptic signalling in neurons. Glutamate receptors are divided into two major groups: metabotropic receptors, which are G-Protein coupled receptors activated by the binding of glutamate, and ionotropic receptors, which are classically understood to be ion channels and activated by glutamate binding. This strict view of the function of ionotropic receptors is being challenged by evidence that they may have metabotropic functions as well (343).

In our work we observed that high *GRIN3A* expression was seen to be associated with better patient prognosis. *GRIN3A* encodes for NMDA receptor subunit 3A (GluN3A). While initially it may seem curious to see that a specific subunit of glutamate receptors correlates with better prognosis in patients, there is a possible explanation that can be garnered from the literature. the GluN3A subunit of NMDA receptors forms atypical NMDA receptors which have been proposed to be dominant negative and antagonise the function of classical NMDA receptors (344). NMDA receptors containing a GluN3A subunit have lower $\mathbf{Ca}^{2+}$ permeability and produce smaller glutamate-evoked whole-cell currents in the central nervous system (344). When viewed in the context of glutamate signalling promoting metastatic potential in melanoma, this is more evidence that glutamate signalling may be playing a role in promoting melanoma progression. *GRIN3A* was screened for its effects on cell proliferation and morphology and it was observed that silencing *GRIN3A* has no effects on cell proliferation or morphology (Figure 5.14) and this again supports the view that *GRIN3A* may be playing a different role from other glutamate receptors, such as *GRIK2*, which was seen to significantly affect cell morphology after silencing.

Other evidence is provided by *GRIN2A*, which forms classical NMDA Receptors. It has been shown to be mutated in 25-33% of melanomas (222,345) and may be a contributing factor to poor prognosis in

patients (346). In our work we observed that *GRIN2A* is mutated in 25% of the 287 melanomas in the TCGA dataset with mutation and copy number variant data. It did not however correlate with patient outcomes. The lower power of the work of D'Mello *et al* (19 patients total) may explain the significance of their findings.

5.5 Conclusion

In chapter 4 we identified that glutamine/glutamate metabolism maybe involved in promoting melanoma proliferation or an amoeboid phenotype via ROCK signalling. In this chapter we assessed the roles that these metabolic pathways play in melanoma patient databases to understand if the results found *in vitro* may have relevance in a clinical setting. A picture arose from the data analysis which points to glutamine and glutamate transport being upregulated during metastasis in melanoma. Links were also established between *ROCK* expression and glutamine metabolism, with *ROCK1* positively correlating with glutamine metabolism and negatively correlating with glycolysis. Additionally, *ROCK2* negatively correlated with glutamine secretion and leucine uptake again supporting the hypothesis that ROCK drives glutamine metabolism.

Transcriptome data from A375M2 melanoma cells where ROCK activity was inhibited by small molecule inhibitors was also analysed in the view of glutamine/glutamate metabolism. It was observed that genes involved in glutamate secretion and glutamate signalling are highly expressed in A375M2 melanomas. Finally, a selection of metabolic genes from the microarray data was screened for their effects on melanoma proliferation and morphology. This screen demonstrated that there is a relationship between cell proliferation and morphology and suggests that melanoma cells require energy from both glycolysis and the TCA cycle to sustain high levels of both. Additionally, glutamate signalling was also observed to play a role in regulating melanoma morphology.

In the next chapter we have shown that the results found in chapter 4, namely that ROCK activity drives melanoma metastasis via regulation of glutamine/glutamate metabolism, may be applicable to the broader, more heterogeneous clinical setting of melanoma. In the next chapter we will return to an *in vitro* setting to further study the metabolic pathways that were examined and discussed in this chapter.

Chapter 6 : An *in vitro* investigation of Glutamine metabolism and glutamate signalling in melanoma

6.1 Introduction

In the previous chapters, we observed that ROCK activity drives higher levels of intracellular glutamine, glutamate and glutathione. In addition, inhibition of ROCK activity led to increase anaerobic respiration in the presences of oxygen. Glutamine and glutamate metabolism was investigated through patient microarray data and it was seen that enzymes involved in glycolysis are upregulated in primary melanomas while genes involved in glutamine metabolism are upregulated in melanoma metastasis. Furthermore, ROCK expression correlated with glutamine metabolism and the TCA cycle while being inversely correlated with glycolytic enzymes. The collected data together suggests that metastatic melanomas become less dependent on the Warburg effect and utilise glutamine/glutamate metabolism to sustain high levels of proliferation in metastatic potential. In short, we have also found evidence that ROCK may promote glutamine metabolism in metastatic melanoma, both through the metabolomic studies conducted as well as through our bioinformatics analysis.

6.1.1 Glutamine/Glutamate transport in melanoma cell proliferation and morphology

Based on the work in the previous chapters we have built a hypothesis that ROCK is promoting melanoma metastasis via the regulation of glutamine/glutamate metabolism and glutamate signalling. In this chapter we aim to test this hypothesis and further understand how glutamine/glutamate metabolism affects the proliferation and morphology of metastatic melanoma and if there is evidence for how this is direct regulated by ROCK. Toward this aim we have two principle objectives: First, we will conduct studies of how interfering with glutamine/glutamate metabolism and signalling regulates melanoma proliferation, melanoma cell morphology and their metabolic profiles. Secondly we aim to link regulation of glutamine/glutamate metabolism and/or glutamate signalling to ROCK expression or activity.

Several amino acid transporters are of interest to us as we observed that the expression of enzymes responsible for glutamine/leucine exchanges (*SLC7A5*/*SLC3A2*) negatively correlates with ROCK expression in melanoma patients. Additionally, *SLC7A11* which encodes for xCT, responsible for glutamate cysteine exchange, was seen to be highly expressed in A375M2 melanoma cells. As discussed in the previous chapter, gln/glu transport has garnered interest in cancer research due to the important roles they play in aiding ‘glutamine addiction’ (347) and maintaining antioxidant homeostasis

(348). For this chapter, six genes involved in gln/glu transport were selected, either on the basis of their potential significance in metastatic melanoma, identified in the previous chapter (*SLC1A5*, *SLC3A2*, *SLC7A5*, and *SLC7A11*), or their putative ability to affect uptake of glutamine from cell culture media (*SLC38A1* and *SLC16A19*). In a similar fashion to the RNAi screen shown in the previous chapter, we are interested in understanding if these genes associated with glutamine/glutamate transport play roles in regulating cell proliferation and/or cell morphology. We will then investigate if the metabolic profiles of melanoma cells where the expression of gln/glu transporters are silenced replicates the profiles of cells where ROCK activity or expression is inhibited.

6.1.2 Glutamate signalling in melanoma cell proliferation and morphology

In the previous chapters we observed that glutamate is secreted by melanoma cells and glutamate signalling may also be playing a role in regulating cell proliferation or morphology. Glutamate signalling is mediated by transmembrane proteins that bind to and are activated by glutamate. There are two major groups of glutamate receptors divided according to their downstream signalling; metabotropic receptors are G-protein coupled receptors while ionotropic receptors are ion channels. Glutamate signalling has already been implicated to be important in melanoma. It has been seen that overexpression of the metabotropic receptors *GRM1* and *GRM5* are sufficient to induce melanoma in mouse models of melanoma (224,226). Additionally, ionotropic receptors such as *GRIN2A* have been seen to be often mutated in melanoma (222) and mutant *GRIN2A* may supports tumour cell survival. Evidence from the previous chapter as well as the literature all support our hypothesis that glutamate signalling plays a role in promoting melanoma proliferation and metastasis.

There is additional evidence that glutamate signalling may play a role in promoting melanoma progression. TCGA data shows that the 26 glutamate receptors genes are mutated in 80.1% out of 287 melanomas from the largest dataset of melanoma sequencing data present on the TCGA (Figure 6.2) (180,181). *GRIN2A* is mutated in 25% of cases followed by *GRID2* which is mutated in 19% of melanomas (Figure 6.3). The data found in the TCGA database supports other published literature which has found *GRIN2A* to be mutated in 22-33% of melanomas (222,345), and has been suggested to have prognostic value (346).

This evidence is further bolstered when compared to the total mutation data in the TCGA. There are 1485 genes found to be mutated in at least one melanoma in the TCGA dataset. The average mutation

rate of these genes is 4.67% (Figure 6.1), There are 151 genes mutated in more than 10% of melanoma. GRIN2A is the 36th most mutated gene in the melanoma dataset.

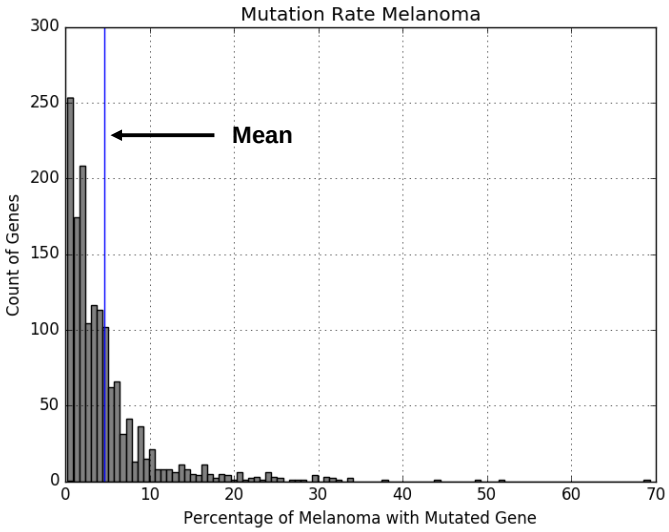

Figure 6.1 Histogram of mutated genes in the TCGA melanoma dataset vs. percentage of melanomas harbouring mutated gene. The mean mutation rate (4.67%) is highlighted with blue line. There are a total of 1485 genes mutated in the TCGA melanoma dataset, comprised of 358 melanoma samples with mutation data.

This evidence further suggests that glutamate signalling may play an important role particularly in melanoma compared to other tumour types. For examples, glutamate receptors are only mutated in 6.1% of chronic lymphocytic leukaemia (Figure 6.2).

While there are many putative glutamate receptors that may be of interest in melanoma (and will warrant future investigation), here we focus on *GRIK2*. The ionotropic glutamate receptor subunit *GRIK2* is highly expressed in A375M2 melanoma cells and there was an indication, in a previous microarray study (140), that expression of *GRIK2* may be regulated by ROCK activity. In addition, silencing of *GRIK2* expression led to significant changes in melanoma cell morphology while not affecting cell proliferation. We will interrogate *GRIK2* further, by confirming that the morphological changes observed in the previous chapter are due to changes in actomyosin.

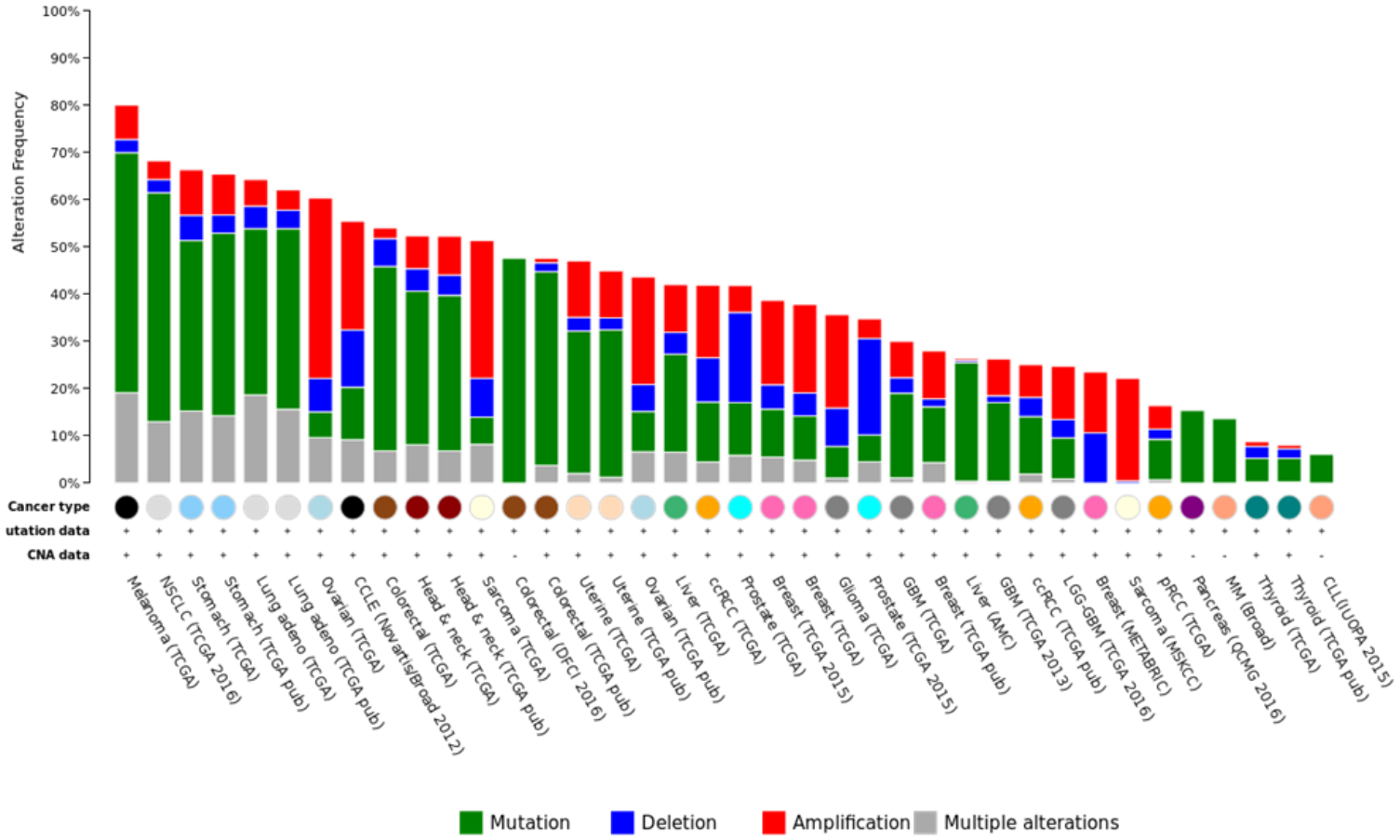

Figure 6.2. Glutamate receptors are often mutated in melanoma. Histogram of genetic alterations of the 26 glutamate receptors in the TCGA database. Melanoma datasets are shown in black in the cancer type segment. Mutations are shown in green, deletions in blue, amplifications in red and multiple alterations in grey. Cancer types are listed in descending order of mutation rates for the 26 glutamate receptor genes. Figure is generated from cbioportal.org. A public repository and web-tool for visualising TCGA data (181). Datasets are selected as having a minimum of 200 samples and having mutation and Copy number variants (CNV) data available.

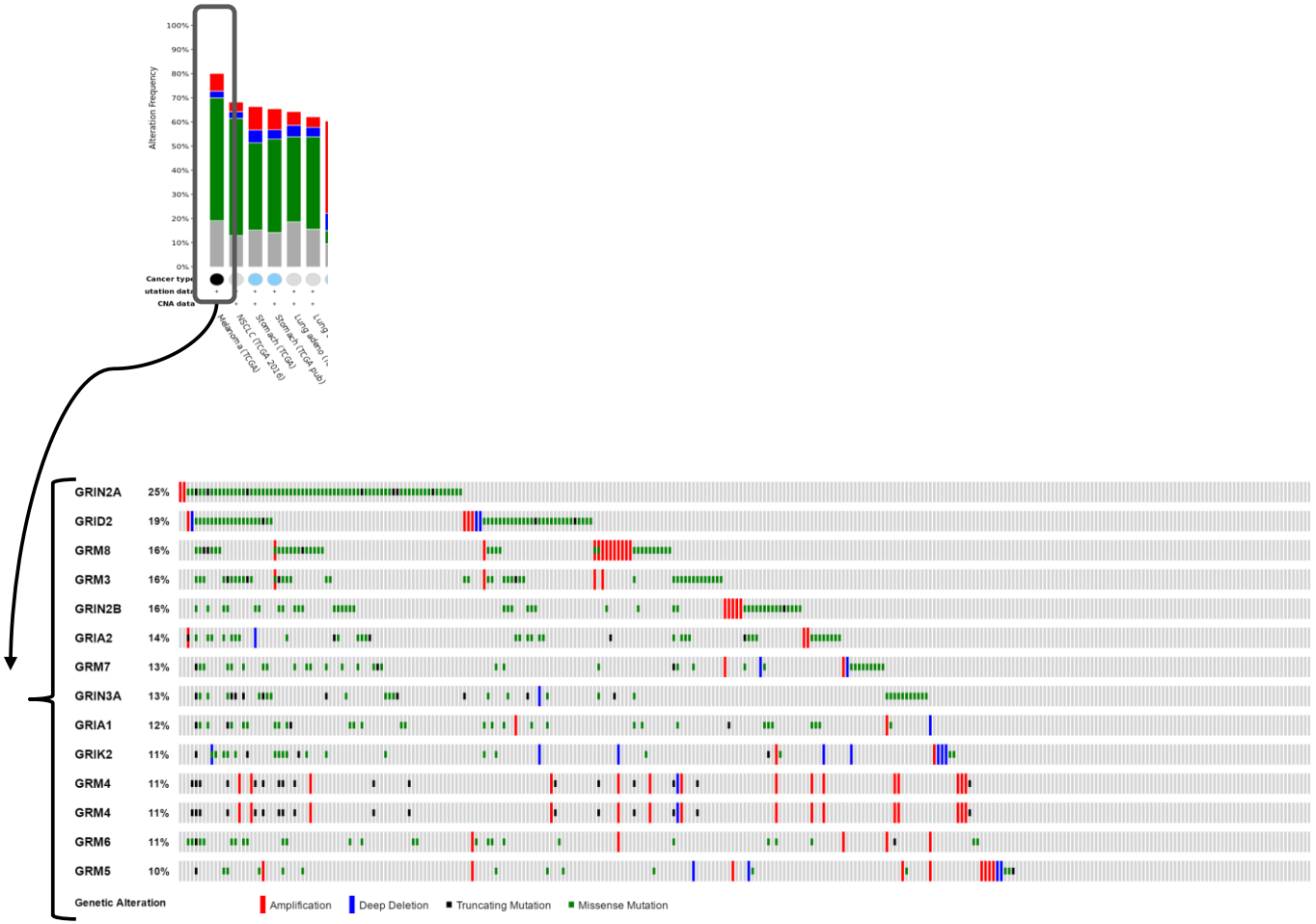

Figure 6.3. Glutamate receptor genes are often genetically altered in melanoma. Individual melanoma sample are plotted along the x-axis along with genetic alterations. Individual glutamate receptor genes are mapped to the y-axis along with the percentage of cases in which genetic alterations are found. Only genes that show genetic alterations in more than 10% of samples are shown in figure. Mutations are shown in green, deletions in blue, amplifications in red and cases with no genetic alterations are in grey. Data and figure generated from cbioportal.org, a public repository of TCGA data(181).

6.1.3 GRIK2 is mutated in A375M2 cells

In the previous chapter we observed that *GRIK2* was highly expressed in A375M2 human melanoma cells and that silencing of *GRIK2* expression led to significant changes in morphology while not affecting cell proliferation. This motivated our further investigation into the role of *GRIK2* in melanoma metastasis. The Catalogue of Somatic Mutations in Cancer (COSMIC)(349) shows that A375 human melanoma cells harbour a mutated form of *GRIK2*. It has a missense C > T mutation, which leads to the substitution of threonine 740 to an isoleucine reside. If mapped to a crystallographic model of GluK2 (*GRIK2*) (350), the mutated residue is T709, located very closely to the glutamate binding domain (Figure 6.4, mutated reside shown in black). This may possibly affect the function of the protein, although further studies would have to verify this. We addressed this possible confounding factor in A375M2 cells by also studying the role of *GRIK2* in a murine model of melanoma, the B16F10 cells.

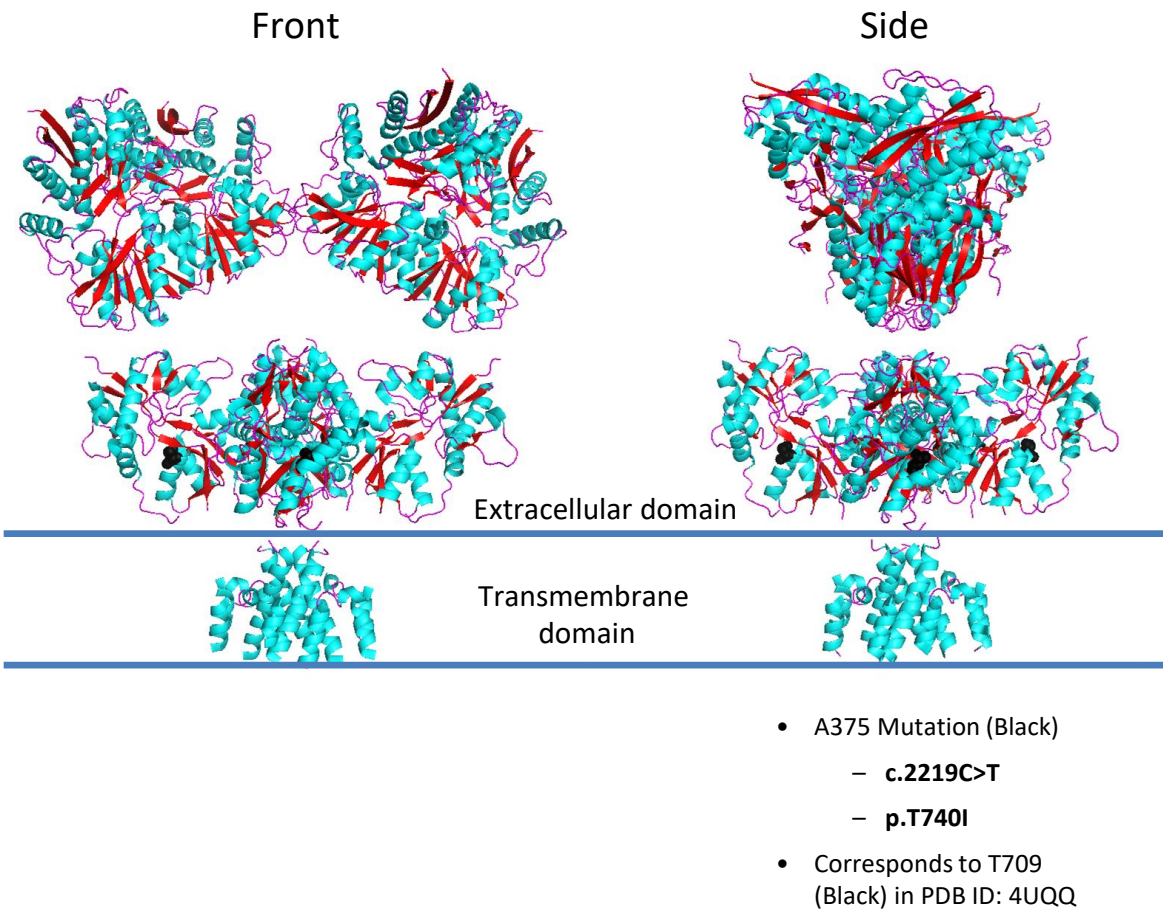

Figure 6.4. *GRIK2* is mutated in A375 human melanoma cells. GluK2 is a transmembrane protein that functions as an ion channel and is activated by glutamate binding. Pymol cartoon visualisation of the GluK2 receptor, a homo-tetramer formed from the expressed *GRIK2* gene. Alpha helices are coloured in blue, beta-sheets in red and unstructured regions in purple. The mutated residue found in A375M2 melanoma cells (residue T740) is shown in Black. (PDB ID: 4UQQ)

6.1.4 Studies of Ionotropic Glutamate receptor antagonists in melanoma

We are also interested in targeting glutamate signalling with small molecule antagonists of ionotropic glutamate receptors to study their effects on melanoma cell proliferation, morphology and the metabolic profiles. This is done out of interest for potential translational research into the application of using drugs targeting glutamate signalling in melanoma. Glutamate antagonists are a class of drugs that have been mainly used to study the functions of glutamate signalling in the central nervous system as well as to treat illnesses associated with aberrant glutamate signalling such as Parkinson's Disease (amantadine)(351), Alzheimer's (Memantine/MK-801)(352), and Depression (ketamine)(353). Many of these drugs such as Memantine, and amantadine are already approved for clinical use in the US and the EU meaning their safety profiles are well established. Should sufficient evidence of glutamate signalling promoting melanoma progression be collected, translating use of currently approved glutamate antagonists in melanoma would be an attractive prospective.

For our studies we have selected four ionotropic glutamate receptor antagonists to test their effect on melanoma cell proliferation (Table 9). Based on the data collect we will select one for metabolomic analysis in human melanoma.

Antagonist	Mechanism	IC_{50} in A549 Lung Carcinoma Cells (Rzeski *et al)*
MK-801 (Diclozipine)	Non-competitive NMDA antagonist	>500 μM
GYKI-52466	Non-competitive AMPA antagonist	~250 μM
CFM-2	Non-competitive AMPA antagonist	~10-100 μM
Memantine	Un-competitive NMDA antagonist	~100-250 μM

Table 9. Glutamate antagonists used in study

Glutamate antagonists were selected based on previously published data demonstrating anti-proliferative effects in lung carcinoma (A549) and rhabdomyosarcoma/medulloblastoma (TE671) (354). Rzeski *et al* used quite high doses of small molecule inhibitors (up to 500 μM) to see a significant effect on cell proliferation. This was replicated in Stepulak *et al* (355) who also demonstrated that AMPA antagonists, GYKI-52466 and CFM-2 inhibit ERK1/2 signalling and reduce phosphorylation of CREB which could explain their anti-proliferative effects. In our study we decided to use lower doses, initially

testing them at 5 μM and 25 μM since we expected any drug of significance, acting at the cell surface and hence not required to penetrate within the cell, to be active at concentrations comparable to the small molecule ROCK inhibitors. Activity at higher concentrations might also be attributable to non-specific, off-target effects.

We will compare the data collected on glutamate antagonists to see if we can replicate the findings found when inhibiting ROCK activity. The metabolic profiles of cells where glutamate signalling is inhibited may particularly reveal similarities and differences between the modes of action of ROCK inhibitors and glutamate antagonists. This will also be compared to the effects of the glutaminase inhibitor 968, which specifically targets glutaminolysis. It is possible that targeting a broad group of glutamate receptors with small molecule inhibitors may affect several signalling pathways in a similar manner to ROCK, while specific inhibition of glutaminolysis may show more narrow effects on proliferation, morphology and the metabolic profile. Data collected from these experiments will further develop the hypothesis that ROCK drives melanoma metastasis through glutamine/glutamate metabolism and glutamine signalling.

6.2 Results

6.2.1 Glutamine and Glutamate Transporters differentially regulate melanoma cell proliferation and morphology

The candidate did not generate the following data shown in this section. Data presented here was generated by Dr. Eva Crosas-Molit and Ms. Beatriz Padilla. It is presented here to help create a larger context for data presented further on.

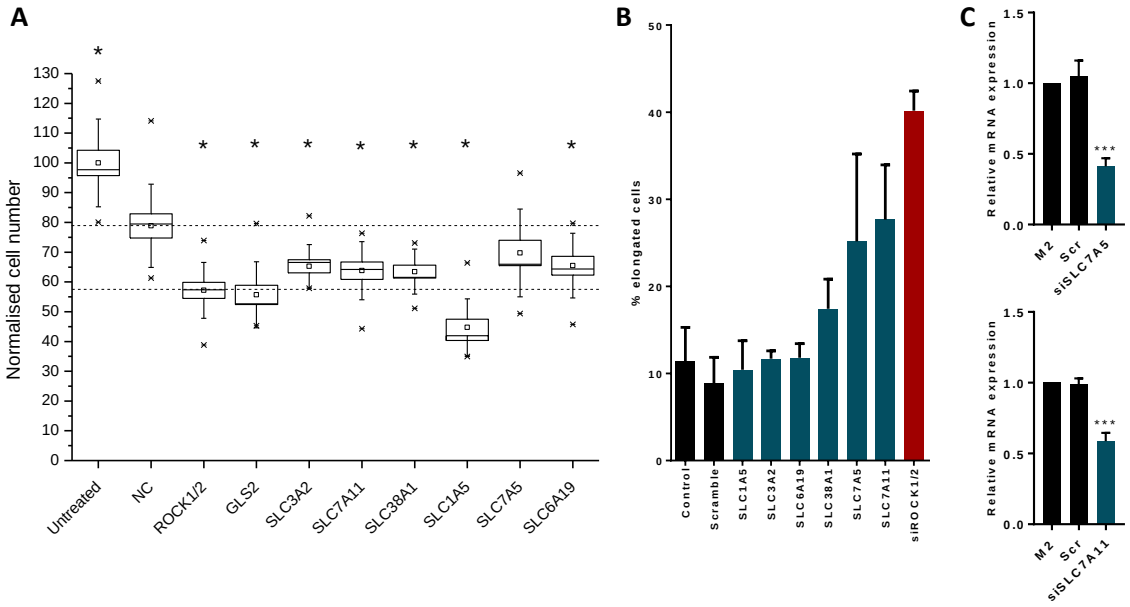

Figure 6.5. Glutamine and glutamate transporters have differential effects on cell proliferation and cell morphology. A) Cell proliferation assay of A375M2 cells siRNA knockdown of genes related to glutamine/glutamate transport. Cell counts are normalised to untreated cells. Measurements were taken 72 hours post transfection. Boxplots show median and 75% confidence interval, whiskers show 95% confidence interval. B) Morphology assay of A375M2 cells seeded on a collagen 1 layer after knockdown of gln/glu transporter genes. Bar charts show mean +/- SEM. C) Verification of Knockdown by qPCR from proliferation and morphological experiments. For all experiments non-targeting siRNA used as negative controls and *ROCK1*/2 knockdowns used as positive controls for both reductions in proliferation and change in morphology. Abbreviations: Untreated Cells and Control are cells without treatment. NC and Scramble are cells treated with non-targeting siRNAs. Experiments are n=4. * - p<0.05, *** p<0.001

In the second RNAi screen, of glutamine and glutamate transporters, it was seen that silencing gene expression of the glutamine transporter *SLC1A5* led to a significant reduction in cell proliferation while not affecting cell morphology. On the other hand, silencing expression of the genes *SLC7A5* and *SLC7A11* encoding the glutamine and glutamate transporters respectively led to a significant change in cellular morphology (Fig. 4), similar to that found in siROCK treated cells. They also affected melanoma proliferation but not to the extent of siSLC1A5 treated cells. Taken together, the data collected on *GLS2* and *SLC1A5* suggests that glutamine transport and glutaminolysis is important for sustaining proliferation, however these may have negligible effects on cell morphology. On the other

hand, genes involved in the secretion of glutamate or exchanging glutamine for leucine seem to be important in sustaining a rounded morphology.

6.2.2 Knockdown of Glutamine/Glutamate Transporters significantly alter the cellular metabolome

Based on the data from the *in vitro* screen of the glutamine/glutamate transporters three receptors were selected for metabolic profiling. In Chapter 4 we elucidated the metabolic profiles of melanoma cells when ROCK activity or expression was ablated. It was seen that glutamine and glutamate metabolism was significantly regulated by ROCK activity. We hypothesize that interfering directly with glutamine and glutamate transport may partially replicate the metabolic profiles observed in our ROCK studies. SLC1A5 was selected because of its large influence on cell proliferation while *SLC7A5* and *SLC7A11* were selected due to their substantial effects on cell morphology. The three genes were knocked down individually *in vitro* using siRNA delivered by the LAH4-L1 pH responsive peptide, nucleic acid delivery system in A375M2 human melanoma cells and intracellular and extracellular metabolomes compared to non-targeting control siRNA treated cells.

Both whole cell HR-MAS NMR metabolomic and NMR metabolomics of the spent media were analysed. The knockdown of these genes has yet to be confirmed by qPCR and/or Western blot in this set of experiments and will be essential future experiments to confirm the validity of the results explained below. Nevertheless, we observed a significant change in both the intracellular and extra-cellular environment of the melanoma cells after knockdown with siRNAs targeting the glutamine/glutamate transporters as opposed to scramble siRNA.

siSLC1A5 treated cells saw a reduction in saturated lipids, methyl groups on lipid chains, lactic acid, phosphocholine and asparagine while there was an increase in alanine, leucine, creatine, glycerophosphocholine, and glycine (Figure 6.6, Figure 6.7). In the spent media there was a very weak change in the spent media profile (Q^2 = 0.157, Figure 6.8) suggesting a decrease in pyroglutamate, methionine, glutamine, leucine, glucose and lysine. There was an increase in lactate, alanine and glutamate (Figure 6.9).

si*SLC7A5* treated cells had an increase in choline, leucine, alanine, creatine, glycerophosphocholine, glycine, and acetate, while the CH2-CH2 bonds and CH3 groups of lipids, lactate and m*yo*-inositol decreased in the cells (Figure 6.6, Figure 6.7). In the spent media there was a decrease in glucose, methionine, glutamine, and leucine while there was an increase of lactate and alanine (Figure 6.9).

si*SLC7A11* treated cells showed decreases in the CH2-CH2 bonds and CH3 groups of lipids, phosphocholine, glutamate, choline, *myo*-inositol, glutathione, asparagine, and acetate, while there was an observed increase in lactate and alanine (Figure 6.6, Figure 6.7). In the spent media we observed a decrease in lactate, pyroglutamate, alanine, glutamine and pyruvate while we observed an increase in glucose, glutamine, isoleucine, and valine (Figure 6.9).

In the spent media there was a change in the lactate/glucose ratio in siSLC1A5 and siSLC7A5 knockdown conditions compared to control, with a respective change in mean lac/glc ratio of 1.41 and 1.09 respectively, this suggests a switch to glycosolysis after knockdown. On the other hand, siSLC7A11 conditions saw a mean decrease of lac/glc of 0.86, which suggests the cells made less use of glycolysis. These changes can be observed in the heatmap below (Figure 6.7).

Additionally there was an increase in glutamate/glutamine ratio (glu/gln) in siSLC1A5 and siSLC7A5 conditions, with a mean increas of 0.04, and 0.05 while there was a decrease in glu/gln of 0.06 in siSLC7A11. This suggests a slight change in the production of glutamate and consumpiton of glutamine in these conditions (Figure 6.7).

There was a slight increase in glutamine uptake in siSLC1A5 and siSLC7A5 conditions, with a mean reduction of glutamine concentrations of 0.01 mM and 0.03 mM respectively. This is counter intuitive as the transporters knocked down are glutamine transporters. One would expect knockdown to inhibit and uptake of glutamine. This is a further point that would need validation although admitedley the effects sizes are quite small.

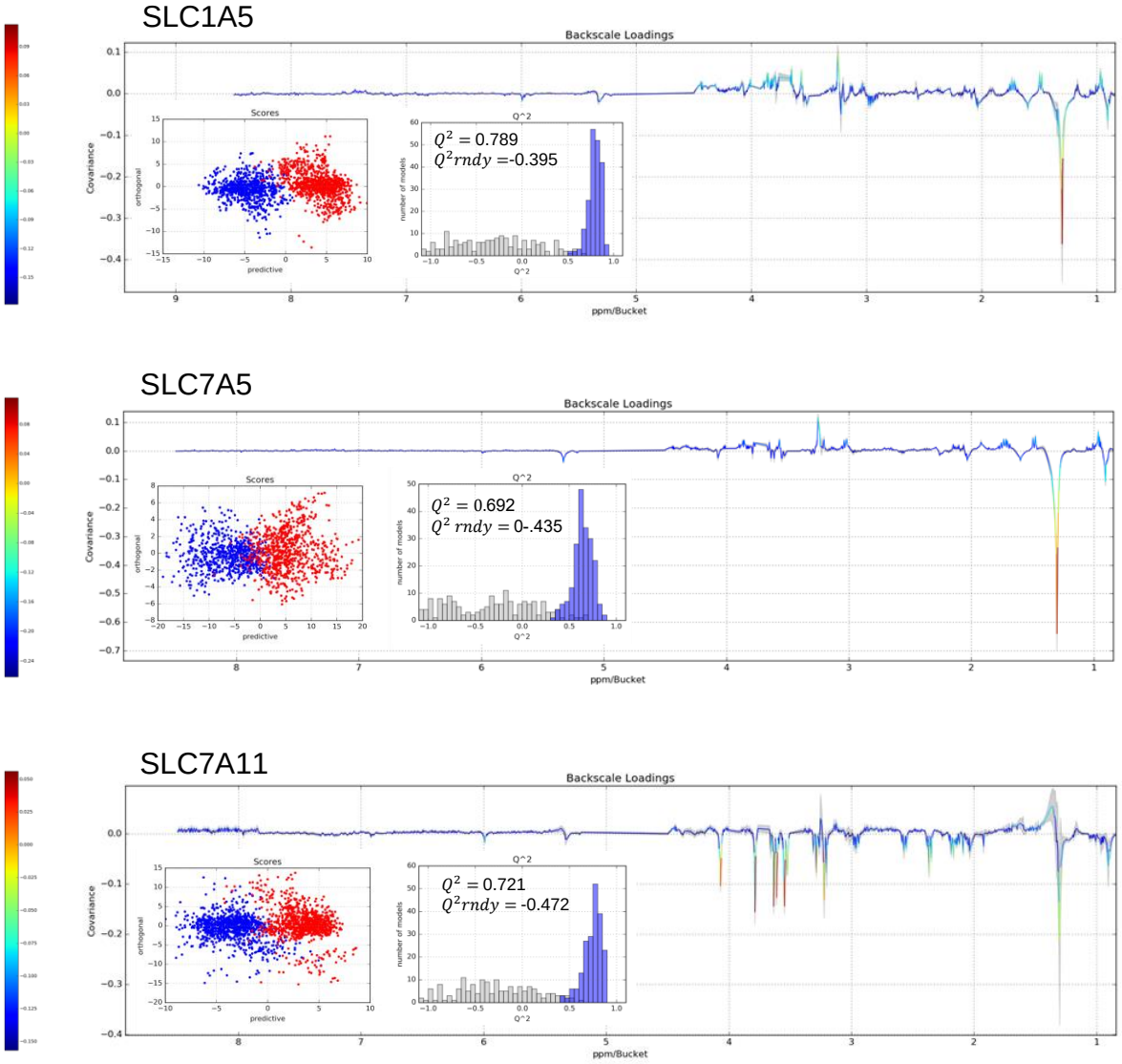

Figure 6.6. Whole cell NMR metabolomics of transporter knockdowns in A375M2 cells. Scores plot, Q^2 histogram and back scale loadings plots of A) siSLC1A5 b) si*SLC7A5* and C) si*SLC7A11* knockdowns compared with Non-targeting siControl. Experiments were conducted n=3 times, and each experimental replicate containing three technical replicates, for a total of 9 samples per experimental condition.

Hierarchical clustering of the whole cell metabolomic data show that *SLC1A5* and *SLC7A5* have more similar profiles to each other than *SLC7A11* (Figure 6.7). This is consistent with the known functions of these genes as *SLC1A5* and *SLC7A5* are glutamine transporters while *SLC7A11* is a cysteine/glutamate exchanger.

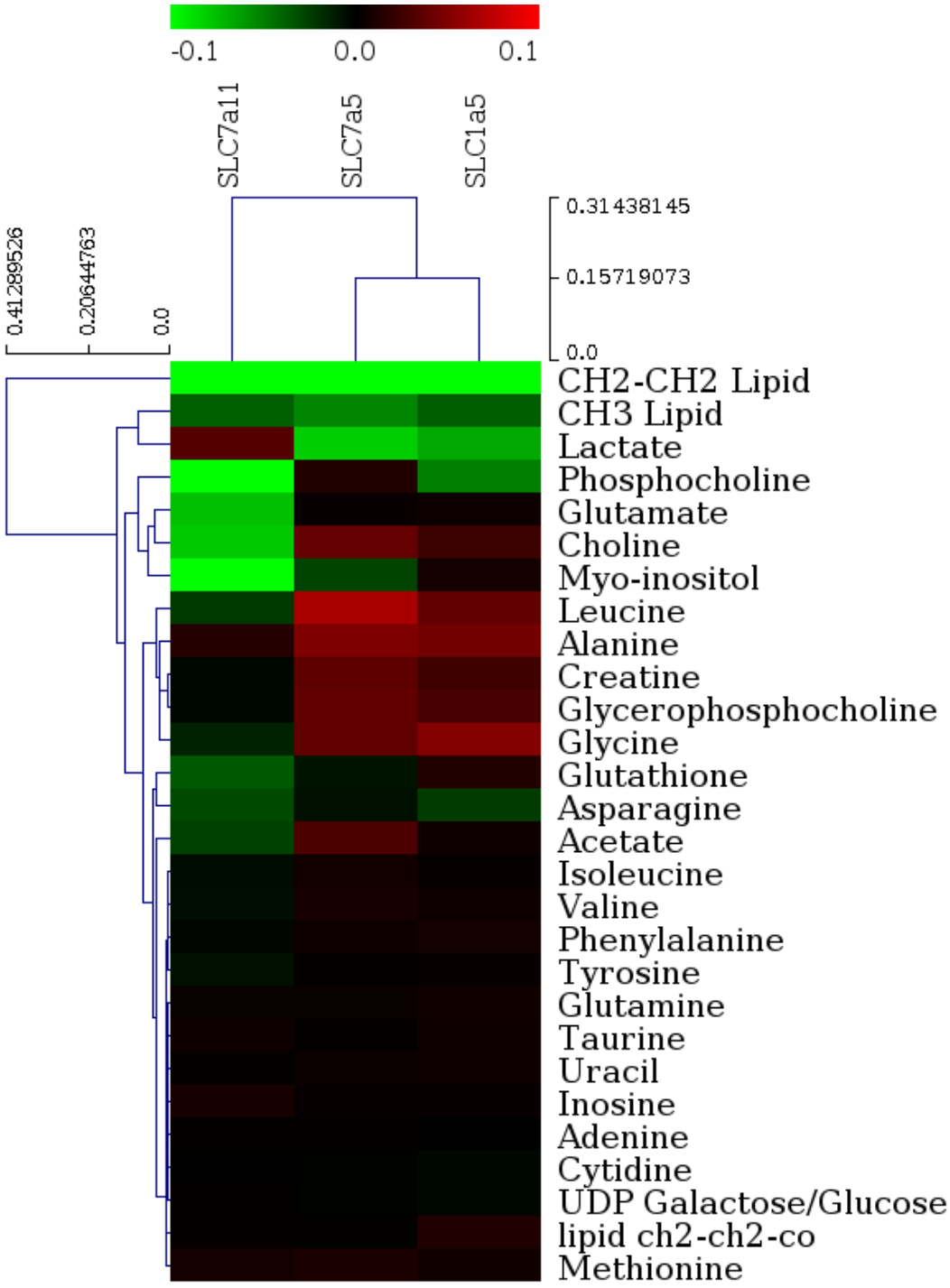

Figure 6.7. Heatmap with hierarchical clustering of loadings from OPLS-DA models for A375M2 whole cell metabolomic data where gln/glut are knockdown by siRNA. Changes are shown relative to transfection with non-targeting siControl.

SLC7A11 has quite a distinct profile in that the observed increases in leucine, alanine, creatine, glycerophosphocholine and glycine see in the glutamine transporters are not seen in the glutamate transporter. In addition, *SLC7A11* knockdown led to a decrease in glutamate and choline not seen in the other two conditions while a substantial reduction in *myo*-inositol was much greater than that

achieved with si*SLC7A5* (none was observed for siSLC1A5). It is curious that there is a decrease in glutamate after *SLC7A11* knockdown as one would expect there to be an accumulation in intracellular glutamate after *SLC7A11* knockdown. It could be that the additional glutamate is be re-directed into other pathways.

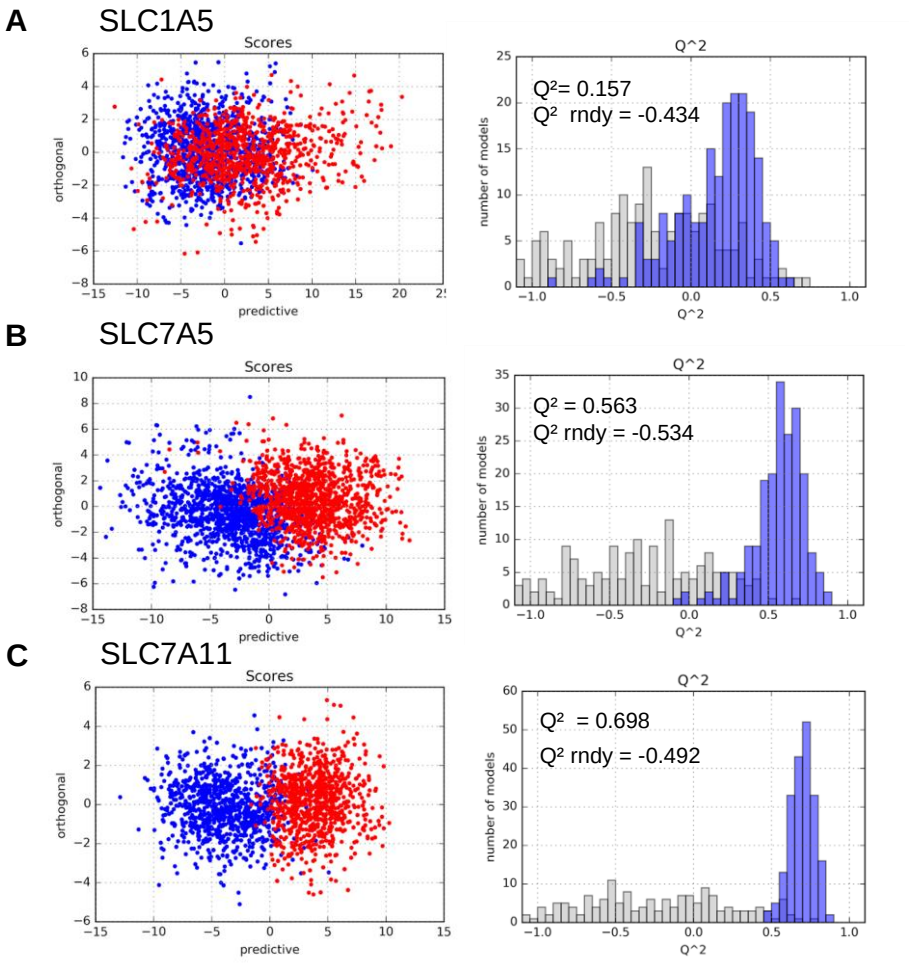

Figure 6.8. Silencing of *SLC7A5* and *SLC7A11* causes strong changes in exometabolome while silencing of SLC1A5 has a weak effect on the exometabolome. OPLS-DA Scores plots and histograms of Q² for models built on generated data (blue) and permutated data (grey) from spent media NMR metabolomics of gln/glu transporter knockdowns, compared with non-targeting siControl treated A375M2 cells. Experiments were conducted n=3 times, and each experimental replicate containing three technical replicates, for a total of 9 samples per experimental condition.

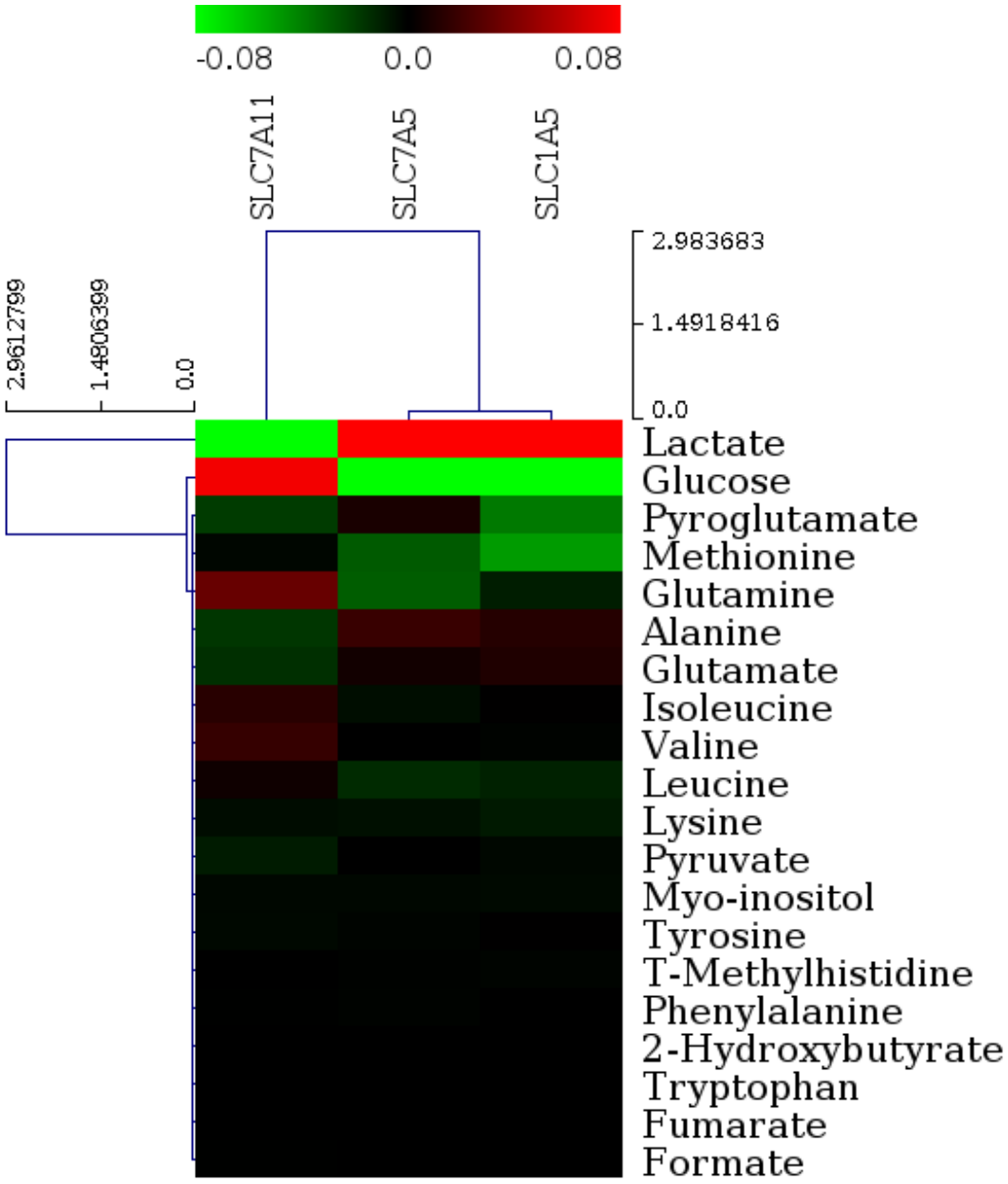

Figure 6.9.Heatmap with hierarchical clustering of OPLS-DA loadings from spent media metabolomics of A375M2 human melanoma cells after gln/glu transporter knockdowns. Changes are shown relative to media of cells transfected with non-targeting siControl.

6.2.4 *GRIK2* knockdown leads to decreased actomyosin contractility

Little is known about the role of ionotropic glutamate receptors in melanoma. Based on work in the previous chapter we investigated if these receptors may play a role in regulating contractility. *GRIK2*, belonging to the Kainate glutamate receptor family was selected to investigate a potential regulation of cell morphology and contractility.

We saw that knockdown of *GRIK2* expression led to elongation of A375M2 cell along with a significant reduction in phosphorylated myosin light chain (Figure 6.10). Knockdown was confirmed by qPCR (Figure 6.10). These results were further validated in A375M2 cells by using individual siRNA oligonucleotides of GRIK2 to rule out off-target effects when using Smart Pools of siRNA. Single OnTarget*plus*™ oligonucleotides targeting *GRIK2* also showed effects in elongating cells and lowering levels of p-MLC2 (Figure 6.11).

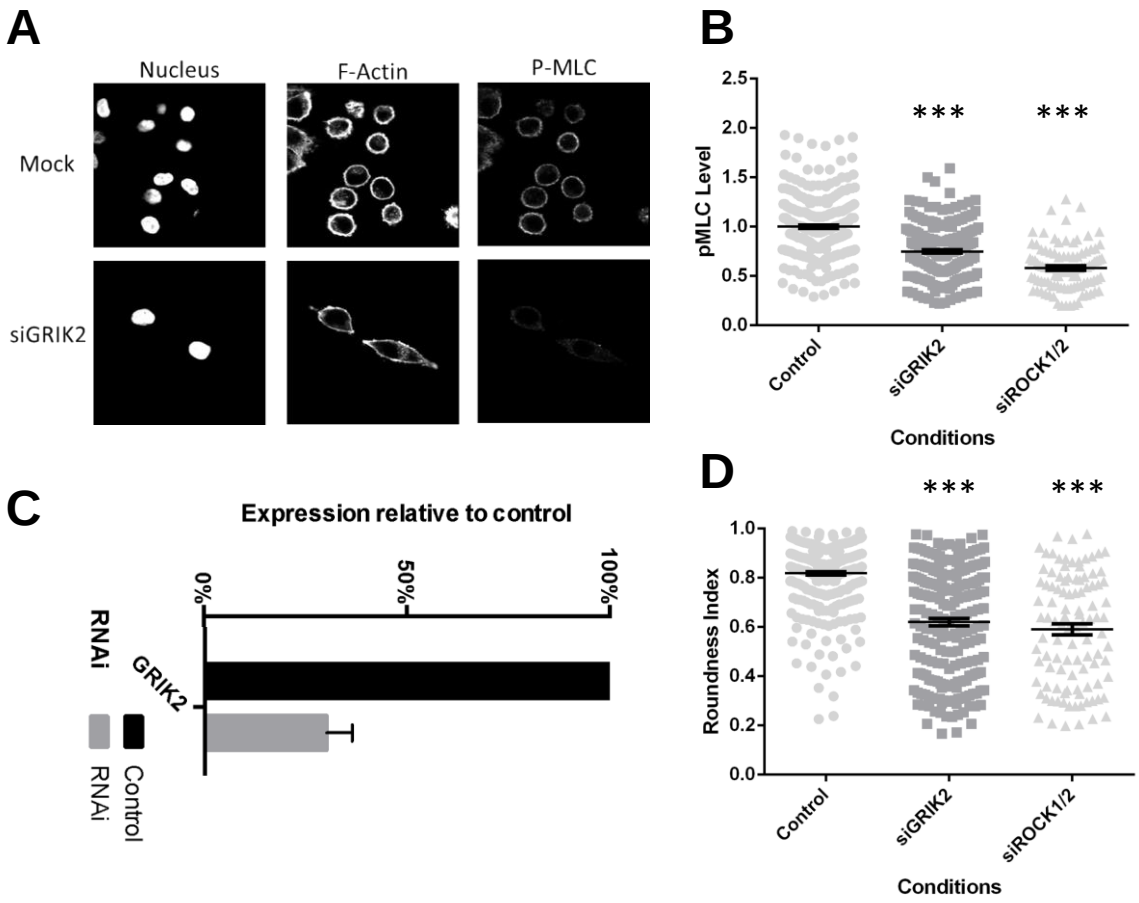

Figure 6.10. *GRIK2* knockdown leads to decreased actomyosin contractility. A) Immunostaining and Confocal imaging of A375M2 cells after *GRIK2* knockdown show cells with more elongated phenotype and less p-MLC2 staining. B) Quantification of p-MLC2 staining in A375M2 cells after *GRIK2* knockdown. ROCK1/2 Knockdown shown for comparison. C) Quantification by qPCR of *GRIK2* knockdown. D) Quantification of roundness index of A375M2 cells after *GRIK2* knockdown. ROCK1/2 knockdown shown for comparison. Error bars show SEM*** = p<0.001. All experiments are n=3. Data generated in collaboration with Simon Chu.

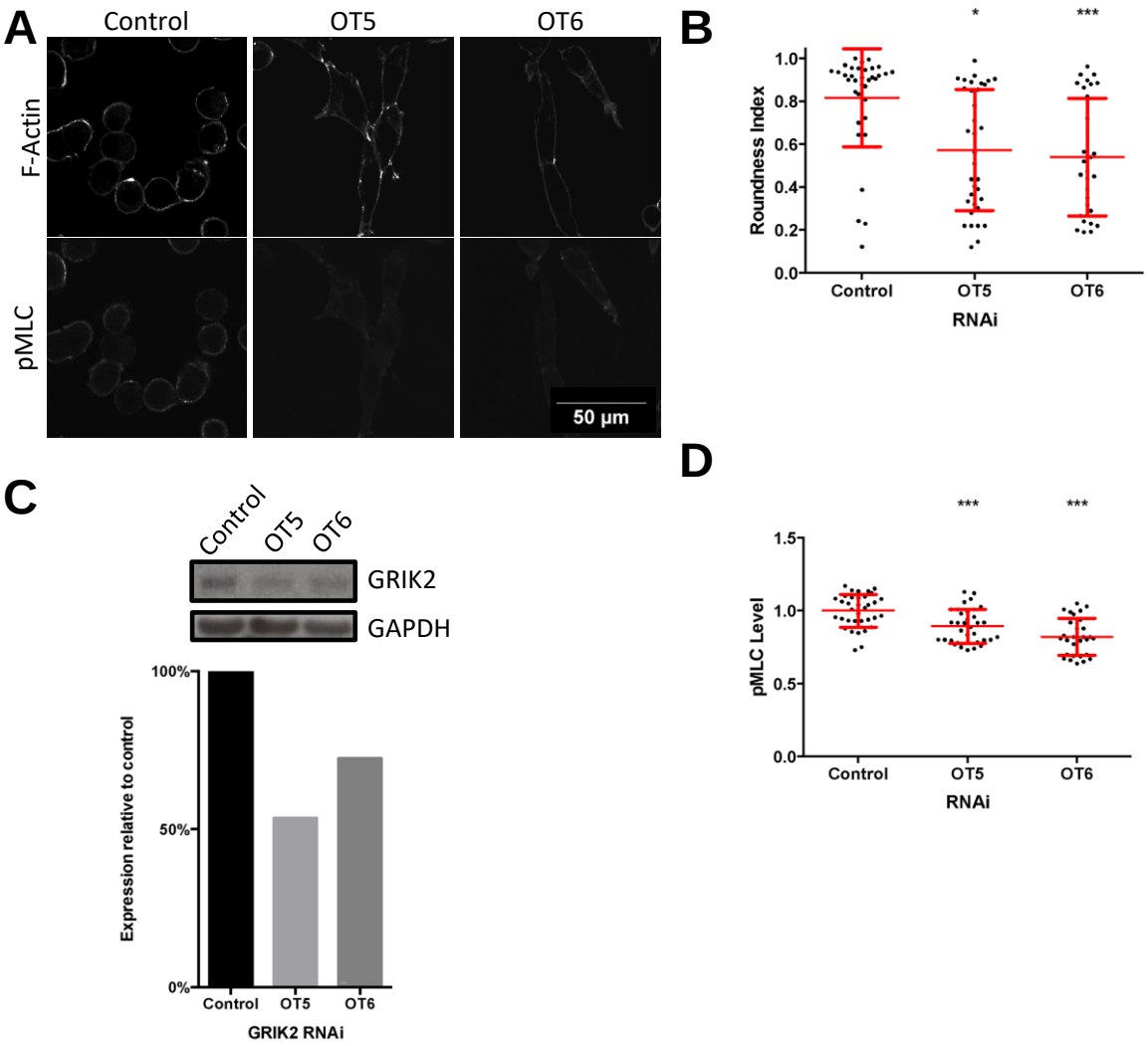

Figure 6.11. *GRIK2* individual oligonucleotide knockdown confirms that *GRIK2* regulates actomyosin contractility. A) Immunostaining and Confocal imaging of A375M2 cells after *GRIK2* knockdown with individual oligonucleotides. B) Quantification of cell rounding after *GRIK2* knockdown with individual oligonucleotides. C) Confirmation of knockdown by western blot (n=1). D) Quantification of p-MLC2 staining (n=3 with 10 cells quantified per experiment). Error bars show SEM * - $p<0.05$, ** $p<0.01$, *** $p<0.001$. Data generated in collaboration with Simon Chu.

6.2.6 Protein levels of GluK2 but not *GRIK2* RNA are regulated by ROCK activity

Work in the previous chapter had shown that RNA levels of *GRIK2* are not significantly altered by ROCK activity as treatment with H1152 did not significantly alter levels of *GRIK2*. However, we did observe that protein levels of GluK2 (*GRIK2*) are significantly reduced after 24-hour treatment with H1152 and Y27632 (Figure 6.12). GluK2 protein levels are reduced by 60% with H1152 while Y27632 leads to a 48.8% reduction in GluK2. This suggests that ROCK activity may be acting post-translationally on *GRIK2* expression and should be replicated with siRNA knockdowns of ROCK. Should knockdowns of ROCK not replicate these findings, it could be explained as an off-target effect of these small molecule inhibitors as both H1152 and Y27632 have been shown to bind to several other kinases such as PKA, PKC and AKT (145).

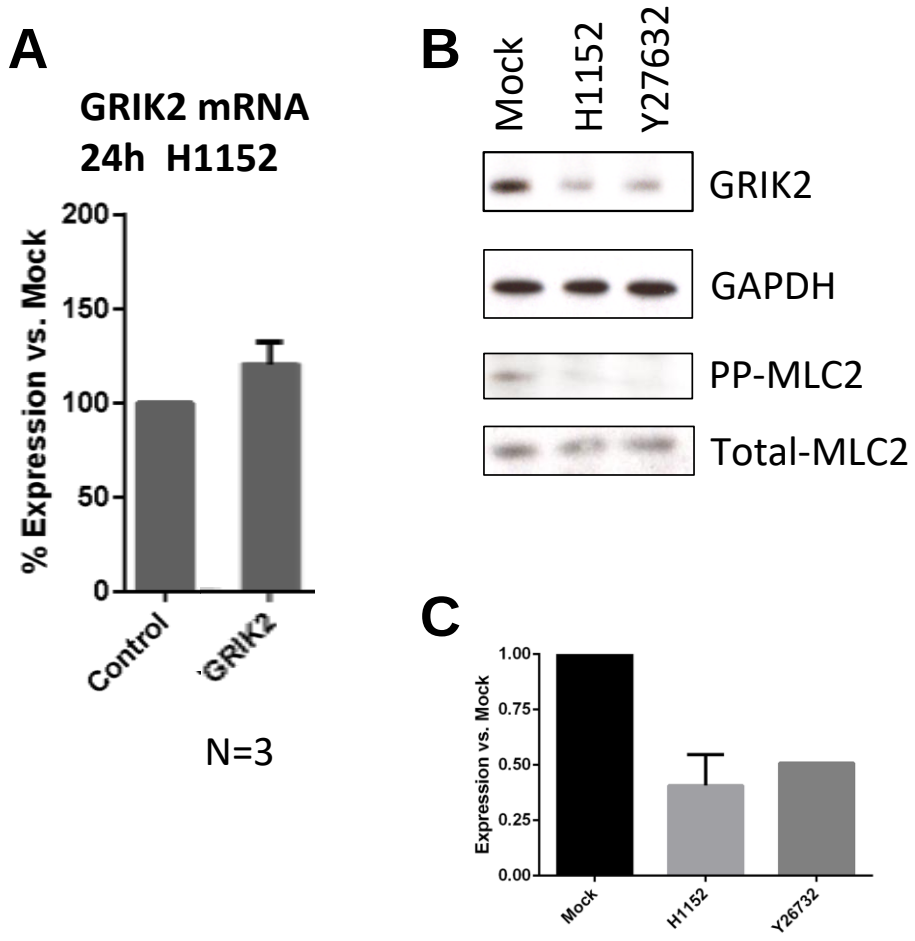

Figure 6.12. Protein levels of GluK2 (GRIK2) but not RNA are regulated by ROCK activity in A375M2 cells. All experiments performed with 25 hour treatments of ROCK inhibitors. A) Quantification of RNA levels of GRIK2 after ROCK inhibition with 5 µM H1152 (n=3). B) Western blot of GluK2 (GRIK2) levels after ROCK inhibition with 5 µM H1152 or 10 µM Y27632. C) Quantification of Western blot in (B) (n=2).

6.2.7 *GRIK2* regulates actomyosin contractility in B16F10 mouse melanoma cells

Studying the role of *GRIK2* in a murine model of melanoma serves two purposes. First it is a first step toward syngeneic *in vitro* studies of glutamate receptors in melanoma. Secondly, we can see if the results observed in A375M2 cells where *GRIK2* is mutated can be replicated in another melanoma cell line. The *GRIK2* gene is 99.01% identical between human and mouse and is 100% identical in the region where *GRIK2* is mutated in A375M2 cells.

We saw in B16F10 mouse melanoma cells that *GRIK2* knockdown again alters cell morphology along with a reduction of phosphorylated myosin light chain (Figure 6.13B). As this work was done on glass coverslips rather than a thick Collagen 1 matrix as in previous data the morphology of these cells remains poorly characterised. However, it is possible to see more protrusions in the knockdown cells when compared to the control cells (Figure 6.13A).

These results strengthen our finding that *GRIK2* regulates melanoma contractility despite the mutation found in A375 human melanoma cells. It is not known if *GRIK2* is mutated in B16 mouse melanoma cells. Knockdown of *GRIK2* did not affect cell proliferation.

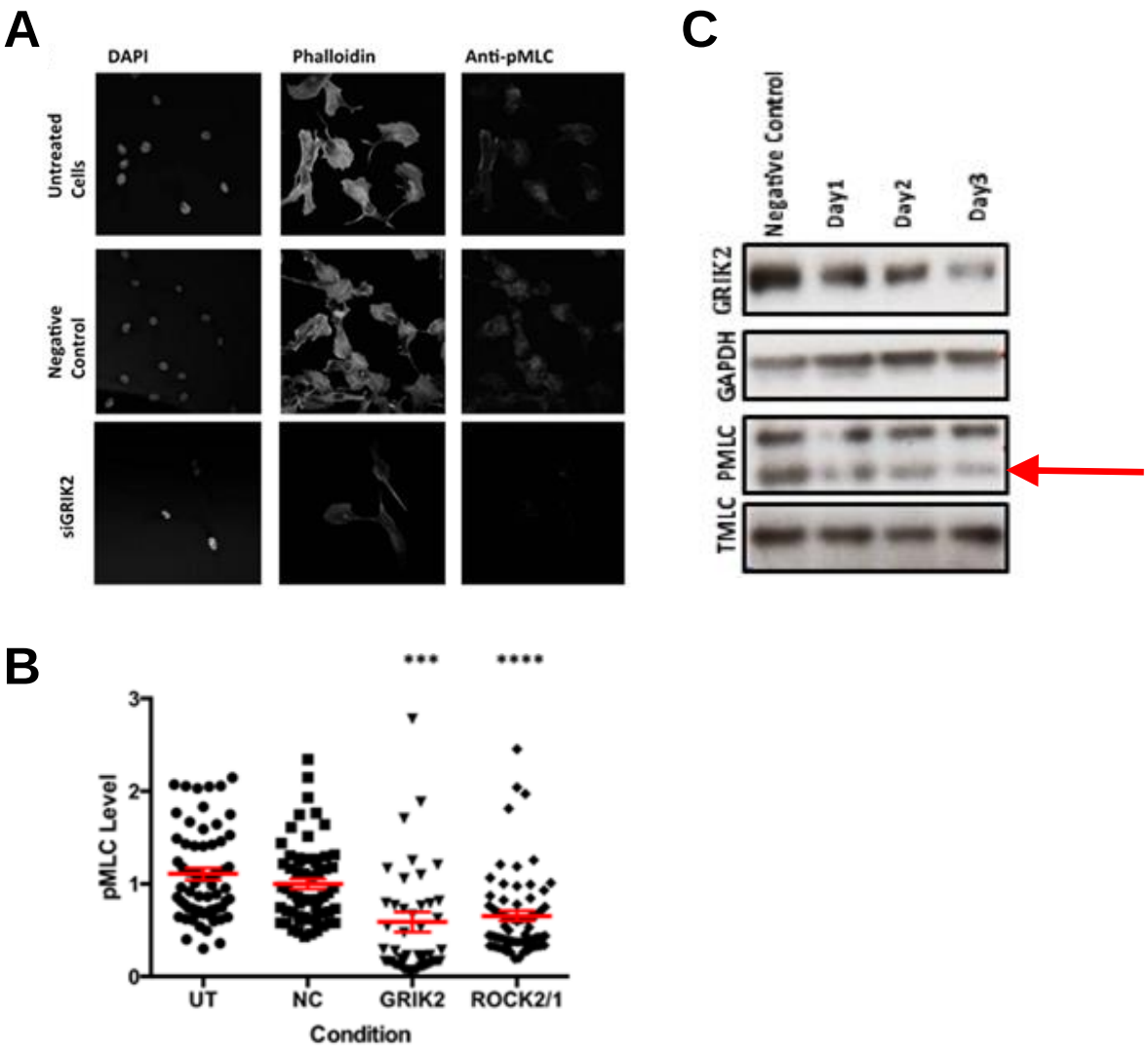

Figure 6.13. *GRIK2* regulates actomyosin contractility in B16F10 mouse melanoma cells. A) Immunostaining and confocal imaging of B16F10 cells after GRIK2 knockdown illustrates reduced levels of p-MLC2. B) Quantification of p-MLC2 levels from images in (A) (n=3). C) Western blot of B16F10 cells after *GRIK2* knockdown confirms optimal knockdown of GluK2 (*GRIK2*) after 72 hours and lowest levels of pp-MLC2 (n=1). Red arrow indicates the band for pp-MLC2. *** - p<0.001 **** p<0.0001. Data generated in collaboration with Sogol Salamipour.

6.2.8 Glutaminase inhibitor stops melanoma cell proliferation

Amino acid transport is an essential step to sustain 'glutamine addiction' in melanoma cells. The glutaminase inhibitor 968 was first proposed by Wang *et al*(158) who demonstrated that 968 binds to glutaminase and can block rho dependent transformation of fibroblasts and inhibit the proliferation of breast cancer and lung cancer cells. More recently it was shown that 968 binds to monomeric glutaminase and thus blocks the active tetrameric form of glutaminase (159).

We saw A375M2 melanomas cells are very sensitive to glutaminase inhibition. Logistic curve fitting of proliferation data show that a 50% reduction in proliferation after 48 hours can be achieved with doses as low as 3.25 μM (Figure 6.14A). In our metabolomic study we used a dose of 10 μM for 24 hours.

6.2.9 968 Significantly Alters the Cellular Metabolome

There was a significant shift in the intracellular metabolome in cells treated with 968 (Q^2 =0.660, Figure 6.14B) however we saw that there was no observable change in consumption or secretion patters in the spent cell culture media (Q^2 = -0.364, Figure 6.14C). In the cells, we observed an increase in phosphocholine, glutamate, glutathione, *myo*-inositol, glycerophosphocholine and a reduction in saturated lipids, acetate, leucine, creatine, valine, CH_3 groups of lipids and choline. The change in phosphocholine levels may be a marker for proliferation as has been shown in several studies investigating the effects of choline kinase in malignant tissue (356). An increase in intracellular phosphocholine in the treatment condition may point to an accumulation due to blocked phospholipid synthesis downstream of phosphocholine.

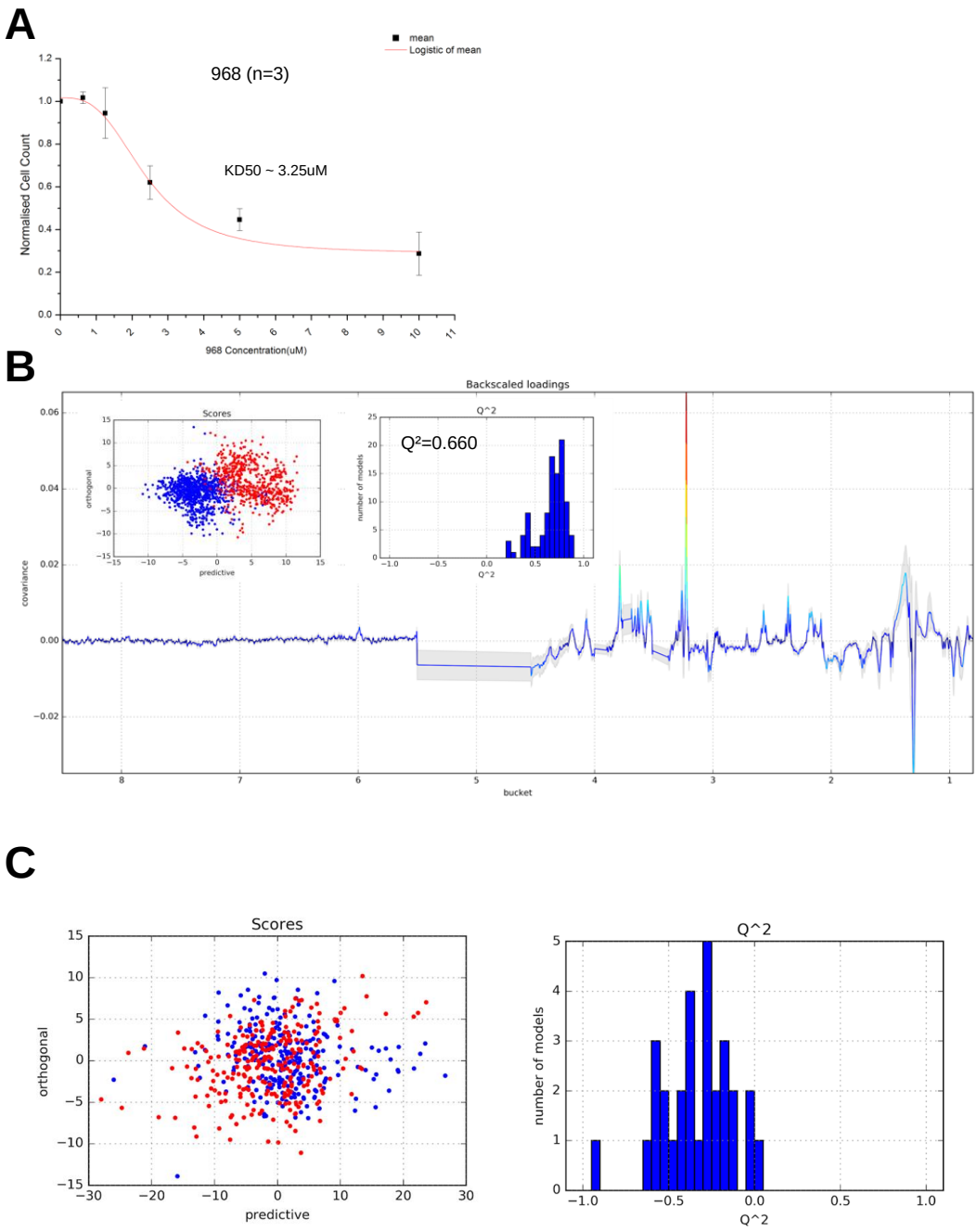

Figure 6.14. 968 Glutaminase inhibitor regulates melanoma proliferation and the metabolic profile while not regulating the exometabolome. Metabolomics of A375M2 cells after 24-hour treatment with 10 μM 968 glutaminase inhibitor. A) The glutaminase inhibitor 968 limits cell proliferation and B) significantly alters the melanoma metabolome. Scores plot, Scores plot, Q² histogram and back scale loadings of OPLS-DA models from HR-MAS NMR of whole A375M2 cells after 968 treatments. C) 968 does not significantly change metabolite consumption patterns in spent media. Scores and Q² histogram of spent media metabolomics of A375M2 cells after 968 treatment. Back scale loadings not shown because of non-significance of data. Experiments were conducted n=3 times, and each experimental replicate containing three technical replicates, for a total of 9 samples per experimental condition.

6.2.10 AMPA/Kainate antagonists but not NMDA antagonists regulate melanoma cell proliferation

At both 5 μM and 25 μM doses we observed that only CFM-2 decreased cell proliferation significantly (Figure 6.15A, B). This is to be expected based on previous studies where GYKI-52466 required 100 μM doses before anti-proliferative effects were observed although this was tested in cell lines unrelated

to melanoma.

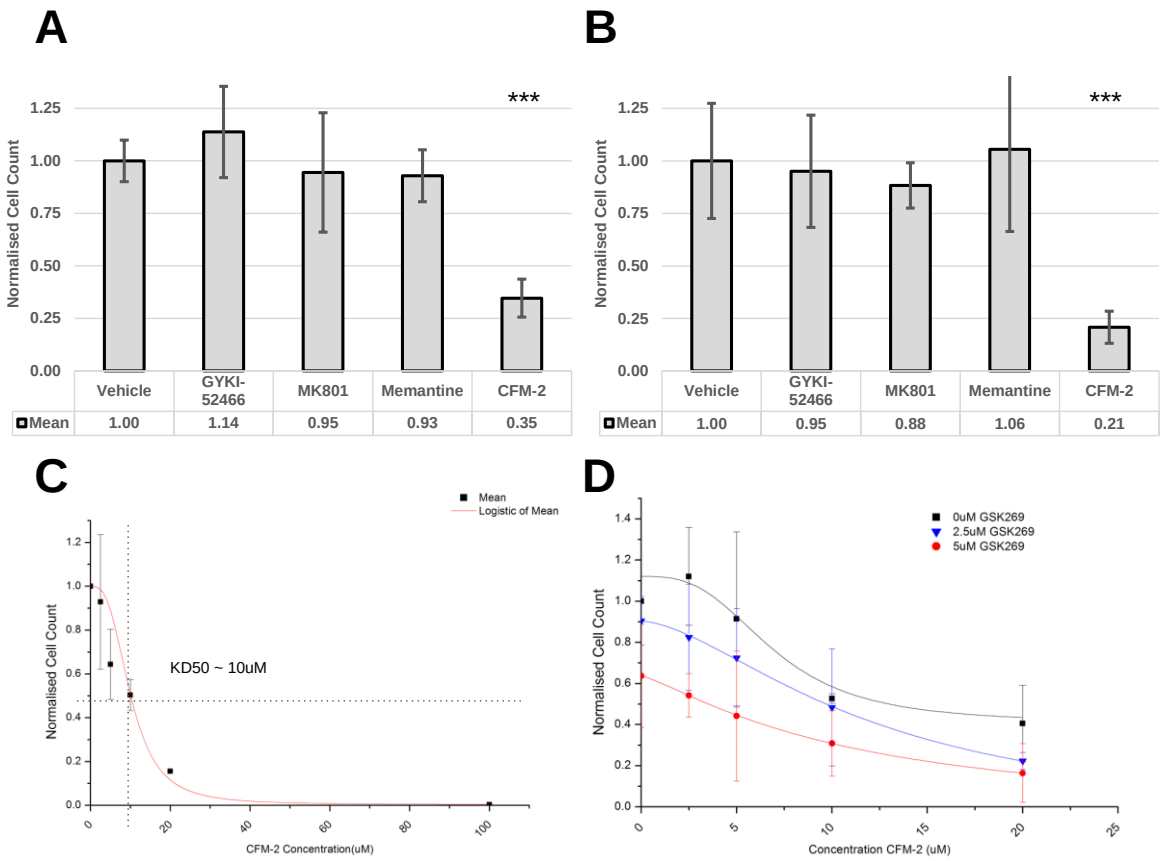

Figure 6.15. The AMPA/Kainate antagonist CFM-2 limits cell proliferation at low doses. A) boxplot of normalised cell count of A375M2 cells after 48-hour treatment with 5 μM of glutamate antagonists. B) Experiment repeated in (A) with 25 μM doses of glutamate antagonists C) Dose-response curve of CFM-2 show a KD50 of about 10 μM. D) CFM-2 combined with the ROCK inhibitor GSK269 have an additive effect of cell proliferation. *** - $p<0.001$ (n=3).

As CFM-2 showed strong effects at even 5 μM, a dose response study was conducted and saw that a 50% reduction in proliferation after 48 hours was observed at 10 μM doses (Figure 6.15C), which was then selected as the dose for all future experiments. It should be noted that initial experiments showed 65% reduction in proliferation of melanoma cells at a 5 μM dose (Figure 6.15A), however further experiments showed a 10 μM dose was required to see 50% reduction in proliferation (Figure 6.15C). This could be explained by possible degradation of CFM-2 with storage. Despite reduced effects, we observed CFM-2 was also tested in combination with the ROCK inhibitor GSK269 with doses of 2.5 μM or 5 μM. It was seen that the two inhibitors have an additive effect on inhibiting cell proliferation (Figure 6.15D).

6.2.11 CFM-2 alters both the intracellular and extracellular metabolic profile of melanoma cells.

As we observed that CFM-2 leads to a significant reduction in cell proliferation. We conducted NMR metabolomic studies of the spent cell culture media and whole cells after a 24-hour treatment with 10 μM CFM-2 (Figure 6.16).

OPLS-DA show that both the intracellular metabolome and spent media shift significantly (Q^2 = 0.626 and Q^2 = 0.626 respectively, Figure 6.16A, B) after treatment with CFM-2. In the cells, there was a decrease in phosphocholine glycerophosphocholine, lactate, glutamate, glutathione, *myo*-inositol, arginine. There was an increase in saturated lipids, acetate, leucine, alanine, creatine, and valine.

In the spent media we observed a reduction in glucose, valine, alanine and 2-hydroxybutryate, while there was an increase in lactate and pyruvate (Figure 6.16C).

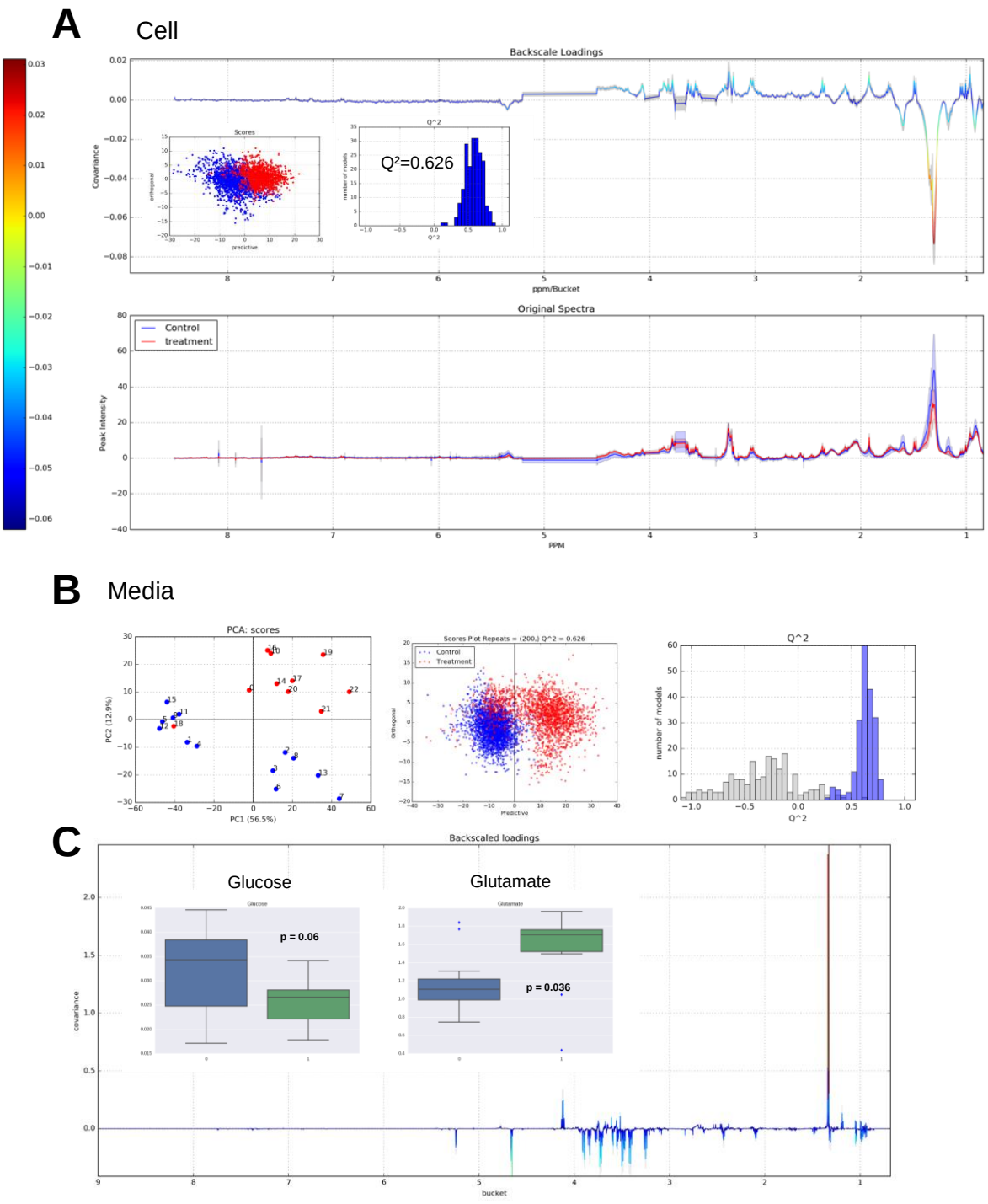

Figure 6.16. AMPA/Kainate antagonist CFM-2 regulates both the endo- and exometabolome. A375M2 cells treated with 10 μM CFM-2 for 24 hours A) CFM-2 significantly alters the intracellular metabolome. Back scaled loadings and mean PQN normalised spectra for control (blue) and CFM-2 treated (red) cells. Scores plot and Q² histogram are inset into the back scaled loadings plot. B, PCA scores, OPLS-DA Scores and Q² histogram of spent cell culture media metabolomics control samples are blue, treatment are red. C) back scale loadings plot of OPLS-DA model for exometabolome. Boxplots of univariate analysis of Glucose and glutamate peaks are inset to highlight the changes in glucose consumption and glutamate secretion after CFM-2 treatment. Experiments were conducted n=3 times, and each experimental replicate containing three technical replicates, for a total of 9 samples per experimental condition.

6.2.12 Hierarchical clustering of small molecule inhibitor metabolomic data

Hierarchical clustering of the gathered metabolomic data demonstrate that the metabolic profiles of melanoma cells between GSK269 and CFM-2 treatments are very similar (Figure 6.17). The only differences being leucine and alanine where we observed an increase in CFM-2 and no change in GSK269. In the cells, a nearly opposite response was observed between cells treated with GSK269 or CFM-2 and cells treated with 968 glutaminase inhibitor. Nearly every measured metabolite showed an opposite response (Figure 6.17).

In the spent media we also see that CFM-2 and GSK269 both have increased consumption of glucose and increased secretion of lactate, despite both drugs having strong anti-proliferative effects. This can be explained either as a metabolic switch as the cells become more dependent on glycolysis for energy. Another possible explanation is that this effect may be a partial response to increased oxidative stress in the cells after ROCK inhibition or blocking glutamate signalling as discussed in earlier chapters. 968 had no significant effect on the spent media again suggesting that these drugs have very different mechanisms of action.

Of interest was the observation was A375M2 cells treated with GSK269 at 1% FBS conditions showed reduced uptake of leucine while at 10% FBS conditions there was no change in extracellular leucine concentrations. As discussed in the previous chapter, ROCK expression is negatively correlated with *SLC7A5* expression

Clustering also reveals subtle changes in the exometabolome of cells cultured in 10%FBS media and 1% FBS media. Pyroglutamate, valine, and glutamine saw slight changes in different serum conditions. This could be explained by different quantities of growth factors included in cell culture media. Cell culture media is commonly supplemented with serum to provide growth factors, however this can add confounding factors and an extra layer of complexity as the components making up serum are not completely profiled. There can also be batch variability of serum between experiments. This study highlights this difficulty and points to a need for replacement systems of serum in future work.

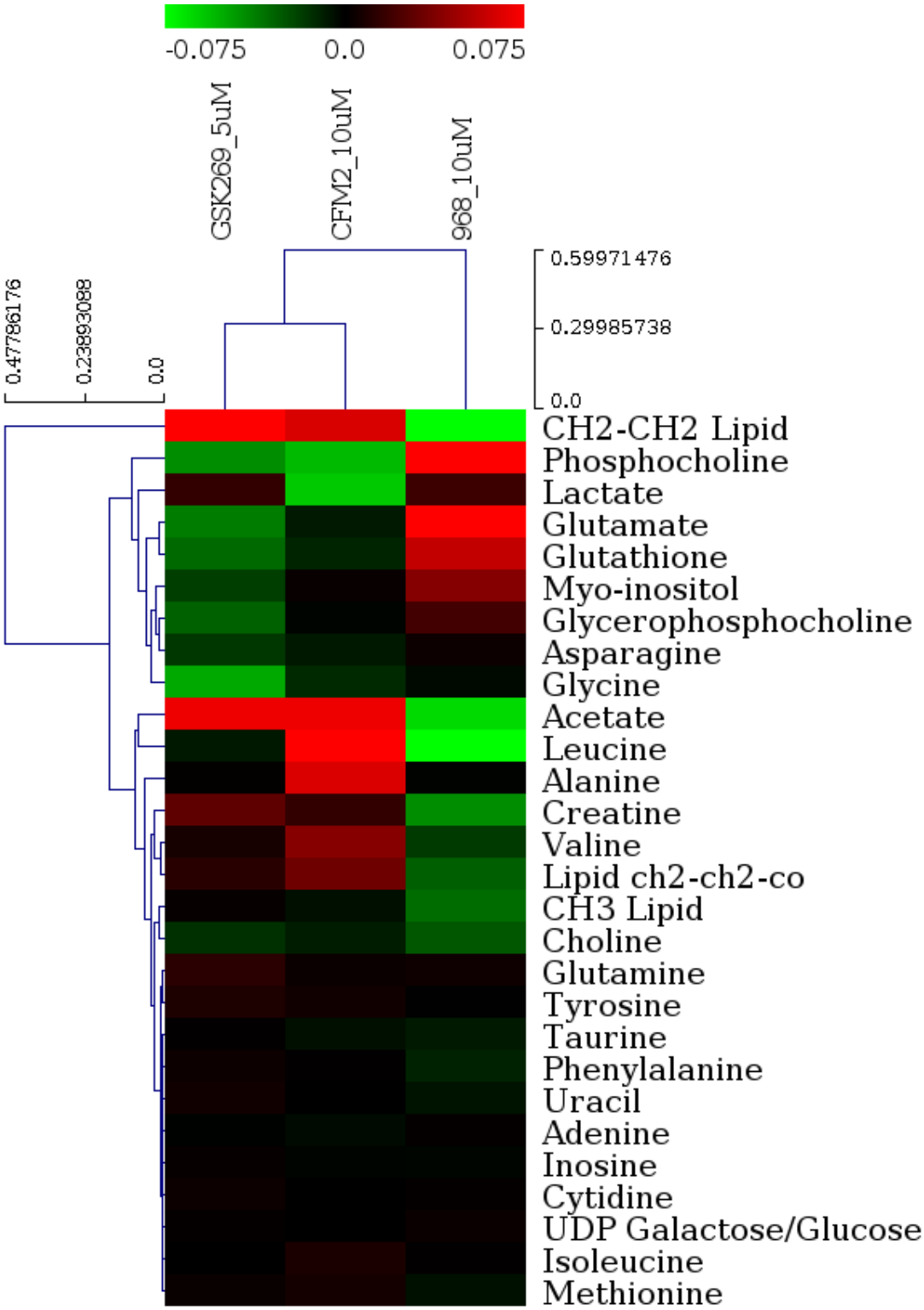

Figure 6.17. Hierarchical clustering of whole cell metabolomics of small molecule inhibitors of ROCK, AMPA/Kainate Signalling and Glutaminase

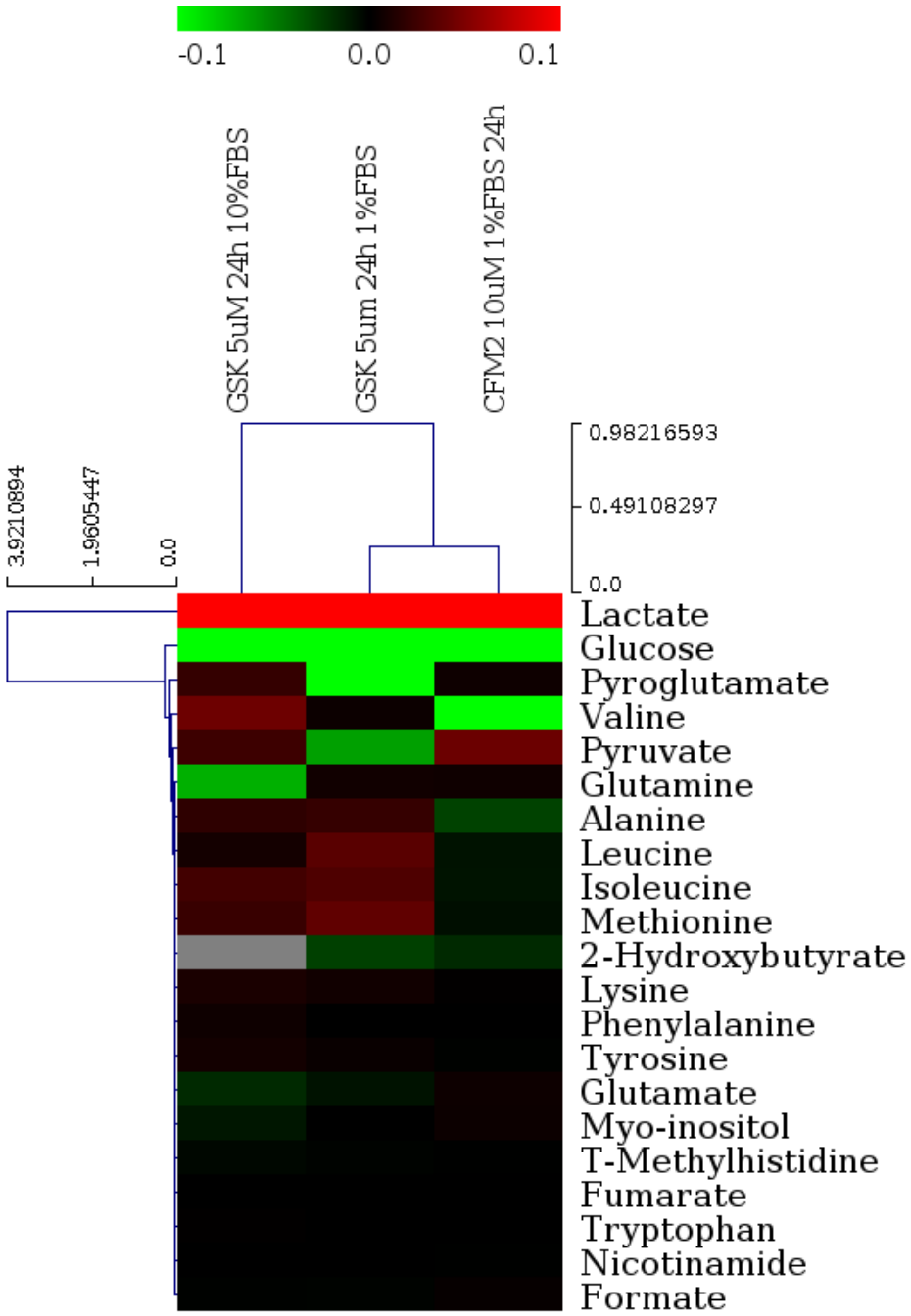

Figure 6.18. Hierarchical clustering of spent media metabolomics of small molecule inhibitors of ROCK, AMPA/Kainate Signalling. Data from glutaminase inhibitor 968 not shown due to non-significance of OPLS-DA models

6.3 Discussion

6.3.1 Glutamine/Glutamate transporters and glutaminase inhibitors affect the metabolome

It may seem obvious that interfering with the transport of major metabolites such as glutamine and glutamate would affect the cellular metabolome. However, it is interesting to observe the difference that different solute carriers have on regulating complex metabolic pathways.

Silencing of *SLC7A5* and *SLC7A11* expression was seen to have a significant effect on melanoma cell morphology while silencing of *SLC1A5* had minimal effects on cell morphology. This data adds an additional layer to current knowledge about amino acid transporters in cancer. As discussed in the previous chapter it has been shown that the LAT1 heterodimer (*SLC3A2*/*SLC7A5*) is coupled with ASCT2 (*SLC1A5*) in maintaining intracellular glutamine pools as ASCT2 brings glutamine into the cell while LAT1 exchanges intracellular glutamine for extracellular leucine (303,331). xCT (*SLC7A11*) exchanges intracellular glutamate for cysteine. We observed in chapter 3 that ROCK promotes levels of intracellular glutamine and glutamate. The fact that both genes involved in secreting glutamine/glutamate promoted a rounded morphology of melanoma cells while the gene involved in glutamine uptake did not influence cell morphology suggests that extracellular glutamate may play and important role in regulating cell morphology. In our studies there is an abundance of glutamine in the cell culture media (4mM) and the exchange of glutamine and leucine may also play an important role in regulating cell morphology. There is a possibility that glutamate may be signalling back to melanoma cells to sustain a rounded type morphology.

SLC3A2 is required to form the functional heterodimers of LAT1 (*SLC7A5*), and xCT (*SLC7A11*). We observed that knockdown of both *SLC7A5* and *SLC7A11* lead to significant elongation of melanoma cells however surprisingly knockdown of *SLC3A2* led to no changes in cell morphology. Knockdown of all three genes had a significant effect on cell proliferation although not to the extent of *SLC1A5* knockdown. Further work will need to be conducted to validate these findings and explain how knockdown of *SLC3A2* does not influence cell morphology to the extent of *SLC7A5* and *SLC7A11* knockdowns. It could be that only low levels of *SLC3A2* are required to maintain levels of *SLC7A5* and *SLC7A11* at the plasma membrane and could not be ablated with transient knockdowns.

Discussion on the results of metabolomic data from knockdowns of the solute carriers needs to start with the caveat that data confirming the knockdowns by qPCR or Western blot are not yet available. Nevertheless, the same siRNA delivery procedure was used as in Chapter 3 while qPCR indicates

these genes were successfully silenced using the same siRNAs in the screen. Most importantly, the metabolic profiles of A375M2 cells treated with the three differing siRNAs are quite distinct. Notably, the metabolome of si*SLC7A5* treated cells is more similar to that of siSLC1A5 treated cells than si*SLC7A11* treated cells. It is tempting to look for common traits between cells where *SLC7A5*, *SLC7A11* and *ROCK1/2* gene expression is silenced or ROCK activity is inhibited to establish a mechanistic link between ROCK and glutamine/glutamate in controlling cell morphology. It is seen that *myo*-inositol decreases after knockdown with both si*SLC7A5* and siSLCA11, and this is not observed in siSLC1A5 treated cells; in chapter 3 it was also observed that *myo*-inositol decreases after ROCK inhibition. In the *in vitro* screen in chapter 5, the m*yo*-inositol transporter *SLC5A3* was also tested and it was seen that it has an effect on cell proliferation and morphology, however it was not one of the largest hits seen in the screen.

We observed in the glutamine transporter knockdowns that there is an increase of lactic acid in the spent media along with corresponding decrease in in glucose. This was seen to be more pronounced in si*SLC7A5* treated cells than in siSLC1A5 treated cells.

As shown in Chapter 3, inhibition of ROCK led to an increase in the Warburg effect seen in the spent media, which would seem counter-intuitive as ROCK promotes cancer cell proliferation. This is seen again with the glutamine transporters. While the ability of the cells to absorb glutamine and other amino acids in the case of *SLC7A5* is blocked, we would expect to observe less lactate in the spent media. Instead we see the opposite effect. On the other hand, knockdown of *SLC7A11* showed a metabolic profile that would be consistent with a decrease in cell proliferation, with a reduced amount of lactic acid and an increased quantity of glucose in the spent media compared to controls. As discussed in the previous chapter, this increase in the Warburg effect after altering glutamine metabolism may be a response of the cells to potential increases in oxidative stress.

Further work needs to be conducted to fully understand the roles that these genes play in regulating the flow of metabolites across the plasma membrane. Thus far we have discussed these genes primarily in their role in regulating glutamine and glutamate transport, however the proteins that are expressed from these genes are not fully understood.

In recent years *SLC7A11* has received additional interest with the elucidation of a novel non-canonical p53 controlled non-apoptotic regulated cell death pathway, called ferroptosis (357). In ferroptosis, p53 inhibits cysteine uptake by repressing the expression of *SLC7A11*. This lack of cysteine then leads to

an increase in lipid reactive oxygen species which promote cell death (358). Ferroptosis is also characterised by morphological changes in the mitochondria. Mitochondria become smaller and have increased membrane density along with a reduction of cristae (359).

As discussed in the previous chapter, ROCK plays an important role in regulating reactive oxygen species in melanomas. ROCK and JAK/STAT signalling pathways cooperate to sustain amoeboid migration(140) and it has been reported that STAT3 and STAT5A bind the *SLC7A11* promoter region and thus repress expression. Inhibiting STAT lead to upregulation of *SLC7A11* in breast cancer(348).

A currently proposed view on how solute carriers may cooperate is that ASCT2 (*SLC1A5)* may aid cells to maintain glutamine homeostasis in cancer cells while LAT1 (*SLC7A5)* mediates the exchange of glutamine and leucine, another essential amino acid in cancers. In addition, xCT (*SLC7A11)* maintains the homeostasis of anti-oxidant species by exchanging cysteine and glutamate (331,347). Solute carriers are general understudied (267). As transmembrane proteins they are attractive drug targets and merit further research.

6.3.2 Glutaminase as a therapeutic target in melanoma

The glutaminase inhibitor 968 affected the intracellular metabolome significantly, but had quite a distinct profile compared to either ROCK or glutamate signalling inhibitors. Interestingly we did not observe a significant change in the metabolism of the spent cell culture media after treatment with 968. As glutaminolysis is blocked, one might suspect that the cells become more reliant on glucose and glycolysis as an energy source, however that was not seen. It could be that the inhibition of glutaminase does not lead to the same levels of oxidative stress as that found in after inhibiting ROCK or glutamate signalling. It is known that both the ROCK inhibitors and the glutamate antagonist CFM-2 alter signalling pathways important to cell survival and proliferation (143,184,355) and the metabolic effects we see after using these drugs could be a response to the added stresses. The glutaminase inhibitor instead is thought to act principally on mitochondrial glutaminase (159,230,360) and so may not have the broad spectrum of effects as the other inhibitors.

Glutaminase is an attractive therapeutic target in cancer therapy as glutamine in normal tissue is not an essential amino acid, however can be conditionally essential during periods of growth or pregnancy (361). Inhibition of glutaminase could function well with rapidly proliferating cells such as cancers. Currently available glutaminase specific inhibitors such as BTPES and 968 have low micro-molar specificity and poor aqueous solubility (265) and so research continues to develop molecules with

improved activity and solubility. Recently another glutaminase inhibitor CB-389 was shown to have anti-tumour activity in triple negative breast cancers (362) and is being brought forward by Calithera Biosciences Inc. in 5 separate phase 1 clinical trials to test in a wide range of solid tumours as well as lymphomas and leukaemia (clinicaltrials.gov search term: 'cb-839').

6.3.3 Targeting metastasis for therapy

Consideration needs to be made when thinking of cancers in terms of cancer stem cells or dormant tumours (113). Several studies have shown that melanomas are highly plastic cells (189,256,363) and even that a neural crest type environment may promote invasiveness in melanomas (363). Melanomas have also been seen to disseminate at early stages of disease (364) and thus it becomes even more important to think of ways of treating not just melanoma proliferation but ways of inhibiting invasive phenotypes. Slowly dividing melanoma cells that retain the capacity to form tumours at distant site would remain a challenge if thinking of targeting melanomas solely with proliferation blocking treatments. There are several ways to approach the disease from this perspective. One possible strategy would be to aim to treat cancer essentially as a chronic disease (365), similar to the way HIV is currently treated. Otherwise strategies need to be developed to ultimately target disseminated tumour cells (366). While many ideas have been proposed, there is currently debate as to the clinical relevance of these strategies(367). From this perspective our initial observations that silencing *GRIK2* expression altered melanoma cell morphology but not proliferation bolstered our interest in understanding the role that glutamate signalling plays in melanoma metastasis.

6.3.4 AMPA antagonists regulate cell proliferation and affect the metabolome

Several groups have shown that AMPA antagonists potentially regulate melanoma cell proliferation (354,355,368). In our studies we confirmed these results and additionally show that CFM-2 was able to reduced proliferation substantially at very low doses. Glutamate receptor antagonists are already used clinically to treat neuronal diseases such as epilepsy. As safety profiles have already been established for some of these drugs it would be an attractive proposal to convert these anti-epileptic drugs to treat melanoma or other cancers. Future research will be done to understand if there are antagonists that also affect cell morphology.

We observed that the metabolic changes associated with CFM-2 treatment resemble those found during ROCK inhibition. As discussed in previous chapters, ROCK inhibition leads to an increase in oxidative stress in melanoma cells and we observed depletion in several key metabolites involved in anti-oxidant

pathways. Changes in glutamine, glutamate, and glutathione concentrations along with an increase in glycolysis observed in the spent media all point to a possible compensatory action by melanoma cells to the increases in oxidative stress. This suggests again that CFM-2 may cause an increase in oxidative stress in melanoma cells, which respond by upregulating anti-oxidant pathways. It has previously been suggested that CFM-2 regulates other kinase signalling pathways in lung cancer(355) and It could be a similar case in melanoma, thus explaining their anti-proliferative effects.

All of these changes observed in ROCK inhibited cells were also observed in cells treated with CFM-2, with the exception of glutamate. CFM-2 treated cells increase the amount of extracellular glutamate as opposed to ROCK inhibited cells in which a decrease in glutamate was observed. A possible explanation could be that melanoma cells attempt to compensate for the blockage of glutamate signalling by increasing the secretion of glutamate. Experiments could be conducted to study the expression of genes required for glutamate production in these conditions.

6.3.5 GRIK2 regulates contractility but not proliferation

In the final part of our study we have focussed on the roles of one subunit of the kainate receptor family, *GRIK2* (called GluK2 or GluR6 at protein level). *GRIK2* codes for the GluR6 protein which forms hetero-tetramers with other kainate receptor subunits at the plasma membrane giving functional proteins with different binding and activation activities (210) while being present as homo-tetramers at the endoplasmic reticulum (369). *GRIK2* has three splice variants which alter the intracellular domain of the protein and thus the possible phosphorylation sites which control trafficking (370). We observed that interfering with *GRIK2* expression in both human and mouse melanoma led to a decrease in myosin phosphorylation and changes in cell morphology while not affecting capacity for cell proliferation. We also observed that *GRIK2* is mutated in 11% of melanomas (Figure 6.3) and *GRIK2* is mutated in our *in vitro* model of human melanoma. The functional consequences of this mutation have still to be elucidated.

There is some contradictory research pointing to the involvement of ionotropic glutamate receptors in malignant disease. Wu *et al* propose that *GRIK2* may have tumour suppressor activity in gastric epithelium as *GRIK2* overexpression leads to decreased invasion (371). Their results contradict our current findings as we propose that *GRIK2* activity promotes the highly invasive, blebbing type migration. This may be due to tissue specific roles of *GRIK2*. Melanomas are of neural crest origin and so they may be re-wiring glutamate signalling pathways to promote a highly invasive phenotype.

The question of how GluK2 regulates actomyosin contractility remains open. GluK2 could promote contractility by facilitating influx of calcium ions into the cell. Calcium is a known promoter of contractility via calmodulin kinase(372) and calcium homeostasis is considered important in tumour progression (76). Another possibility is that GluR6 could be regulating contractility via G-protein coupled signalling pathways as suggested in Rodrigues *et al* (343). Tashiro *et al* showed that filopodial motility of hippocampal mossy fibres were regulated by kainate receptors (373). They suggested that kainate receptors may be sensors for axonal filopodia to probe the local environment for synapse formation. In non-neuronal cells it is well established that the Rho GTPase cdc42, promotes filopodia formation in a variety of cell types (374). This highlights again the possible parallels between cells of neural crest origin, of which melanocytes and thus melanomas are part.

There is a gap in the literature to look systematically at ionotropic glutamate receptors signalling in melanoma. Currently studies have focussed almost exclusively at the expression of the glutamate receptors themselves. The downstream targets of iGluR and more specifically kainate signalling has thus far been ignored. This is due to a general ignorance of the complexes that stabilize kainite receptors and the signalling pathways in which kainate receptors take part. Their functions are still being elucidated in neurons, as reviewed in (210,375). The difficulties in elucidating the functions of kainate receptors is in part due to the difficulty in studying the specific functions of ionotropic receptors because there is a lack of specific agonists and antagonists. Further research into the binding partners of kainate receptors and their downstream signalling targets could also reveal interesting novel therapeutic targets of metastasis.

A final interesting observation was that GluK2 expression (*GRIK2*) is dependent on ROCK activity while RNA expression of *GRIK2* does not seem to be affected by ROCK activity. There could be several explanations for this observation. ROCK may be trafficking and/or stabilizing the protein at the plasma membrane. It has already been shown that ROCK1 regulates the transport of GLUT3 to the plasma membrane (156). It has been shown that phosphorylation of GluK2 by PKC at the S846 enhances SUMOylation at K886. This ultimately accelerates endocytosis of GluK2 and trafficking to late endosomes for degradation (370). It has been suggested that substrates of PKC are readily phosphorylated by ROCK, but not vice versa (376), so it would not be surprising to find that ROCK could phosphorylate GluK2. What would be surprising would be to find that ROCK activity has the opposite effect in terms of trafficking GluK2 than PKC. The limitation of our study is that this data has

thus far been observed with two ROCK inhibitors H1152 and Y27632, however we have not validated these results with *ROCK* knockdown. It remains a possibility that these results could be due to off target effects of ROCK inhibitors as they have been known to also inhibit the activity of PKA and PKC (145). Further studies will need to be conducted to confirm this finding.

We did not observe any change in cell proliferation after *GRIK2* knockdown while there was a large reduction in cell proliferation when using the AMPA receptor antagonist CFM-2. This could be due to differential effects of specific glutamate receptor subunits or could be due to the broader effects of small molecule inhibitors compared to genetic silencing. More work should be conducted to tease out which glutamate receptor subunits are responsible for melanoma proliferation. In the previous chapter we made observations on how different NMDA receptor subtypes may work in the opposite manner in promoting melanoma progression. For example, *GRIN2A* is often mutated in melanomas(377) and may contribute to poor prognosis (346) while we observed that *GRIN3A* forms atypical NMDA receptors (344) and correlates with better prognosis in patients. This data adds another layer of complexity as we now see that kainate receptors may also contribute to certain aspects of tumour progression by promoting a highly invasive phenotype while not regulating proliferation.

6.3.6 Toward a mechanistic explanation of the regulation of metabolism by ROCK

In this chapter we have explored how interfering with cellular metabolism at different stages of metabolic and signalling pathways influence cell proliferation, morphology and metabolism. We have not yet arrived at a complete mechanistic explanation for how ROCK may regulate cellular metabolism as thus far the collected data is circumstantial and based on correlations. ROCK is already known to be in a tight interplay with several other signalling hubs such as p53(184,378), c-Myc(379), PI3K/AKT-mTOR(380,381), so attempting to pick apart the subtle roles that it may be playing in regulating cell metabolism is quite an undertaking. We have seen through the metabolomics work that several metabolites and thus pathways may be regulated either directly or indirectly through ROCK activity. Despite these challenges, there are possible explanations gained from the literature that should be explored in the future to arrive at a mechanistic explanation for the observations made in this work.

6.3.6.1.1 ROCK activating c-Myc

c-Myc is a major oncogene and has been extensively linked to playing a major role in rewiring cancer cell metabolism. It has been termed the ‘master regulator’ of cancer metabolism (382,383) (264,266,383-387). It has been shown in prostate cancer that ROCK directly phosphorylates c-Myc

(379) so it is not a stretch to hypothesize that the same situation could be true in melanomas. Future work could be conducted to identify what aspects of regulating cancer metabolism ROCK and Myc overlap and if there are areas that are specific to one protein or the other.

6.3.6.1.2 ROCK and reactive oxygen species and p53

P53 is known as the gatekeeper of cell growth and division (388) and is known to regulate metabolism by regulating the expression of genes involved in glycolysis, fatty acid metabolism, and oxidative stress (389). It is established that p53 can regulate RhoA/ROCK signalling. A mutant gain of function form of P53 found in some tumours has also been shown to promote the Warburg effect by upregulating RhoA/ROCK signalling (155). In mouse endothelial fibroblasts it has been shown that p53 regulates RhoA activation and a loss of p53 leads to increased cell migration due to RhoA/ROCK signalling (160). Additionally, p53 can regulate RhoE expression, which is a ROCK suppressor (390).

There is also some evidence that ROCK can interact with p53. Vermula *et al* show via immunoprecipitation assay that ROCK1 can interact with and stabilise p53 in splenocytes (391). In their model of haemolytic anaemia, ROCK1 deficient mice had increased survival compared to wild type mice. While there is little available in the literature, further studies could be conducted to see how ROCK interacts with p53 and thus cellular metabolism.

6.3.6.1.3 ROCK direct phosphorylation of metabolic targets (GLS, GRIK, Transporters)

Experiments could be designed to investigate if ROCK directly interacts with GLS or glutamate receptors such as GluK2 (*GRIK2*). This could be conducted by co-immunoprecipitation (co-IP) to see if ROCK and the candidate proteins interact in complex. More specific kinase assays could be conducted with $^{32}\mathbf{P}$ to see if GLS or GluK2 are direct substrates of ROCK. On a broader scale, novels substrates of ROCK could be identified with phosphor-proteomics studies. Phospho-proteomics is a rapidly growing field and there is already a study into how the phosphor-proteome changes during resistance to BRAF inhibitors in melanoma (4). A potential study that could be conducted would be to identify substrates of ROCK in melanoma and how the phosphor-proteome changes after ROCK inhibition or in knockdown/knock-out models of ROCK in melanoma.

6.4 Conclusion

In this chapter we aimed to gain a deeper understanding of how interfering with glutamine/glutamate metabolism, transport and glutamate signalling affects cell proliferation, morphology and metabolic profiles. In addition, we made preliminary attempts to directly connect ROCK activity with aspects of cellular metabolism.

The data presented in this chapter shows that glutamine/glutamate transporters play different roles in regulating melanoma proliferation and morphology. Genes involved in glutamine import showed strong effects on cell proliferation while genes involved in glutamine/glutamate secretion showed strong regulation of cell morphology and regulated cell proliferation to a much smaller extent.

Glutamate signalling was also investigated; it was seen that NMDA receptor antagonists did not inhibit cell proliferation while the AMPA/kainate antagonist CFM-2 strongly inhibited cell proliferation at low doses. The glutaminase inhibitor 968 also showed strong regulation of cell proliferation at low doses. Both treatments significantly altered the metabolic profiles of melanoma cells. CFM-2 led to a metabolic profile that was comparable to that of the ROCK inhibitor GSK269 while 968 led to a very distinct metabolic profile. Additionally, 968 treatments did not lead to a change in the spent cell culture media while CFM-2 and GSK269 both led to increases in the Warburg effect, possible as a response to oxidative stress.

Data presented in this chapter support the hypothesis that glutamate signalling plays an important role in regulating melanoma proliferation, cell morphology and that ROCK may play a role in regulating ionotropic glutamate signalling. Silencing of genes involved in glutamate secretion led to elongation of melanoma cells. Silencing of *GRIK2*, a gene encoding for the ionotropic glutamate receptor GluK2, also led to cell elongation and reduced actomyosin contractility. Inhibiting ROCK activity with small molecule inhibitors led to a reduction in protein levels of GluK2 while not affecting the expression of *GRIK2*.

Chapter 7 : Conclusion and Future Work

7.1 Overview of Work

Malignant Melanoma remains he deadliest form of skin cancer despite incredible advances in treatment that have come into the clinic in the past five years. In addition, non-response or development of resistance remains an important issue when attempting to treat melanoma patients. Rho-ROCK signalling has been thought to be an attractive therapeutic target for treating a variety of cancers since the early 2000s (125).

Cancer metabolism has long been known to be altered compared to normal tissue and the past two decades have seen a renaissance of research into cancer metabolism as the scientific community has entered the post-genomic era aided by technological developments allowing for -omics level studies of the metabolic landscape of biological systems (161).

In this body of work, we aimed to address a gap in knowledge of if and how ROCK regulates melanoma cell metabolism to sustain increased levels of cell proliferation and invasion. We started by examining if altering ROCK activity in metastatic melanoma would change the cellular metabolome by interfering with ROCK activity or expression in human and murine melanomas. We observed that altering ROCK activity led to significant changes in several metabolites and metabolic pathways that are important in maintaining cell proliferation and anti-oxidant pathways. In particular glutamine and glutamate metabolism was suggested to be the most regulated pathway by ROCK activity. We also saw that ROCK1 and ROCK2 may play differing role in regulating cell metabolism, however further research should elucidate these differences

We then aimed to understand if the results found *in vitro* could be more broadly applicable in a clinical setting. We studied how genes involved in glutamine and glutamate pathways are expressed in both primary melanomas and metastasized melanomas using publically available transcriptome data. We observed that genes involved in glycolysis were more expressed in primary tumours compared to normal tissue while genes involved in glutamine and glutamate metabolism were more expressed in metastatic melanomas compared to primary melanomas. It was also observed that genes involved in glutamine metabolism correlated with ROCK expression while ROCK expression negatively correlated with genes involved in glycolysis. *In vitro* we tested the expression of a selection of genes in A375M2 cells and observed that *SLC7A11*, a gene involved in glutamate, cysteine exchange and *GRIK2*, encoding for an ionotropic glutamate receptor, are highly expressed. *GRIK2* was also seen to regulate cell morphology and not cell proliferation. It was also observed that the expression of the

transglutaminase gene *TGM2*, which is upregulated in metastatic melanomas compared to primary melanomas, is regulated by ROCK activity. These results lend support to our *in vitro* findings that glutamine metabolism and ROCK play an important role in the progression of melanoma in the metastatic cascade.

We then took a closer look at these pathways with further *in vitro* studies, examining their roles in cell proliferation, morphology, and actomyosin contractility in models of metastatic melanoma. We aimed to see if the metabolic phenotype observed in our studies of ROCK could be replicated by targeting genes involved in glutamine and glutamate transport. Silencing of genes involved in glutamine influx showed regulation of cell proliferation while genes involved in glutamine/leucine exchange and glutamate/cysteine exchange showed significant effects on cell morphology. This pointed to a potential role in glutamate signalling in melanoma morphology.

We further investigated the role of *GRIK2* in melanoma cell morphology and observed that silencing of GRIK2 led to more elongated cells and a decrease in actomyosin contractility in both human and murine melanomas. Additionally, we observed that ROCK activity regulated the expression of GluK2, the expressed protein of *GRIK2*, while not regulating the expression of *GRIK2*. These demonstrate that contractility in melanoma is regulated by glutamate receptors.

We finally aimed to understand the effects of glutamate receptor antagonists in melanoma. Several glutamate antagonists are already approved for clinical use for several neurodegenerative diseases and so the translation of these drugs into treating melanoma represents an attractive proposal. We observed that blanket targeting of the AMPA/kainate receptor subgroup with CFM-2 at low doses showed substantial decreases in cell proliferation and led to a metabolic profile similar to that found in melanoma cells after ROCK inhibition. Interestingly, we observed that CFM-2 led to an increase in the Warburg effect in melanoma cells, similar to what we had observed with ROCK inhibitors. This was not seen with the glutaminase inhibitor 968, which showed strong anti-proliferative effects at low concentrations and a significant change in intracellular metabolism, but no change in the exometabolome. While in this work we studied the effects of the small molecule inhibitors on melanoma proliferation and the metabolic profiles, future work should elucidate their effects also on cell morphology and actomyosin contractility.

In this thesis we have shown that ROCK regulates the metabolic profiles of metastatic melanomas and is correlated with glutamine/glutamate metabolism and glutamate signalling while being negatively correlated with glycolysis.

7.2 Discussion/Model

From the data presented in this thesis we have implicated ROCK activity with a variety of metabolic pathways (Figure 7.1). We correlated ROCK with intracellular glutamine, glutamate and glutathione levels. It is known that ROCK can directly phosphorylate c-Myc(379) which is a known regulator of cellular metabolism in cancer(266,382,383). Therefore, it is possible that ROCK can promote glutaminolysis via c-Myc. It is also known that ROCK supresses reactive oxygen species to promote survival in metastatic melanoma. The picture that is forming from this work is that metabolism is intrinsically tied to several signalling pathways and anti-oxidant homeostasis. While the role of ROCK in regulating Reactive oxygen species has been previously proposed(184), to date a role for ROCK in cancer cell metabolism has not been examined in depth.

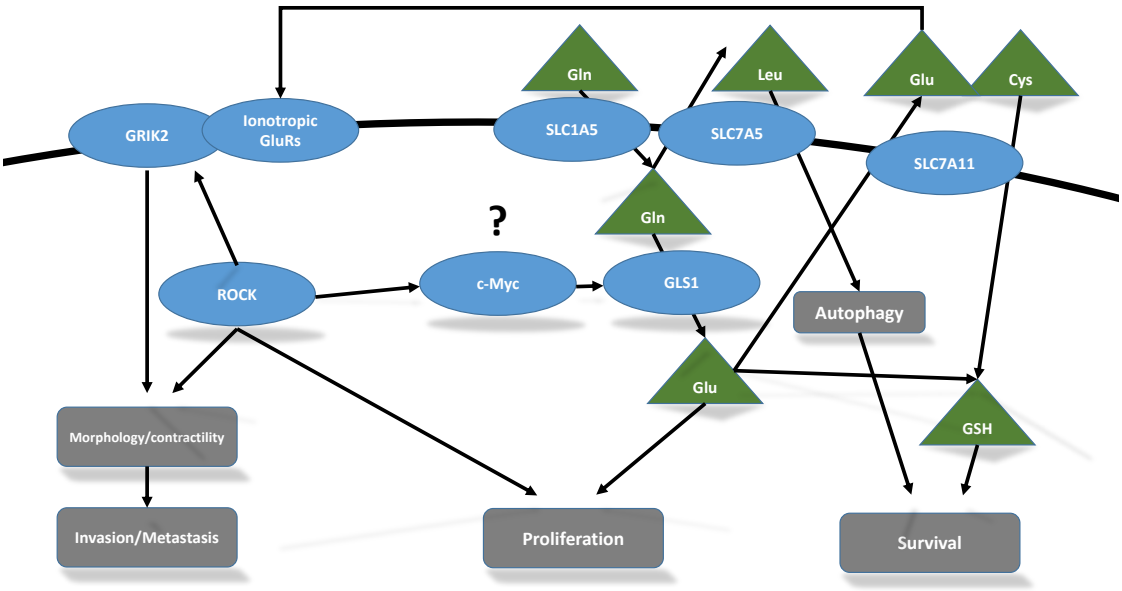

Figure 7.1. Proposed model for regulation of cellular metabolism and glutamate signalling by ROCK. ROCK promotes actomyosin contractility and thus cell proliferation and metastasis. In this work we have shown associations of ROCK activity with both glutamine/glutamate metabolism and glutamate signalling. ROCK activity regulates the protein levels of ionotropic glutamate receptors such as GluK2. In the literature it has been shown that ROCK regulates the function of c-MYC, which is known as a key regulator of cancer cell metabolism. ROCK could be potentially regulating cellular metabolism via activation of c-MYC or other proteins involved in regulating cellular metabolism such as p53.

We have seen that blocking glutamate signalling pharmacologically can block cell proliferation while knocking down representative ionotropic glutamate receptor genes can lower contractility in melanoma cells. Blanket inhibition of glutamate receptors with small molecule inhibitors lead to significant changes in proliferation while targeting individual members will lead to a more nuanced view of which family members contribute to different cellular functions.

Not shown in our model but that is however very important to mention is the role that ROCK was observed to play in supressing the Warburg effect. We consistently observed increases in the Warburg effect after ROCK inhibition in the spent cell culture media. Whether this is to compensate for a blockage of glutamine metabolism or as a response to increased oxidative stress in these cells is yet to be established.

7.3 Future Work

As with many research projects, this results of this study creates many more questions than it can answer. We have made associations between ROCK activity and glutamine/glutamate transport, metabolism and glutamate signalling. However, no definitive mechanistic explanations have been proven in this work.

Future work will also aim to investigate other metabolic pathways that were observed to be regulated by ROCK activity or expression in melanoma. In this work we have focussed primarily on glutamine and glutamate metabolic pathways and have overlooked many other finding that the metabolomic studies have suggested. For example, we have only taken a cursory look into what *myo*-inositol could be doing in melanoma cells in terms of promoting cell proliferation or cell morphology. Inositide signalling is a large area of biomedical research in itself, linked with PLCγ and PTEN (236).

We also saw significant changes in how lipid bodies are changed in melanoma cells after perturbing ROCK activity or expression. ROCK plays a major role in regulating the actin cytoskeleton and influencing modes of migration in cancer cells. It would be interesting to understand if the changes in lipids are a consequence of or partially responsible for the changes in cell shape induced by ROCK signalling. Some preliminary work has been performed with live imaging of A375M2 cells using di-4-ANEPPDHQ (Figure 7.2), a fluorescent dye that emits at two different wavelengths depending on the fluidity of cellular membranes, allowing for live cell imaging of lipid order in cells(392). It will be interesting to see how fluorescence microscopy compares to the NMR metabolomic data showed in this thesis.

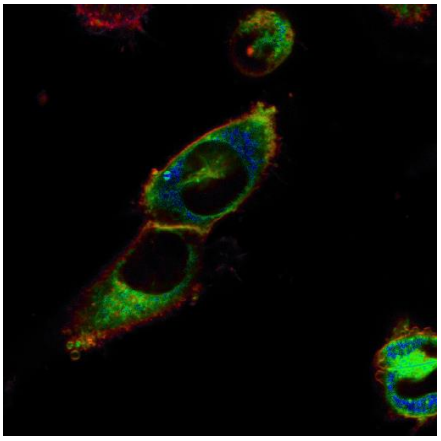

Figure 7.2. Live fluorescence imaging of A375M2 human melanoma cells plated on plastic and stained with di-4-ANEPPDHQ. Colours represent rigidity of cell membrane with green representing rigid membrane and red representing more fluid membranes. Blue is oversaturated pixels.

Future work would also aim to add additional layers of information regarding ROCK and melanoma cells. Additional experimental systems such as proteomic and phospho-proteomics could add new insight to the substrates of ROCK in melanoma and how these affect cellular metabolism. Multi-block OPLS algorithms (82,83) could be incorporated to help identify trends within melanoma cells that may not be apparent using network analysis that requires *a priori* knowledge of biological pathways.

It will take many years to tease apart how different members of each pathway contribute to specific effects in cancer cells. Eventually it is hoped that the data presented here can contribute to further understanding of cancer progression and eventually support the progress toward novel therapies for melanoma and other forms of cancer.

Appendix A: Full Gene Lists

Genes used in Database Searches and Gene Set Enrichment Analysis

Total Unique Genes	**HMDB Search 'glut*'**	**Glycolysis**	**TCA Cycle**	**Glutaminolysis**	**Ionotropic Glutamate Receptors**	**Metabotropic Glutamate Receptors**	**Gln/Glu Transporter**	**Glc Transport**
AADAT	AADAT	HK1	DLD	SLC1A5	GRIA1	GRM1	SLC7A1	SLC2A1
AASS	AADAT	HK2	OGDH	SLC38A1	GRIA2	GRM2	SLC7A2	SLC2A2
ABAT	AASS	HK3	SULA2	GLS1	GRIA3	GRM3	SLC7A3	*SLC2A3*
ACO1	ABAT	TPI1	SUCLG1	GLS2	GRIA4	GRM4	SLC7A4	SLC2A4
ACO2	ADC	GCK	SUCLG2	GOT1	GRID1	GRM5	*SLC7A5*	SLC2A14
ADC	AGXT2	PFKM	SDHD	GOT2	GRID2	GRM6	SLC7A6	SLC5A1
AGXT	ALDH18A1	PFKL	SDHC	GLUD1	GRIK1	GRM7	SLC7A7	SLC5A2
AGXT2	ASNS	PFKP	SDHA	GLUD2	GRIK2	GRM8	SLC7A8	SLC5A4
ALDH18A1	BCAT1	GAPDH	SDHB	GPT	GRIK3		SLC7A9	SLC5A9
ALDH4A1	BCAT2	GAPDHS	FH		GRIK4		SLC7A10	SLC5A10
ASNS	CCBL1	PGAM1	MDH1		GRIK5		*SLC7A11*	
BCAT1	CCBL2	PGAM2	ME1		GRIN1		SLC3A1	
BCAT2	CTPS2	ENO1	ME2		GRIN2A		*SLC3A2*	
CAD	DNPEP	ENO2	ME3		GRIN2B		SLC1A1	
CCBL1	EARS2	ENO3	PC		GRIN2C		SLC1A2	
CCBL2	ENPEP	PKM2	CS		GRIN2D		SLC1A3	
CS	EPRS	PKLR	ACO1		GRIN3A		SLC1A6	
CTPS1	FPGS	LDHAL6B	ACO2		GRIN3B		SLC1A7	
CTPS2	FTCD	LDHA	IDH3				SLC1A5	
DLD	GAD1	LDHB	IDH1					

DNPEP	GAD2	LDHC	IDH2					
EARS2	GCLC	SLC2A1	IDH3B					
ENO1	GCLM	SLC2A2	IDH3G					
ENO2	GFPT1	SLC2A4						
ENO3	GFPT2							
ENPEP	GGT1							
EPRS	GGT5							
F13A1	GGT6							
FH	GGT7							
FOLH1	GGT7							
FPGS	GIG18							
FTCD	GLS							
GAD1	GLS2							
GAD2	GLUL							
GAPDH	GLYATL1							
GAPDHS	GOT1							
GATC	GOT1L1							
GCK	GOT2							
GCLC	GPT							
GCLM	GPT2							
GFPT1	GRIA1							
GFPT2	GRIK1							
GGCX	GRIK3							
GGT1	GSS							

GGT2	LGSN							
GGT3P	NAGS							
GGT5	OAT							
GGT6	OPLAH							
GGT7	PET112							
GIG18	PFAS							
GLS	PIG59							
GLS1	PSAT1							
GLS2	QARS							
GLUD1	QRSL1							
GLUD2	SLC25A18							
GLUL	SLC25A22							
GLYATL1	TAT							
GMPS	SLC16A1							
GOT1	SLC16A10							
GOT1L1	SLC1A5							
GOT2	SLC38A3							
GPT	SLC7A8							
GPT2	AASS							
GRIA1	AGXT							
GRIA2	ALDH4A1							
GRIA3	CAD							
GRIA4	CTPS1							
GRID1	F13A1							

GRID2	FOLH1							
GRIK1	GATC							
GRIK2	GGCX							
GRIK3	GGT2							
GRIK4	GGT3P							
GRIK5	GLUD1							
GRIN1	GLUD2							
GRIN2A	GMPS							
GRIN2B	GRIA2							
GRIN2C	GRIK2							
GRIN2D	GRIN1							
GRIN3A	GRIN2A							
GRIN3B	GRIN2B							
GRM1	GRIN2C							
GRM2	GRIN2D							
GRM3	GRIN3A							
GRM4	GRIN3B							
GRM5	GRM1							
GRM6	GRM4							
GRM7	GRM7							
GRM8	GRM8							
GSR	GSR							
GSS	NADSYN1							
HK1	PPAT							

HK2	RIMKLA							
HK3	RIMKLB							
IDH1	SLC1A1							
IDH2	SLC1A2							
IDH3	SLC1A3							
IDH3B	SLC1A6							
IDH3G	SLC1A7							
LDHA	*SLC7A11*							
LDHAL6B	TGM1							
LDHB	TGM2							
LDHC	TGM3							
LGSN	TGM4							
MDH1	TGM5							
ME1	TGM6							
ME2	TGM7							
ME3								
NADSYN1								
NAGS								
OAT								
OGDH								
OPLAH								
PC								
PET112								
PFAS								

PFKL								
PFKM								
PFKP								
PGAM1								
PGAM2								
PIG59								
PKLR								
PKM2								
PPAT								
PSAT1								
QARS								
QRSL1								
RIMKLA								
RIMKLB								
SDHA								
SDHB								
SDHC								
SDHD								
SLC16A1								
SLC16A10								
SLC1A1								
SLC1A2								
SLC1A3								
SLC1A5								

SLC1A6								
SLC1A7								
SLC25A18								
SLC25A22								
SLC2A1								
SLC2A14								
SLC2A2								
SLC2A3								
SLC2A4								
SLC38A1								
SLC38A3								
SLC3A1								
SLC3A2								
SLC5A1								
SLC5A10								
SLC5A2								
SLC5A4								
SLC5A9								
SLC7A1								
SLC7A10								
SLC7A11								
SLC7A2								
SLC7A3								
SLC7A4								

SLC7A5								
SLC7A6								
SLC7A7								
SLC7A8								
SLC7A9								
SUCLG1								
SUCLG2								
SULA2								
TAT								
TGM1								
TGM2								
TGM3								
TGM4								
TGM5								
TGM6								
TGM7								
TPI1								

Genes Upregulated in Databases

Avery		**Talantov**		**Kabbarah**		**Riker**		**Xu**		**TCGA**	
Primary Melanomas				Metastatic Melanomas							
Gene	Pathway	Gene	Pathway	Gene	Pathway			Gene	Pathway	Gene	Pathway
SLC2A3	glucose transport	ASNS	Asparagine synthesis	AASS	Glutamate synthesis			ACO2	TCA cycle	BCAT1	Branched Amino Acid Synthesis
		CAD	Pyrimidine Synthesis	ASNS	Asparagine synthesis			ALDH18A1	Proline Synthesis	HK3	Glycolysis
		ENO1	Glycolysis	DLD	Glycolysis			ASNS	Asparagine synthesis	SLC7A7	Glutamine Transport
		ENO2	Glycolysis	ENO2	Glycolysis			BCAT1	Branched Amino Acid Synthesis	TGM2	Transglutaminase
		GOT2	Glutaminolysis	GFPT1	Glycolysis			DLD	Lipoamide dehydrogenase		
		GRIK1	Glutamate receptor	GLS	Glutaminolysis			ENO2	Glycolysis		
		GRIK2	Glutamate receptor	PPAT	Purine Synthesis			ENO3	Glycolysis		
		GRIN2D	Glutamate receptor	TGM2	Transglutaminase			FOLH1	Glutamate synthesis		
		ME2	TCA Cycle					GFPT1	Glycolysis		
		OGDH	Glycolysis					GGCX	Glutamate Carboxylation		
		PFKL	Glycolysis					GLS	Glutaminolysis		
		PFKP	Glycolysis					GRIA4	Glutamate Receptor		
		PKM2	Glycolysis					GSR	Antioxidant homeostasis		
		PPAT	Purine Synthesis					HK3	Glycolysis		
		SLC1A5	Glutamine transport					MDH1	TCA cycle		
		SLC2A3	Glucose Transport					ME2	TCA cycle		
		SLC3A2	Glutamine transport					PPAT	Purine Synthesis		
		SLC7A1	Amino Acid transport					SLC16A1	Lactate Transport		
		SLC7A5	Glutamine transport					SLC7A2	Arginine, Lysine Transport		

		SLC7A8	Glutamine transport					*SLC7A5*	Glutamine Transport		
		TGM4	Transglutaminase					SLC7A7	Glutamine Transport		
		TPI1	Glycolysis					TGM2	Transglutaminase		

Genes Downregulated in Databases

Primary Melanoma				Metastatic Melanoma							
Avery		Talantov		Kabbarah		Riker		Xu		TCGA	
Gene	Pathway	Gene	Pathway	Gene	Pathway	Gene	Pathway	Gene	Pathway	Gene	Pathway
CCBL2	Kynurenic Acid Synthesis	ACO1	TCA Cycle	F13A1	Transglutaminase	GRIA3	Glutamate Receptor	F13A1	Transglutaminase	TGM1	Transglutaminase
CS	TCA cycle	F13A1	Transglutaminase	GPT	Glycolysis	TGM1	Transglutaminase	GGT5	Glutathione catabolism	TGM3	Transglutaminase
GCLM	Glutathione Synthesis	GAD1	GABA synthesis	GRM5	Glutamate Receptor			GPT	Glycolysis	TGM5	Transglutaminase
GGCX	Glutamate Carboxylation	GAPDHS	Glycolysis	SLC2A1	Glucose Transport			GRIK4	Glutamate Receptor		
IDH1	TCA cycle	GLS2	Glutaminolysis	TGM1	Transglutaminase			NADSYN1	NAD synthesis		
OAT	Glutamate/GABA synthesis	GLUD2	Glutaminolysis	TGM3	Transglutaminase			PKLR	Glycolysis		
PFKM	Glycolysis	GPT	Glycolysis					SLC2A1	Glucose Transport		
PSAT1	Serine Synthesis	GRIA1	Glutamate Receptor					TGM1	Transglutaminase		
SDHA	TCA cycle	GRIN2A	Glutamate Receptor					TGM3	Transglutaminase		
SDHC	TCA cycle	IDH2	TCA Cycle					TGM5	Transglutaminase		
SLC3A2	Glutamine Transport	ME1	TCA Cycle								
SLC5A10	Glucose Transport	ME3	TCA Cycle								
SLC7A8	Glutamine Transport	OAT	Glutamate/GABA Synthesis								
TGM7	Transglutaminase	OPLAH	Glutamate Synthesis								
		PC	TCA Cycle								

		PSAT1	Serine Synthesis								
		SLC16A10	Amino Acid Transport								
		SLC1A2	Glutamate import								
		SLC1A6	Glutamate import								
		SLC2A1	Glucose Transport								
		SLC38A1	Glutamine Transport								
		SLC5A1	Glucose Transport								
		SUCLG1	TCA cycle								
		TGM1	Transglutaminase								
		TGM3	Transglutaminase								
		TGM5	Transglutaminase								

Appendix B: Notes on Metabolite Assignment

Metabolomics software has developed greatly in recent years with the advent of both publically available (Bayesil automated assignment for liquid NMR (393)) and commercial software (ChenomX) to aid metabolite assignment. A full discussion on the methods is beyond the scope of this work however a few notes and figures are presented here to give an idea of the efforts made to verify metabolite assignments.

A challenge that comes with 1D NMR metabolomics are overlapping spectra that increase difficulty in making confident assignments of metabolites. One method to increase confidence is to include 2 dimensional NMR experiments which can spread peaks over a second dimension, thus increasing the separation between individual peaks. Due to the long time-frames required for obtaining 2D spectra, we obtained J-Res, COSY, and HSQC 2D spectra for one sample per condition studied. Figure 7.3 shows a representative 2D homonuclear correlation spectroscopy (COSY) experiment.

Software aided assignment is also become more accessible. Bayesil is an online web took that allows for fully automated metabolite assignment for plasma, serum or cerebrospinal fluid (393), and can have some use with other fluids if used with caution. The Chenomx software package allows users to overlay 1D spectra of standard compound atop the spectra of interest and creates a summed spectrum (Figure 7.4). This increases confidence in assignments as users can easily visualise if all resonances from a candidate metabolite are present in the spectra of study.

These additional techniques are very useful to assign spectra, however they do not yet replace the value of human expertise and the data previously published. (60). This is particularly true for HR-MAS NMR as most developed software is made specifically for liquid NMR.

	METABOLITE	CHEBI ID	PPM
1	Acetate	CHEBI:15366	1.92
2	Alanine	CHEBI:16449	1.48
3	Asparagine	CHEBI:22653	2.80
4	Aspartate	CHEBI:22660	2.73
5	Choline	CHEBI:15354	3.21
6	Creatine	CHEBI:16919	3.02
7	Glucose	CHEBI:17234	3.44
8	Glutamate	CHEBI:18237	2.36
9	Glutamine	CHEBI:28300	2.46
10	Glycerophosphocholine	CHEBI:16870	3.26
11	Triglycerides	CHEBI:17855	4.47
12	Inosine	CHEBI:17596	8.19
13	Isoleucine	CHEBI:24898	1.03
14	Lactate	CHEBI:78320	1.33
15	Leucine	CHEBI:25017	0.97
16	Lipid CH2-CH2-CO		2.25
17	Methyl Group of Lipids CH3		0.90
18	*Myo*-Inositol	CHEBI:17268	3.55
19	Phenylalanine	CSID 136705	7.35
20	Phosphocholine	CHEBI:18132	3.23
21	Lipid Chain CH2-CH2		1.30
22	Tyrosine	CHEBI:18186	6.90
23	Valine	CHEBI:27266	5.33
24	Unsaturated Lipid Chain		1.04

Table 10. Assignments used for HR-MAS NMR experiments including Chemical Entities of Biological Interest Database (ChEBI) accession number where available.

	METABOLITE	CHEBI ID	PPM
1	Leucine	CHEBI:25017	0.97
2	Isoleucine	CHEBI:24898	1.01
3	Valine	CHEBI:27266	1.04
4	Lactate	CHEBI:78320	1.33
5	Alanine	CHEBI:16449	1.48
6	Methionine	CHEBI:16811	2.14
7	Glutamate	CHEBI:18237	2.33
8	Pyruvate	CHEBI:32816	2.38
9	Pyroglutamate	CHEBI:16010	2.41
10	Glutamine	CHEBI:28300	2.44
11	Lysine	CHEBI:25094	3.04
12	*Myo*-inositol	CHEBI:17268	4.07
13	Glucose	CHEBI:17234	5.24
14	Fumarate	CHEBI:18012	6.52
15	T-Methyl histidine	CHEBI 10960	7.04
16	Tyrosine	CHEBI:18186	7.19
17	Phenylalanine	CHEBI:28044	7.33
18	Tryptophan	CHEBI:27897	7.55
19	Formate	CHEBI:30751	8.46
20	Nicotinamide	CHEBI:17154	8.72

Table 11. Assignments of cell culture media NMR metabolomics including Chemical Entities of Biological Interest Database (ChEBI) accession number.

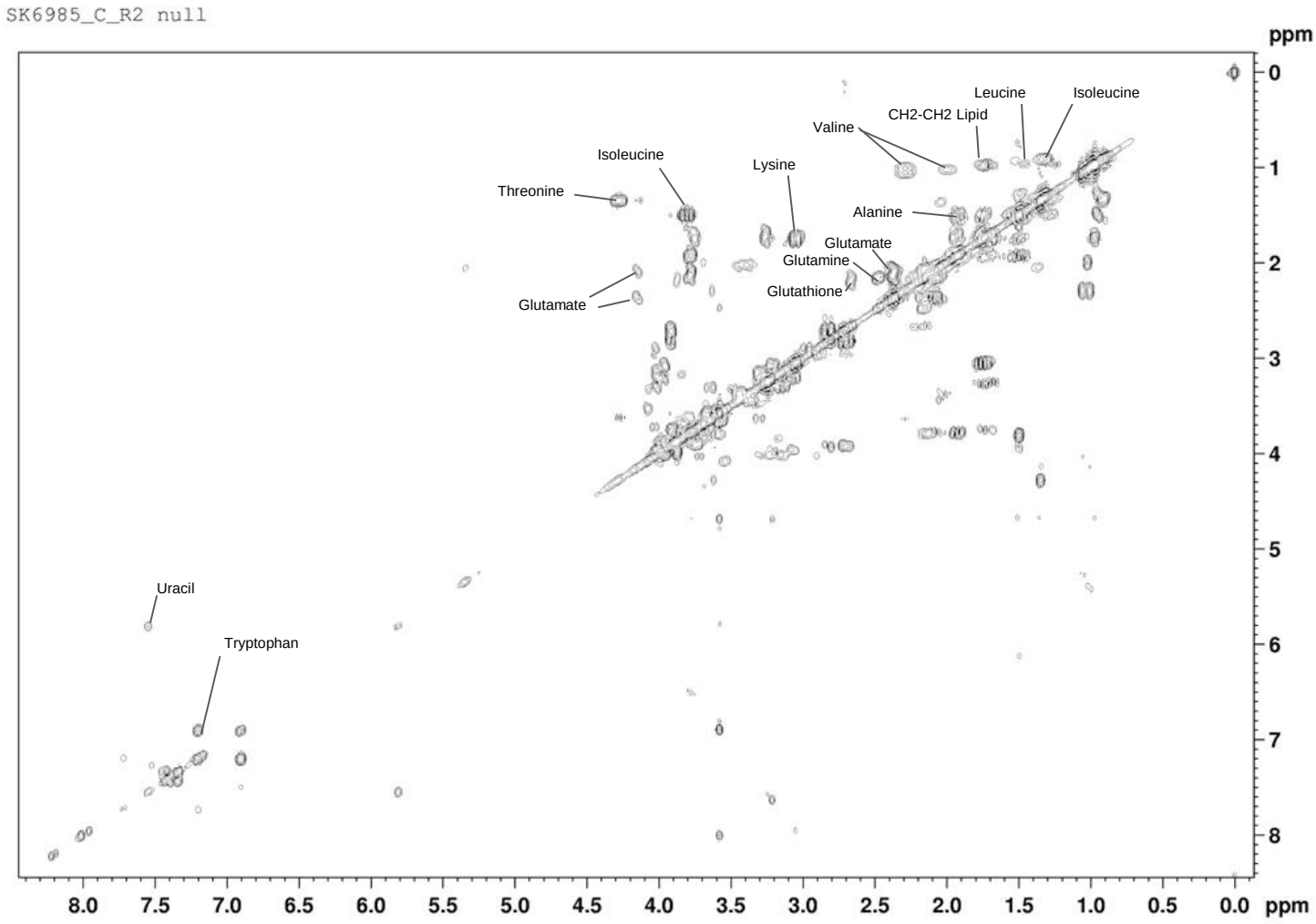

Figure 7.3. Representative 2D COSY ^{1}H HR-MAS NMR spectra of ROCK2 KO murine melanomas. A partial assignment is shown of identified metabolites. the spectrum was obtained on a 400 MHz Bruker spectrometer.

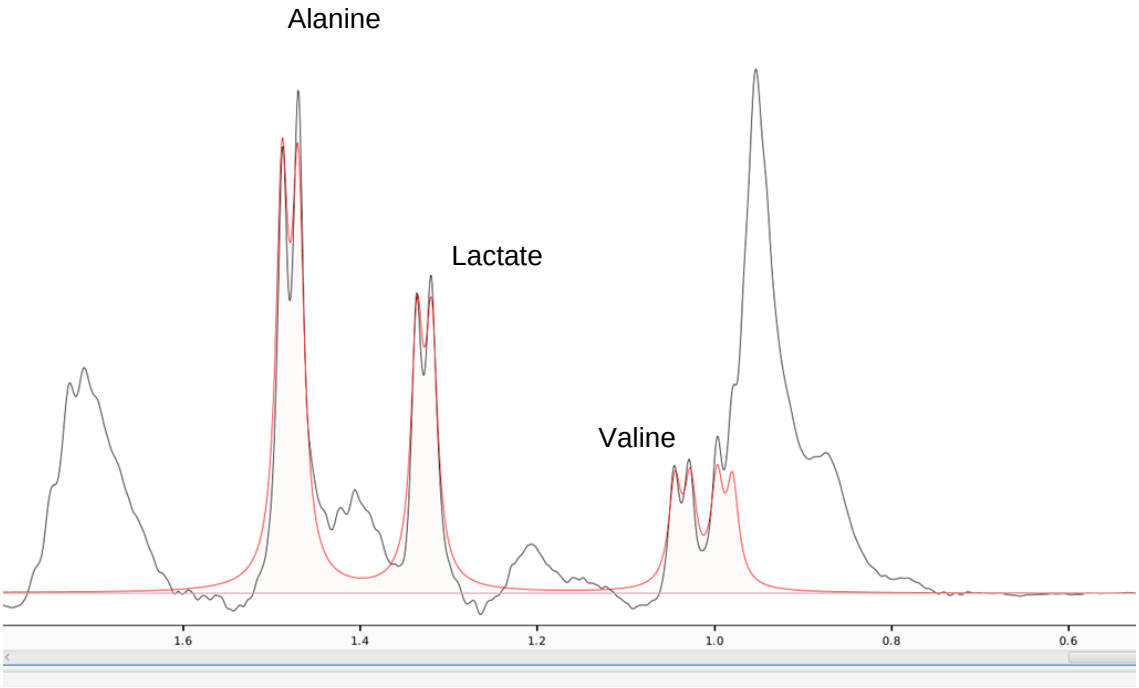

Figure 7.4. Representative metabolite assignment with Chenomx software. Chenomx permits users to overlay NMR spectra of standard compounds (red) with the NMR spectrum under study (black). A particular strength of the Chenomx software is the ability to account for shifting of peaks due to changes in pH between samples. The spectrum shown here is a 1D ^{1}H HR-MAS NMR of ROCK2 KO murine melanoma obtained on a 400 MHz Bruker spectrometer.

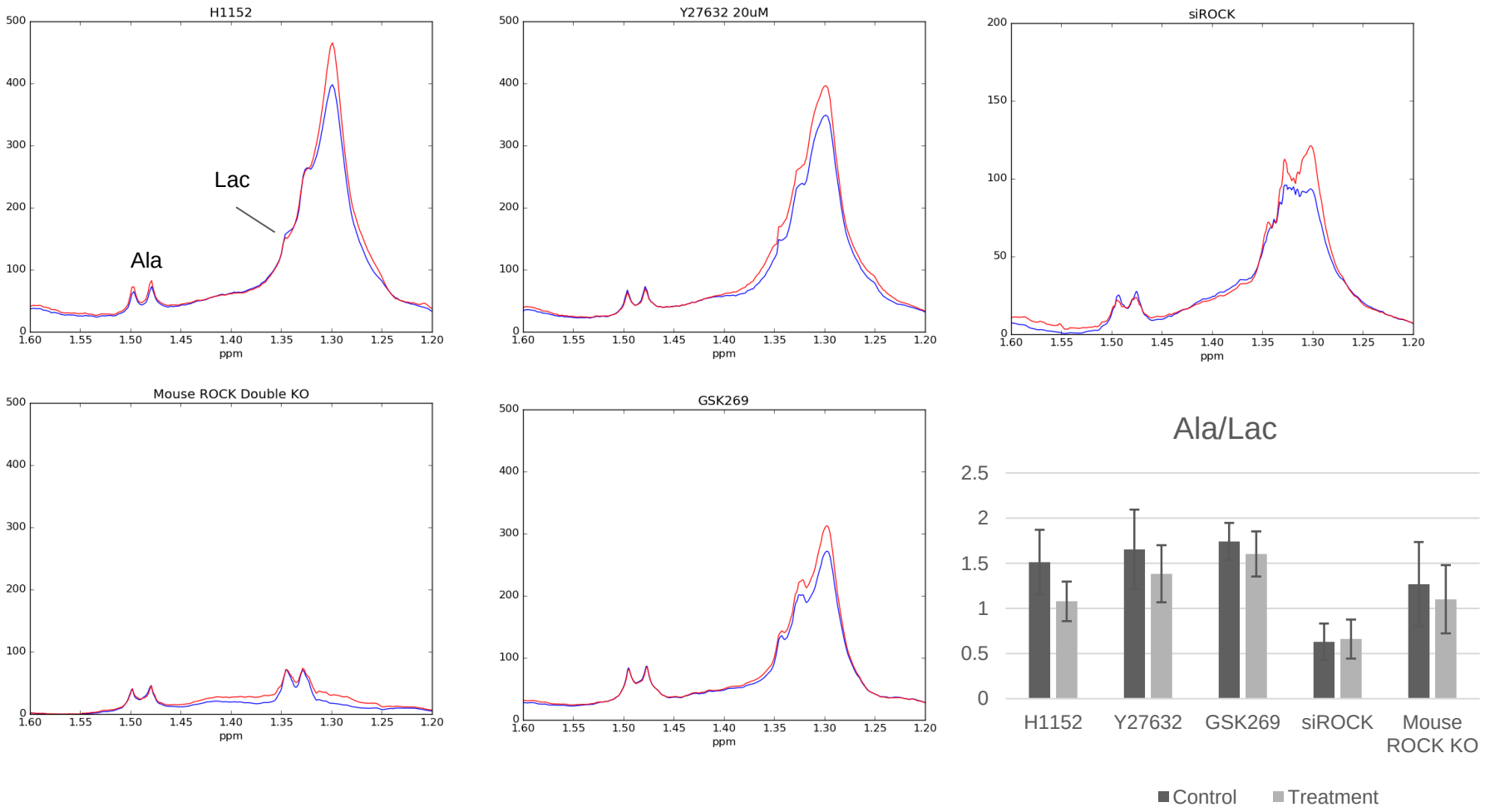

Figure 7.5. H1152 interferes with the redox state of melanoma cells. Left) Mean PQN normalised ^{1}H HR-MAS NMR spectra of melanoma cells where ROCK activity has been interfered with. Control spectra are plotted in blue while treatment spectra re plotted in red. Spectra highlight the changes in Alanine (Ala) and Lactate (Lac). Right) The ratios between Alanine and Lactate are shown between control cells and treatment cells. All experiments are n=3 with 3 internal replicates per experiment.

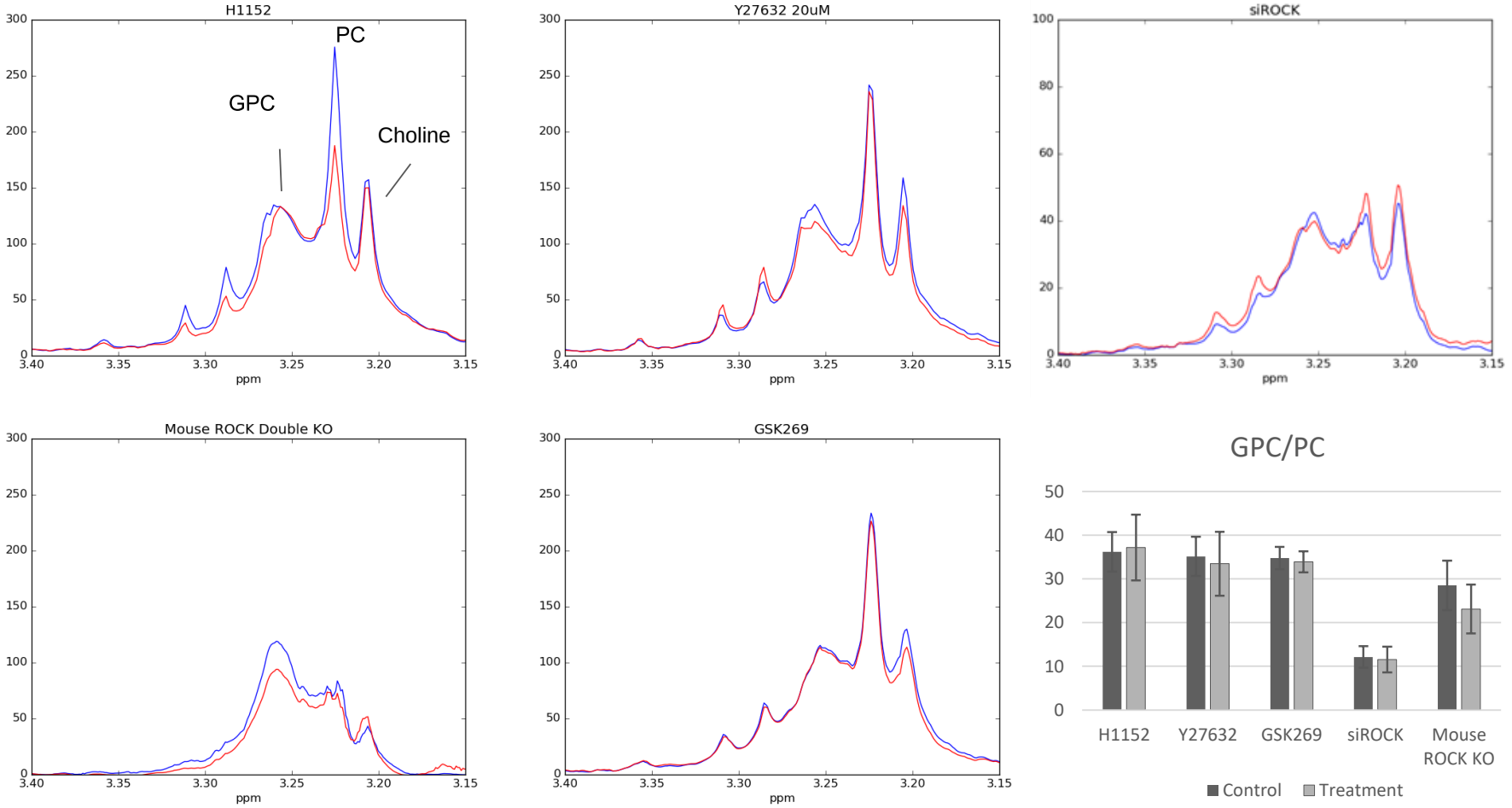

Figure 7.6 GPC/PC ratio of mouse melanoma cells decrease after KO of ROCK. Left) Mean PQN normalised ^{1}H HR-MAS NMR spectra of melanoma cells where ROCK activity has been interfered with. Control spectra are plotted in blue while treatment spectra re plotted in red. Spectra highlight the changes in choline, Phosphocholine (PC), and glycerophosphocholine (GPC). Right) The ratios between GPC and PC are shown between control cells and treatment cells. All experiments are n=3 with 3 internal replicates per experiment.

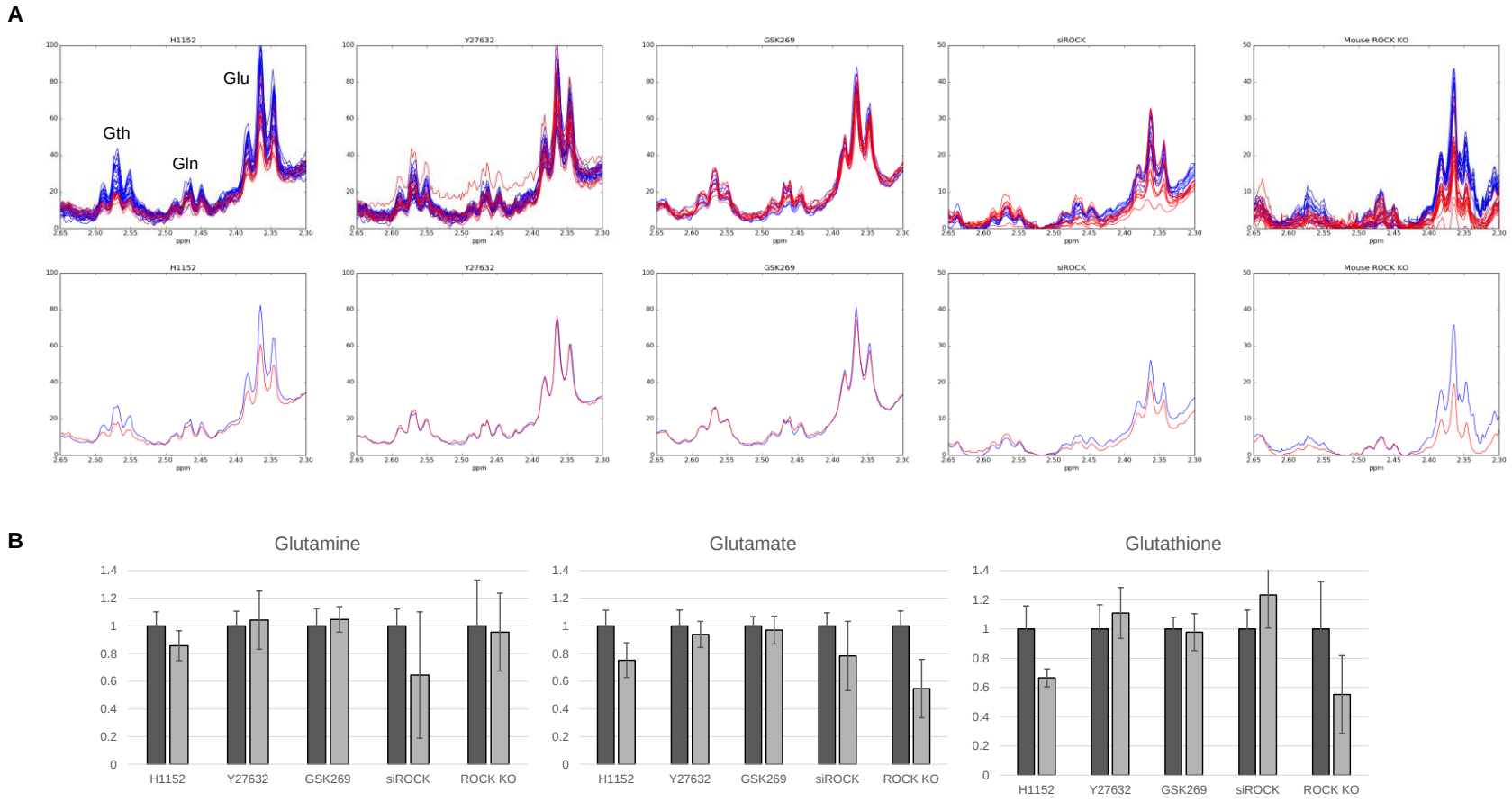

Figure 7.7 Glutamine, glutamate and glutathione are altered by different levels of ROCK activity. A) Top: Spectral overlays of ^{1}H HR-MAS NMR of human and murine melanoma cells highlighting the spectral regions with glutathione (Gth), glutamine (Gln), and glutamate (Glu). Control cells are plotted in blue while treatment cells are plotted in red. From left to right the treatments are H1152, Y27632, GSK269, siROCK and ROCK double knock-out. Below: mean spectra from the same data to illustrated the differences in controls (blue) vs. treatment (red). B) Bar charts taken from data in A illustrating the relative changes in signal intensity of melanoma cells are interfering with ROCK expression/activity. Bar Charts show mean +/-standard error of the mean (minimum n=3 with 3 internal replicates in each experiment for a total of 9 samples per condition).

References

1. McLaren, E. (2014) Deaths Registered in England and Wales: 2014. Office for National Statistics
2. CRUK. (2016) Skin cancer incidence statistics. CRUK
3. Sadok, A., McCarthy, A., Caldwell, J., Collins, I., Garrett, M. D., Yeo, M., Hooper, S., Sahai, E., Kuemper, S., Mardakheh, F. K., and Marshall, C. J. (2015) Rho kinase inhibitors block melanoma cell migration and inhibit metastasis. *Cancer research* **75**, 2272-2284
4. Smit, M. A., Maddalo, G., Greig, K., Raaijmakers, L. M., Possik, P. A., van Breukelen, B., Cappadona, S., Heck, A. J., Altelaar, A. F., and Peeper, D. S. (2014) ROCK1 is a potential combinatorial drug target for BRAF mutant melanoma. *Molecular systems biology* **10**, 772
5. Kuemper, S., Mardakheh, F. K., McCarthy, A., Yeo, M., Stamp, G. W., Paul, A., Worboys, J., Sadok, A., Jorgensen, C., Guichard, S., and Marshall, C. J. (2016) Rho-associated kinase (ROCK) function is essential for cell cycle progression, senescence and tumorigenesis. *eLife* **5**
6. Mehlen, P., and Puisieux, A. (2006) Metastasis: a question of life or death. *Nat Rev Cancer* **6**, 449-458
7. Ascierto, P. A., Kirkwood, J. M., Grob, J.-J., Simeone, E., Grimaldi, A. M., Maio, M., Palmieri, G., Testori, A., Marincola, F. M., and Mozzillo, N. (2012) The role of BRAF V600 mutation in melanoma. *Journal of Translational Medicine* **10**, 85-85
8. Camacho, L. H. (2015) CTLA-4 blockade with ipilimumab: biology, safety, efficacy, and future considerations. *Cancer Medicine* **4**, 661-672
9. Ott, P. A., and Hodi, F. S. (2016) Talimogene Laherparepvec for the Treatment of Advanced Melanoma. *Clinical cancer research : an official journal of the American Association for Cancer Research*
10. CRUK. (2015) Cancer Mortality Statistics.
11. Reed, K. B., Brewer, J. D., Lohse, C. M., Bringe, K. E., Pruitt, C. N., and Gibson, L. E. (2012) Increasing Incidence of Melanoma Among Young Adults: An Epidemiological Study in Olmsted County, Minnesota. *Mayo Clinic Proceedings* **87**, 328-334
12. Spagnolo, F., Ghiorzo, P., and Queirolo, P. (2014) Overcoming resistance to BRAF inhibition in BRAF-mutated metastatic melanoma. *Oncotarget* **5**, 10206-10221

13. Drake, C. G., Lipson, E. J., and Brahmer, J. R. (2014) Breathing new life into immunotherapy: review of melanoma, lung and kidney cancer. *Nature reviews. Clinical oncology* **11**, 24-37

14. Martin, O. A., Anderson, R. L., Narayan, K., and MacManus, M. P. (2016) Does the mobilization of circulating tumour cells during cancer therapy cause metastasis? *Nature reviews. Clinical oncology* **advance online publication**

15. Vander Heiden, M. G., Cantley, L. C., and Thompson, C. B. (2009) Understanding the Warburg effect: the metabolic requirements of cell proliferation. *Science* **324**

16. Hsu, P. P., and Sabatini, D. M. (2008) Cancer cell metabolism: Warburg and beyond. *Cell* **134**

17. Warburg, O. (1956) On the Origin of Cancer Cells. *Science* **123**, 309-314

18. Warburg, O. (1966) **The Prime Cause and Prevention of Cancer**.

19. Weinhouse, S., Warburg, O., Burk, D., and Schade, A. L. (1956) On Respiratory Impairment in Cancer Cells. *Science* **124**, 267

20. Warburg, O., Wind, F., and Negelein, E. (1927) THE METABOLISM OF TUMORS IN THE BODY. *The Journal of General Physiology* **8**, 519-530

21. Pavlova, Natalya N., and Thompson, Craig B. The Emerging Hallmarks of Cancer Metabolism. *Cell Metabolism* **23**, 27-47

22. Wise, D. R., and Thompson, C. B. (2010) Glutamine addiction: a new therapeutic target in cancer. *Trends in biochemical sciences* **35**, 427-433

23. Hensley, C. T. (2013) Glutamine and cancer: cell biology, physiology, and clinical opportunities. **123**, 3678-3684

24. Cohen, A., Holmen, S., and Colman, H. (2013) IDH1 and IDH2 Mutations in Gliomas. *Current neurology and neuroscience reports* **13**, 345

25. Flavahan, W. A., Drier, Y., Liau, B. B., Gillespie, S. M., Venteicher, A. S., Stemmer-Rachamimov, A. O., Suvà, M. L., and Bernstein, B. E. (2016) Insulator dysfunction and oncogene activation in IDH mutant gliomas. *Nature* **529**, 110-114

26. Nicholson, J. K., and Lindon, J. C. (2008) Systems biology: Metabonomics. *Nature* **455**, 1054-1056

27. Oliver, S. G., Winson, M. K., Kell, D. B., and Baganz, F. (1998) Systematic functional analysis of the yeast genome. *Trends in Biotechnology* **16**, 373-378

28. Fiehn, O. (2002) Metabolomics--the link between genotypes and phenotypes. *Plant molecular biology* **48**, 155-171

29. Nicholson, J. K., Lindon, J. C., and Holmes, E. (1999) 'Metabonomics': understanding the metabolic responses of living systems to pathophysiological stimuli via multivariate statistical analysis of biological NMR spectroscopic data. *Xenobiotica; the fate of foreign compounds in biological systems* **29**, 1181-1189

30. Horning, E. C., and Horning, M. G. (1971) Metabolic Profiles: Gas-Phase Methods for Analysis of Metabolites. *Clinical Chemistry* **17**, 802-809

31. Pauling, L., Robinson, A. B., Teranishi, R., and Cary, P. (1971) Quantitative Analysis of Urine Vapor and Breath by Gas-Liquid Partition Chromatography. *Proceedings of the National Academy of Sciences* **68**, 2374-2376

32. Moon, R. B., and Richards, J. H. (1973) Determination of intracellular pH by 31P magnetic resonance. *The Journal of biological chemistry* **248**, 7276-7278

33. Brown, F. F., Campbell, I. D., Kuchel, P. W., and Rabenstein, D. C. (1977) Human erythrocyte metabolism studies by 1H spin echo NMR. *FEBS Letters* **82**, 12-16

34. Daniels, A., Williams, R. J. P., and Wright, P. E. (1976) Nuclear magnetic resonance studies of the adrenal gland and some other organs. *Nature* **261**, 321-323

35. Peng, B., Li, H., and Peng, X. X. (2015) Functional metabolomics: from biomarker discovery to metabolome reprogramming. *Protein & Cell* **6**, 628-637

36. Beckonert, O., Keun, H. C., Ebbels, T. M. D., Bundy, J., Holmes, E., Lindon, J. C., and Nicholson, J. K. (2007) Metabolic profiling, metabolomic and metabonomic procedures for NMR spectroscopy of urine, plasma, serum and tissue extracts. *Nat. Protocols* **2**, 2692-2703

37. Fang, M., Ivanisevic, J., Benton, H. P., Johnson, C. H., Patti, G. J., Hoang, L. T., Uritboonthai, W., Kurczy, M. E., and Siuzdak, G. (2015) Thermal Degradation of Small Molecules: A Global Metabolomic Investigation. *Analytical chemistry* **87**, 10935-10941

38. Derenne, A., Van Hemelryck, V., Lamoral-Theys, D., Kiss, R., and Goormaghtigh, E. (2013) FTIR spectroscopy: A new valuable tool to classify the effects of polyphenolic compounds on cancer cells. *Biochimica et Biophysica Acta (BBA) - Molecular Basis of Disease* **1832**, 46-56

39. Cherney, D. P., Ekman, D. R., Dix, D. J., and Collette, T. W. (2007) Raman spectroscopy-based metabolomics for differentiating exposures to triazole fungicides using rat urine. *Analytical chemistry* **79**, 7324-7332

40. Ellis, D. I., and Goodacre, R. (2006) Metabolic fingerprinting in disease diagnosis: biomedical applications of infrared and Raman spectroscopy. *The Analyst* **131**, 875-885

41. Hanahan, D., and Weinberg, R. A. (2012) Hallmarks of cancer: the next generation. *Cell* **144**

42. Cascante, M., and Marin, S. (2008) Metabolomics and fluxomics approaches. *Essays In Biochemistry* **45**, 67-82

43. Nargund, S., Joffe, M. E., Tran, D., Tugarinov, V., and Sriram, G. (2013) Nuclear Magnetic Resonance Methods for Metabolic Fluxomics. in *Systems Metabolic Engineering: Methods and Protocols* (Alper, S. H. ed.), Humana Press, Totowa, NJ. pp 335-351

44. Collino, S., Martin Fç-, P. J., and Rezzi, S. (2013) Clinical metabolomics paves the way towards future healthcare strategies. *British Journal of Clinical Pharmacology* **75**, 619-629

45. Khoo, S. H., and Al-Rubeai, M. (2007) Metabolomics as a complementary tool in cell culture. *Biotechnology and applied biochemistry* **47**, 71-84

46. Edwards, J. C. Principles of NMR.

47. Arnold, J. (1996) An NMR premier for life scientists: By Henry Rattle. P 124. Partneship Press, Fareham, PO16 7YB, UK. 1995. £12.95 ISBN 0-9516436-3-0. *Biochemical Education* **24**, 67-67

48. Mescher, M., Merkle, H., Kirsch, J., Garwood, M., and Gruetter, R. (1998) Simultaneous in vivo spectral editing and water suppression. *NMR in Biomedicine* **11**, 266-272

49. Wilkinson, A. D. M. (1997) *Compredindium of Chemical Terminology*, 2nd ed., Blackwell Scientific Publications, Oxford, UK

50. Harwood, L. M. C. (1996) *Introduction to Organic Spectroscopy*, Oxford University Press, USA

51. Ravera, E., Luchinat, C., and Parigi, G. (2016) Basic facts and perspectives of Overhauser DNP NMR. *Journal of Magnetic Resonance* **264**, 78-87

52. Dumez, J.-N. (2016) Perspectives on hyperpolarised solution-state magnetic resonance in chemistry. *Magnetic Resonance in Chemistry*, n/a-n/a

53. Bornet, A., Maucourt, M., Deborde, C., Jacob, D., Milani, J., Vuichoud, B., Ji, X., Dumez, J.-N., Moing, A., Bodenhausen, G., Jannin, S., and Giraudeau, P. (2016) Highly Repeatable

Dissolution Dynamic Nuclear Polarization for Heteronuclear NMR Metabolomics. *Analytical chemistry* **88**, 6179-6183

54. Dumez, J. N., Milani, J., Vuichoud, B., Bornet, A., Lalande-Martin, J., Tea, I., Yon, M., Maucourt, M., Deborde, C., Moing, A., Frydman, L., Bodenhausen, G., Jannin, S., and Giraudeau, P. (2015) Hyperpolarized NMR of plant and cancer cell extracts at natural abundance. *The Analyst* **140**, 5860-5863

55. Nelson, S. J., Kurhanewicz, J., Vigneron, D. B., Larson, P. E., Harzstark, A. L., Ferrone, M., van Criekinge, M., Chang, J. W., Bok, R., Park, I., Reed, G., Carvajal, L., Small, E. J., Munster, P., Weinberg, V. K., Ardenkjaer-Larsen, J. H., Chen, A. P., Hurd, R. E., Odegardstuen, L. I., Robb, F. J., Tropp, J., and Murray, J. A. (2013) Metabolic imaging of patients with prostate cancer using hyperpolarized [1-(1)(3)C]pyruvate. *Sci Transl Med* **5**, 198ra108

56. Halle-Wittenberg, M.-L.-U. Solid-State NMR Methodology.

57. Mehring, M. (1983) Principles of High Resolution NMR in Solids.

58. Watts, A. (2005) Solid-state NMR in drug design and discovery for membrane-embedded targets. *Nat Rev Drug Discov* **4**, 555-568

59. Beckonert, O., Coen, M., Keun, H. C., Wang, Y., Ebbels, T. M. D., Holmes, E., Lindon, J. C., and Nicholson, J. K. (2010) High-resolution magic-angle-spinning NMR spectroscopy for metabolic profiling of intact tissues. *Nat. Protocols* **5**, 1019-1032

60. Sitter, B., Sonnewald, U., Spraul, M., Fjosne, H. E., and Gribbestad, I. S. (2002) High-resolution magic angle spinning MRS of breast cancer tissue. *NMR Biomed* **15**, 327-337

61. Tripathi, P., Somashekar, B. S., Ponnusamy, M., Gursky, A., Dailey, S., Kunju, P., Lee, C. T., Chinnaiyan, A. M., Rajendiran, T. M., and Ramamoorthy, A. (2013) HR-MAS NMR tissue metabolomic signatures cross-validated by mass spectrometry distinguish bladder cancer from benign disease. *J Proteome Res* **12**, 3519-3528

62. Dettmer, K., Nürnberger, N., Kaspar, H., Gruber, M. A., Almstetter, M. F., and Oefner, P. J. (2011) Metabolite extraction from adherently growing mammalian cells for metabolomics studies: optimization of harvesting and extraction protocols. *Analytical and Bioanalytical Chemistry* **399**, 1127-1139

63. Matheus, N., Hansen, S., Rozet, E., Peixoto, P., Maquoi, E., Lambert, V., Noël, A., Frédérich, M., Mottet, D., and Tullio, P. (2014) An Easy, Convenient Cell and Tissue Extraction Protocol for Nuclear Magnetic Resonance Metabolomics. *Phytochemical Analysis* **25**, 342-349

64. Duarte, I. F., Marques, J., Ladeirinha, A. F., Rocha, C., Lamego, I., Calheiros, R., Silva, T. M., Marques, M. P., Melo, J. B., Carreira, I. M., and Gil, A. M. (2009) Analytical approaches toward successful human cell metabolome studies by NMR spectroscopy. *Analytical chemistry* **81**, 5023-5032

65. Vermeer, L. S., Fruhwirth, G. O., Pandya, P., Ng, T., and Mason, A. J. (2012) NMR Metabolomics of MTLn3E Breast Cancer Cells Identifies a Role for CXCR4 in Lipid and Choline Regulation. *Journal of Proteome Research* **11**, 2996-3003

66. Kozlowska, J., Rivett, D. W., Vermeer, L. S., Carroll, M. P., Bruce, K. D., James Mason, A., and Rogers, G. B. (2013) A relationship between Pseudomonal growth behaviour and cystic fibrosis patient lung function identified in a metabolomic investigation. *Metabolomics* **9**, 1262-1273

67. Kozlowska, J., Vermeer, L. S., Rogers, G. B., Rehnnuma, N., Amos, S.-B. T. A., Koller, G., McArthur, M., Bruce, K. D., and Mason, A. J. (2014) Combined Systems Approaches Reveal Highly Plastic Responses to Antimicrobial Peptide Challenge in <italic>Escherichia coli</italic>. *PLoS Pathog* **10**, e1004104

68. Rogers, G. B., Kozlowska, J., Keeble, J., Metcalfe, K., Fao, M., Dowd, S. E., Mason, A. J., McGuckin, M. A., and Bruce, K. D. (2014) Functional divergence in gastrointestinal microbiota in physically-separated genetically identical mice. *Scientific Reports* **4**, 5437

69. Nielsen, N.-P. V., Carstensen, J. M., and Smedsgaard, J. (1998) Aligning of single and multiple wavelength chromatographic profiles for chemometric data analysis using correlation optimised warping. *Journal of Chromatography A* **805**, 17-35

70. Vu, N. T., and Laukens, K. (2013) Getting Your Peaks in Line: A Review of Alignment Methods for NMR Spectral Data. *Metabolites* **3**

71. Savorani, F., Tomasi, G., and Engelsen, S. B. (2010) icoshift: A versatile tool for the rapid alignment of 1D NMR spectra. *Journal of Magnetic Resonance* **202**, 190-202

72. Sousa, S. A. A., Magalhães, A., and Ferreira, M. M. C. (2013) Optimized bucketing for NMR spectra: Three case studies. *Chemometrics and Intelligent Laboratory Systems* **122**, 93-102

73. Ebbels, T. M. D., and Cavill, R. (2009) Bioinformatic methods in NMR-based metabolic profiling. *Progress in Nuclear Magnetic Resonance Spectroscopy* **55**, 361-374

74. Heinemann, J., Mazurie, A., Tokmina-Lukaszewska, M., Beilman, G. J., and Bothner, B. (2014) Application of support vector machines to metabolomics experiments with limited replicates. *Metabolomics* **10**, 1121-1128

75. Hall, L. M., Hill, D. W., Menikarachchi, L. C., Chen, M. H., Hall, L. H., and Grant, D. F. (2015) Optimizing artificial neural network models for metabolomics and systems biology: an example using HPLC retention index data. *Bioanalysis* **7**, 939-955

76. Chen, T., Cao, Y., Zhang, Y., Liu, J., Bao, Y., Wang, C., Jia, W., and Zhao, A. (2013) Random Forest in Clinical Metabolomics for Phenotypic Discrimination and Biomarker Selection. *Evidence-Based Complementary and Alternative Medicine* **2013**, 11

77. Trygg, J., and Wold, S. (2002) Orthogonal projections to latent structures (O-PLS). *Journal of Chemometrics* **16**, 119-128

78. Ebbels, T. M., Lindon, J. C., and Coen, M. (2011) Processing and modeling of nuclear magnetic resonance (NMR) metabolic profiles. *Methods Mol Biol* **708**, 365-388

79. Westerhuis, J. A., Hoefsloot, H. C. J., Smit, S., Vis, D. J., Smilde, A. K., van Velzen, E. J. J., van Duijnhoven, J. P. M., and van Dorsten, F. A. (2008) Assessment of PLSDA cross validation. *Metabolomics* **4**, 81-89

80. Cavill, R., Jennen, D., Kleinjans, J., and Briedé, J. J. (2015) Transcriptomic and metabolomic data integration. *Briefings in Bioinformatics*

81. Dharuri, H., Demirkan, A., van Klinken, J. B., Mook-Kanamori, D. O., van Duijn, C. M., 't Hoen, P. A. C., and Willems van Dijk, K. (2014) Genetics of the human metabolome, what is next? *Biochimica et Biophysica Acta (BBA) - Molecular Basis of Disease* **1842**, 1923-1931

82. Wangen, L. E., and Kowalski, B. R. (1989) A multiblock partial least squares algorithm for investigating complex chemical systems. *Journal of Chemometrics* **3**, 3-20

83. Boccard, J., and Rutledge, D. N. (2013) A consensus orthogonal partial least squares discriminant analysis (OPLS-DA) strategy for multiblock Omics data fusion. *Analytica Chimica Acta* **769**, 30-39

84. Macklin, D. N., Ruggero, N. A., and Covert, M. W. (2014) The future of whole-cell modeling. *Current Opinion in Biotechnology* **28**, 111-115

85. Karr, Jonathan R., Sanghvi, Jayodita C., Macklin, Derek N., Gutschow, Miriam V., Jacobs, Jared M., Bolival, B., Jr., Assad-Garcia, N., Glass, John I., and Covert, Markus W. A Whole-Cell Computational Model Predicts Phenotype from Genotype. *Cell* **150**, 389-401

86. Ben Yahia, B., Malphettes, L., and Heinzle, E. (2015) Macroscopic modeling of mammalian cell growth and metabolism. *Applied Microbiology and Biotechnology* **99**, 7009-7024

87. Shakhova, O. (2014) Neural crest stem cells in melanoma development. *Current opinion in oncology* **26**, 215-221

88. Shakhova, O., and Sommer, L. (2013) Testing the cancer stem cell hypothesis in melanoma: the clinics will tell. *Cancer letters* **338**, 74-81

89. Boiko, A. D., Razorenova, O. V., van de Rijn, M., Swetter, S. M., Johnson, D. L., Ly, D. P., Butler, P. D., Yang, G. P., Joshua, B., Kaplan, M. J., Longaker, M. T., and Weissman, I. L. (2010) Human melanoma-initiating cells express neural crest nerve growth factor receptor CD271. *Nature* **466**, 133-137

90. Fecher, L. A., Cummings, S. D., Keefe, M. J., and Alani, R. M. (2007) Toward a molecular classification of melanoma. *Journal of clinical oncology : official journal of the American Society of Clinical Oncology* **25**, 1606-1620

91. Holderfield, M., Deuker, M. M., McCormick, F., and McMahon, M. (2014) Targeting RAF kinases for cancer therapy: BRAF-mutated melanoma and beyond. *Nat Rev Cancer* **14**, 455-467

92. Davies, H., Bignell, G. R., Cox, C., Stephens, P., Edkins, S., Clegg, S., Teague, J., Woffendin, H., Garnett, M. J., Bottomley, W., Davis, N., Dicks, E., Ewing, R., Floyd, Y., Gray, K., Hall, S., Hawes, R., Hughes, J., Kosmidou, V., Menzies, A., Mould, C., Parker, A., Stevens, C., Watt, S., Hooper, S., Wilson, R., Jayatilake, H., Gusterson, B. A., Cooper, C., Shipley, J., Hargrave, D., Pritchard-Jones, K., Maitland, N., Chenevix-Trench, G., Riggins, G. J., Bigner, D. D., Palmieri, G., Cossu, A., Flanagan, A., Nicholson, A., Ho, J. W. C., Leung, S. Y., Yuen, S. T., Weber, B. L., Seigler, H. F., Darrow, T. L., Paterson, H., Marais, R., Marshall, C. J., Wooster, R., Stratton, M. R., and Futreal, P. A. (2002) Mutations of the BRAF gene in human cancer. *Nature* **417**, 949-954

93. Fedorenko, I. V., Gibney, G. T., Sondak, V. K., and Smalley, K. S. (2015) Beyond BRAF: where next for melanoma therapy? *Br J Cancer* **112**, 217-226

94. Kauffmann, R. M., and Chen, S. L. (2014) Workup and Staging of Malignant Melanoma. *Surgical Clinics of North America* **94**, 963-972

95. Orgaz, J. L., and Sanz-Moreno, V. (2013) Emerging molecular targets in melanoma invasion and metastasis. *Pigment cell & melanoma research* **26**, 39-57

96. Mukherjee, S. (2010) The Emperor of All Maladies: A Biography of Cancer. Scribner

97. Routhier, A., Astuccio, M., Lahey, D., Monfredo, N., Johnson, A., Callahan, W., Partington, A., Fellows, K., Ouellette, L., Zhidro, S., Goodrow, C., Smith, A., Sullivan, K., Simone, P., Le, L., Vezuli, B., Zohni, M., West, E., Gleason, D., and Bryan, B. (2010) Pharmacological inhibition of Rho-kinase signaling with Y-27632 blocks melanoma tumor growth. *Oncology reports* **23**, 861-867

98. Dummer, R., Hauschild, A., Lindenblatt, N., Pentheroudakis, G., and Keilholz, U. (2015) Cutaneous melanoma: ESMO Clinical Practice Guidelines for diagnosis, treatment and follow-up. *Annals of Oncology* **26**, v126-v132

99. Andtbacka, R. H., Kaufman, H. L., Collichio, F., Amatruda, T., Senzer, N., Chesney, J., Delman, K. A., Spitler, L. E., Puzanov, I., Agarwala, S. S., Milhem, M., Cranmer, L., Curti, B., Lewis, K., Ross, M., Guthrie, T., Linette, G. P., Daniels, G. A., Harrington, K., Middleton, M. R., Miller, W. H., Jr., Zager, J. S., Ye, Y., Yao, B., Li, A., Doleman, S., VanderWalde, A., Gansert, J., and Coffin, R. S. (2015) Talimogene Laherparepvec Improves Durable Response Rate in Patients With Advanced Melanoma. *Journal of clinical oncology : official journal of the American Society of Clinical Oncology* **33**, 2780-2788

100. Hoeller, C., Michielin, O., Ascierto, P. A., Szabo, Z., and Blank, C. U. (2016) Systematic review of the use of granulocyte-macrophage colony-stimulating factor in patients with advanced melanoma. *Cancer immunology, immunotherapy : CII* **65**, 1015-1034

101. Long, G. V., Stroyakovskiy, D., Gogas, H., Levchenko, E., de Braud, F., Larkin, J., Garbe, C., Jouary, T., Hauschild, A., Grob, J. J., Chiarion Sileni, V., Lebbe, C., Mandalà, M., Millward, M., Arance, A., Bondarenko, I., Haanen, J. B. A. G., Hansson, J., Utikal, J., Ferraresi, V., Kovalenko, N., Mohr, P., Probachai, V., Schadendorf, D., Nathan, P., Robert, C., Ribas, A., DeMarini, D. J., Irani, J. G., Casey, M., Ouellet, D., Martin, A.-M., Le, N., Patel, K., and Flaherty, K. (2014) Combined BRAF and MEK Inhibition versus BRAF Inhibition Alone in Melanoma. *New England Journal of Medicine* **371**, 1877-1888

102. Sosman, J. A., Kim, K. B., Schuchter, L., Gonzalez, R., Pavlick, A. C., Weber, J. S., McArthur, G. A., Hutson, T. E., Moschos, S. J., Flaherty, K. T., Hersey, P., Kefford, R., Lawrence, D., Puzanov, I., Lewis, K. D., Amaravadi, R. K., Chmielowski, B., Lawrence, H. J., Shyr, Y., Ye, F., Li, J., Nolop, K. B., Lee, R. J., Joe, A. K., and Ribas, A. (2012) Survival in BRAF V600–Mutant Advanced Melanoma Treated with Vemurafenib. *New England Journal of Medicine* **366**, 707-714

103. Puzanov, I., Amaravadi, R. K., McArthur, G. A., Flaherty, K. T., Chapman, P. B., Sosman, J. A., Ribas, A., Shackleton, M., Hwu, P., Chmielowski, B., Nolop, K. B., Lin, P. S., and Kim, K. B. (2015) Long-term outcome in BRAF(V600E) melanoma patients treated with vemurafenib: Patterns of disease progression and clinical management of limited progression. *European journal of cancer (Oxford, England : 1990)* **51**, 1435-1443

104. Haarberg, H. E., and Smalley, K. S. M. (2014) Resistance to Raf inhibition in cancer. *Drug discovery today. Technologies* **11**, 1-116

105. Robert, C., Karaszewska, B., Schachter, J., Rutkowski, P., Mackiewicz, A., Stroiakovski, D., Lichinitser, M., Dummer, R., Grange, F., Mortier, L., Chiarion-Sileni, V., Drucis, K., Krajsova, I., Hauschild, A., Lorigan, P., Wolter, P., Long, G. V., Flaherty, K., Nathan, P., Ribas, A., Martin, A.-M., Sun, P., Crist, W., Legos, J., Rubin, S. D., Little, S. M., and Schadendorf, D. (2014) Improved Overall Survival in Melanoma with Combined Dabrafenib and Trametinib. *New England Journal of Medicine* **372**, 30-39

106. Postow, M. A., Chesney, J., Pavlick, A. C., Robert, C., Grossmann, K., McDermott, D., Linette, G. P., Meyer, N., Giguere, J. K., Agarwala, S. S., Shaheen, M., Ernstoff, M. S., Minor, D., Salama, A. K., Taylor, M., Ott, P. A., Rollin, L. M., Horak, C., Gagnier, P., Wolchok, J. D., and Hodi, F. S. (2015) Nivolumab and Ipilimumab versus Ipilimumab in Untreated Melanoma. *New England Journal of Medicine* **372**, 2006-2017

107. Larkin, J., Ascierto, P. A., Dréno, B., Atkinson, V., Liszkay, G., Maio, M., Mandalà, M., Demidov, L., Stroyakovskiy, D., Thomas, L., de la Cruz-Merino, L., Dutriaux, C., Garbe, C., Sovak, M. A., Chang, I., Choong, N., Hack, S. P., McArthur, G. A., and Ribas, A. (2014) Combined Vemurafenib and Cobimetinib in BRAF-Mutated Melanoma. *New England Journal of Medicine* **371**, 1867-1876

108. Larkin, J., Chiarion-Sileni, V., Gonzalez, R., Grob, J. J., Cowey, C. L., Lao, C. D., Schadendorf, D., Dummer, R., Smylie, M., Rutkowski, P., Ferrucci, P. F., Hill, A., Wagstaff, J., Carlino, M. S., Haanen, J. B., Maio, M., Marquez-Rodas, I., McArthur, G. A., Ascierto, P. A., Long, G. V., Callahan, M. K., Postow, M. A., Grossmann, K., Sznol, M., Dreno, B., Bastholt, L., Yang, A., Rollin, L. M., Horak, C., Hodi, F. S., and Wolchok, J. D. (2015) Combined Nivolumab and Ipilimumab or Monotherapy in Untreated Melanoma. *New England Journal of Medicine* **373**, 23-34

109. Steeg, P. S., and Theodorescu, D. (2008) Metastasis: a therapeutic target for cancer. *Nature clinical practice. Oncology* **5**, 206-219

110. Sleeman, J., and Steeg, P. S. (2010) Cancer metastasis as a therapeutic target. *European Journal of Cancer* **46**, 1177-1180

111. Mansfield, A. S., and Markovic, S. N. (2013) Inhibition of angiogenesis for the treatment of metastatic melanoma. *Current oncology reports* **15**, 492-499

112. Carmeliet, P., and Jain, R. K. (2000) Angiogenesis in cancer and other diseases. *Nature* **6801**

113. Senft, D., and Ronai, Z. A. (2016) Immunogenic, cellular, and angiogenic drivers of tumor dormancy--a melanoma view. *Pigment cell & melanoma research* **29**, 27-42

114. Pantel, K., and Brakenhoff, R. H. (2004) Dissecting the metastatic cascade. *Nat Rev Cancer* **4**, 448-456

115. Mina, L. A., and Sledge, G. W., Jr. (2011) Rethinking the metastatic cascade as a therapeutic target. *Nature reviews. Clinical oncology* **8**, 325-332

116. Koumoutsakos, P., Pivkin, I., and Milde, F. (2013) The Fluid Mechanics of Cancer and Its Therapy. *Annual Review of Fluid Mechanics* **45**, 325-355

117. Drake, C. G., Jaffee, E., and Pardoll, D. M. (2006) Mechanisms of immune evasion by tumors. *Advances in immunology* **90**, 51-81

118. Valastyan, S., and Weinberg, Robert A. Tumor Metastasis: Molecular Insights and Evolving Paradigms. *Cell* **147**, 275-292

119. Yamaguchi, H., and Condeelis, J. (2007) Regulation of the actin cytoskeleton in cancer cell migration and invasion. *Biochimica et Biophysica Acta (BBA) - Molecular Cell Research* **1773**, 642-652

120. Friedl, P., and Wolf, K. (2010) Plasticity of cell migration: a multiscale tuning model. *J Cell Biol* **188**

121. Friedl, P., and Alexander, S. (2011) Cancer Invasion and the Microenvironment: Plasticity and Reciprocity. *Cell* **147**, 992-1009

122. Giampieri, S., Manning, C., Hooper, S., Jones, L., Hill, C. S., and Sahai, E. (2009) Localised and reversible TGFβ signalling switches breast cancer cells from cohesive to single cell motility. *Nature cell biology* **11**, 1287-1296

123. Parri, M., and Chiarugi, P. (2010) Rac and Rho GTPases in cancer cell motility control. *Cell Communication and Signaling* **8**, 1-14

124. Friedl, P., and Wolf, K. (2010) Plasticity of cell migration: a multiscale tuning model. *The Journal of Cell Biology* **188**, 11-19

125. Sahai, E., and Marshall, C. J. (2002) RHO-GTPases and cancer. *Nat Rev Cancer* **2**, 133-142

126. Ridley, A. J. Rho GTPases and actin dynamics in membrane protrusions and vesicle trafficking. *Trends in Cell Biology* **16**, 522-529

127. Madaule, P., and Axel, R. (1985) A novel ras-related gene family. *Cell* **41**, 31-40

128. Ridley, A. J. (2004) Rho proteins and cancer. *Breast cancer research and treatment* **84**, 13-19

129. Nakagawa, O., Fujisawa, K., Ishizaki, T., Saito, Y., Nakao, K., and Narumiya, S. (1996) ROCK-I and ROCK-II, two isoforms of Rho-associated coiled-coil forming protein serine/threonine kinase in mice. *FEBS Lett* **392**, 189-193

130. Riento, K., and Ridley, A. J. (2003) Rocks: multifunctional kinases in cell behaviour. *Nature reviews. Molecular cell biology* **4**, 446-456

131. Jacobs, M., Hayakawa, K., Swenson, L., Bellon, S., Fleming, M., Taslimi, P., and Doran, J. (2006) The structure of dimeric ROCK I reveals the mechanism for ligand selectivity. *The Journal of biological chemistry* **281**, 260-268

132. The PyMOL Molecular Graphics System. (LLC, S. ed., 1.8 Ed.

133. Jacobs, M., Hayakawa, K., Swenson, L., Bellon, S., Fleming, M., Taslimi, P., and Doran, J. (2006) The Structure of Dimeric ROCK I Reveals the Mechanism for Ligand Selectivity. *Journal of Biological Chemistry* **281**, 260-268

134. Yamaguchi, H., Kasa, M., Amano, M., Kaibuchi, K., and Hakoshima, T. Molecular Mechanism for the Regulation of Rho-Kinase by Dimerization and Its Inhibition by Fasudil. *Structure* **14**, 589-600

135. Leung, T., Manser, E., Tan, L., and Lim, L. (1995) A novel serine/threonine kinase binding the Ras-related RhoA GTPase which translocates the kinase to peripheral membranes. *The Journal of biological chemistry* **270**, 29051-29054

136. Leung, T., Chen, X. Q., Manser, E., and Lim, L. (1996) The p160 RhoA-binding kinase ROK alpha is a member of a kinase family and is involved in the reorganization of the cytoskeleton. *Molecular and cellular biology* **16**, 5313-5327

137. Croft, D. R., and Olson, M. F. (2006) The Rho GTPase effector ROCK regulates cyclin A, cyclin D1, and p27Kip1 levels by distinct mechanisms. *Molecular and cellular biology* **26**, 4612-4627

138. Kümper, S., Mardakheh, F. K., McCarthy, A., Yeo, M., Stamp, G. W., Paul, A., Worboys, J., Sadok, A., Jørgensen, C., Guichard, S., and Marshall, C. J. (2016) Rho-associated kinase (ROCK) function is essential for cell cycle progression, senescence and tumorigenesis. *eLife* **5**, e12203

139. Provenzano, P. P., Inman, D. R., Eliceiri, K. W., Trier, S. M., and Keely, P. J. (2008) Contact Guidance Mediated Three-Dimensional Cell Migration is Regulated by Rho/ROCK-Dependent Matrix Reorganization. *Biophysical Journal* **95**, 5374-5384

140. Sanz-Moreno, V., Gaggioli, C., Yeo, M., Albrengues, J., Wallberg, F., Viros, A., Hooper, S., Mitter, R., Féral, Chloé C., Cook, M., Larkin, J., Marais, R., Meneguzzi, G., Sahai, E., and Marshall, Chris J. ROCK and JAK1 Signaling Cooperate to Control Actomyosin Contractility in Tumor Cells and Stroma. *Cancer cell* **20**, 229-245

141. Amano, M., Ito, M., Kimura, K., Fukata, Y., Chihara, K., Nakano, T., Matsuura, Y., and Kaibuchi, K. (1996) Phosphorylation and Activation of Myosin by Rho-associated Kinase (Rho-kinase). *Journal of Biological Chemistry* **271**, 20246-20249

142. Kawano, Y., Fukata, Y., Oshiro, N., Amano, M., Nakamura, T., Ito, M., Matsumura, F., Inagaki, M., and Kaibuchi, K. (1999) Phosphorylation of Myosin-Binding Subunit (Mbs) of Myosin Phosphatase by Rho-Kinase in Vivo. *The Journal of Cell Biology* **147**, 1023-1038

143. Wei, L., Surma, M., Shi, S., Lambert-Cheatham, N., and Shi, J. (2016) Novel Insights into the Roles of Rho Kinase in Cancer. *Archivum immunologiae et therapiae experimentalis* **64**, 259-278

144. Shang, X., Marchioni, F., Sipes, N., Evelyn, C. R., Jerabek-Willemsen, M., Duhr, S., Seibel, W., Wortman, M., and Zheng, Y. (2012) Rational design of small molecule inhibitors targeting RhoA subfamily Rho GTPases. *Chemistry & biology* **19**, 699-710

145. Feng, Y., LoGrasso, P. V., Defert, O., and Li, R. (2016) Rho Kinase (ROCK) Inhibitors and Their Therapeutic Potential. *Journal of Medicinal Chemistry* **59**, 2269-2300

146. Yamamoto, K., Maruyama, K., Himori, N., Omodaka, K., Yokoyama, Y., Shiga, Y., Morin, R., and Nakazawa, T. (2014) The novel Rho kinase (ROCK) inhibitor K-115: a new candidate drug for neuroprotective treatment in glaucoma. *Investigative ophthalmology & visual science* **55**, 7126-7136

147. Shimizu, T., and Liao, J. K. (2016) Rho Kinases and Cardiac Remodeling. *Circulation Journal* **advpub**

148. Morgan-Fisher, M., Wewer, U. M., and Yoneda, A. (2013) Regulation of ROCK Activity in Cancer. *Journal of Histochemistry and Cytochemistry* **61**, 185-198

149. Wong, M. (2014) Actelion Pharmaceuticals and CoTherix held liable for fighting off competition to Tracleer® by interfering with rival Asahi's development of fasudil. Quora.com

150. Sugi, T., and Nishio, F. (2006) Process for producing an oral sustained-release preparation of fasudil hydrochloride. Google Patents

151. Vogel, C. J., Smit, M. A., Maddalo, G., Possik, P. A., Sparidans, R. W., van der Burg, S. H., Verdegaal, E. M., Heck, A. J., Samatar, A. A., Beijnen, J. H., Altelaar, A. F., and Peeper, D. S. (2015) Cooperative induction of apoptosis in NRAS mutant melanoma by inhibition of MEK and ROCK. *Pigment cell & melanoma research* **28**, 307-317

152. Nakashima, M., Adachi, S., Yasuda, I., Yamauchi, T., Kawaguchi, J., Hanamatsu, T., Yoshioka, T., Okano, Y., Hirose, Y., Kozawa, O., and Moriwaki, H. (2011) Inhibition of Rho-associated coiled-coil containing protein kinase enhances the activation of epidermal growth factor receptor in pancreatic cancer cells. *Mol Cancer* **10**, 79

153. Nakashima, M., Adachi, S., Yasuda, I., Yamauchi, T., Kozawa, O., and Moriwaki, H. (2010) Rho-kinase regulates negatively the epidermal growth factor-stimulated colon cancer cell proliferation. *International journal of oncology* **36**, 585-592

154. Orgaz, J. L., Pandya, P., Dalmeida, R., Karagiannis, P., Sanchez-Laorden, B., Viros, A., Albrengues, J., Nestle, F. O., Ridley, A. J., Gaggioli, C., Marais, R., Karagiannis, S. N., and Sanz-Moreno, V. (2014) Diverse matrix metalloproteinase functions regulate cancer amoeboid migration. *Nature communications* **5**, 4255

155. Zhang, C., Liu, J., Liang, Y., Wu, R., Zhao, Y., Hong, X., Lin, M., Yu, H., Liu, L., Levine, A. J., Hu, W., and Feng, Z. (2013) Tumour-associated mutant p53 drives the Warburg effect. *Nature communications* **4**, 2935

156. Chun, K.-H., Araki, K., Jee, Y., Lee, D.-H., Oh, B.-C., Huang, H., Park, K. S., Lee, S. W., Zabolotny, J. M., and Kim, Y.-B. (2012) Regulation of Glucose Transport by ROCK1 Differs from That of ROCK2 and Is Controlled by Actin Polymerization. *Endocrinology* **153**, 1649-1662

157. Huang, H., Lee, D.-H., Zabolotny, J. M., and Kim, Y.-B. (2013) Metabolic actions of Rho-kinase in periphery and brain. *Trends in Endocrinology & Metabolism* **24**, 506-514

158. Wang, J. B., Erickson, J. W., Fuji, R., Ramachandran, S., Gao, P., Dinavahi, R., Wilson, K. F., Ambrosio, A. L., Dias, S. M., Dang, C. V., and Cerione, R. A. (2010) Targeting mitochondrial glutaminase activity inhibits oncogenic transformation. *Cancer cell* **18**, 207-219

159. Stalnecker, C. A., Ulrich, S. M., Li, Y., Ramachandran, S., McBrayer, M. K., DeBerardinis, R. J., Cerione, R. A., and Erickson, J. W. (2015) Mechanism by which a recently discovered allosteric inhibitor blocks glutamine metabolism in transformed cells. *Proceedings of the National Academy of Sciences* **112**, 394-399

160. Gadea, G., de Toledo, M., Anguille, C., and Roux, P. (2007) Loss of p53 promotes RhoA–ROCK-dependent cell migration and invasion in 3D matrices. *J Cell Biol* **178**, 23-30

161. Kell, D. B., and Oliver, S. G. (2016) The metabolome 18 years on: a concept comes of age. *Metabolomics* **12**, 1-8

162. Abbate, V., Liang, W., Patel, J., Lan, Y., Capriotti, L., Iacobucci, V., Bui, T. T., Chaudhuri, P., Kudsiova, L., Vermeer, L. S., Chan, P. F. L., Kong, X., Drake, A. F., Lam, J. K. W., Bansal, S. S., and Mason, A. J. (2013) Manipulating the pH response of 2,3-diaminopropionic acid rich

peptides to mediate highly effective gene silencing with low-toxicity. *Journal of Controlled Release* **172**, 929-938

163. Lam, J. K. W., Liang, W., Lan, Y., Chaudhuri, P., Chow, M. Y. T., Witt, K., Kudsiova, L., and Mason, A. J. (2012) Effective endogenous gene silencing mediated by pH responsive peptides proceeds via multiple pathways. *Journal of controlled release : official journal of the Controlled Release Society* **158**, 293-303

164. Dettmer, K., Nurnberger, N., Kaspar, H., Gruber, M. A., Almstetter, M. F., and Oefner, P. J. (2011) Metabolite extraction from adherently growing mammalian cells for metabolomics studies: optimization of harvesting and extraction protocols. *Anal Bioanal Chem* **399**, 1127-1139

165. Dieterle, F., Ross, A., Schlotterbeck, G., and Senn, H. (2006) Probabilistic quotient normalization as robust method to account for dilution of complex biological mixtures. Application in 1H NMR metabonomics. *Analytical chemistry* **78**, 4281-4290

166. Kohl, S. M., Klein, M. S., Hochrein, J., Oefner, P. J., Spang, R., and Gronwald, W. (2012) State-of-the art data normalization methods improve NMR-based metabolomic analysis. *Metabolomics* **8**, 146-160

167. Worley, B., and Powers, R. (2014) MVAPACK: A Complete Data Handling Package for NMR Metabolomics. *ACS Chemical Biology* **9**, 1138-1144

168. Furusjö, E., Svenson, A., Rahmberg, M., and Andersson, M. (2006) The importance of outlier detection and training set selection for reliable environmental QSAR predictions. *Chemosphere* **63**, 99-108

169. Wishart, D. S., Tzur, D., Knox, C., Eisner, R., Guo, A. C., Young, N., Cheng, D., Jewell, K., Arndt, D., Sawhney, S., Fung, C., Nikolai, L., Lewis, M., Coutouly, M. A., Forsythe, I., Tang, P., Shrivastava, S., Jeroncic, K., Stothard, P., Amegbey, G., Block, D., Hau, D. D., Wagner, J., Miniaci, J., Clements, M., Gebremedhin, M., Guo, N., Zhang, Y., Duggan, G. E., Macinnis, G. D., Weljie, A. M., Dowlatabadi, R., Bamforth, F., Clive, D., Greiner, R., Li, L., Marrie, T., Sykes, B. D., Vogel, H. J., and Querengesser, L. (2007) HMDB: the Human Metabolome Database. *Nucleic acids research* **35**, D521-526

170. Ulrich, E. L., Akutsu, H., Doreleijers, J. F., Harano, Y., Ioannidis, Y. E., Lin, J., Livny, M., Mading, S., Maziuk, D., Miller, Z., Nakatani, E., Schulte, C. F., Tolmie, D. E., Kent Wenger, R., Yao, H., and Markley, J. L. (2008) BioMagResBank. *Nucleic acids research* **36**, D402-408

171. Saeed, A. I., Sharov, V., White, J., Li, J., Liang, W., Bhagabati, N., Braisted, J., Klapa, M., Currier, T., Thiagarajan, M., Sturn, A., Snuffin, M., Rezantsev, A., Popov, D., Ryltsov, A., Kostukovich, E., Borisovsky, I., Liu, Z., Vinsavich, A., Trush, V., and Quackenbush, J. (2003) TM4: a free, open-source system for microarray data management and analysis. *BioTechniques* **34**, 374-378

172. Xia, J., Mandal, R., Sinelnikov, I. V., Broadhurst, D., and Wishart, D. S. (2012) MetaboAnalyst 2.0--a comprehensive server for metabolomic data analysis. *Nucleic acids research* **40**, W127-133

173. Xia, J., Sinelnikov, I. V., Han, B., and Wishart, D. S. (2015) MetaboAnalyst 3.0--making metabolomics more meaningful. *Nucleic acids research* **43**, W251-257

174. Subramanian, A., Tamayo, P., Mootha, V. K., Mukherjee, S., Ebert, B. L., Gillette, M. A., Paulovich, A., Pomeroy, S. L., Golub, T. R., Lander, E. S., and Mesirov, J. P. (2005) Gene set enrichment analysis: A knowledge-based approach for interpreting genome-wide expression profiles. *Proceedings of the National Academy of Sciences* **102**, 15545-15550

175. Avery-Kiejda, K. A., Bowden, N. A., Croft, A. J., Scurr, L. L., Kairupan, C. F., Ashton, K. A., Talseth-Palmer, B. A., Rizos, H., Zhang, X. D., Scott, R. J., and Hersey, P. (2011) P53 in human melanoma fails to regulate target genes associated with apoptosis and the cell cycle and may contribute to proliferation. *BMC cancer* **11**, 203

176. Talantov, D., Mazumder, A., Yu, J. X., Briggs, T., Jiang, Y., Backus, J., Atkins, D., and Wang, Y. (2005) Novel genes associated with malignant melanoma but not benign melanocytic lesions. *Clinical cancer research : an official journal of the American Association for Cancer Research* **11**, 7234-7242

177. Xu, L., Shen, S. S., Hoshida, Y., Subramanian, A., Ross, K., Brunet, J. P., Wagner, S. N., Ramaswamy, S., Mesirov, J. P., and Hynes, R. O. (2008) Gene expression changes in an animal melanoma model correlate with aggressiveness of human melanoma metastases. *Molecular cancer research : MCR* **6**, 760-769

178. Kabbarah, O., Nogueira, C., Feng, B., Nazarian, R. M., Bosenberg, M., Wu, M., Scott, K. L., Kwong, L. N., Xiao, Y., Cordon-Cardo, C., Granter, S. R., Ramaswamy, S., Golub, T., Duncan, L. M., Wagner, S. N., Brennan, C., and Chin, L. (2010) Integrative Genome Comparison of Primary and Metastatic Melanomas. *PLoS ONE* **5**, e10770

179. Riker, A. I., Enkemann, S. A., Fodstad, O., Liu, S., Ren, S., Morris, C., Xi, Y., Howell, P., Metge, B., Samant, R. S., Shevde, L. A., Li, W., Eschrich, S., Daud, A., Ju, J., and Matta, J. (2008) The gene expression profiles of primary and metastatic melanoma yields a transition point of tumor progression and metastasis. *BMC Medical Genomics* **1**, 13

180. Cerami, E., Gao, J., Dogrusoz, U., Gross, B. E., Sumer, S. O., Aksoy, B. A., Jacobsen, A., Byrne, C. J., Heuer, M. L., Larsson, E., Antipin, Y., Reva, B., Goldberg, A. P., Sander, C., and Schultz, N. (2012) The cBio cancer genomics portal: an open platform for exploring multidimensional cancer genomics data. *Cancer discovery* **2**, 401-404

181. Gao, J., Aksoy, B. A., Dogrusoz, U., Dresdner, G., Gross, B., Sumer, S. O., Sun, Y., Jacobsen, A., Sinha, R., Larsson, E., Cerami, E., Sander, C., and Schultz, N. (2013) Integrative analysis of complex cancer genomics and clinical profiles using the cBioPortal. *Science signaling* **6**, pl1

182. Guan, J., Gupta, R., and Filipp, F. V. (2015) Cancer systems biology of TCGA SKCM: Efficient detection of genomic drivers in melanoma. *Scientific Reports* **5**, 7857

183. Rath, N., and Olson, M. F. (2012) Rho-associated kinases in tumorigenesis: re-considering ROCK inhibition for cancer therapy. *EMBO reports* **13**, 900-908

184. Herraiz, C., Calvo, F., Pandya, P., Cantelli, G., Rodriguez-Hernandez, I., Orgaz, J. L., Kang, N., Chu, T., Sahai, E., and Sanz-Moreno, V. (2016) Reactivation of p53 by a Cytoskeletal Sensor to Control the Balance Between DNA Damage and Tumor Dissemination. *JNCI Journal of the National Cancer Institute* **108**

185. Cantelli, G., Orgaz, J. L., Rodriguez-Hernandez, I., Karagiannis, P., Maiques, O., Matias-Guiu, X., Nestle, F. O., Marti, R. M., Karagiannis, S. N., and Sanz-Moreno, V. (2015) TGF-beta-Induced Transcription Sustains Amoeboid Melanoma Migration and Dissemination. *Current biology : CB* **25**, 2899-2914

186. Giard, D. J., Aaronson, S. A., Todaro, G. J., Arnstein, P., Kersey, J. H., Dosik, H., and Parks, W. P. (1973) In Vitro Cultivation of Human Tumors: Establishment of Cell Lines Derived From a Series of Solid Tumors. *Journal of the National Cancer Institute* **51**, 1417-1423

187. Fidler, I. J. (1975) Biological behavior of malignant melanoma cells correlated to their survival in vivo. *Cancer research* **35**, 218-224

188. Doe, C., Bentley, R., Behm, D. J., Lafferty, R., Stavenger, R., Jung, D., Bamford, M., Panchal, T., Grygielko, E., Wright, L. L., Smith, G. K., Chen, Z., Webb, C., Khandekar, S., Yi, T., Kirkpatrick, R., Dul, E., Jolivette, L., Marino, J. P., Jr., Willette, R., Lee, D., and Hu, E. (2007) Novel Rho kinase inhibitors with anti-inflammatory and vasodilatory activities. *The Journal of pharmacology and experimental therapeutics* **320**, 89-98

189. Sanz-Moreno, V., Gadea, G., Ahn, J., Paterson, H., Marra, P., Pinner, S., Sahai, E., and Marshall, C. J. (2008) Rac activation and inactivation control plasticity of tumor cell movement. *Cell* **135**, 510-523

190. Griffin, J. L., Mann, C. J., Scott, J., Shoulders, C. C., and Nicholson, J. K. (2001) Choline containing metabolites during cell transfection: an insight into magnetic resonance spectroscopy detectable changes. *FEBS Lett* **509**, 263-266

191. Feng, J., Li, J., Wu, H., and Chen, Z. (2013) Metabolic responses of HeLa cells to silica nanoparticles by NMR-based metabolomic analyses. *Metabolomics* **9**, 874-886

192. DeBerardinis, R. J., Mancuso, A., Daikhin, E., Nissim, I., Yudkoff, M., Wehrli, S., and Thompson, C. B. (2007) Beyond aerobic glycolysis: Transformed cells can engage in glutamine metabolism that exceeds the requirement for protein and nucleotide synthesis. *Proc Natl Acad Sci U S A* **104**, 19345-19350

193. Kailavasan, M., Rehman, I., Reynolds, S., Bucur, A., Tozer, G., and Paley, M. (2014) NMR-based evaluation of the metabolic profile and response to dichloroacetate of human prostate cancer cells. *NMR Biomed* **27**, 610-616

194. Stewart, J. D., Marchan, R., Lesjak, M. S., Lambert, J., Hergenroeder, R., Ellis, J. K., Lau, C.-H., Keun, H. C., Schmitz, G., Schiller, J., Eibisch, M., Hedberg, C., Waldmann, H., Lausch, E., Tanner, B., Sehouli, J., Sagemueller, J., Staude, H., Steiner, E., and Hengstler, J. G. (2012) Choline-releasing glycerophosphodiesterase EDI3 drives tumor cell migration and metastasis. *Proceedings of the National Academy of Sciences* **109**, 8155-8160

195. Ratnikov, B., Aza-Blanc, P., Ronai, Z. A., Smith, J. W., Osterman, A. L., and Scott, D. A. (2015) Glutamate and asparagine cataplerosis underlie glutamine addiction in melanoma. *Oncotarget* **6**, 7379-7389

196. Seidlitz, E. P., Sharma, M. K., Saikali, Z., Ghert, M., and Singh, G. (2009) Cancer cell lines release glutamate into the extracellular environment. *Clinical & Experimental Metastasis* **26**, 781-787

197. Sharma, M. K., Seidlitz, E. P., and Singh, G. (2010) Cancer cells release glutamate via the cystine/glutamate antiporter. *Biochemical and biophysical research communications* **391**, 91-95

198. Nagana Gowda, G. A., Gowda, Y. N., and Raftery, D. (2015) Massive Glutamine Cyclization to Pyroglutamic Acid in Human Serum Discovered Using NMR Spectroscopy. *Analytical chemistry* **87**, 3800-3805

199. Rodriguez-Hernandez, I., Cantelli, G., Bruce, F., and Sanz-Moreno, V. (2016) *Rho, ROCK and actomyosin contractility in metastasis as drug targets [version 1; referees: 2 approved]*,

200. Jackson, A. L., and Linsley, P. S. (2004) Noise amidst the silence: off-target effects of siRNAs? *Trends in Genetics* **20**, 521-524

201. Jackson, A. L., and Linsley, P. S. (2010) Recognizing and avoiding siRNA off-target effects for target identification and therapeutic application. *Nat Rev Drug Discov* **9**, 57-67

202. DeBerardinis, R. J., and Cheng, T. (2010) Q's next: the diverse functions of glutamine in metabolism, cell biology and cancer. *Oncogene* **29**

203. Wang, Q., Beaumont, K. A., Otte, N. J., Font, J., Bailey, C. G., van Geldermalsen, M., Sharp, D. M., Tiffen, J. C., Ryan, R. M., Jormakka, M., Haass, N. K., Rasko, J. E., and Holst, J. (2014) Targeting glutamine transport to suppress melanoma cell growth. *International journal of cancer* **135**, 1060-1071

204. Huang, W., Choi, W., Chen, Y., Zhang, Q., Deng, H., He, W., and Shi, Y. (2013) A proposed role for glutamine in cancer cell growth through acid resistance. *Cell Res* **23**, 724-727

205. Altman, B. J., Stine, Z. E., and Dang, C. V. (2016) From Krebs to clinic: glutamine metabolism to cancer therapy. *Nat Rev Cancer* **advance online publication**

206. Fu, Y. M., Zhang, H., Ding, M., Li, Y. Q., Fu, X., Yu, Z. X., and Meadows, G. G. (2004) Specific amino acid restriction inhibits attachment and spreading of human melanoma via modulation of the integrin/focal adhesion kinase pathway and actin cytoskeleton remodeling. *Clin Exp Metastasis* **21**, 587-598

207. Jourdain, P., Allaman, I., Rothenfusser, K., Fiumelli, H., Marquet, P., and Magistretti, P. J. (2016) L-Lactate protects neurons against excitotoxicity: implication of an ATP-mediated signaling cascade. *Sci Rep* **6**, 21250

208. Willard, S. S., and Koochekpour, S. (2013) Glutamate, Glutamate Receptors, and Downstream Signaling Pathways. *International Journal of Biological Sciences* **9**, 948-959

209. Traynelis, S. F., Wollmuth, L. P., McBain, C. J., Menniti, F. S., Vance, K. M., Ogden, K. K., Hansen, K. B., Yuan, H., Myers, S. J., and Dingledine, R. (2010) Glutamate Receptor Ion Channels: Structure, Regulation, and Function. *Pharmacological Reviews* **62**, 405-496

210. Contractor, A., Mulle, C., and Swanson, G. T. (2011) Kainate receptors coming of age: milestones of two decades of research. *Trends Neurosci* **34**, 154-163

211. Ohtani, Y., Harada, T., Funasaka, Y., Nakao, K., Takahara, C., Abdel-Daim, M., Sakai, N., Saito, N., Nishigori, C., and Aiba, A. (2008) Metabotropic glutamate receptor subtype-1 is essential for in vivo growth of melanoma. *Oncogene* **27**, 7162-7170

212. Song, Z., He, C.-D., Liu, J., Sun, C., Lu, P., Li, L., Gao, L., Zhang, Y., Xu, Y., Shan, L., Liu, Y., Zou, W., Zhang, Y., Gao, H., and Gao, W. (2012) Blocking glutamate-mediated signalling inhibits human melanoma growth and migration. *Experimental dermatology* **21**, 926-931

213. Namkoong, J., Shin, S. S., Lee, H. J., Marin, Y. E., Wall, B. A., Goydos, J. S., and Chen, S. (2007) Metabotropic glutamate receptor 1 and glutamate signaling in human melanoma. *Cancer research* **67**, 2298-2305

214. Yip, D., Le, M. N., Chan, J. L., Lee, J. H., Mehnert, J. A., Yudd, A., Kempf, J., Shih, W. J., Chen, S., and Goydos, J. S. (2009) A phase 0 trial of riluzole in patients with resectable stage III and IV melanoma. *Clinical cancer research : an official journal of the American Association for Cancer Research* **15**, 3896-3902

215. Choi, K. Y., Chang, K., Pickel, J. M., Badger, J. D., 2nd, and Roche, K. W. (2011) Expression of the metabotropic glutamate receptor 5 (mGluR5) induces melanoma in transgenic mice. *Proc Natl Acad Sci U S A* **108**, 15219-15224

216. Ishiuchi, S., Tsuzuki, K., Yoshida, Y., Yamada, N., Hagimura, N., Okado, H., Miwa, A., Kurihara, H., Nakazato, Y., Tamura, M., Sasaki, T., and Ozawa, S. (2002) Blockage of Ca(2+)-permeable AMPA receptors suppresses migration and induces apoptosis in human glioblastoma cells. *Nat Med* **8**, 971-978

217. Ishiuchi, S., Yoshida, Y., Sugawara, K., Aihara, M., Ohtani, T., Watanabe, T., Saito, N., Tsuzuki, K., Okado, H., Miwa, A., Nakazato, Y., and Ozawa, S. (2007) Ca2+-permeable AMPA receptors regulate growth of human glioblastoma via Akt activation. *The Journal of neuroscience : the official journal of the Society for Neuroscience* **27**, 7987-8001

218. van Vuurden, D. G., Yazdani, M., Bosma, I., Broekhuizen, A. J., Postma, T. J., Heimans, J. J., van der Valk, P., Aronica, E., Tannous, B. A., Wurdinger, T., Kaspers, G. J., and Cloos, J. (2009) Attenuated AMPA receptor expression allows glioblastoma cell survival in glutamate-rich environment. *PLoS One* **4**, e5953

219. Beretta, F., Bassani, S., Binda, E., Verpelli, C., Bello, L., Galli, R., and Passafaro, M. (2009) The GluR2 subunit inhibits proliferation by inactivating Src-MAPK signalling and induces apoptosis by means of caspase 3/6-dependent activation in glioma cells. *European Journal of Neuroscience* **30**, 25-34

220. Ripka, S., Riedel, J., Neesse, A., Griesmann, H., Buchholz, M., Ellenrieder, V., Moeller, F., Barth, P., Gress, T. M., and Michl, P. (2010) Glutamate receptor GRIA3--target of CUX1 and mediator of tumor progression in pancreatic cancer. *Neoplasia (New York, N.Y.)* **12**, 659-667

221. Ribeiro, M. P., Nunes-Correia, I., Santos, A. E., and Custodio, J. B. (2014) The combination of glutamate receptor antagonist MK-801 with tamoxifen and its active metabolites potentiates their antiproliferative activity in mouse melanoma K1735-M2 cells. *Exp Cell Res* **321**, 288-296

222. Prickett, T. D., Zerlanko, B. J., Hill, V. K., Gartner, J. J., Qutob, N., Jiang, J., Simaan, M., Wunderlich, J., Gutkind, J. S., Rosenberg, S. A., and Samuels, Y. (2014) Somatic mutation of GRIN2A in malignant melanoma results in loss of tumor suppressor activity via aberrant NMDAR complex formation. *J Invest Dermatol* **134**, 2390-2398

223. Pollock, P. M., Cohen-Solal, K., Sood, R., Namkoong, J., Martino, J. J., Koganti, A., Zhu, H., Robbins, C., Makalowska, I., Shin, S.-S., Marin, Y., Roberts, K. G., Yudt, L. M., Chen, A., Cheng, J., Incao, A., Pinkett, H. W., Graham, C. L., Dunn, K., Crespo-Carbone, S. M., Mackason, K. R., Ryan, K. B., Sinsimer, D., Goydos, J., Reuhl, K. R., Eckhaus, M., Meltzer, P. S., Pavan, W. J., Trent, J. M., and Chen, S. (2003) Melanoma mouse model implicates metabotropic glutamate signaling in melanocytic neoplasia. *Nature genetics* **34**, 108-112

224. Schiffner, S., Chen, S., Becker, J. C., and Bosserhoff, A. K. (2012) Highly pigmented Tg(Grm1) mouse melanoma develops non-pigmented melanoma cells in distant metastases. *Experimental dermatology* **21**, 786-788

225. Wen, Y., Li, J., Koo, J., Shin, S.-S., Lin, Y., Jeong, B.-S., Mehnert, J., Chen, S., Cohen-Solal, K., and Goydos, J. S. (2014) Activation of the Glutamate Receptor GRM1 Enhances Angiogenic Signaling to Drive Melanoma Progression. *Cancer research* **74**, 2499-2509

226. Choi, K. Y., Chang, K., Pickel, J. M., Badger, J. D., and Roche, K. W. (2011) Expression of the metabotropic glutamate receptor 5 (mGluR5) induces melanoma in transgenic mice. *Proceedings of the National Academy of Sciences of the United States of America* **108**, 15219-15224

227. Marin, Y. E., Namkoong, J., Shin, S. S., Raines, J., Degenhardt, K., White, E., and Chen, S. (2005) Grm5 expression is not required for the oncogenic role of Grm1 in melanocytes. *Neuropharmacology* **49 Suppl 1**, 70-79

228. Brand, K. A., and Hermfisse, U. (1997) Aerobic glycolysis by proliferating cells: a protective strategy against reactive oxygen species. *FASEB journal : official publication of the Federation of American Societies for Experimental Biology* **11**, 388-395

229. Lee, M., and Yoon, J. H. (2015) Metabolic interplay between glycolysis and mitochondrial oxidation: The reverse Warburg effect and its therapeutic implication. *World Journal of Biological Chemistry* **6**, 148-161

230. Baenke, F., Chaneton, B., Smith, M., Van Den Broek, N., Hogan, K., Tang, H., Viros, A., Martin, M., Galbraith, L., Girotti, M. R., Dhomen, N., Gottlieb, E., and Marais, R. (2016) Resistance to BRAF inhibitors induces glutamine dependency in melanoma cells. *Molecular Oncology* **10**, 73-84

231. Nishioka, T., Nakayama, M., Amano, M., and Kaibuchi, K. (2012) Proteomic screening for Rho-kinase substrates by combining kinase and phosphatase inhibitors with 14-3-3zeta affinity chromatography. *Cell structure and function* **37**, 39-48

232. Nishino, H., Tokuda, H., Satomi, Y., Masuda, M., Osaka, Y., Yogosawa, S., Wada, S., Mou, X. Y., Takayasu, J., Murakoshi, M., Jinnno, K., and Yano, M. (2004) Cancer prevention by antioxidants. *BioFactors (Oxford, England)* **22**, 57-61

233. Fuchs-Tarlovsky, V. (2013) Role of antioxidants in cancer therapy. *Nutrition (Burbank, Los Angeles County, Calif.)* **29**, 15-21

234. Herraiz, C., Crosas-Molist, E., and Sanz-Moreno, V. (2016) Reactive oxygen species and tumor dissemination: Allies no longer. *Molecular & Cellular Oncology* **3**, e1127313

235. Le Gal, K., Ibrahim, M. X., Wiel, C., Sayin, V. I., Akula, M. K., Karlsson, C., Dalin, M. G., Akyurek, L. M., Lindahl, P., Nilsson, J., and Bergo, M. O. (2015) Antioxidants can increase melanoma metastasis in mice. *Sci Transl Med* **7**, 308re308

236. Wilson, Miranda S. C., Livermore, Thomas M., and Saiardi, A. (2013) Inositol pyrophosphates: between signalling and metabolism. *Biochemical Journal* **452**, 369-379

237. Gillaspy, G. E. (2011) The cellular language of *myo*-inositol signaling. *The New phytologist* **192**, 823-839

238. Serkova, N. J., Gamito, E. J., Jones, R. H., O'Donnell, C., Brown, J. L., Green, S., Sullivan, H., Hedlund, T., and Crawford, E. D. (2008) The metabolites citrate, *myo*-inositol, and spermine are potential age-independent markers of prostate cancer in human expressed prostatic secretions. *Prostate* **68**, 620-628

239. Hecht, S. S., Kenney, P. M. J., Wang, M., Trushin, N., Agarwal, S., Venket Rao, A., and Upadhyaya, P. (1999) Evaluation of butylated hydroxyanisole, *myo*-inositol, curcumin, esculetin, resveratrol and lycopene as inhibitors of benzo[a]pyrene plus 4-(methylnitrosamino)-1-(3-pyridyl)-1-butanone-induced lung tumorigenesis in A/J mice. *Cancer letters* **137**, 123-130

240. Hecht, S. S., Kenney, P. M. J., Wang, M., and Upadhyaya, P. (2001) Dose–response study of *myo*-inositol as an inhibitor of lung tumorigenesis induced in A/J mice by benzo[a]pyrene and 4-(methylnitrosamino)-1-(3-pyridyl)-1-butanone. *Cancer letters* **167**, 1-6

241. Lam, S., McWilliams, A., leRiche, J., MacAulay, C., Wattenberg, L., and Szabo, E. (2006) A Phase I Study of *myo*-Inositol for Lung Cancer Chemoprevention. *Cancer Epidemiology Biomarkers & Prevention* **15**, 1526-1531

242. Kallenberg, K., Bock, H. C., Helms, G., Jung, K., Wrede, A., Buhk, J. H., Giese, A., Frahm, J., Strik, H., Dechent, P., and Knauth, M. (2009) Untreated glioblastoma multiforme: increased *myo*-inositol and glutamine levels in the contralateral cerebral hemisphere at proton MR spectroscopy. *Radiology* **253**, 805-812

243. Howells, S. L., Maxwell, R. J., Peet, A. C., and Griffiths, J. R. (1992) An investigation of tumor 1H nuclear magnetic resonance spectra by the application of chemometric techniques. *Magnetic resonance in medicine* **28**, 214-236

244. Beckonert, O., Monnerjahn, J., Bonk, U., and Leibfritz, D. (2003) Visualizing metabolic changes in breast-cancer tissue using 1H-NMR spectroscopy and self-organizing maps. *NMR Biomed* **16**, 1-11

245. Nordenberg, J., Panet, C., Wasserman, L., Malik, Z., Fuchs, A., Stenzel, K. H., and Novogrodsky, A. (1987) The anti-proliferative effect of lithium chloride on melanoma cells and its reversion by *myo*-inositol. *Br J Cancer* **55**, 41-46

246. Baenke, F., Peck, B., Miess, H., and Schulze, A. (2013) Hooked on fat: the role of lipid synthesis in cancer metabolism and tumour development. *Disease Models and Mechanisms* **6**, 1353-1363

247. Beloribi-Djefaflia, S., Vasseur, S., and Guillaumond, F. (2016) Lipid metabolic reprogramming in cancer cells. *Oncogenesis* **5**, e189

248. Balog, J., Sasi-Szabó, L., Kinross, J., Lewis, M. R., Muirhead, L. J., Veselkov, K., Mirnezami, R., Dezső, B., Damjanovich, L., Darzi, A., Nicholson, J. K., and Takáts, Z. (2013) Intraoperative Tissue Identification Using Rapid Evaporative Ionization Mass Spectrometry. *Science Translational Medicine* **5**, 194ra193-194ra193

249. Griffin, J. L., and Shockcor, J. P. (2004) Metabolic profiles of cancer cells. *Nat Rev Cancer* **4**, 551-561

250. Lock, F. E., and Hotchin, N. A. (2009) Distinct Roles for ROCK1 and ROCK2 in the Regulation of Keratinocyte Differentiation. *PLoS ONE* **4**, e8190

251. Yoneda, A., Multhaupt, H. A. B., and Couchman, J. R. (2005) The Rho kinases I and II regulate different aspects of *myo*sin II activity. *J Cell Biol* **170**, 443-453

252. Noma, K., Rikitake, Y., Oyama, N., Yan, G., Alcaide, P., Liu, P.-Y., Wang, H., Ahl, D., Sawada, N., Okamoto, R., Hiroi, Y., Shimizu, K., Luscinskas, F. W., Sun, J., and Liao, J. K. ROCK1 mediates leukocyte recruitment and neointima formation following vascular injury. *The Journal of Clinical Investigation* **118**, 1632-1644

253. Shi, J., Wu, X., Surma, M., Vemula, S., Zhang, L., Yang, Y., Kapur, R., and Wei, L. (2013) Distinct roles for ROCK1 and ROCK2 in the regulation of cell detachment. *Cell Death Dis* **4**, e483

254. Schatton, T., and Frank, M. H. (2008) Cancer stem cells and human malignant melanoma. *Pigment cell & melanoma research* **21**, 39-55

255. Zimmerer, R. M., Korn, P., Demougin, P., Kampmann, A., Kokemüller, H., Eckardt, A. M., Gellrich, N.-C., and Tavassol, F. (2013) Functional features of cancer stem cells in melanoma cell lines. *Cancer Cell International* **13**, 1-14

256. Taddei, M. L., Giannoni, E., Morandi, A., Ippolito, L., Ramazzotti, M., Callari, M., Gandellini, P., and Chiarugi, P. (2014) Mesenchymal to amoeboid transition is associated with stem-like features of melanoma cells. *Cell Communication and Signaling : CCS* **12**, 24

257. Ravi, M., Paramesh, V., Kaviya, S. R., Anuradha, E., and Solomon, F. D. (2015) 3D cell culture systems: advantages and applications. *Journal of cellular physiology* **230**, 16-26

258. Allen, D. D., Caviedes, R., Cardenas, A. M., Shimahara, T., Segura-Aguilar, J., and Caviedes, P. A. (2005) Cell lines as in vitro models for drug screening and toxicity studies. *Drug development and industrial pharmacy* **31**, 757-768

259. Tabassum, D. P., and Polyak, K. (2015) Tumorigenesis: it takes a village. *Nat Rev Cancer* **15**, 473-483

260. McMillin, D. W., Negri, J. M., and Mitsiades, C. S. (2013) The role of tumour-stromal interactions in modifying drug response: challenges and opportunities. *Nat Rev Drug Discov* **12**, 217-228

261. Hirt, C., Papadimitropoulos, A., Mele, V., Muraro, M. G., Mengus, C., Iezzi, G., Terracciano, L., Martin, I., and Spagnoli, G. C. (2014) "In vitro" 3D models of tumor-immune system interaction. *Advanced drug delivery reviews* **79-80**, 145-154

262. Gillet, J. P., Varma, S., and Gottesman, M. M. (2013) The clinical relevance of cancer cell lines. *JNCI Journal of the National Cancer Institute* **105**, 452-458

263. Sanz-Moreno, V., Gadea, G., Ahn, J., Paterson, H., Marra, P., Pinner, S., Sahai, E., and Marshall, C. J. (2008) Rac activation and inactivation control plasticity of tumor cell movement. *Cell* **135**

264. Ratnikov, B. I., Scott, D. A., Osterman, A. L., Smith, J. W., and Ronai, Z. A. (2016) Metabolic rewiring in melanoma. *Oncogene*

265. Lukey, M. J., Wilson, K. F., and Cerione, R. A. (2013) Therapeutic strategies impacting cancer cell glutamine metabolism. *Future medicinal chemistry* **5**, 1685-1700

266. Dang, C. V. (2010) Rethinking the Warburg effect with Myc micromanaging glutamine metabolism. *Cancer research* **70**, 859-862

267. Cesar-Razquin, A., Snijder, B., Frappier-Brinton, T., Isserlin, R., Gyimesi, G., Bai, X., Reithmeier, R. A., Hepworth, D., Hediger, M. A., Edwards, A. M., and Superti-Furga, G. (2015) A Call for Systematic Research on Solute Carriers. *Cell* **162**, 478-487

268. Hay, N. (2016) Reprogramming glucose metabolism in cancer: can it be exploited for cancer therapy? *Nat Rev Cancer* **16**, 635-649

269. Filipp, F. V., Ratnikov, B., De Ingeniis, J., Smith, J. W., Osterman, A. L., and Scott, D. A. (2012) Glutamine-fueled mitochondrial metabolism is decoupled from glycolysis in melanoma. *Pigment cell & melanoma research* **25**, 732-739

270. Hernandez-Davies, J. E., Tran, T. Q., Reid, M. A., Rosales, K. R., Lowman, X. H., Pan, M., Moriceau, G., Yang, Y., Wu, J., Lo, R. S., and Kong, M. (2015) Vemurafenib resistance reprograms melanoma cells towards glutamine dependence. *J Transl Med* **13**, 210

271. Brazma, A., Hingamp, P., Quackenbush, J., Sherlock, G., Spellman, P., Stoeckert, C., Aach, J., Ansorge, W., Ball, C. A., Causton, H. C., Gaasterland, T., Glenisson, P., Holstege, F. C., Kim, I. F., Markowitz, V., Matese, J. C., Parkinson, H., Robinson, A., Sarkans, U., Schulze-Kremer, S., Stewart, J., Taylor, R., Vilo, J., and Vingron, M. (2001) Minimum information about a microarray experiment (MIAME)-toward standards for microarray data. *Nature genetics* **29**, 365-371

272. Wu, C., Zhu, J., and Zhang, X. (2013) Network-based differential gene expression analysis suggests cell cycle related genes regulated by E2F1 underlie the molecular difference between smoker and non-smoker lung adenocarcinoma. *BMC Bioinformatics* **14**, 1-16

273. Macneil, L. T., and Walhout, A. J. (2011) Gene regulatory networks and the role of robustness and stochasticity in the control of gene expression. *Genome Res* **21**

274. de la Fuente, A. (2010) From 'differential expression' to 'differential networking' - identification of dysfunctional regulatory networks in diseases. *Trends Genet* **26**

275. Segal, E., Shapira, M., Regev, A., Pe'er, D., Botstein, D., Koller, D., and Friedman, N. (2003) Module networks: identifying regulatory modules and their condition-specific regulators from gene expression data. *Nature genetics* **34**

276. Masin, M., Vazquez, J., Rossi, S., Groeneveld, S., Samson, N., Schwalie, P. C., Deplancke, B., Frawley, L. E., Gouttenoire, J., Moradpour, D., Oliver, T. G., and Meylan, E. (2014) GLUT3 is induced during epithelial-mesenchymal transition and promotes tumor cell proliferation in non-small cell lung cancer. *Cancer Metab* **2**, 11

277. Krzeslak, A., Wojcik-Krowiranda, K., Forma, E., Jozwiak, P., Romanowicz, H., Bienkiewicz, A., and Brys, M. (2012) Expression of GLUT1 and GLUT3 glucose transporters in endometrial and breast cancers. *Pathology oncology research : POR* **18**, 721-728

278. Ha, T. K., and Chi, S. G. (2012) CAV1/caveolin 1 enhances aerobic glycolysis in colon cancer cells via activation of SLC2A3/GLUT3 transcription. *Autophagy* **8**, 1684-1685

279. Rhodes, D. R., Barrette, T. R., Rubin, M. A., Ghosh, D., and Chinnaiyan, A. M. (2002) Meta-Analysis of Microarrays. *Cancer research* **62**, 4427

280. Vié, N., Copois, V., Bascoul-Mollevi, C., Denis, V., Bec, N., Robert, B., Fraslon, C., Conseiller, E., Molina, F., Larroque, C., Martineau, P., Del Rio, M., and Gongora, C. (2008) Overexpression of phosphoserine aminotransferase PSAT1 stimulates cell growth and increases chemoresistance of colon cancer cells. *Molecular Cancer* **7**, 14-14

281. Oliveros, J. C. (2007) VENNY. An interactive tool for comparing lists with Venn Diagrams.

282. Singh, U. S., Pan, J., Kao, Y. L., Joshi, S., Young, K. L., and Baker, K. M. (2003) Tissue transglutaminase mediates activation of RhoA and MAP kinase pathways during retinoic acid-induced neuronal differentiation of SH-SY5Y cells. *The Journal of biological chemistry* **278**, 391-399

283. Singh, U. S., Kunar, M. T., Kao, Y. L., and Baker, K. M. (2001) Role of transglutaminase II in retinoic acid-induced activation of RhoA-associated kinase-2. *The EMBO journal* **20**, 2413-2423

284. Janiak, A., Zemskov, E. A., and Belkin, A. M. (2006) Cell surface transglutaminase promotes RhoA activation via integrin clustering and suppression of the Src-p190RhoGAP signaling pathway. *Mol Biol Cell* **17**, 1606-1619

285. Nurminskaya, M. V., and Belkin, A. M. (2012) Cellular functions of tissue transglutaminase. *International review of cell and molecular biology* **294**, 1-97

286. Benjamini, Y., and Hochberg, Y. (1995) Controlling the false discovery rate: a practical and powerful approach to multiple testing. *Journal of the royal statistical society. Series B (Methodological)*, 289-300

287. Goswami, M. T., Chen, G., Chakravarthi, B. V., Pathi, S. S., Anand, S. K., Carskadon, S. L., Giordano, T. J., Chinnaiyan, A. M., Thomas, D. G., Palanisamy, N., Beer, D. G., and Varambally, S. (2015) Role and regulation of coordinately expressed de novo purine biosynthetic enzymes PPAT and PAICS in lung cancer. *Oncotarget* **6**, 23445-23461

288. Reitman, Z. J., and Yan, H. (2010) Isocitrate Dehydrogenase 1 and 2 Mutations in Cancer: Alterations at a Crossroads of Cellular Metabolism. *JNCI Journal of the National Cancer Institute* **102**, 932-941

289. Cardaci, S., and Ciriolo, M. R. (2012) TCA cycle defects and cancer: when metabolism tunes redox state. *International journal of cell biology* **2012**

290. Zeng, L., Morinibu, A., Kobayashi, M., Zhu, Y., Wang, X., Goto, Y., Yeom, C. J., Zhao, T., Hirota, K., Shinomiya, K., Itasaka, S., Yoshimura, M., Guo, G., Hammond, E. M., Hiraoka, M., and Harada, H. (2015) Aberrant IDH3alpha expression promotes malignant tumor growth by inducing HIF-1-mediated metabolic reprogramming and angiogenesis. *Oncogene* **34**, 4758-4766

291. Tatsukawa, H., Furutani, Y., Hitomi, K., and Kojima, S. (2016) Transglutaminase 2 has opposing roles in the regulation of cellular functions as well as cell growth and death. *Cell Death Dis* **7**, e2244

292. Di Giacomo, G., Lentini, A., Beninati, S., Piacentini, M., and Rodolfo, C. (2009) In vivo evaluation of type 2 transglutaminase contribution to the metastasis formation in melanoma. *Amino acids* **36**, 717-724

293. Xu, L., Begum, S., Hearn, J. D., and Hynes, R. O. (2006) GPR56, an atypical G protein-coupled receptor, binds tissue transglutaminase, TG2, and inhibits melanoma tumor growth and metastasis. *Proceedings of the National Academy of Sciences* **103**, 9023-9028

294. Erdem, S., Yegen, G., Telci, D., Yildiz, I., Tefik, T., Issever, H., Kilicaslan, I., and Sanli, O. (2015) The increased transglutaminase 2 expression levels during initial tumorigenesis predict

increased risk of metastasis and decreased disease-free and cancer-specific survivals in renal cell carcinoma. *World journal of urology* **33**, 1553-1560

295. Miyoshi, N., Ishii, H., Mimori, K., Tanaka, F., Hitora, T., Tei, M., Sekimoto, M., Doki, Y., and Mori, M. (2010) TGM2 is a novel marker for prognosis and therapeutic target in colorectal cancer. *Ann Surg Oncol* **17**, 967-972

296. Mangala, L. S., Fok, J. Y., Zorrilla-Calancha, I. R., Verma, A., and Mehta, K. (2007) Tissue transglutaminase expression promotes cell attachment, invasion and survival in breast cancer cells. *Oncogene* **26**, 2459-2470

297. Kotsakis, P., and Griffin, M. (2007) Tissue transglutaminase in tumour progression: friend or foe? *Amino acids* **33**, 373-384

298. Chhabra, A., Verma, A., and Mehta, K. (2009) Tissue transglutaminase promotes or suppresses tumors depending on cell context. *Anticancer Res* **29**, 1909-1919

299. Li, L., Watson, C. J., Dubourd, M., Bruton, A., Xu, M., Cooke, G., and Baugh, J. A. (2016) HIF-1-Dependent TGM1 Expression is Associated with Maintenance of Airway Epithelial Junction Proteins. *Lung*

300. van der Velden, J. J., van Geel, M., Nellen, R. G., Jonkman, M. F., McGrath, J. A., Nanda, A., Sprecher, E., van Steensel, M. A., McLean, W. H., and Cassidy, A. J. (2015) Novel TGM5 mutations in acral peeling skin syndrome. *Experimental dermatology* **24**, 285-289

301. Prasad, P. D., Wang, H., Huang, W., Kekuda, R., Rajan, D. P., Leibach, F. H., and Ganapathy, V. (1999) Human LAT1, a subunit of system L amino acid transporter: molecular cloning and transport function. *Biochemical and biophysical research communications* **255**, 283-288

302. Wagner, C. A., Lang, F., and Bröer, S. (2001) Function and structure of heterodimeric amino acid transporters. *American Journal of Physiology - Cell Physiology* **281**, C1077-C1093

303. Nicklin, P., Bergman, P., Zhang, B., Triantafellow, E., Wang, H., Nyfeler, B., Yang, H., Hild, M., Kung, C., Wilson, C., Myer, V. E., MacKeigan, J. P., Porter, J. A., Wang, Y. K., Cantley, L. C., Finan, P. M., and Murphy, L. O. (2009) Bidirectional Transport of Amino Acids Regulates mTOR and Autophagy. *Cell* **136**, 521-534

304. Glick, D., Barth, S., and Macleod, K. F. (2010) Autophagy: cellular and molecular mechanisms. *The Journal of pathology* **221**, 3-12

305. Marino, M. L., Pellegrini, P., Di Lernia, G., Djavaheri-Mergny, M., Brnjic, S., Zhang, X., Hagg, M., Linder, S., Fais, S., Codogno, P., and De Milito, A. (2012) Autophagy is a protective mechanism for human melanoma cells under acidic stress. *The Journal of biological chemistry* **287**

306. Sheen, J. H., Zoncu, R., Kim, D., and Sabatini, D. M. (2011) Defective regulation of autophagy upon leucine deprivation reveals a targetable liability of human melanoma cells in vitro and in vivo. *Cancer cell* **19**, 613-628

307. Feral, C. C., Nishiya, N., Fenczik, C. A., Stuhlmann, H., Slepak, M., and Ginsberg, M. H. (2005) CD98hc (SLC3A2) mediates integrin signaling. *Proc Natl Acad Sci U S A* **102**, 355-360

308. Boulter, E., Estrach, S., Errante, A., Pons, C., Cailleteau, L., Tissot, F., Meneguzzi, G., and Féral Cé, C. (2013) CD98hc (SLC3A2) regulation of skin homeostasis wanes with age. *The Journal of Experimental Medicine* **210**, 173-190

309. Broer, A., Rahimi, F., and Broer, S. (2016) Deletion of Amino Acid Transporter ASCT2 (SLC1A5) Reveals an Essential Role for Transporters SNAT1 (SLC38A1) and SNAT2 (SLC38A2) to Sustain Glutaminolysis in Cancer Cells. *The Journal of biological chemistry* **291**, 13194-13205

310. Fuchs, B. C., Finger, R. E., Onan, M. C., and Bode, B. P. (2007) ASCT2 silencing regulates mammalian target-of-rapamycin growth and survival signaling in human hepatoma cells. *American journal of physiology. Cell physiology* **293**, C55-63

311. Liu, Y., Yang, L., An, H., Chang, Y., Zhang, W., Zhu, Y., Xu, L., and Xu, J. (2015) High expression of Solute Carrier Family 1, member 5 (SLC1A5) is associated with poor prognosis in clear-cell renal cell carcinoma. *Sci Rep* **5**, 16954

312. Shimizu, K., Kaira, K., Tomizawa, Y., Sunaga, N., Kawashima, O., Oriuchi, N., Tominaga, H., Nagamori, S., Kanai, Y., Yamada, M., Oyama, T., and Takeyoshi, I. (2014) ASC amino-acid transporter 2 (ASCT2) as a novel prognostic marker in non-small cell lung cancer. *Br J Cancer* **110**, 2030-2039

313. van Geldermalsen, M., Wang, Q., Nagarajah, R., Marshall, A. D., Thoeng, A., Gao, D., Ritchie, W., Feng, Y., Bailey, C. G., Deng, N., Harvey, K., Beith, J. M., Selinger, C. I., O'Toole, S. A., Rasko, J. E., and Holst, J. (2016) ASCT2/SLC1A5 controls glutamine uptake and tumour growth in triple-negative basal-like breast cancer. *Oncogene* **35**, 3201-3208

314. Wang, Q., Hardie, R. A., Hoy, A. J., van Geldermalsen, M., Gao, D., Fazli, L., Sadowski, M. C., Balaban, S., Schreuder, M., Nagarajah, R., Wong, J. J., Metierre, C., Pinello, N., Otte, N. J., Lehman, M. L., Gleave, M., Nelson, C. C., Bailey, C. G., Ritchie, W., Rasko, J. E., and Holst, J. (2015) Targeting ASCT2-mediated glutamine uptake blocks prostate cancer growth and tumour development. *The Journal of pathology* **236**, 278-289

315. Witte, D., Ali, N., Carlson, N., and Younes, M. (2002) Overexpression of the neutral amino acid transporter ASCT2 in human colorectal adenocarcinoma. *Anticancer Res* **22**, 2555-2557

316. Hassanein, M., Hoeksema, M. D., Shiota, M., Qian, J., Harris, B. K., Chen, H., Clark, J. E., Alborn, W. E., Eisenberg, R., and Massion, P. P. (2013) SLC1A5 mediates glutamine transport required for lung cancer cell growth and survival. *Clinical cancer research : an official journal of the American Association for Cancer Research* **19**, 560-570

317. Hassanein, M., Qian, J., Hoeksema, M. D., Wang, J., Jacobovitz, M., Ji, X., Harris, F. T., Harris, B. K., Boyd, K. L., Chen, H., Eisenberg, R., and Massion, P. P. (2015) Targeting SLC1a5-mediated glutamine dependence in non-small cell lung cancer. *International journal of cancer* **137**, 1587-1597

318. Shimizu, A., Kaira, K., Kato, M., Yasuda, M., Takahashi, A., Tominaga, H., Oriuchi, N., Nagamori, S., Kanai, Y., Oyama, T., Asao, T., and Ishikawa, O. (2015) Prognostic significance of L-type amino acid transporter 1 (LAT1) expression in cutaneous melanoma. *Melanoma Res* **25**, 399-405

319. Huang, F., Zhao, Y., Zhao, J., Wu, S., Jiang, Y., Ma, H., and Zhang, T. (2014) Upregulated SLC1A5 promotes cell growth and survival in colorectal cancer. *International journal of clinical and experimental pathology* **7**, 6006-6014

320. Shennan, D. B., Thomson, J., Barber, M. C., and Travers, M. T. (2003) Functional and molecular characteristics of system L in human breast cancer cells. *Biochim Biophys Acta* **1611**, 81-90

321. Broer, A., Wagner, C. A., Lang, F., and Broer, S. (2000) The heterodimeric amino acid transporter 4F2hc/y+LAT2 mediates arginine efflux in exchange with glutamine. *The Biochemical journal* **349 Pt 3**, 787-795

322. Thakkar, A. D., Raj, H., Chakrabarti, D., Ravishankar, Saravanan, N., Muthuvelan, B., Balakrishnan, A., and Padigaru, M. (2010) Identification of Gene Expression Signature in Estrogen Receptor Positive Breast Carcinoma. *Biomarkers in Cancer* **2**, 1-15

323. Kaji, M., Kabir-Salmani, M., Anzai, N., Jin, C. J., Akimoto, Y., Horita, A., Sakamoto, A., Kanai, Y., Sakurai, H., and Iwashita, M. (2010) Properties of L-type amino acid transporter 1 in epidermal ovarian cancer. *International journal of gynecological cancer : official journal of the International Gynecological Cancer Society* **20**, 329-336

324. Januchowski, R., Zawierucha, P., Andrzejewska, M., Rucinski, M., and Zabel, M. (2013) Microarray-based detection and expression analysis of ABC and SLC transporters in drug-resistant ovarian cancer cell lines. *Biomedicine & pharmacotherapy = Biomedecine & pharmacotherapie* **67**, 240-245

325. Kobayashi, K., Ohnishi, A., Promsuk, J., Shimizu, S., Kanai, Y., Shiokawa, Y., and Nagane, M. (2008) Enhanced tumor growth elicited by L-type amino acid transporter 1 in human malignant glioma cells. *Neurosurgery* **62**, 493-504

326. Oda, K., Hosoda, N., Endo, H., Saito, K., Tsujihara, K., Yamamura, M., Sakata, T., Anzai, N., Wempe, M. F., Kanai, Y., and Endou, H. (2010) L-type amino acid transporter 1 inhibitors inhibit tumor cell growth. *Cancer science* **101**, 173-179

327. Ichinoe, M., Mikami, T., Yoshida, T., Igawa, I., Tsuruta, T., Nakada, N., Anzai, N., Suzuki, Y., Endou, H., and Okayasu, I. (2011) High expression of L-type amino-acid transporter 1 (LAT1) in gastric carcinomas: comparison with non-cancerous lesions. *Pathol Int* **61**, 281-289

328. Betsunoh, H., Fukuda, T., Anzai, N., Nishihara, D., Mizuno, T., Yuki, H., Masuda, A., Yamaguchi, Y., Abe, H., Yashi, M., Fukabori, Y., Yoshida, K., and Kamai, T. (2013) Increased expression of system large amino acid transporter (LAT)-1 mRNA is associated with invasive potential and unfavorable prognosis of human clear cell renal cell carcinoma. *BMC cancer* **13**, 509

329. Janpipatkul, K., Suksen, K., Borwornpinyo, S., Jearawiriyapaisarn, N., Hongeng, S., Piyachaturawat, P., and Chairoungdua, A. (2014) Downregulation of LAT1 expression suppresses cholangiocarcinoma cell invasion and migration. *Cellular signalling* **26**, 1668-1679

330. Deitmer, J. W., Broer, A., and Broer, S. (2003) Glutamine efflux from astrocytes is mediated by multiple pathways. *Journal of neurochemistry* **87**, 127-135

331. Bhutia, Y. D., Babu, E., Ramachandran, S., and Ganapathy, V. (2015) Amino Acid transporters in cancer and their relevance to "glutamine addiction": novel targets for the design of a new class of anticancer drugs. *Cancer research* **75**, 1782-1788

332. Huang, Y., Dai, Z., Barbacioru, C., and Sadee, W. (2005) Cystine-glutamate transporter SLC7A11 in cancer chemosensitivity and chemoresistance. *Cancer research* **65**, 7446-7454

333. Lyons, S. A., Chung, W. J., Weaver, A. K., Ogunrinu, T., and Sontheimer, H. (2007) Autocrine glutamate signaling promotes glioma cell invasion. *Cancer research* **67**, 9463-9471

334. Chen, R. S., Song, Y. M., Zhou, Z. Y., Tong, T., Li, Y., Fu, M., Guo, X. L., Dong, L. J., He, X., Qiao, H. X., Zhan, Q. M., and Li, W. (2009) Disruption of xCT inhibits cancer cell metastasis via the caveolin-1/beta-catenin pathway. *Oncogene* **28**, 599-609

335. Timmerman, L. A., Holton, T., Yuneva, M., Louie, R. J., Padro, M., Daemen, A., Hu, M., Chan, D. A., Ethier, S. P., van 't Veer, L. J., Polyak, K., McCormick, F., and Gray, J. W. (2013) Glutamine sensitivity analysis identifies the xCT antiporter as a common triple-negative breast tumor therapeutic target. *Cancer cell* **24**, 450-465

336. Dai, L., Cao, Y., Chen, Y., Kaleeba, J. A., Zabaleta, J., and Qin, Z. (2015) Genomic analysis of xCT-mediated regulatory network: Identification of novel targets against AIDS-associated lymphoma. *Oncotarget* **6**, 12710-12722

337. Dai, L., Cao, Y., Chen, Y., Parsons, C., and Qin, Z. (2014) Targeting xCT, a cystine-glutamate transporter induces apoptosis and tumor regression for KSHV/HIV-associated lymphoma. *Journal of hematology & oncology* **7**, 30

338. Ishimoto, T., Nagano, O., Yae, T., Tamada, M., Motohara, T., Oshima, H., Oshima, M., Ikeda, T., Asaba, R., Yagi, H., Masuko, T., Shimizu, T., Ishikawa, T., Kai, K., Takahashi, E., Imamura, Y., Baba, Y., Ohmura, M., Suematsu, M., Baba, H., and Saya, H. (2011) CD44 variant regulates redox status in cancer cells by stabilizing the xCT subunit of system xc(-) and thereby promotes tumor growth. *Cancer cell* **19**, 387-400

339. Takeuchi, S., Wada, K., Toyooka, T., Shinomiya, N., Shimazaki, H., Nakanishi, K., Nagatani, K., Otani, N., Osada, H., Uozumi, Y., Matsuo, H., and Nawashiro, H. (2013) Increased xCT expression correlates with tumor invasion and outcome in patients with glioblastomas. *Neurosurgery* **72**, 33-41; discussion 41

340. Kinoshita, H., Okabe, H., Beppu, T., Chikamoto, A., Hayashi, H., Imai, K., Mima, K., Nakagawa, S., Ishimoto, T., Miyake, K., Yokoyama, N., Ishiko, T., and Baba, H. (2013) Cystine/glutamic acid transporter is a novel marker for predicting poor survival in patients with hepatocellular carcinoma. *Oncology reports* **29**, 685-689

341. Shiozaki, A., Iitaka, D., Ichikawa, D., Nakashima, S., Fujiwara, H., Okamoto, K., Kubota, T., Komatsu, S., Kosuga, T., Takeshita, H., Shimizu, H., Nako, Y., Sasagawa, H., Kishimoto, M., and Otsuji, E. (2014) xCT, component of cysteine/glutamate transporter, as an independent prognostic factor in human esophageal squamous cell carcinoma. *Journal of gastroenterology* **49**, 853-863

342. Robert, S. M., Buckingham, S. C., Campbell, S. L., Robel, S., Holt, K. T., Ogunrinu-Babarinde, T., Warren, P. P., White, D. M., Reid, M. A., Eschbacher, J. M., Berens, M. E., Lahti, A. C., Nabors, L. B., and Sontheimer, H. (2015) SLC7A11 expression is associated with seizures and predicts poor survival in patients with malignant glioma. *Sci Transl Med* **7**, 289ra286

343. Rodrigues, R. J., and Lerma, J. (2012) Metabotropic signaling by kainate receptors. *Wiley Interdisciplinary Reviews: Membrane Transport and Signaling* **1**, 399-410

344. Perez-Otano, I., Larsen, R. S., and Wesseling, J. F. (2016) Emerging roles of GluN3-containing NMDA receptors in the CNS. *Nat Rev Neurosci* **advance online publication**

345. Wei, X., Walia, V., Lin, J. C., Teer, J. K., Prickett, T. D., Gartner, J., Davis, S., Program, N. C. S., Stemke-Hale, K., Davies, M. A., Gershenwald, J. E., Robinson, W., Robinson, S., Rosenberg, S. A., and Samuels, Y. (2011) Exome sequencing identifies GRIN2A as frequently mutated in melanoma. *Nature genetics* **43**, 442-446

346. D'Mello S, A., Flanagan, J. U., Green, T. N., Leung, E. Y., Askarian-Amiri, M. E., Joseph, W. R., McCrystal, M. R., Isaacs, R. J., Shaw, J. H., Furneaux, C. E., During, M. J., Finlay, G. J., Baguley, B. C., and Kalev-Zylinska, M. L. (2014) Evidence That GRIN2A Mutations in Melanoma Correlate with Decreased Survival. *Frontiers in oncology* **3**, 333

347. Bhutia, Y. D., and Ganapathy, V. (2016) Glutamine transporters in mammalian cells and their functions in physiology and cancer. *Biochimica et Biophysica Acta (BBA) - Molecular Cell Research* **1863**, 2531-2539

348. Linher-Melville, K., Haftchenary, S., Gunning, P., and Singh, G. (2015) Signal transducer and activator of transcription 3 and 5 regulate system Xc- and redox balance in human breast cancer cells. *Molecular and cellular biochemistry* **405**, 205-221

349. Forbes, S. A., Beare, D., Gunasekaran, P., Leung, K., Bindal, N., Boutselakis, H., Ding, M., Bamford, S., Cole, C., Ward, S., Kok, C. Y., Jia, M., De, T., Teague, J. W., Stratton, M. R., McDermott, U., and Campbell, P. J. (2015) COSMIC: exploring the world's knowledge of somatic mutations in human cancer. *Nucleic acids research* **43**, D805-D811

350. Meyerson, J. R., Kumar, J., Chittori, S., Rao, P., Pierson, J., Bartesaghi, A., Mayer, M. L., and Subramaniam, S. (2014) Structural mechanism of glutamate receptor activation and desensitization. *Nature* **514**, 328-334

351. Blanpied, T. A., Clarke, R. J., and Johnson, J. W. (2005) Amantadine inhibits NMDA receptors by accelerating channel closure during channel block. *The Journal of neuroscience : the official journal of the Society for Neuroscience* **25**, 3312-3322

352. Galimberti, D., and Scarpini, E. (2016) Old and new acetylcholinesterase inhibitors for Alzheimer's disease. *Expert opinion on investigational drugs*, 1-7

353. Zanos, P., Moaddel, R., Morris, P. J., Georgiou, P., Fischell, J., Elmer, G. I., Alkondon, M., Yuan, P., Pribut, H. J., Singh, N. S., Dossou, K. S., Fang, Y., Huang, X. P., Mayo, C. L., Wainer, I. W., Albuquerque, E. X., Thompson, S. M., Thomas, C. J., Zarate, C. A., Jr., and Gould, T. D. (2016) NMDAR inhibition-independent antidepressant actions of ketamine metabolites. *Nature* **533**, 481-486

354. Rzeski, W., Turski, L., and Ikonomidou, C. (2001) Glutamate antagonists limit tumor growth. *Proc Natl Acad Sci U S A* **98**, 6372-6377

355. Stepulak, A., Sifringer, M., Rzeski, W., Brocke, K., Gratopp, A., Pohl, E. E., Turski, L., and Ikonomidou, C. (2007) AMPA antagonists inhibit the extracellular signal regulated kinase pathway and suppress lung cancer growth. *Cancer biology & therapy* **6**, 1908-1915

356. Glunde, K., Bhujwalla, Z. M., and Ronen, S. M. (2011) Choline metabolism in malignant transformation. *Nature reviews. Cancer* **11**, 835-848

357. Jiang, L., Kon, N., Li, T., Wang, S. J., Su, T., Hibshoosh, H., Baer, R., and Gu, W. (2015) Ferroptosis as a p53-mediated activity during tumour suppression. *Nature* **520**, 57-62

358. Dixon, S. J., Lemberg, K. M., Lamprecht, M. R., Skouta, R., Zaitsev, E. M., Gleason, C. E., Patel, D. N., Bauer, A. J., Cantley, A. M., Yang, W. S., Morrison, B., 3rd, and Stockwell, B. R. (2012) Ferroptosis: an iron-dependent form of nonapoptotic cell death. *Cell* **149**, 1060-1072

359. Xie, Y., Hou, W., Song, X., Yu, Y., Huang, J., Sun, X., Kang, R., and Tang, D. (2016) Ferroptosis: process and function. *Cell Death Differ* **23**, 369-379

360. Lim, J. H., Luo, C., Vazquez, F., and Puigserver, P. (2014) Targeting mitochondrial oxidative metabolism in melanoma causes metabolic compensation through glucose and glutamine utilization. *Cancer research* **74**, 3535-3545

361. Watford, M. (2015) Glutamine and glutamate: Nonessential or essential amino acids? *Animal Nutrition* **1**, 119-122

362. Gross, M. I., Demo, S. D., Dennison, J. B., Chen, L., Chernov-Rogan, T., Goyal, B., Janes, J. R., Laidig, G. J., Lewis, E. R., Li, J., Mackinnon, A. L., Parlati, F., Rodriguez, M. L., Shwonek, P. J., Sjogren, E. B., Stanton, T. F., Wang, T., Yang, J., Zhao, F., and Bennett, M. K. (2014) Antitumor activity of the glutaminase inhibitor CB-839 in triple-negative breast cancer. *Molecular cancer therapeutics* **13**, 890-901

363. Ghislin, S., Deshayes, F., Lauriol, J., Middendorp, S., Martins, I., Al-Daccak, R., and Alcaide-Loridan, C. (2012) Plasticity of melanoma cells induced by neural cell crest conditions and three-dimensional growth. *Melanoma Res* **22**, 184-194

364. Friberg, S., and Nystrom, A. (2015) Cancer Metastases: Early Dissemination and Late Recurrences. *Cancer growth and metastasis* **8**, 43-49

365. Folkman, J., and Kalluri, R. (2004) Cancer without disease. *Nature* **427**, 787

366. Ghajar, C. M. (2015) Metastasis prevention by targeting the dormant niche. *Nat Rev Cancer* **15**, 238-247

367. Uhr, J. W., and Pantel, K. (2011) Controversies in clinical cancer dormancy. *Proc Natl Acad Sci U S A* **108**, 12396-12400

368. Ribeiro, M. P., Custodio, J. B., and Santos, A. E. (2016) Ionotropic glutamate receptor antagonists and cancer therapy: time to think out of the box? *Cancer Chemother Pharmacol*

369. Coussen, F. (2009) Molecular determinants of kainate receptor trafficking. *Neuroscience* **158**, 25-35

370. Nasu-Nishimura, Y., Jaffe, H., Isaac, J. T., and Roche, K. W. (2010) Differential regulation of kainate receptor trafficking by phosphorylation of distinct sites on GluR6. *The Journal of biological chemistry* **285**, 2847-2856

371. Wu, C. S., Lu, Y. J., Li, H. P., Hsueh, C., Lu, C. Y., Leu, Y. W., Liu, H. P., Lin, K. H., Hui-Ming Huang, T., and Chang, Y. S. (2010) Glutamate receptor, ionotropic, kainate 2 silencing by DNA hypermethylation possesses tumor suppressor function in gastric cancer. *International journal of cancer* **126**, 2542-2552

372. Fukata, Y., Amano, M., and Kaibuchi, K. (2001) Rho-Rho-kinase pathway in smooth muscle contraction and cytoskeletal reorganization of non-muscle cells. *Trends Pharmacol Sci* **22**

373. Tashiro, A., Dunaevsky, A., Blazeski, R., Mason, C. A., and Yuste, R. (2003) Bidirectional Regulation of Hippocampal Mossy Fiber Filopodial Motility by Kainate Receptors: A Two-Step Model of Synaptogenesis. *Neuron* **38**, 773-784

374. Nobes, C. D., and Hall, A. (1995) Rho, rac, and cdc42 GTPases regulate the assembly of multimolecular focal complexes associated with actin stress fibers, lamellipodia, and filopodia. *Cell* **81**, 53-62

375. Lerma, J., and Marques, Joana M. Kainate Receptors in Health and Disease. *Neuron* **80**, 292-311

376. Kang, J. H., Jiang, Y., Toita, R., Oishi, J., Kawamura, K., Han, A., Mori, T., Niidome, T., Ishida, M., Tatematsu, K., Tanizawa, K., and Katayama, Y. (2007) Phosphorylation of Rho-associated kinase (Rho-kinase/ROCK/ROK) substrates by protein kinases A and C. *Biochimie* **89**, 39-47

377. Wei, X., Walia, V., Lin, J. C., Teer, J. K., Prickett, T. D., Gartner, J., Davis, S., Stemke-Hale, K., Davies, M. A., Gershenwald, J. E., Robinson, W., Robinson, S., Rosenberg, S. A., and Samuels, Y. (2011) Exome sequencing identifies GRIN2A as frequently mutated in melanoma. *Nature genetics* **43**, 442-446

378. Gadea, G., de Toledo, M., Anguille, C., and Roux, P. (2007) Loss of p53 promotes RhoA–ROCK-dependent cell migration and invasion in 3D matrices. *The Journal of Cell Biology* **178**, 23-30

379. Zhang, C., Zhang, S., Zhang, Z., He, J., Xu, Y., and Liu, S. (2014) ROCK has a crucial role in regulating prostate tumor growth through interaction with c-Myc. *Oncogene* **33**, 5582-5591

380. Bourguignon, L. Y., Singleton, P. A., Zhu, H., and Diedrich, F. (2003) Hyaluronan-mediated CD44 interaction with RhoGEF and Rho kinase promotes Grb2-associated binder-1 phosphorylation and phosphatidylinositol 3-kinase signaling leading to cytokine (macrophage-colony stimulating factor) production and breast tumor progression. *The Journal of biological chemistry* **278**, 29420-29434

381. Li, Z., Dong, X., Wang, Z., Liu, W., Deng, N., Ding, Y., Tang, L., Hla, T., Zeng, R., Li, L., and Wu, D. (2005) Regulation of PTEN by Rho small GTPases. *Nature cell biology* **7**, 399-404

382. Miller, D. M., Thomas, S. D., Islam, A., Muench, D., and Sedoris, K. (2012) c-Myc and Cancer Metabolism. *Clinical cancer research : an official journal of the American Association for Cancer Research* **18**, 5546-5553

383. Dang, C. V. (2012) MYC on the path to cancer. *Cell* **149**

384. Gordan, J. D., Thompson, C. B., and Simon, M. C. (2007) HIF and c-Myc: sibling rivals for control of cancer cell metabolism and proliferation. *Cancer cell* **12**

385. Shim, H., Dolde, C., Lewis, B. C., Wu, C. S., Dang, G., Jungmann, R. A., Dalla-Favera, R., and Dang, C. V. (1997) c-Myc transactivation of LDH-A: implications for tumor metabolism and growth. *Proc Natl Acad Sci U S A* **94**

386. Soucek, L., Whitfield, J., Martins, C. P., Finch, A. J., Murphy, D. J., Sodir, N. M., Karnezis, A. N., Swigart, L. B., Nasi, S., and Evan, G. I. (2008) Modelling Myc inhibition as a cancer therapy. *Nature* **455**

387. Wise, D. R., DeBerardinis, R. J., Mancuso, A., Sayed, N., Zhang, X. Y., Pfeiffer, H. K., Nissim, I., Daikhin, E., Yudkoff, M., McMahon, S. B., and Thompson, C. B. (2008) Myc regulates a transcriptional program that stimulates mitochondrial glutaminolysis and leads to glutamine addiction. *Proc Natl Acad Sci U S A* **105**, 18782-18787

388. Levine, A. J. (1997) p53, the cellular gatekeeper for growth and division. *Cell* **88**, 323-331

389. Puzio-Kuter, A. M. (2011) The Role of p53 in Metabolic Regulation. *Genes & Cancer* **2**, 385-391

390. Ongusaha, P. P., Kim, H.-G., Boswell, S. A., Ridley, A. J., Der, C. J., Dotto, G. P., Kim, Y.-B., Aaronson, S. A., and Lee, S. W. (2006) RhoE Is a Pro-Survival p53 Target Gene that Inhibits ROCK I-Mediated Apoptosis in Response to Genotoxic Stress. *Current Biology* **16**, 2466-2472

391. Vemula, S., Shi, J., Mali, R. S., Ma, P., Liu, Y., Hanneman, P., Koehler, K. R., Hashino, E., Wei, L., and Kapur, R. (2012) ROCK1 functions as a critical regulator of stress erythropoiesis and survival by regulating p53. *Blood* **120**, 2868-2878

392. Owen, D. M., Rentero, C., Magenau, A., Abu-Siniyeh, A., and Gaus, K. (2012) Quantitative imaging of membrane lipid order in cells and organisms. *Nat Protoc* **7**, 24-35

393. Ravanbakhsh, S., Liu, P., Bjordahl, T. C., Mandal, R., Grant, J. R., Wilson, M., Eisner, R., Sinelnikov, I., Hu, X., Luchinat, C., Greiner, R., and Wishart, D. S. (2015) Accurate, Fully-Automated NMR Spectral Profiling for Metabolomics. *PLoS ONE* **10**, e0124219